AXIAL PERFORMANCE OF CONTINUOUS-FLIGHT PILE IN FROZEN SOIL

by

Shuai Gao

A thesis submitted in partial fulfillment of the requirements for the degree of

Doctor of Philosophy

in

GEOTECHNICAL ENGINEERING

Department of Civil and Environmental Engineering

University of Alberta

ABSTRACT

Piles are commonly used in the Canadian Arctic as a foundation solution. Steel pipe shaft pile, which is a conventional pile type in the Arctic, is placed in an oversized pre-drilled hole and then the annulus is backfilled with gravel slurries or grout designed to cure (i.e., a process called freezeback) at cold temperatures. However, the construction is labor-intensive and freezeback is time-consuming. Additionally, conventional steel pipe piles may provide lower adfreeze strength between backfill and frozen soil than other methods.

As an innovative foundation option, continuous-flight piles consist of a steel tube with continuous spiral flights and a tapered lower segment. These piles can be installed by applying a compressive load and torque to the pile head. Owing to the difference in pile construction and soil-pile interface, continuous-flight piles have advantages such as large capacities, rapid installation, lightweight, and reusability in non-frozen soils. Consequently, continuous-flight piles may present a better solution for deep foundations in the Canadian Arctic region. However, currently there is not any design guideline or research on the application of continuous-flight piles in permafrost regions. The short-term strength and long-term creep settlement of the continuous-flight pile in the frozen ground may be different from conventional predrilled steel pipe piles. Understanding the effects of pile shaft features and frozen soil conditions on the axial performance of continuous-flight piles will provide valuable information for the pile design in permafrost.

To address these gaps, a research program was conducted to characterize the installation and determine the axial behaviour of continuous-flight piles in frozen soils. Some specific hypotheses of the research program are: 1) the continuous-flight pile can be screwed into a pilot hole in frozen soil; 2) the water content, salinity, temperature of soils and pile shaft feature will affect the performance of piles; 3) the geotechnical failure may occur locally at the soil beneath the pile threads instead of at the soil-shaft shear surface, based on research of this pile type in non-

frozen soils; 4) because of the failure pattern, the short-term capacity of the continuous-flight pile may be greater than conventional piles of similar size, and the long-term creep rates may be less than that of conventional piles.

The research of model pile testing in frozen soils was carried out at the Cold Regions Geotechnical Research Center, University of Alberta. Twelve short-term or constant displacement rate tests, four long-term or constant load tests, and seven installation tests were conducted. Continuous-flight pile segments with a diameter of 89 mm and a height of 300 mm were installed and loaded in frozen soils to investigate the installation torque, short-term axial pile capacities, long-term settlement, and load-transfer mechanism. The effects of porewater salinity (0 and 10 ppt), soil temperature (0 to -5 °C), soil's water content (20% to 27%), and pile shaft feature were examined. Strain gauges were installed on the pile surface to measure the internal stress distribution during axial loading and the torque during installation. Pile segments were installed in an undersized pilot hole in warm frozen soils using an electric rotary motor. Results showed that installation was refused at a minimum temperature of -1.88 ºC in 10 ppt soil and -1.0 ºC in non-saline soil due to the limitation of the lab equipment. The test pile carried more load than the smooth pile in the cold frozen soil (-5 ºC). The short-term ultimate pile capacity increased significantly when soil temperature decreased from -1 ºC to -5 ºC. The pile capacity increased with decreasing salinity in cold frozen soils while the effect of salinity on the pile capacity in warm frozen soils (-1 ºC) could be neglected. Cylindrical shearing mode and individual bearing mode were observed for continuous-flight piles in warm and cold frozen soils, respectively.

In conclusion, this research introduces a novel pile type that may be suitable for residential and commercial projects in Canadian Arctic communities. Findings from this research are anticipated to contribute to the safe and economic construction of infrastructure across Northern and Western Canada.

Preface

A version of Chapter 3 has been published in the Canadian Geotechnical Journal, which the candidate, Dr. David Sego, and Dr. Lijun Deng co-authored. The candidate's contribution to the content of this research included planning, coordinating, managing, and conducting the laboratory test program, data processing and analyzation.

A version of Chapter 4 has been published in the Canadian Geotechnical Journal, which the candidate, Dr. David Sego, and Dr. Lijun Deng co-authored. The candidate's contribution to the content of this research included planning, coordinating, managing, and conducting the laboratory test program, data processing and analyzation.

A version of Chapter 5 will be submitted to a peer-reviewed journal, which the candidate, Dr. David Sego, and Dr. Lijun Deng co-authored. The candidate's contribution to the content of this research included planning, coordinating, managing, and conducting the laboratory test program, data processing and analyzation.

Acknowledgements

I would like to express my deepest gratitude to my supervisor, Dr. Lijun Deng, for providing me with the opportunity to pursue my research interests, and for his unwavering support, encouragement, and guidance throughout my graduate studies. His expertise, experience, and invaluable feedback have been instrumental in shaping the direction and focus of my research. I am also deeply indebted to Dr. David Sego, and Dr. Michael Hendry for their invaluable insights, critiques, and support as members of my thesis committee.

I would like to thank the financial support from the Natural Sciences and Engineering Research Council of Canada and the China Scholarship Council. I am grateful to Krinner Canada Inc. for their financial and technical support and are grateful to Tomas Johansson and Benoit Trudeau. I appreciate Mr. Lucas Duerksen, Mr. Gleb Aleksandrovich Laskevich, Dr. Jianzhou Wang, and Dr. Jia Bin, Dr. Weidong Li, Chao Liu, for their invaluable assistance in the laboratory work. I am also grateful to my colleagues and friends for their support and camaraderie throughout my time as a graduate student.

I am particularly thankful to my wife Jiajia Xu and my daughter Luna Gao, for their trust, love, and support. Without their encouragement and understanding, this journey would not have been possible.

Finally, I would like to acknowledge the debt of gratitude that I owe to the participants of my study, who graciously shared their time, experiences, and insights with me.

Table of Contents

List of Tables

List of Figures

List of Symbols in Chapter 3 to 5

α, β Empirical parameters in unfrozen water content predictive equation;

γ Shear strain on pile shaft;

ε Axial strain on pile shaft;

ε_{sg} Normal internal strain of pile shaft;

θ Negative temperature in ºC;

θ_0 Reference temperature taken as -1 ºC;

σ Axial stress on pile shaft (kPa);

σ_{sg} Normal internal stress of pile shaft (kPa);

σ_y Tensile yield strength of pile (kPa);

τ Shear stress on pile shaft (kPa);

τ_{ad} Adfreeze strength of pile (kPa);

τ_u Internal shear strength of frozen soil (kPa);

τ_y Yield shear strength of pile (kPa);

a Pile toe radius or half width of a strip footing;

A Cross-sectional area of pile;

A_{shaft} Contacting area of pile shaft;

$A_{threads}$ Contacting area of threads;

b Screw anchor diameter in Ladanyi and Johnston (1974);

B, n Creep parameters of frozen soil;

CSM Cylindrical Shear Mode;

D Smooth shaft diameter of pile (mm);

E Young's modulus of steel i.e. the pile material (210 GPa);

f_s Average sleeve resistance (kPa);

G Shear modulus of steel i.e. the pile material;

I Influencing factor when calculating plate bearing stress vs. pile settlement rate;

IBM Individual Bearing Mode;

J Polar moment of inertia of the pile tubular cross-section;

L Length of pile that was embedded in the soil (mm);

LC Load cell;

L_{ij} Length of shaft segment of pile between i and j (mm);

LP Linear Potentiometer;

L_{th} Length of helical threads that was embedded in the soil (mm);

m_{salt} Mass of salt ions in the frozen soil (g);

m_{water} Mass of porewater in the frozen soil (kg);

N Crowd load of pile;

N_c Bearing capacity factor of frozen soil;

N_y Yield crowd load of pile;

q Unit plate bearing stress (kPa);

Q Internal shaft load of pile (kN);

q_b Unit plate bearing strength from short-term axial loading test (kPa);

Q_{head} Axial load on the pile head (kN);

Q_{plate} Plate bearing resistance (kN);

Q_{shaft} Adfreeze resistance (kN);

r Inner radius of pile shaft (40.85 mm);

R Outer radius of pile shaft (44.45 mm);

s Pile settlement (mm);

$\dot{s}$ Pile settlement rate (mm/h);

S Salinity of soil (ppt);

SG Strain Gauge;

S_{th} Spacing between each thread (mm);

T Temperature of soil (℃) in Chapter 3 and 4; installation torque in Chapter 5;

TC Thermocouple;

t_{soil} Temperature of soil (℃) in Chapter 5;

T_y Yield installation torque;

w Gravimetric water content of soil (%);

w_0 Initial gravimetric water content (%);

w_{th} Width of threads (mm);

w_u Unfrozen gravimetric water content (%).

List of Publications

Gao, S., Bin, J., Sego, D., and Deng, L. 2020. Axial performance of screw micropiles subjected to quick loads in frozen soils. GeoVirtual 2020-Resilience of Innovation, in proceedings of 73rd Canadian Geotechnical Society Conference, (the annual conference of Canadian Geotechnical Society), pp. 8.

Gao, S., Sego, D., and Deng, L. 2021. Pile foundations in permafrost, Canadian Geotechnique, 2 (4): 42-45.

Chapter 3:

Gao, S., Sego, D., and Deng, L. 2023a. Short-term axial loading of continuous-flight pile segment in frozen soil, Canadian Geotechnical Journal, 60(4): 541-554.

Chapter 4:

Gao, S., Sego, D., and Deng, L. 2023b. Long-term axial performance of continuous-flight pile in frozen soil, Canadian Geotechnical Journal, e-first article, doi: 10.1139/cgj-2022-0461.

Chapter 5:

Gao, S., Sego, D., and Deng, L. 2023c. Laboratory investigation of torsional installation method for continuous-flight pile in frozen soil (to be submitted to a peer-reviewed journal).

1 Introduction

1.1 Background

Permafrost refers to the ground that remains at or below 0 °C for at least two consecutive years, regardless of soil type, ground ice distribution, or thermal regime (Andersland and Ladanyi 2004). In Canada, half of the land surface lies in permafrost regions (Johnston 1981), mainly in the arctic and subarctic regions, which include Yukon, Northwest Territories, Nunavut, northern Quebec, and Labrador (Figure 1.1). To design foundations in permafrost, it is important to consider how ground temperature varies over time and depth. These variations can be illustrated by the "trumpet curve" (Figure 1.2a), which shows the magnitude and depth of ground temperature fluctuations that correlate with air temperature. Figure 1.2b shows examples of ground temperature measurements taken in Inuvik, NWT (Holubec 2008).

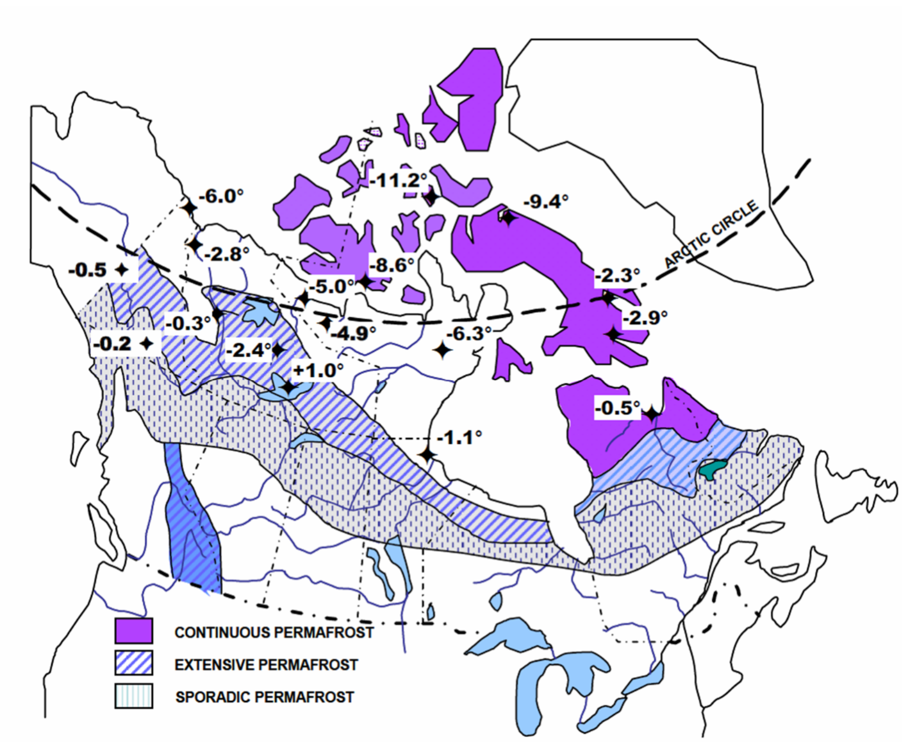

Figure 1.1 Permafrost distribution in Canada (after Holubec 2008).

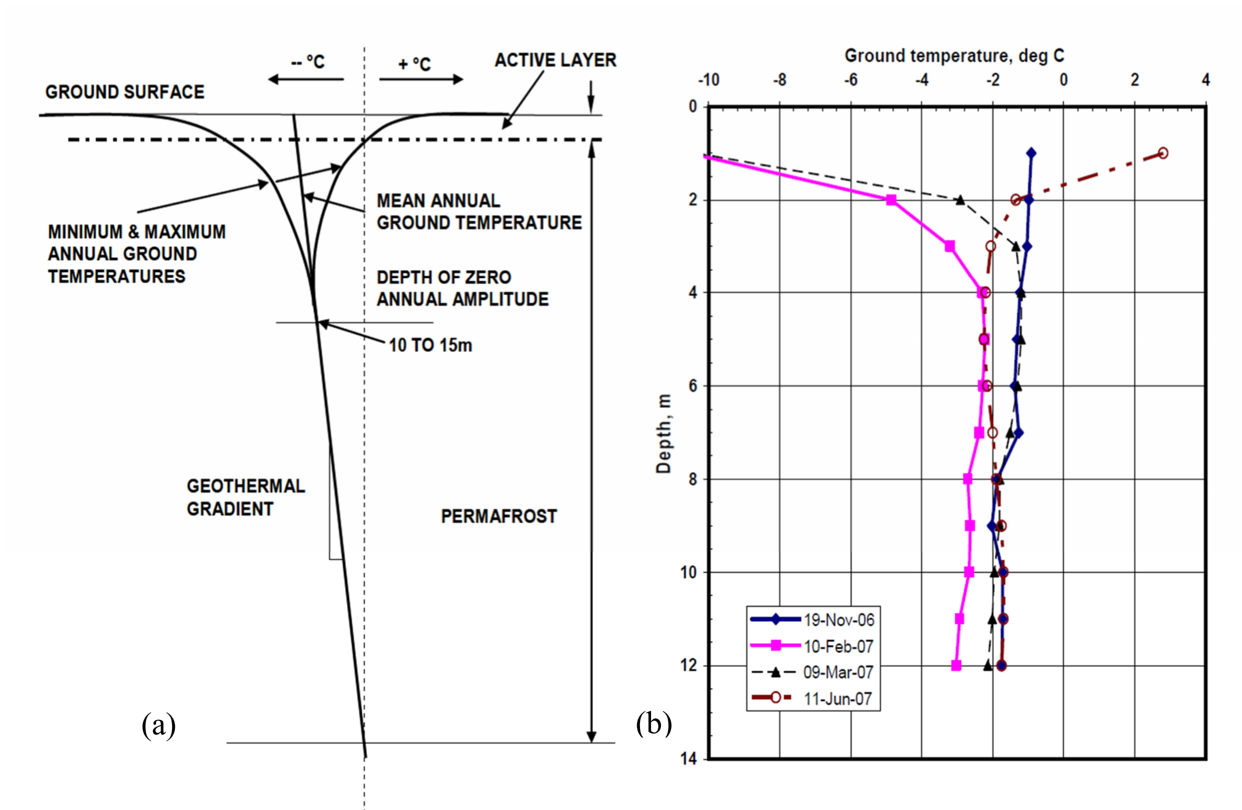

Figure 1.2 (a). "Trumpet curve" of schematic ground temperature profile; (b) ground temperature measured between 2006 and 2007 in Inuvik, NWT (after Holubec 2008).

Piles are commonly used for foundations in permafrost in the Canadian Arctic to support superstructures (e.g., buildings) and above-ground infrastructures (e.g., utilidor). Piles transmit the structural loads to deep soils where the supporting strength of the soil remains relatively stable throughout the life of the structure. Piles in permafrost are typically socketed into bedrock and therefore be deep, despite the relatively low structural loads. In the permafrost regions of Canada, piles are mostly prefabricated and can be installed mechanically. This installation approach eliminates the need for an open excavation, which could cause significant thermal disturbance in the ground (Andersland and Ladanyi 2004).

Pile types used in the permafrost generally include timber, steel, concrete, and composite (steel/concrete) piles. The selection of a particular pile type depends on various factors, including soil type, temperature profiles, load conditions, availability of material, construction equipment, the cost of transportation, and pile installation (Scher 1996). Conventional foundations in cold regions are straight-shaft smooth pipe pile foundations embedded into the permafrost to elevate the supported structures above the ground surface. The pile is usually placed in pre-drilled borehole and the annulus is backfilled with gravel or a cement-based slurry designed to be back-frozen (i.e., freezeback) at cold temperatures (Figure 1.3a). Despite its common use, this foundation type has several disadvantages: the pile may be expensive to construct; the construction and considerable freezeback may be time-consuming; and the pile capacity may not be maximized because the capacity relies on the adfreeze bond strength of the shaft surface that is usually smaller than the strength of adjacent frozen soil (Biggar 1991).

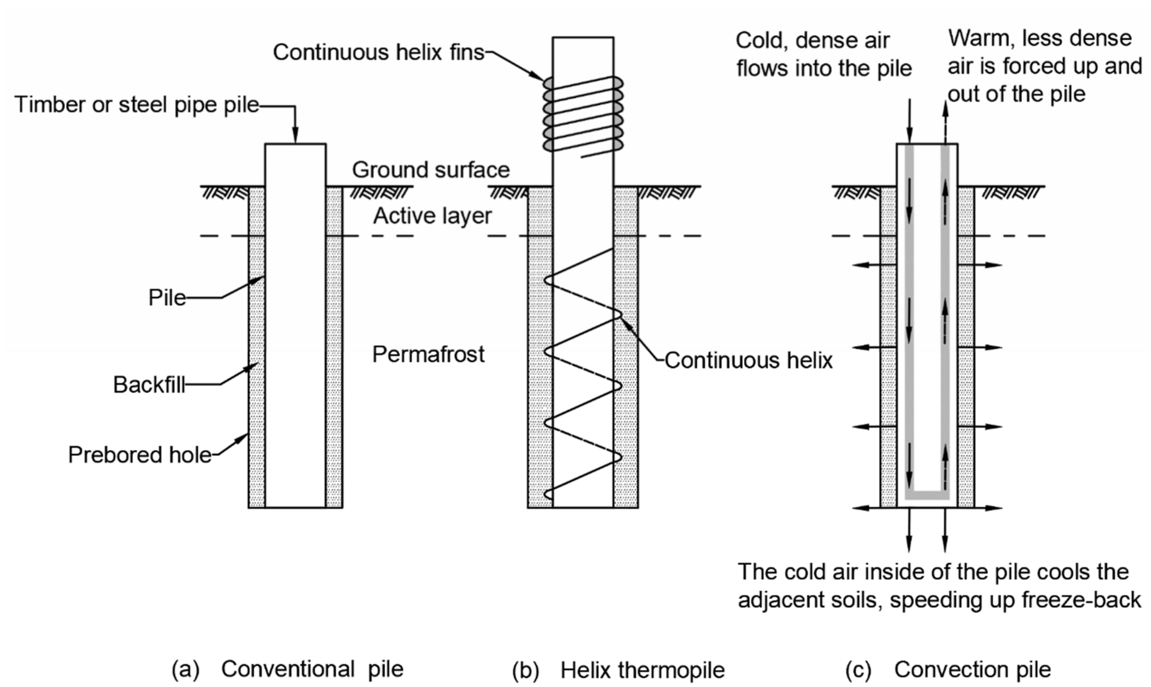

Figure 1.3 Pile types used in the Canadian Arctic (drawing are not to scale, after Gao et al. 2021).

The design of piles in permafrost should consider several potential modes of failure or serviceability criteria. Geotechnical evaluations are required to estimate the minimum embedment depth considering ground temperature, axial shear failure, long-term creep settlement, frost heave and jacking. Piles should resist short-term and sustained loads and have sufficient resistance to counteract upward pull occurring within the active layer from frost heave and frost jacking. Often, creep settlement dominates the pile design, particularly in ice-rich and warm permafrost. Climate change also poses a risk to the integrity of permafrost and pile foundations. Permafrost and frozen ground can thaw in response to climate warming. Changes in permafrost temperatures and active layer thickness will affect the pile performance significantly.

In addition, piles must be protected within the active layer against material deterioration from physical, chemical, and biological actions. In Inuvik, many timber piles have failed because of material damage near the ground surface (Figure 1.4a and 1.4b). In recent years, there have been several cases where new piles or shallow foundations failed to meet the serviceability criteria because of the malfunction of the active or passive freezing system intended to assist with their performance. Wood blocking systems can be a viable solution for remediating buildings that have experienced severe damage to their timber piles (Liu et al. 2022). Instead of remediating failed timber piles, a stack of timber logs is placed on the ground surface (Figure 1.4c and 1.4d). This wood blocking can be positioned underneath the building or outside its edges, making it both easy to install and cost-effective. A case study of a wood blocking system with a health monitoring program in Inuvik was elaborated by Liu et al. (2022). Wood blocking can still settle due to freeze and thaw cycles in the active layer. The top wedge of the wood blocking support will need to be adjusted to close the gaps caused by the settlement.

Several new pile types (Figure 1.3b and 1.3c) have been introduced to the Canadian Arctic in the past few decades, such as helix thermopiles and convection piles. A helix thermopile is a combination of a thermosyphon and an adfreeze pile that incorporates thin-bladed helixes on the pile surface (Zhang and Hoeve 2015). They work together to extract heat from the permafrost during winter. A convection pile is an adfreeze steel pipe pile. Convection forms naturally and extracts the heat from adjacent soils during the winter when the air temperature is colder than the ground temperature, and dormant during the summer. This has a cooling effect on the adjacent soil and improves pile performance.

Figure 1.4 (a) Decayed timber pile supporting an apartment building; (b) failed pile under the utilidor; (c) and (d) wood block system supporting residental buildings in Inuvik, NWT.

Continuous-flight piles or screw micropiles have been recently introduced to Canadian foundation industry as a new foundation type. The continuous-flight pile consists of a steel tube with continuous spiral threads welds on the lower half of the pile shaft and a closed-end tapered pile tip, with a galvanized coating to provide corrosion resistance. The installation method of continuous-flight pile is different from conventional piles. Firstly, continuous-flight piles are screwed into the ground by applying a torque to the pile head while a downward force is also applied to make the pile advance downward. No pre-drilling is required prior to the pile installation unless in the gravelly ground; therefore, the ground disturbance is minimum, and the pile is immediately loadable after installation. Because no soil is removed prior to installation, this pile type can be classified as displacement pile, and the increase in lateral earth pressure caused by installation could potentially lead to a higher capacity than conventional piles. Secondly, grouting and freezeback is not involved in the construction of continuous-flight piles. Therefore, no curing time is needed, and the piles are immediately loadable after installation.

1.2 Problem Statements and Hypotheses

As a new introduced pile type, continuous-flight piles are anticipated to serve as an optimized foundation type for infrastructure systems in the permafrost regions of Canada. However, there is not any previous research on the axial loading behavior of this pile type in permafrost. The load transfer mechanism along with the pile and the pile-soil interaction failure mechanism are still unknown. Also, there is not any relevant research on pile foundations that are installed into permafrost by the torsional method. Understanding the effects of pile shaft feature, soil temperature, salinity, and water content on the installation and axial performance of continuous-flight piles will provide valuable information for the pile design in the permafrost.

Specific hypotheses of this research program are:

- The continuous-flight piles can be screwed into a pilot hole of the warm frozen soils;
- The soil's water content, salinity, temperature, and pile shaft feature will affect the installation and axial performance of continuous-flight piles;
- The geotechnical failure may occur locally at the soil beneath the pile threads instead of at the soil-shaft shear surface, based on research of this pile type in non-frozen soils. The presence of threads may push the shear failure plane outward to

the edge of the threads. The increased shear strength and plate bearing resistance in the native soil will therefore significantly increase the limit capacity of the threaded segment.

- Failure pattern of cylindrical shear mode or individual end bearing mode may occur. The increased resistance in the native soil leads to a higher short-term capacity of continuous-flight piles than conventional piles of similar size, and the long-term creep rates may be less than that of conventional piles.

1.3 Research Objectives

To guide the field application of continuous-flight pile in permafrost of Canada, the specific objectives of this research are as follows:

- Investigate the effects of pile shaft feature, soil temperature, salinity, and water content on the axial performance and installation torque of continuous-flight pile;
- Determine the short-term stress-strain behaviour and strength of continuous-flight pile in frozen ground;
- Investigate the long-term creep settlement of continuous-flight pile in frozen ground;
- Understand the load transfer mechanism along the pile and pile-soil interaction failure mechanism in permafrost;
- Provide a guide for the application of the continuous-flight piles in permafrost.

1.4 Scope and Significance of Present Research

The research characterized the axial behavior and installation torque of continuous-flight piles in frozen soils, using the facilities in the Cold Regions Geotechnical Research Center at the University of Alberta. A laboratory experimental program was developed to examine the effects of soil temperature, salinity, water content and pile shaft shape upon the continuous-flight pile performance. The laboratory model pile testing system consists of a soil-pile test cell with two chambers: inner chamber for the soil and the outer chamber accommodating the circulation of coolant for temperature control, a temperature-control bath, a servo-control hydraulic loading equipment, model pile segments, and a data acquisition system. The continuous-flight pile segments with a diameter of 89 mm and a height of 30 cm were installed and loaded in frozen soils. The pile head load was recorded using a load cell. Pile head displacements and ground surface settlements were recorded from the corresponding linear potentiometers. A series of thermocouples were embedded in the soil chamber to record the soil temperature. Also, strain gauges were used to measure the internal strains along the pile segment. The measured strains were thereafter converted into axial forces and installation torques to characterize the behavior of piles in frozen soils.

Two types of loading tests are conducted in the laboratory: short-term or constant displacement rate loading test, and long-term or constant loading test. The short-term constant displacement rate was 2.2 mm/h, which was within the strain rate range adopted in the literature. The load capacity obtained from the short-term loading tests were referenced to determine the loading increments for the long-term loading tests. The soil type, water content, salinities, temperature are selected to cover the range of conditions encountered in coastal Canadian Arctic communities.

The significance of the present study to geotechnical academic and industrial communities are stated as follows. A laboratory experimental loading system for continuous-flight piles in frozen soils was developed at the University of Alberta as part of the present research program. The experimental program developed techniques and hardware that will aid future research on frozen soil-foundation-structure interaction. Experience was gained in model construction, instrumentation, continuous-flight pile installation, axial loading, and data acquisition. By examining the effects of key parameters on the axial performance, the behavior of piles with a similar geometry and soil conditions in the field can be anticipated. This research provided a solution to estimate the installation skin friction, side shear resistance, unit plate bearing resistance, and long-term creep settlement of continuous-flight piles. The proposed analytical calculation to the load transfer and installation torque can improve understanding the performance of continuous-flight piles in frozen soils. The required installation torque measured in the laboratory tests could be referenced to guide the field application of continuous-flight piles in permafrost of Canada.

Therefore, the outcomes of the present research are anticipated to provide an innovative foundation type that may be more cost-effective and more capable than conventional foundations. The findings from present research will also help promote the broader application of continuous-flight piles in existing and emerging industries such as residential and commercial buildings, railways, bridges, pipelines, power-transmission towers, and other infrastructure systems. In addition, the findings are expected to contribute to the safe and economic construction of infrastructure of indigenous communities, and to help support the economic growth and expansion of communities and industrial infrastructure across Northern Canada and Western Canada associated with climate change.

1.5 Thesis Outline

The thesis contains six chapters. A short description of each chapter and appendix is summarized as follows:

Chapter 1: Introduction

The introduction includes the research background, problem statement and hypotheses, research objectives, scope, and significance of the research.

Chapter 2: Literature Review

A review of the literature related to the mechanical properties of frozen soils, overview of piles foundations practice in cold regions, factors influencing pile adfreeze strength and creep settlement, numerical modeling, and design method of pile foundations in frozen soils is reported in the literature review.

Chapter 3: Short-Term Axial Loading of Continuous-Flight Pile Segment in Frozen Soil

This chapter includes a review of the short-term axial performance of continuous-flight pile in frozen soils. A version of this chapter constitutes the paper that has been published in the Canadian Geotechnical Journal.

Chapter 4: Long-Term Axial Performance of Continuous-Flight Pile in Frozen Soil

This chapter includes a review of the long-term axial performance of continuous-flight pile in frozen soils. A version of this chapter constitutes the paper that has been published to the Canadian Geotechnical Journal.

Chapter 5: Laboratory Investigation of Torsional Installation Method for Continuous-Flight Pile in Frozen Soil

This chapter includes a review of the laboratory investigation of torsional installation method for continuous-flight pile in frozen soils. A version of this chapter constitutes the paper that will be submitted to a peer-reviewed journal.

Chapter 6: Summary of Conclusions

In the final chapter, a summary of the conclusions of all the parts is reported. The limitations of present research and recommendations for further research are given. In addition, recommendations for continuous-flight pile design in warm permafrost is provided.

Appendix A: Additional laboratory tests photos and drawings are presented in this appendix.

Appendix B: Additional test results are presented in this appendix.

Appendix C: An example of data processing sheet is presented in this appendix.

2 Literature Review

The behavior and design of pile foundations for the infrastructure in cold regions have been the focus of research in the past. It is important to have detailed information on subsurface soil conditions for design and construction purposes. This section reviews the mechanical properties of frozen soils, overview of pile foundation practice in permafrost, pile adfreeze strength and creep settlement correlation between frozen soil and pile foundation, and state-of-art research and design of pile foundations in frozen soils.

2.1 Introduction to Frozen Soil Mechanical Properties

Understanding the mechanical properties of frozen soils is crucial in developing safe and reliable infrastructure in cold regions. Foundation design and construction in non-frozen soils are heavily reliant on the mechanical properties of soils, such as shear strength, deformability, and compressibility. However, in permafrost regions, additional factors must be considered, such as soil frost susceptibility or thermal conductivity, adfreeze bond strength, and stress-strain relationships. The complexity of these properties in frozen soils arises from their interdependence on various factors, including soil type, unfrozen water and ice content, saturation, soil temperature, stress, and loading rate. For instance, in a given frozen soil, the strength and creep deformation behavior are primarily influenced by ice content, temperature, salinity, and loading or strain rate.

2.1.1 Factors Influencing Frozen Soil Strength and Creep Settlement

2.1.1.1 Total Moisture Content and Ice Content

The total moisture content is a crucial factor that significantly affect the strength and creep behavior of frozen soils. In cold regions, the total moisture content of a frozen soil exists in two phases: ice and water. This condition significantly affects the soil's thermal, hydraulic, and mechanical properties, including creep, shear strength, and bearing properties (Scher 1996). As the moisture content increases, the pore water in the soil increases, which leads to an increase in the ice content. This increase in ice content leads to an increase in the strength of the frozen soil due to the increase in interlocking between soil particles. However, if the moisture content becomes too high, it may lead to a decrease in strength due to a reduction in the air-void ratio and an increase in the ice lenses, leading to soil heaving and cracking. The ratio of water to ice primarily depends on the soil temperature, grain size, pressure, and mineral content of the water.

Nerseova and Tsytovich (1963) categorized soil water into three distinct states: gaseous, bounded, and free. They defined weakly bounded water as adsorbed water that undergoes a phase change when exposed to sub-zero temperatures, and strongly bounded water as liquid water that remains in that state even at sub-zero temperatures. Free water, on the other hand, freezes at 0 °C at one atmosphere.

The relationship between unfrozen water and temperature in saline soils and ice is described in detail in Ogata et al. (1983). Generally, ice crystals are formed of fresh water excluding impurities, such as salt ions, from the pure crystalline ice structure into the remaining unfrozen water. As the temperature decreases, the salt ions are excluded into the remaining unfrozen brine solution further depressing its freezing point. This process continues until pore solution become a matrix of ice crystals and salt ions with no liquid brine at the eutectic temperature, which is -21.3 ºC for a sodium chloride solution.

To predict the unfrozen water content, Anderson and Tice (1972) and Dillon and Andersland (1966) proposed two methods based on specific surface area and temperature. Dillon and Andersland also accounted for soil activity, clay mineral type, and freezing point depression of pore water. Tice et al. (1976) developed a method for predicting phase composition curves based on liquid limit measurements, which applies to soils with a liquid limit of less than 100 or with no excessive soluble salts. They suggested the following equation to estimate unfrozen water content w_u:

$$w_u = \alpha|T|^{\beta} \tag{2-1}$$

where T is the soil temperature in ºC, and α and β are empirical parameters. Sheng et al. (1995) utilized volumetric water content θ to predict the unfrozen volumetric water content θ_u:

$$\theta_u = \theta e^{(a|T|^b)} \tag{2-2}$$

where θ is the initial volumetric water content, and a and b are fitting parameters that depend on the specific surface area and pore geometry of the soil. Hivon (1991) developed a method to predict the unfrozen water content of saline soils using data obtained experimentally. Then, the effects of unfrozen water content on the strength of frozen saline soil were discussed. A decrease in strength with an increase in unfrozen water content was observed.

2.1.1.2 Soil Temperature

Temperature has a significant impact on the mechanical behavior of frozen soils, as it directly affects the strength of ice and the amount of unfrozen water content. Generally, a decrease in temperature increases the strength of a frozen soil, but also makes it more brittle, resulting in a greater drop in strength after reaching its peak and an increase in the ratio of compressive to tensile strength (as shown in Figure 2.1, Andersland and Ladanyi 2004). Li et al. (2004) concluded that the uniaxial compressive strength of frozen clay linearly increases with decreasing temperature; however, Chen and Lin (2019) proposed that the relationship between the compressive strength and temperature of frozen soil can be expressed by an exponential function (Ren et al. 2023). Previous attempts to use the theory of reaction rate processes to express the relationship between temperature and strength variation in frozen soils have been limited, and the theory is currently viewed as only an approximation.

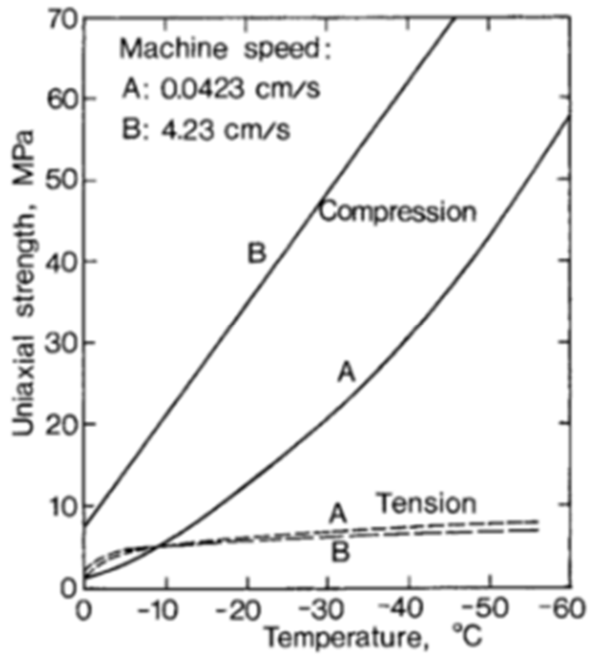

Figure 2.1 Frozen silt uniaxial strength versus temperature (after Andersland and Ladanyi 2004; Haynes and Karalius 1977).

2.1.1.3 Salinity

In many arctic regions, the porewater or pore-ice can be saline due to marine influence during soil deposition or subsequent reworking caused by inundation over geological time (Hivon and Sego 1991; Miller and Johnson 1990). Porewater salinities as high as 46 ppt have been reported in the Baffin Island region (Hanna 1989). In some cases, high "salinity" encountered in the lower Mackenzie Valley can be attributed to local bedrock (limestone and possibly gypsum) rather than marine salinity (Hivon and Sego 1991). Electrical conductivity is often used to determine salinity, and porewater chemistry is not always analyzed. Nixon (1988) presented a simple laboratory test procedure to measure salinity. The permafrost design engineer must determine if any soil chemistry could significantly alter the soil's thermal and physical behavior.

In saline soils, the freezing progress leads to the formation of ice crystals which contain almost fresh water as the salts are expelled upon freezing. As the temperature drops, the ice crystals grow, enveloping both the crystals themselves and the soil particles in a highly concentrated brine solution. Despite the surface tension effects, all medium to fine-grained soils will have some portion of the porewater remain unfrozen, even at temperatures as low as -5 to -10 °C. However, in saline soils, the amount of unfrozen porewater is considerably greater due to the high salt concentrations. Accurately representing the unfrozen moisture content curve in geothermal analyses is crucial. The impact of salinity on the engineering properties of saline soils has been conducted by Nixon and Lem (1984). In frozen saline soil, there is effectively less "bonding" compared to freshwater soil, resulting in considerably less favorable strength and creep deformation characteristics. This phenomenon is confirmed by Hivon and Sego (1995) who investigated the effect of salinity on the frozen soil strength using uniaxial compression tests.

2.1.2 Frozen Soil Strength

Strength properties, such as compressive, shear, and tensile strength, are critical considerations in design. In unfrozen or thawed soils, the strength primarily depends on cohesion and friction between soil particles (Scher 1996). It is generally accepted that the cohesion is time, strain rate and temperature dependent as opposed to friction which is usually constant (Andersland and Al-Nouri 1970). The soil type and grain size distribution are important with respect to the nature of the strength and the amount of unfrozen water, i.e., fine-grained soils having much higher unfrozen water content than coarse-grained soils. Unfrozen soil strength is typically not dependent on loading rate or time. However, in frozen soils, the presence of ice significantly impacts strength-deformation behavior. Ice exhibits non-Newtonian behavior with strong time-dependent plastic deformation (Scher 1996). The relative volumes of ice and soil particles influence the strength-deformation behavior at a given temperature and loading rate (Goughnour and Andersland 1968).

The presence of unfrozen water in frozen soils is due to freezing point depression and salt exclusion within the saline pore fluid.

The observations by Ladanyi and Morel (1990) suggest that the strength behavior of frozen soils can not be predicted by simply adding the strengths of the ice and unfrozen soil components. It was also observed that the tensile strength of ice leads to a dilatancy hardening effect, which causes the frozen sand to behave like it is under confinement even under unconfined compression. Oliphant and Tice (1982) further investigated the mechanisms of strength in frozen soil and identified three components: the strength of the ice, the strength of the soil, and the interaction between the ice and soil. Additionally, Ersoy and Torgrol (1978) found that the effect of strain rate on the measured strength of frozen soils is less significant compared to the effect of temperature.

Hivon and Sego (1995) summarized an extensive laboratory program undertaken to study the influence of soil type, temperature, and salinity on the strength of three different frozen soils under conditions of unconfined constant strain rate tests. They concluded an increase in temperature and salinity (unfrozen water content) causes a significant decrease of strength (Figure 2.2). A predictive model of soil strength in terms of salinity and temperature was presented.

It is important to note that due to their time-dependent behavior, the long-term strength of frozen soils used for design purposes will generally be much smaller than the ultimate or short-term strength. To better understand the interactive relationships between ice content, temperature, strain rate, and confining pressure with frozen soil strengths, researchers have conducted numerous studies. Summaries of frozen soil strengths versus the interactive relationships with ice content, temperature, strain rate, and confining pressure are provided in Andersland and Anderson (1978), Kaplar (1974), and Tsytovich (1975).

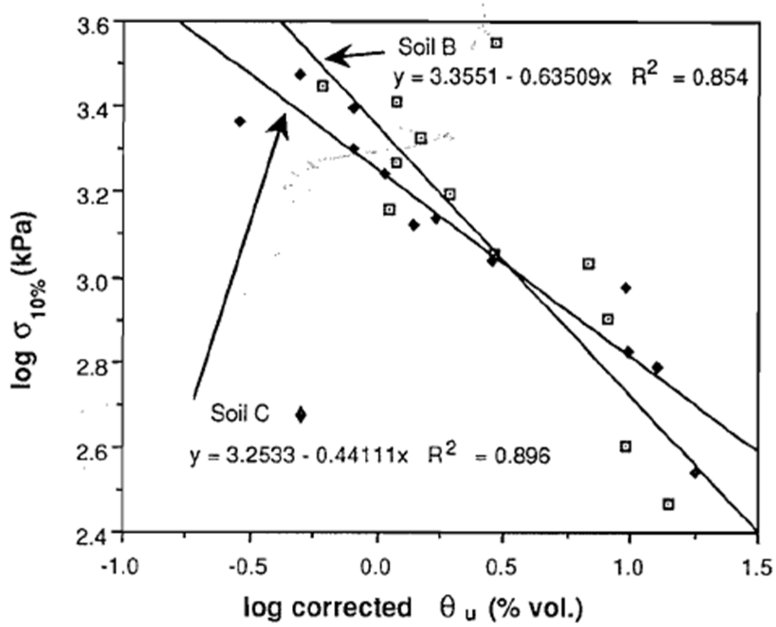

Figure 2.2 Soil strength versus corrected unfrozen water content (after Hivon and Sego 1995).

2.1.3 General Soil Creep Equation

In frozen soil mechanics, it is usually assumed that the total strain, ε, as a result of a deviatoric stress increment is expressed in Equation 2-3:

$$\varepsilon = \varepsilon_0 + \varepsilon^{(c)} \tag{2-3}$$

where ε_0 is the instantaneous strain and $\varepsilon^{(c)}$ is the delayed or creep strain.

For long term problems, such as the behaviour of foundations in permafrost, the short-term response (including elastic, plastic, and primary creep portions) is summed together to form a pseudo-instantaneous plastic strain, $\varepsilon^{(i)}$ (Hult 1966; Ladanyi 1972):

$$\varepsilon = \varepsilon^{(i)} + \dot{\varepsilon}_{min}^{(c)} \tag{2-4}$$

where $\dot{\varepsilon}_{min}^{(c)} = \frac{d\varepsilon^{(c)}}{dt}$ is the minimum (or steady-state) creep rate and t is time. On the basis of available experimental experience with frozen soils (Hult 1966 and Ladanyi 1972), both $\varepsilon^{(i)}$ and $\dot{\varepsilon}_{min}^{(c)}$ be expressed conveniently by the power law approximations:

$$\varepsilon^{(i)} = \varepsilon_k \left(\frac{\sigma}{\sigma_{k\theta}}\right)^k \tag{2-5}$$

and

$$\dot{\varepsilon}_{min}^{(c)} = \dot{\varepsilon}_c \left(\frac{\sigma}{\sigma_{c\theta}}\right)^n \tag{2-6}$$

where $\sigma_{k\theta}$ is a temperature-dependent total deformation modulus, corresponding to the reference strain ε_k, same relationship as $\dot{\varepsilon}_c$ and $\sigma_{c\theta}$.

The values of *k* and *n* can be obtained from uniaxial compression creep tests. For a general state of stress and assuming the validity of von mises flow rule and volume constancy for all plastic deformations, including creep strains, the power type creep equation can be written as (Odqvist 1966):

$$\dot{\varepsilon}_{min}^{(c)} = \dot{\varepsilon}_c \left(\frac{\sigma_e}{\sigma_{c\theta}}\right)^n \text{ (Norton-Bayley power law creep equation)} \tag{2-7}$$

where σ_e and $\dot{\varepsilon}_c$ are the equivalent stress and strain rate, respectively, defined by

$$\sigma_e^2 = 3J_2^{'} = \frac{1}{2}[(\sigma_1 - \sigma_2)^2 + (\sigma_2 - \sigma_3)^2 + (\sigma_3 - \sigma_1)^2] \tag{2-8}$$

$$\varepsilon_e^2 = \frac{4}{3}\dot{I}_2' = \frac{1}{2}[(\dot{\varepsilon}_1 - \dot{\varepsilon}_2)^2 + (\dot{\varepsilon}_2 - \dot{\varepsilon}_3)^2 + (\dot{\varepsilon}_3 - \dot{\varepsilon}_1)^2] \tag{2-9}$$

where $J_2^{'}$ and $\dot{I}_2^{'}$ denote second invariants of stress and strain rate deviation tensor, respectively, and $\sigma_{c\theta}$ is the creep proof stress (creep modulus) obtained in uniaxial compression creep tests at a constant temperature. It should be noted that for axial symmetry, such as in triaxial compression tests on cylindrical specimens, $\sigma_e = (\sigma_1 - \sigma_3)$ and $\dot{\varepsilon}_e = \dot{\varepsilon}_1$, so the power law of equation becomes:

$$\dot{\varepsilon}_1{}^{(c)} = \dot{\varepsilon}_c (\frac{\sigma_1 - \sigma_3}{\sigma_{c\theta}})^n \tag{2-10}$$

For a plane strain case, assuming material incompressibility, $\sigma_e = \frac{\sqrt{3}}{2}(\sigma_1 - \sigma_3)$ and $\dot{\varepsilon}_e = \frac{2}{\sqrt{3}}\dot{\varepsilon}_1$.

Then, $\dot{\varepsilon}_1{}^{(c)} = \left(\frac{\sqrt{3}}{2}\right)^{n+1} \dot{\varepsilon}_c \left(\frac{\sigma_1-\sigma_3}{\sigma_{c\theta}}\right)^n$. Finally, for a simple shear case one can write for an incompressible material:

$$\tau = \frac{1}{2}(\sigma_1 - \sigma_3) \tag{2-11}$$

$$\dot{\gamma} = 2\dot{\varepsilon}_1 \tag{2-12}$$

Then,

$$\dot{\gamma} = 3^{\frac{n+1}{2}} \dot{\varepsilon}_c \left(\frac{\tau}{\sigma_{c\theta}}\right)^n \tag{2-13}$$

With the ice present as pore cement or discrete veins, ice phase behaviour will probably dominate any load-deformation relationship determined for frozen soil. Studies of creep in ice are therefore a useful starting point in the development of appropriate stress-strain relationships for frozen soils.

Glen's (1955) flow law is the most well-known method for predicting constant secondary strain rate, and it has been utilized by numerous authors, including Morgenstern et al. (1980), Sego and Morgenstern (1983):

$$\dot{\varepsilon} = B\sigma^n \tag{2-14}$$

where the value of B is determined by the temperature and type of ice, while the value of n can vary based on the level of stress.

Nixon and Lem (1984) investigated the creep behavior of fine-grained saline frozen soils and the concept of secondary steady-state was utilized. It was noted that at temperature close to the freezing point depression where the unfrozen water content is high, it would be important to differentiate between consolidation and creep effects. Nixon and Pharr (1984) examined the creep behavior of saturated saline frozen gravel, and they observed that neither a secondary creep stage nor a minimum strain rate developed during testing. Hivon (1991) conducted an extensive laboratory program to investigate the influence of soil type, temperature, and salinity on the creep of three different frozen soils using unconfined constant stress tests (Figure 2.3). The results showed that an increase in stress and an increase in salinity cause a decrease in the time to failure and an increase in the strain rate at failure. Hivon (1991) summarized all of the creep parameters necessary to predict the strain versus time for Sayles (1968), Vyalov et al. (1988) and Gardner et al. (1984) models. Table 2.1 lists the obtained creep parameters *B* and *n* for sand (A), silty sand (B), and fine silty sand (C) at the different salinities from Hivon (1991).

Yang et al. (2010) investigated the creep behavior of warm ice-rich frozen sand using a series of experimental data under different stress levels at temperatures of -1 °C, -1.5 °C, and -2 °C. They concluded the creep characteristic of warm ice-rich frozen sand is significantly influenced by the stress levels. A statistical damage constitutive model was proposed based on the experimental results and the validity of the model was verified. Wang et al. (2014) proposed a simple frozen soil creep model by combining Maxwell, Kelvin and Bingham body, with a parabolic yield criteria. Then the model was verified by the direct shear creep tests on frozen fine sand, and the calculated creep strains agree in general with test data (Figure 2.4). Yao et al. (2017) proposed a frozen soil creep model with shear strength attenuation based on parameters obtained from compression and triaxial shear tests. It was noted that the progressive development of creep strain from primary to tertiary stage can be captured reasonably from their model.

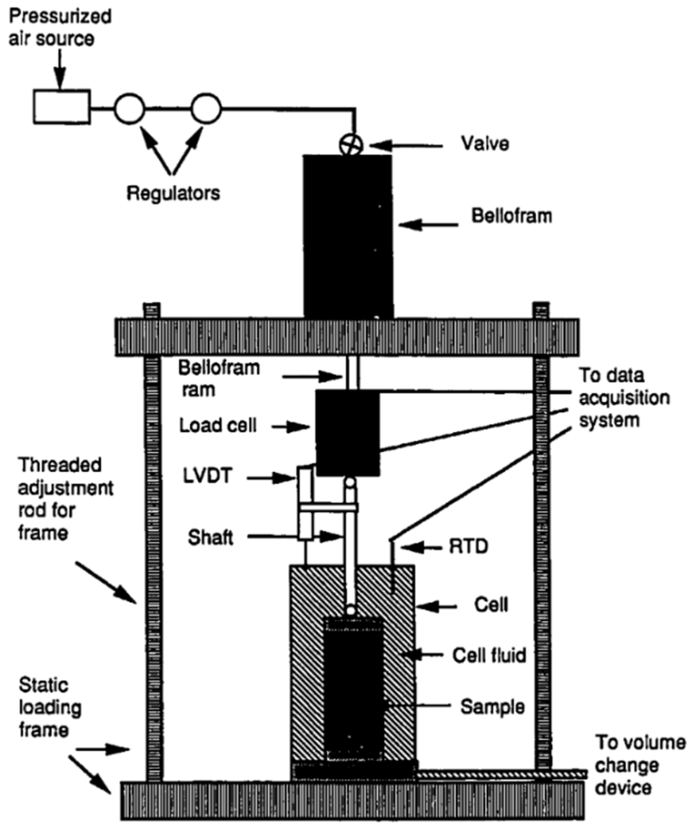

Figure 2.3 Constant stress compression test set-up (after Hivon 1991).

Table 2.1 Creep parameters obtained from Hivon (1991)

B and n VALUES for $\dot{\varepsilon}_m = B\,\sigma^n$

Soil	Salinity (ppt)	B (%/hour)	n
A	0	8.3×10^{-9}	12.2
A	5	0.162	4.6
A	10	0.511	4.2
A	30	36.8	6.7
B	0	9.0×10^{-7}	13.3
B	5	7.9×10^{-5}	12.9
B	10	0.010	11.0
B	30	49.9	4.9
C	0	2.4×10^{-10}	25.6
C	5	5.4×10^{-6}	18.3
C	10	0.0054	14.0
C	30	57.9	3.25

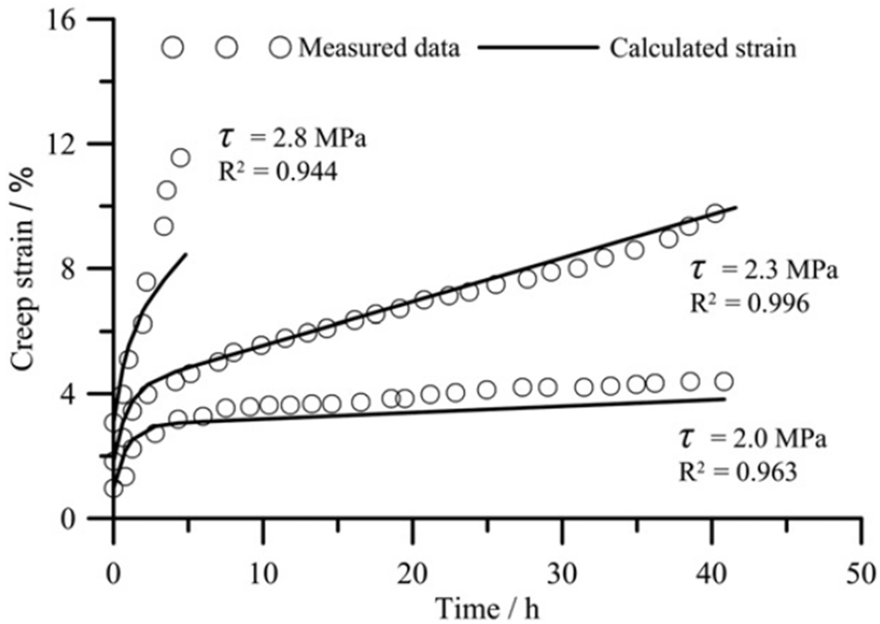

Figure 2.4 Comparison between calculated and measured creep strain from direct shear creep tests (after Wang et al. 2004).

2.2 Overview of Pile Foundations Practice in Permafrost Regions

The straight-shaft smooth timber or steel pipe pile is the conventional foundation used in permafrost regions (Figure 2.5). These piles are usually placed into a pre-drilled, oversized hole with the annulus between the pile shaft and the borehole wall, which is backfilled with a soil-water or grout slurry (Biggar and Sego 1993a, b). The design of the piles is governed by the adfreeze strength between the pile shaft and frozen backfill and the time-dependent creep deformation (Weaver and Morgenstern 1981, Heydinger 1987, Ladanyi et al. 1995). Loading tests of model piles in frozen sand show that smooth straight-shaft piles fail in a brittle manner (Ladanyi and Guichaoua 1985) and have relatively low axial capacities because the shear failure is mobilized at the pile-backfill interface and the adfreeze strength is typically smaller than the strength of adjacent frozen soil.

Figure 2.5 Timber piles are used for residental building and steel pipe piles are supporting commercial buildings in Inuvik, NWT.

Due to their brittle load-displacement behaviour, relatively low axial capacities, and long-term creep deformation, conventional piles may not be appropriate when large capacity and small settlement are required. To enhance their performance, conventional piles may be modified in the following ways: 1) use roughened or corrugated pile shafts; 2) add shaft protrusions such as helix, screws, and lugs; and 3) use a tapered shaft pile.

The surface finish of the pile is critical to the development of surface adfreeze strength (Sego and Smith 1989). A roughened or corrugated shaft surface will move the shear failure surface from the pile- backfill interface outward to the backfill-soil interface or inside the frozen soil, thus significantly increasing the axial capacities. There is ample evidence that the axial capacities of piles are increased by roughening or corrugating the pile shaft (Thomas and Luscher 1980, Weaver and Morgenstern 1981, Andersland and Alwahhab 1983, Holubec and Brzezinski 1989). Compared to conventional smooth piles, roughened or corrugated piles showed more plastic response to short-term loads, and their long-term behaviour could be better predicted (Ladanyi and Theriault 1990). Holubec (1990) conducted field tests of threaded pipe piles backfilled with either a grout or clean uniformly graded coarse sand or fine gravel, as an alternative to the sand slurry pipe. The concepts in the development of the grout and granular thread bar piles are discussed and field load test results are given to compare the capacities of the two proposed piles designs against the sand slurry pipe in short term creep tests. A trifold increase in the axial capacity was observed.

Pile shaft protrusions can change the pile performance significantly. Previous investigations confirmed that protruded piles provide increased axial capacities and reduced creep settlement. Due to their high capacity, protruded piles have many engineering applications. For example, flighted piles were used as foundations for transmission towers in Manitoba (Cutherbertson-Black 2001) and helical piles for the TransAlaska oil pipeline (Zubeck and Liu 2003, Andersland and Ladanyi 2004).

Long (1973) discussed the merit of using rings or helices on piles in lieu of smooth shaft surfaces to avoid the limitation of adfreeze load transfer. Thermal piles with a flight, a 40-mm-wide protrusion welded onto the pile shaft surface, were investigated using field (Dubois 1994) and laboratory tests (Cuthbertson-Black 2001). Johnston and Ladanyi (1972, 1974) conducted field tests in Northern Manitoba to evaluate the creep behaviour and load capacity of single-helix anchor piles and grouted rod anchors. Zubeck and Liu (2003) and Liu et al. (1999, 2007) conducted a full-scale laboratory test and ted their experience with helical piles in Alaska permafrost. Aldaeef and Rayhani (2022) studied the axial short-term pull-out capacity and creep behavior of helical piles in frozen ice-rich silt in the field. Nevertheless, the critical disadvantages of protruded piles are the difficulty in their installation (Johnston and Ladanyi 1974) and the freezeback time can last as long as three months (Biggar and Sego 1993a).

The shape of the pile is often modified to change the load transfer process. Tapered shaft tends to increase the axial compressive capacity and reduce creep settlement. Research on the performance of tapered piles in permafrost is lacking; it was claimed, however, that a slightly tapered pile may increase the axial capacity and reduce the settlement in permafrost, even if the adfreeze bond fails (Andersland and Ladanyi 2004). Due to the taper, an increase in the shaft resistance was observed because the soil adjacent to the pile was forced to expand radially; additional lateral pressures developed and led to increases in shear stresses across the pile-soil surface. Ladanyi and Guichaoua (1985) showed that creep settlement of a slightly tapered pile depends on the pile taper and its diameter, the interface friction and adhesion, and the soil resistance against being pushed aside by the pile axial movement. For a power law type of frozen soil behavior, the penetration resistance of such a pile continues to increase, even after the ice at the interface is broken.

Zhang and Hoeve (2015) recently introduced helix thermopiles to the Canadian Arctic (Figure 2.6). A helix thermopile is a type of pile that combines thin-bladed helixes on the surface with a convection pile, while a convection pile is an adfreeze steel pipe pile. They work together to extract heat from the permafrost to the air, helping to maintain low soil temperatures and preserve the adfreeze bond capacity of the soil. Convection forms naturally and extracts the heat from adjacent soils during the winter when the air temperature is colder than the ground temperature, and dormant during the summer. This has a cooling effect on the ground and improves pile performance. Maintaining low permafrost temperatures can also mitigate the effects of climate change on permafrost and ensure the stability of structures built on or near permafrost. The performance of helix thermopile foundation was evaluated by Zhang and Hoeve (2015). This passive transfer of heat increases soil strength and reduce the pile creep rate, making the helix thermopile an effective solution for foundation design in permafrost regions.

Figure 2.6 Helix thermopile foundations under the RCMP building in Inuvik, NWT.

2.3 Pile Adfreeze Strength

Adfreeze strength or bond between the soil and the surface of a pile, post, foundation, etc., which is a very important soil strength that must be considered when designing foundations. Adfreeze bonds determine a part of the load-carrying capacity of most foundations, especially piling. Creep occurs in the adfreeze bond at the contact surface between the pile and the surrounding soil. The adfreeze strength is primarily temperature-dependent, but is also varies with soils type, moisture content, and surface characteristics of the piling or foundation. Adfreeze bonds are also important when assessing frost jacking (Figure 2.7).

Weaver and Morgenstern (1981) recommended that the adfreeze bond strength is related to the long-term cohesion. The long-term adfreeze strength (τ_{lt}) can be estimated as:

$$\tau_{lt} = m \cdot c_{lt} \tag{2-15}$$

where m = the pile material roughness coefficient:

= 0.6 for steel and concrete

= 0.7 for uncreosoted wood

= 1.0 for corrugated or tapered steel pile (Weaver and Morgenstern 1981)

c_{lt} = the long-term cohesion, kPa, of the frozen soil at the design ground temperature (Figure 2.8).

Figure 2.7 Steel pile failure due to frost jacking in Yellowknife, NWT.

The results of constant displacement rate model pile tests conducted by Parmeswaran (1978) showed the highest adfreeze bond strength measured were for untreated wood, followed by concrete, and sandblasted steel. When pile surfaces were sandblasted, Sego and Smith (1989) observed an increase in the adfreeze bond strength of approximately 100% for model piles in sand, and Biggar and Sego (1989) observed an increase of more than 300% during field pile load tests.

Laboratory measurements of adfreeze strength of Ottawa fine sand to three different types of model piles under constant rates of loading are reported by Parameswaran (1978), the peak adfreeze strength measured by short-term tests under constant loading rates increases with increasing rate of displacement of the pile, according to a power law.

It is well documented that decrease of the temperature of a frozen soil increases the adfreeze strength of pile because of the reduction of unfrozen water and the increased cohesion of the ice (Sayles and Haines 1974; Parmeswaran 1980). At temperatures near the freezing point of the pore water, adfreeze bonds are weak and the soil is highly susceptible to time dependent deformation. A summary of the variation of adfreeze bond strength with changes in temperature in non-saline frozen soils is reported in Weaver and Morgenstern (1981), and in saline permafrost reported in Velli et al. (1973).

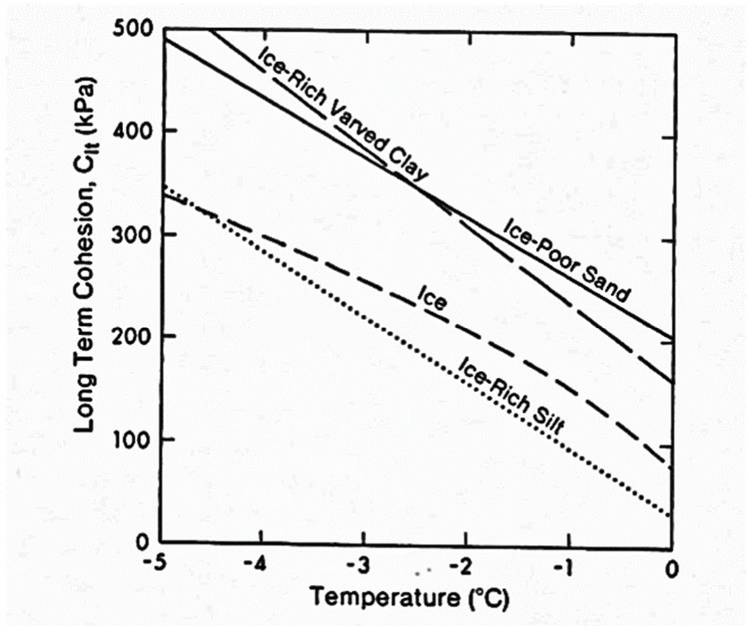

Figure 2.8 Long-term cohesion of frozen soils (after Weaver and Morgenstern 1981).

Nixon and McRoberts (1976) developed an expression for pile displacement velocity based upon work by Johnston and Ladanyi (1972). The formulation assumes that the constitutive behavior of the soil may be described by a simple power law, that the pile displaces at a constant rate (secondary creep), and that the deformation of the frozen ground around the pile shaft is idealized as shearing of concentric cylinders. Their relationship supports Vyalov's observation, indicating that doubling the pile diameter would reduce allowable shaft stress by approximately 30%. Frederking (1979) and Saeki et al. (1986) also report a reduction in adfreeze bond strength with increasing pile diameter in tests of piles frozen into an ice sheet.

Field loading tests of piles were conducted in saline permafrost and seasonally frozen rock to examine the effect of modifications to the pile surface and the backfill material and to compare their performance to piles installed using practice at that time (Biggar and Sego 1993 a and 1993b). In order to better define the effects of soil salinity, and pile surface and backfill modification on pile performance, a model pile testing program was conducted. The paper reviews the factors pertinent to pile design and testing in saline frozen soils and describes the results of constant displacement rate tests on model piles (Biggar and Sego 1993c, Figure 2.9). It was observed that salinity in the backfill material caused substantial reductions in adfreeze strength and rougher shaft surfaces significantly increased the adfreeze strength. A study was undertaken to examine pile performance in soil at salinities in which either adfreeze bond strength or time-dependent deformation governs the pile capacity. Thereby, guidance on which pile configuration provides optimum performance in the various native soil conditions was provided by Biggar (1991).

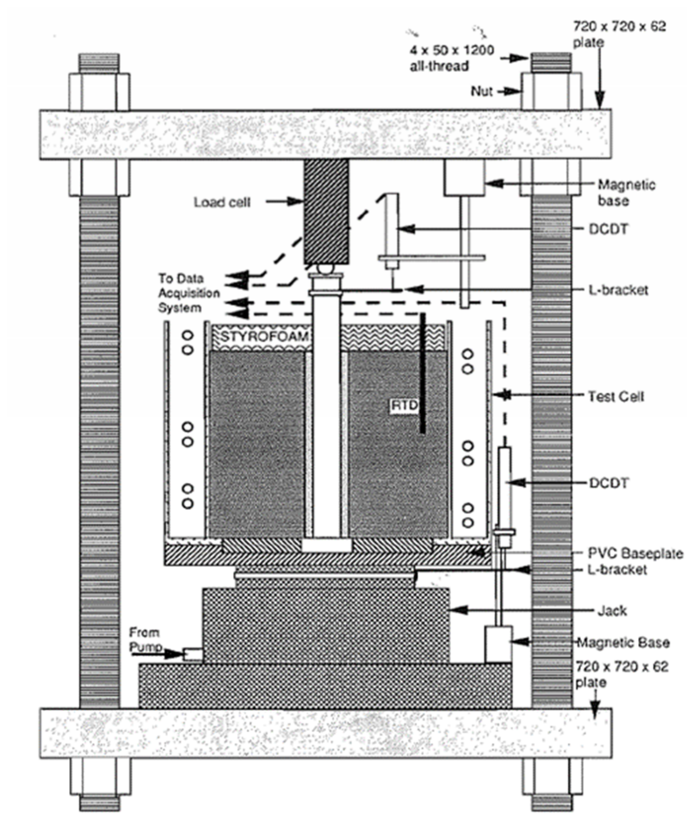

Figure 2.9 Model pile test loading equipment (after Biggar and Sego 1993c).

Biggar et al. (1996) conducted a long-term field load testing program on steel pipe piles installed with pre-bored holes backfilled with different materials, and to compare the results with the theory on model pile tests conducted at the University of Alberta (Biggar 1993c). Biggar and Kong (2001) gave more information about the time-dependent field performance of grout-backfilled piles or anchors in permafrost and compared the results with design guidelines based on allowable pile deformations and creep in ice-rich and saline permafrost.

Tang et al. (2019) investigated the effects of permafrost degradation on the axial behavior of concrete piles in warm permafrost. Quick axial compression tests were conducted on concrete piles installed in frozen soils in the cold room laboratory (Figure 2.10). Results showed that adfreeze bond strength was not reached near the pile tip. Piles in frozen soils could still gain the tip resistance at a displacement as much as 10% pile diameter and did not reach the plunging failure at such a displacement. They also compared the unit shaft resistance and adfreeze strength obtained from laboratory tests with the past studies (Table 2.2).

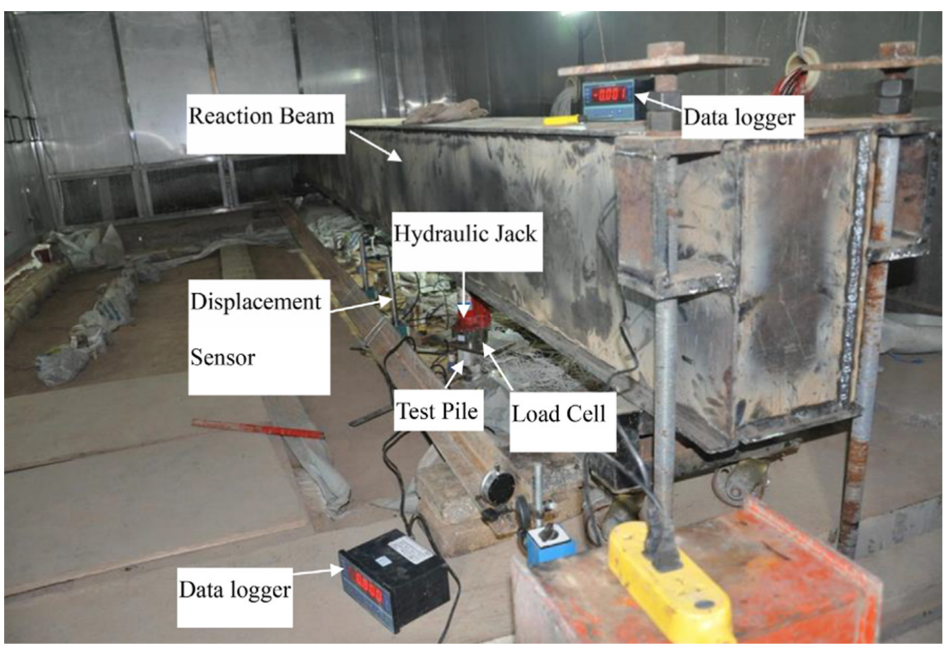

Figure 2.10 Laboratory loading setup from Tang et al. (2019).

Table 2.2 Summary of shaft resistance and adfreeze strength from Tang et al. (2019) and selected literature (after Tang et al. 2019)

Pile type	Soil type	w (%)	T (°C)	Maximum q_s (kPa)	τ_{ad} (kPa)	Reference
Concrete	Silt (ML)	30	−2.35	962 (P5-S1)	962	Present study
			−1.34	750 (P3-S1)	750	
			−1.10	564 (P4-S1)	564	
	Clay (CH)	10	−2.29	154 (P5-S2)	154	
			−1.52	347 (P3-S2)	347	
			−1.20	305 (P4-S2)	305	
			−2.11	10 (P5-S3)	N/A	
			−1.46	40 (P4-S3)	N/A	
			−1.28	20 (P3-S3)	N/A	
Smooth concrete	N/A	18	−5 to −10	960	960	Tsytovish and Sumgin (1959)
Smooth Timber				610	610	
Timber	Sand	18	−6	560–1800	560–1800	Parameswaran (1978)
Concrete				800	800	
Steel H-section				180–600	180–600	
N/A	Sand	N/A	−5	N/A	294	Weaver and Morgenstern (1981)
Steel	Saline	18	−5.5	244	244	Biggar and Sego (1993a, 1993b)
	Grout	16.7	−5.1	412	412	

Aldaeef and Rayhani (2019) investigated the load transfer behavior of conventional and helical piles in frozen soft clay utilizing in-situ pile load tests. Then, Aldaeef and Rayhani (2021a) introduced a new method to predict load transfer of conventional and helical piles in ice-rich frozen soils based on the freezing ground temperature and the temperature-dependent cohesion. It was showed that the predicted pile capacities matched well with the measured load capacities in the frozen ground. They investigated the shear strength between frozen sand and steel, and the ratio between the internal friction of the frozen sand and the interface friction of the steel-frozen sand element was assessed (Aldaeef and Rayhani 2021b).

2.4 Creep Settlements of Foundations in Frozen Soils

Residential houses or some commercial buildings are commonly supported on spread footings in the Canadian Arctic. It is well accepted that the creep settlement governs the design of shallow and deep foundations. Ladanyi and Johnston (1974) developed a method to predict the creep settlement and the bearing capacity of frozen soils under deep circular loads. The theory utilizes experimentally determined creep parameters of frozen soil and is specifically intended for designing deep circular footings and screw anchors embedded in permafrost soils. The theoretical solution was verified against the results from screw anchor field tests and satisfactory agreement was observed (Figure 2.11).

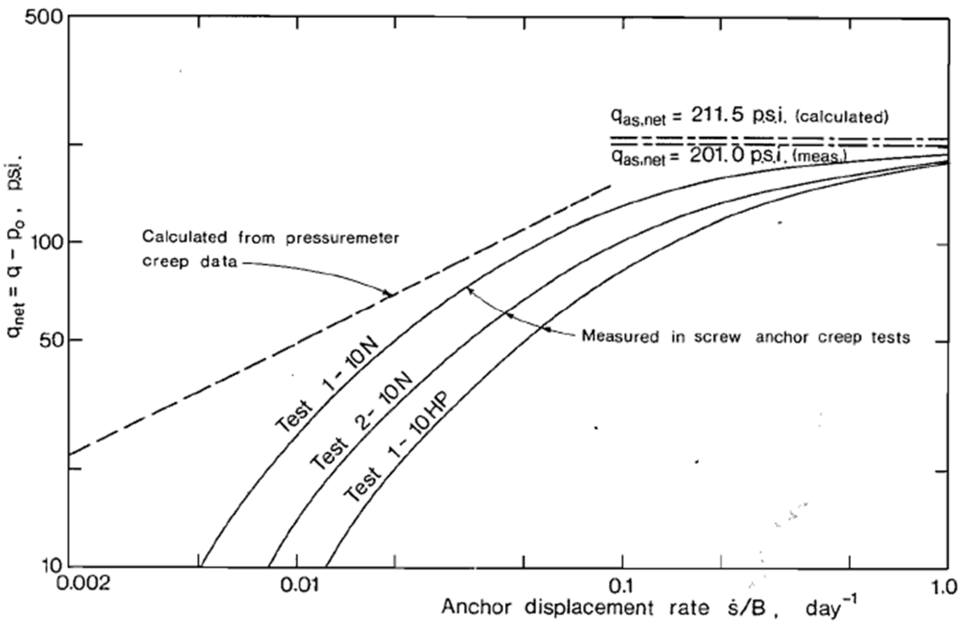

Figure 2.11 Comparison of calculated and measured creep rates and point resistance of screw anchors in permafrost (after Ladanyi and Johnston 1974).

Ladanyi (1975) predicted the creep settlement and time-dependent bearing capacity of strip footing in frozen soil using a simple mathematical model of an expanding cylindrical cavity. Nixon (1978) proposed a settlement analysis for spread footings on permafrost:

$$\dot{s} = I \cdot a \cdot B \cdot q^n \tag{2-16}$$

where $\dot{s}$ is the pile settlement rate, I is an influencing factor which depends only on n, a is the half-width of the footing, and B and n are experimental secondary creep parameters. It was suggested that allowable footing loads will be controlled by limiting long-term settlements rather than considering the soil strength alone.

To design pile foundation in the permafrost, it is also necessary to have a constitutive creep, or time-dependent strain rate relationship. Nixon (1978) suggested that limitation of long-term pile settlements will control the design loadings. Morgenstern et al. (1980) gave a comprehensive review of literature related to the behaviour of friction piles in ice and ice-rich soil. In order to rationalize existing adfreeze strength design procedures and extend settlement based designs previously developed for ice-rich soils to both friction and end-bearing piles in ice-poor frozen soils, a compilation of data on allowable adfreeze strength data, frozen soil creep data, and pile design procedures has been undertaken to facilitate selecting allowable loads on piles in a broad range of permafrost soils (Weaver and Morgenstern 1981).

The creep settlement of pile in frozen soil is a function of the time, pile diameter, and soil type and temperature. Weaver and Morgenstern (1981) developed a series of equations for predicting allowable shear stress and pile capacity versus creep settlement. The salinity of the soil also greatly affects the creep rates (Nixon 1988, Miller and Johnson 1990). Figure 2.12 illustrates the predicted creep settlement rate versus applied load and soil salinity.

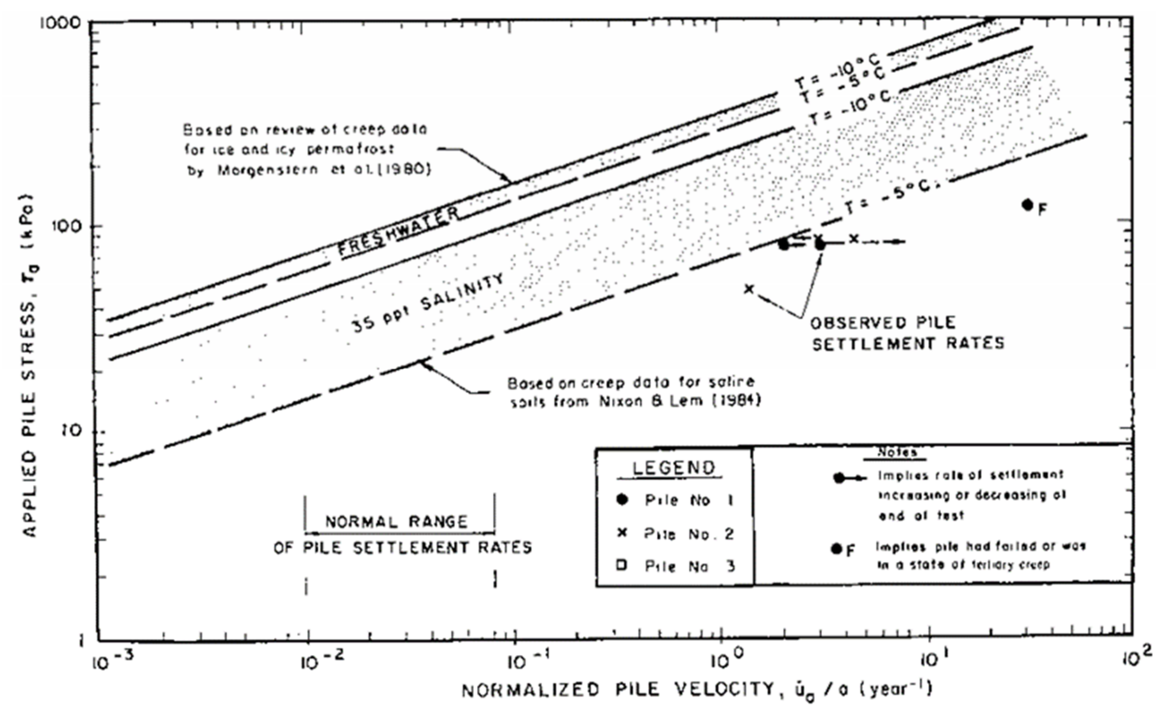

Figure 2.12 Prediction for creep settlement for freshwater and saline soils (after Nixon 1988).

For a frozen soil subjected to simple shear under plane strain conditions, Johnston and Ladanyi (1972) show that the flow law for a general state of stress reduces to

$$\dot{\gamma} = 3^{(n+1)/2} B \tau^{n} \tag{2-17}$$

For a flow law having two terms may be written as

$$\dot{\gamma} = 3^{(n_1+1)/2} B_1 \tau^{n_1} + 3^{(n_2+1)/2} B_2 \tau^{n_2} \tag{2-18}$$

Considering the problem of a pile in the frozen ground at a constant temperature, it is assumed that the pile material is considerably more rigid in the long-term than the surrounding frozen soil and that the shear stress is distributed uniformly along the pile shaft (Figure 2.13). The shear stress τ_a is therefore given by

$$\tau_a = P/2\pi a L \tag{2-19}$$

where *P* is load on the pile, *a* is the pile radius, and *L* is the embedded length in permafrost.

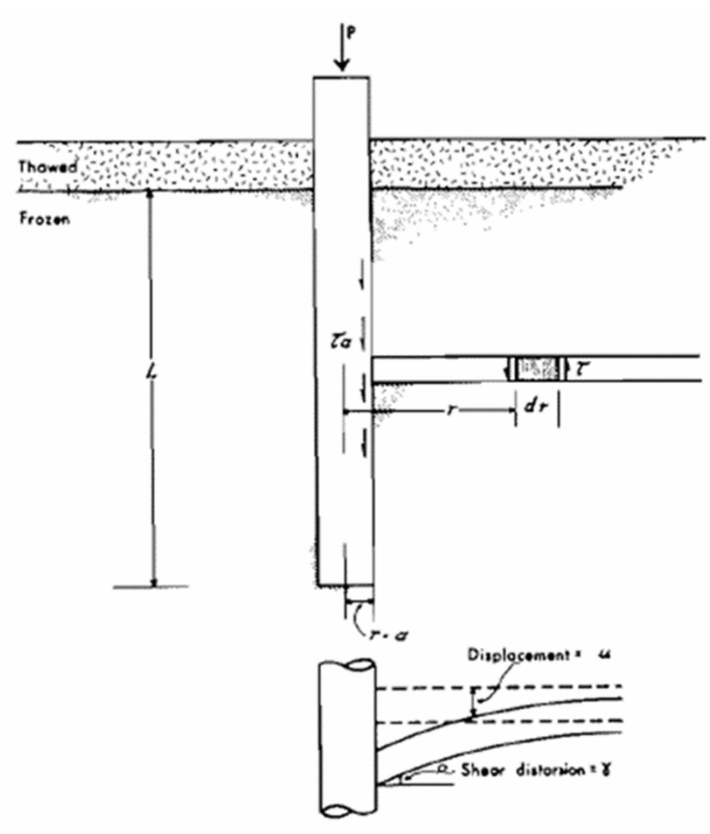

Figure 2.13 Shear stresses and strains in frozen soil (after Nixon and McRoberts 1976).

The end-bearing stresses are assumed to be zero (Sanger 1969). Following the analysis of Nadai (1963) and Johnston and Ladanyi (1972), it can be shown that for a weightless soil the applied shear stress, τ_a, at $r = a$ is related to the shear stress, τ, at any other radius by

$$\tau = \tau_a(a/r) \tag{2-20}$$

Substituting this equation for the shear stress in the flow law expressed by (2-20), we obtain

$$\dot{\gamma} = 3^{(n_1+1)/2}B_1(\frac{\tau_a a}{r})^{n_1} + 3^{(n_2+1)/2}B_2(\frac{\tau_a a}{r})^{n_2} \tag{2-21}$$

As shown in Figure 2.13, the shear distortion is related to the displacement by

$$\gamma = -\frac{du}{dr} \tag{2-22}$$

where u is the displacement at any radius and similarly the shear strain rate, $\dot{\gamma}$, is related to the displacement rate, $\dot{u}$, by

$$\dot{\gamma} = -\frac{d\dot{u}}{dr} \tag{2-23}$$

Combination of (2-21) and (2-23) yields

$$\frac{d\dot{u}}{dr} = -3^{(n_1+1)/2}B_1(\frac{\tau_a a}{r})^{n_1} - 3^{(n_2+1)/2}B_2(\frac{\tau_a a}{r})^{n_2} \tag{2-24}$$

This equation may be integrated to obtain the displacement rate. At the pile radius, a, the soil displacement rate equals the pile displacement rate, $\dot{u}_a$, and

$$\text{at } r = a, \dot{u} = \dot{u}_a \tag{2-25}$$

Introducing this boundary condition, we obtain

$$\dot{u} = -3^{\frac{n_1+1}{2}}B_1(\tau_a a)^{n_1}(\frac{r^{1-n_1}}{1-n_1}) + \frac{3^{\frac{n_1+1}{2}}B_1\tau_a^{n_1}a}{1-n_1} - 3^{\frac{n_2+1}{2}}B_2(\tau_a a)^{n_2}(\frac{r^{1-n_2}}{1-n_2}) + \frac{3^{(n_2+1)/2}B_2\tau_a^{n_2}a}{1-n_2} + \dot{u}_a \tag{2-26}$$

We apply the other boundary condition that at an infinite radius the displacement rate is zero, that is

$$\text{at } r = \infty, \dot{u} = 0 \tag{2-27}$$

Equations (2-26) and (2-27) provide the following equation for the displacement rate of the pile

$$\dot{u} = \frac{3^{(n_1+1)/2} B_1 \tau_a^{n_1} a}{n_1 - 1} + \frac{3^{(n_2+1)/2} B_2 \tau_a^{n_2} a}{n_2 - 1} \quad (2\text{-}28)$$

Equation (2-28) relates the steady pile displacement rate u_a to the applied shaft shear stress τ_a, in terms of the pile radius a, and the constant B and n determined from uniaxial creep data for the frozen soil in question.

As for the lateral behavior, conventional pile foundations subject to lateral loading were investigated using field tests (Rowley et al. 1973, 1975). Foriero and Ladanyi (1991a, b) developed a general approach to the problem of a laterally loaded pile in a creeping soil using elastoviscoplastic theory. The practical advantage of that approach was that it provided solutions to those classic elastoplastic problems, for which the steady-state solution of the viscoplastic problem reduces to the conventional elastoplastic solution.

Nixon and Lem (1984) conducted 34 creep tests and 11 time-dependent strength laboratory tests in the saline soils. Then, they combined the creep analysis for vertical and laterally loaded piles in permafrost with data on the creep of saline fine-grained soils to present the preliminary design charts for piles in saline permafrost (Neukirchner and Nixon 1987). In 1988, a limited program of pile load testing was carried out to confirm or modify the initial pile loadings based on previously published material (Nixon 1988).

2.5 Numerical Modeling of Pile Foundations in Frozen Soils

Nixon and McRoberts (1976) used the finite difference procedure to simulate the behavior of a compressible pile embedded in an ice-rich soil or ice. A reasonably good agreement is observed between both the displacements and the shear stresses along the shaft. A finite element computer program RDPIL.FOR for laterally loaded pile in a viscoelastic layered soil was developed by Foriero and Ladanyi (1990). The program used a Maxwell model to accommodate the initial elastic subgrade modulus, which is independent of time. Foriero and Ladanyi (1995) utilised a viscoplasticity theory to provide a general approach to the problem of creep in frozen soils. Then a finite element computer program was developed to verify the validity of the proposed model, which focused on a layer of the soil-pile system under both plane strain and plane stress conditions (finite element meshes are shown in Figure 2.14). It concluded that finite element computations yielded lower results than the analytical solution as shown in Figure 2.15. The finite element method provided the capability for evaluating soil-pile interaction under lateral loading.

In order to increase the use of helical piers as a cost effective foundation alternative, Zubeck and Liu (2003) presented the experience with helical piers in Alaska and gave a design example using the developed finite element analysis and creep results. The analysis incorporated four models: the Large Model, Small Model, Installation Failure Model, and Creep Model. The creep equation of Equation (2-7) was adopted in the finite element analysis. Liu et al. (2007) used the computer program ANSYS to present a study of the behaviour of helical pier foundations in frozen ground, the Drucker-Prager yield criteria was used to describe the yield surface for the soil elements (Figure 2.16). The numerical analysis yielded valuable insights into the creep behavior of helical piers in frozen ground, specifically regarding the magnitude of settlement that can be anticipated over extended periods.

Foriero et al. (2005) utilized MATLAB as the FEM computer program to investigate the laterally loaded pile in permafrost by considering the temperature variation as function of depth. The creep parameters used in the simulations were obtained from quasi-static cone penetration tests. The simulated results showed a good agreement with the measured values of the bending moments and demonstrated a clear distinction between stationary and non-stationary creep (Figure 2.17).

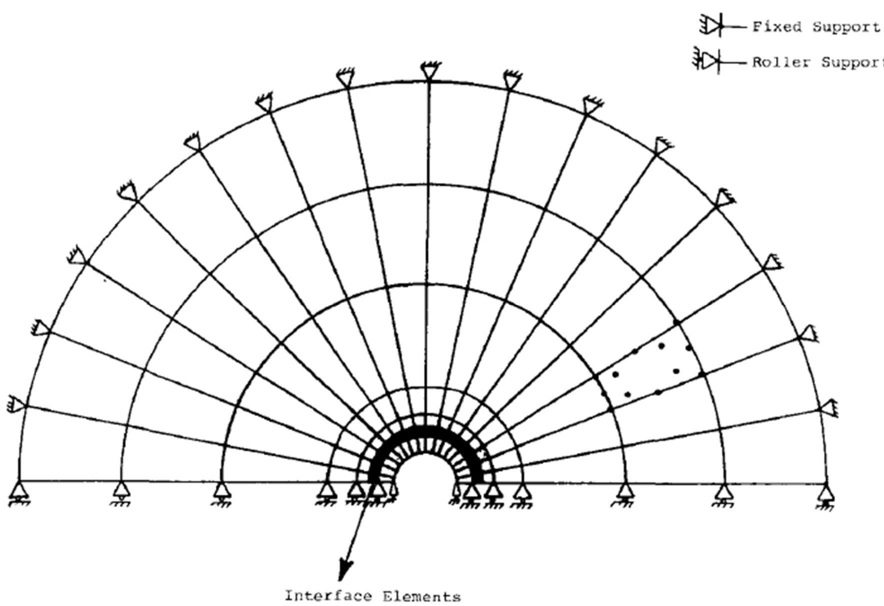

Figure 2.14 Finite element meshes in Foriero and Ladanyi (1995).

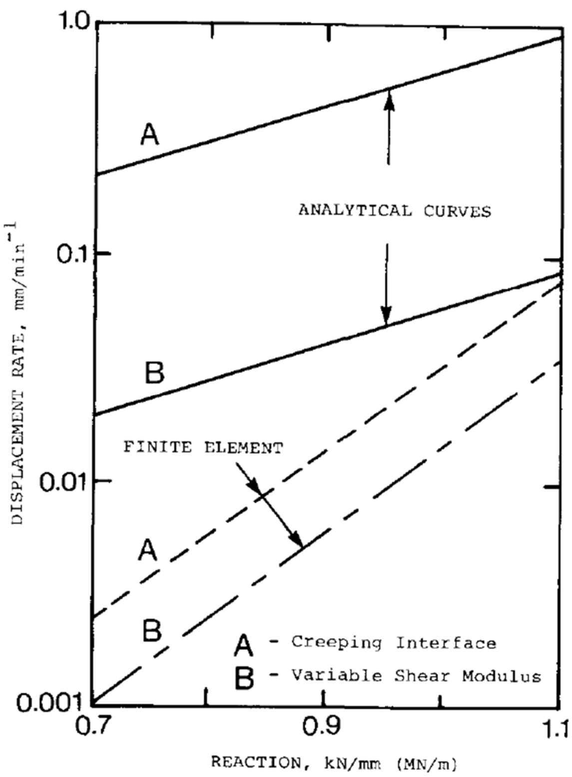

Figure 2.15 Comparison results between finite element and analyical solution (Foriero and Ladanyi 1995).

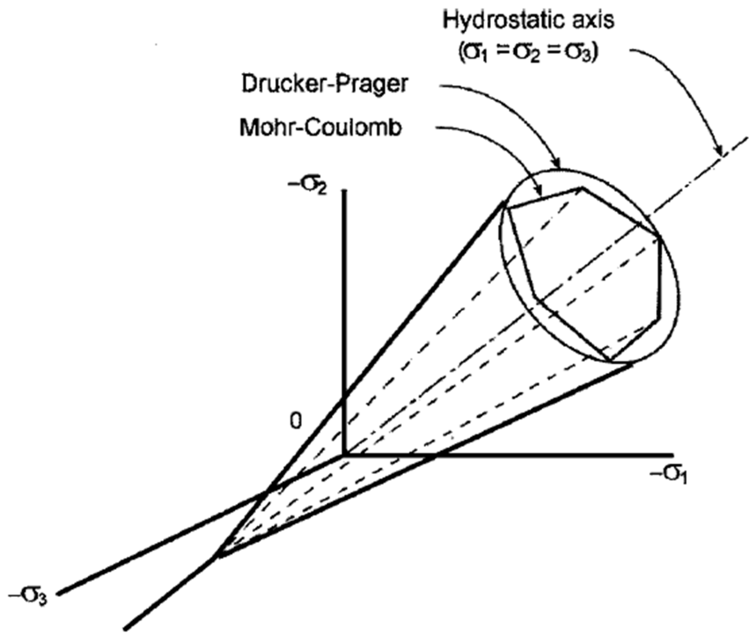

Figure 2.16 Drucker-Prager circular cone yield surface (Liu et al. 2007).

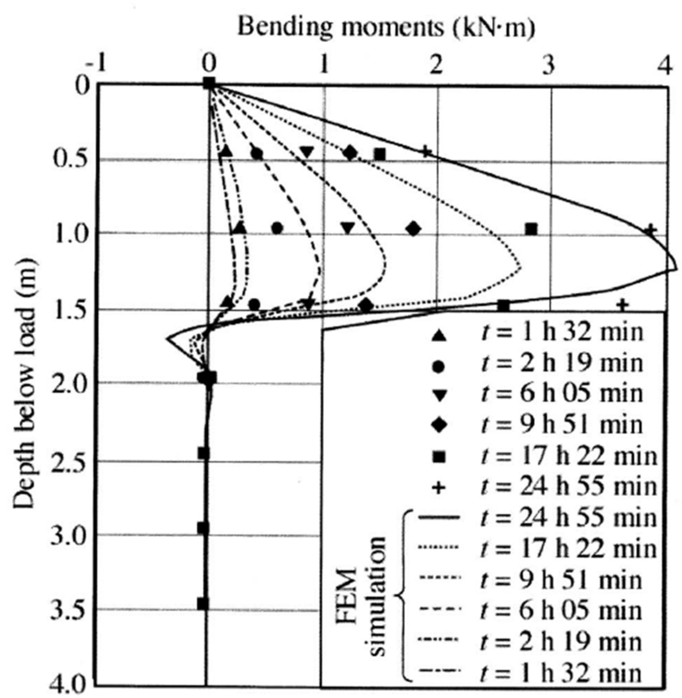

Figure 2.17 Comparison of bending moments between finite element simulation and field measurements (Foriero et al. 2005).

Crowther (2013) utilized a commercially available computer program LPile that uses *p-y* curves to model lateral pile loading and soil interaction. The strength and strain criteria account for frozen soil particle size, temperature, and load duration in the construction of *p-y* curves were discussed. It showed that the deflections calculated using LPile and the strength criteria were in the range of those measured during the lateral pile load tests performed in Inuvik.

2.6 Design Method of Pile Foundations in Frozen Soils

The design of pile foundations in frozen soils in most cases is based on limiting long-term creep settlements. Creep settlements are a function of the pile-soil adfreeze stress and temperature. In addition to compressive loads, design of all piling in non-permafrost and permafrost areas must also consider the detrimental seasonal frost effects associated with heave and jacking. The correct design of a pile foundation depends on predicting accurately the depth of the active layer and long-term ground temperatures, after construction has been completed.

The entire design procedure is summarized in Figure 2.18. Weaver and Morgenstern's (1981) method distinguish between ice-rich and ice-poor frozen soils, and they suggested that portions of frozen ground with temperatures above -1 °C can be neglected. Heydinger (1987) provided an overview of the 1980's art on piles in permafrost and identified research needs. Pile types, installation methods, design techniques and testing procedures are discussed.

Nottingham and Christopherson (1983) presented a design concept for driven piles in permafrost. They defined maximum adfreeze limits using short term loading criteria, followed by long term loading to establish long term adfreeze limits based on creep deflection.

Design methods of laterally loaded piles were proposed and discussed in Nixon (1984) and Neukirchner and Nixon (1987). A design approach is presented by (Crowther 1990) to analyze laterally loaded piles embedded in layered frozen soil. The design approach makes use of a commercially available computer solution that uses *p-y* curves to model soil and pile interaction. Shear strength and strain criteria for both ice-rich and ice-poor soil are presented for use in constructing *p-y* curves.

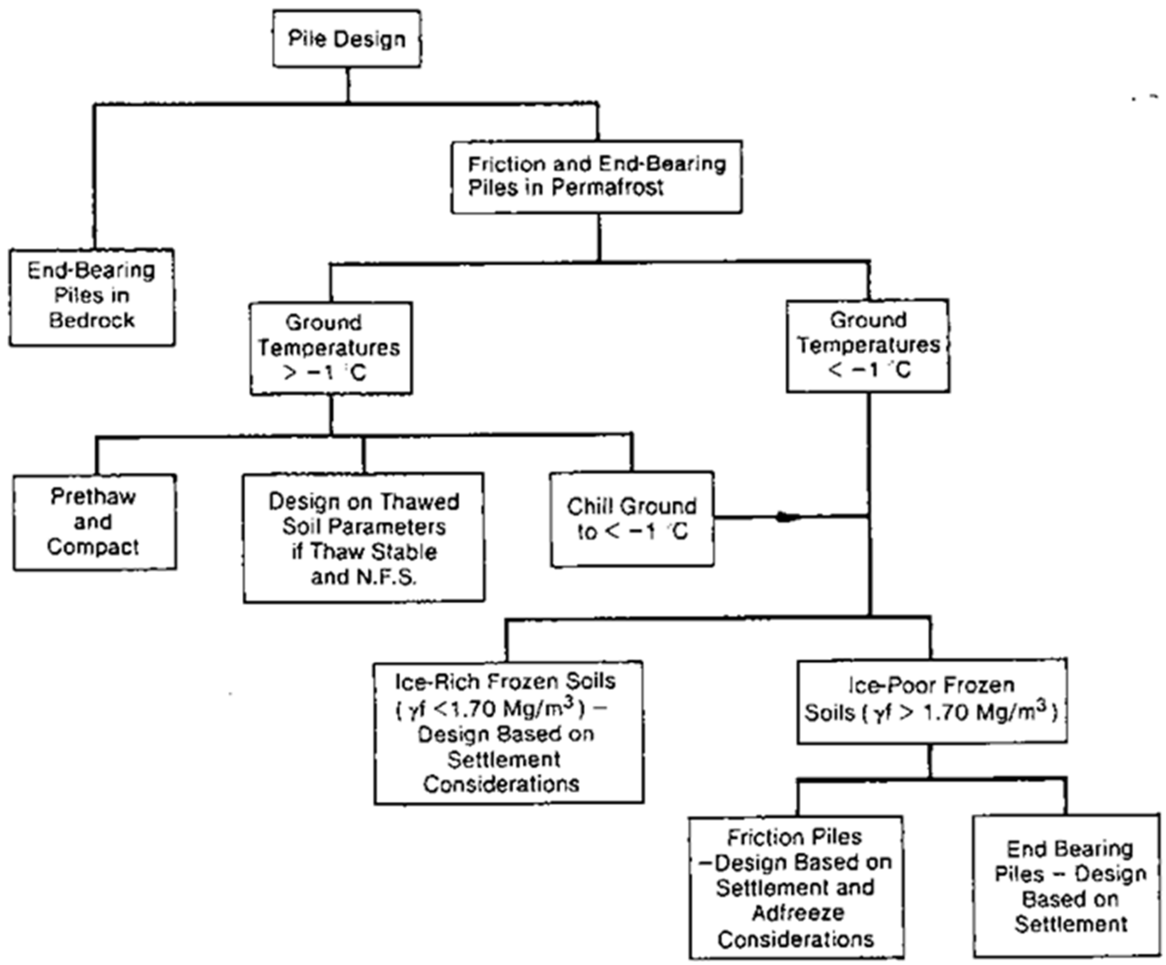

Figure 2.18 Proposed pile design procedure (Weaver and Morgenstern 1981).

Zhang and Hoeve (2015) proposed a geotechnical design of thermopile foundation for a building in Inuvik, NWT. Geotechnical evaluations were undertaken to estimate the necessary pile embedment depths, considering specified pile long-term creep settlement criteria and design criteria to mitigate potential frost jacking.

Hoeve and Trimble (2018) provided an overview of the current state of the practice of adfreeze piles. This practice is based on a theoretical basis that was developed between the 1970s and 1990s, with practical construction considerations considered. It was suggested that piles should be designed using service loads rather than factored loads to avoid unnecessary conservatism. An approach to maintaining appropriate conservatism under serviceability limit state was proposed. The flow law model of Equation (2-14) and (2-28) were used to determine the pile secondary creep rate. The design input included ground temperature, pile diameter, active layer thickness at the end of design life, and frost heave considerations. Compression loading and frost-jacking resistance were also considered. The study also provided an example of an adfreeze pile design in Old Crow, Yukon using the current design method, which recommended a minimum length of 5 meters to resist front heave (Figure 2.19).

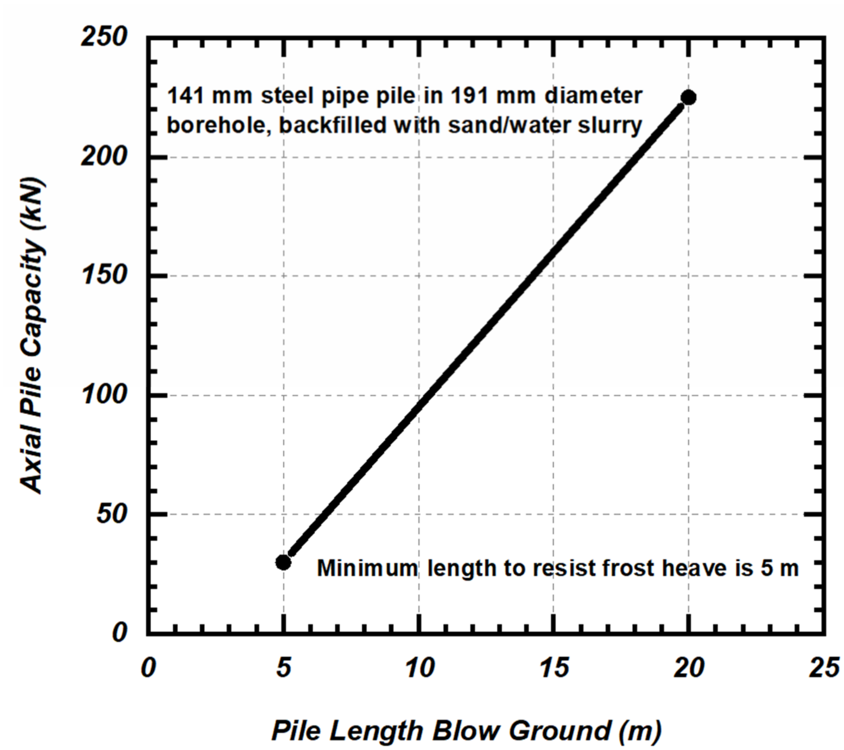

Figure 2.19 Slotted pile capacity versus length for building piles of New Community Centre, Old Crow, YT (after Hoeve and Trimble 2018).

2.7 Summary

- Foundation design in permafrost is heavily rely on the mechanical properties of frozen soils, which are complex due to their interdependence on various factors, including soil type, unfrozen water and ice content, saturation, soil temperature, salinity, stress, and loading rate.
- Straight-shaft smooth timber or pipe pile are commonly used in Canadian Arctic communities since 1950s. New improved pile foundations has been introduced to the industry practice recently and performance of these pile has been investigated.
- Section 2.3 and 2.4 provide a detailed explanation of the factors that may impact the adfreeze strength and creep settlement of a pile foundation.
- Section 2.5 summarizes the research of numerical modeling of pile foundations in frozen soils and a thorough review of pile design in permafrost is list section 2.6.

From the literature review, it can be concluded that most of the research projects are focused on the conventional predrilled piles that are backfilled with grout or gravel in the frozen ground. However, the cost of conventional piles is very high; the construction is labor-intensive and freeze-back is time-consuming. Since the construction season in the Canadian Arctic is short, typically from May to October, it is critical to shorten the duration of pile foundation construction; predrilled piles may provide lower adfreeze bond strength between backfill and frozen soil than other methods. Effects of climate change, which warms the permafrost and deepens the active layer, may require alternative pile types and installation methods; piles currently used are more suitable for commercial projects than residential housing projects in permafrost; notably, there was a scarcity of research on the axial load distribution during load testing; while there are several studies on the installation torque of screw piles in unfrozen soil, there is no published research on the torque of continuous-flight piles required to install the pile in frozen soils. Thus, communities of northern Canada need affordable piles for residential houses and commercial applications.

Continuous-flight piles have demonstrated the advantages such as lightweight, large capacities, reusability, and rapid installation, in the non-frozen soils of Canada. Continuous-flight piles develop their axial capacity primarily through the continuous-flights on the shaft. Although research on continuous-flight pile applications in permafrost has not been conducted, past studies of smooth and protruded piles in permafrost may imply that continuous-flight piles, as a result of the shaft screws and tapered shape, will provide much larger capacities and smaller creep displacement than conventional pile foundations in permafrost. The installation process may further increase the confining stress on adjacent soils and therefore increase the capacities. The new pile type may be potentially used in the permafrost of Canada and render advantageous against conventional steel pipe piles. In summary, research on the axial performance of continuous-flight pile in frozen ground is needed prior to the application of this pile type.

3 Short-Term Axial Loading of Continuous-Flight Pile Segment in Frozen Soil[1]

3.1 Introduction

Pile foundations are commonly used in the Canadian Arctic. The short-term capacities and long-term creep behavior of piles have to be considered in their design. Field testing of full-scale piles were common for investigating their axial performance in permafrost. For example, Nixon (1988) examined the pile settlement and creep rates of piles in saline permafrost under constant load. A field load test program of piles with different shaft treatments and backfills in saline permafrost was conducted by Biggar and Sego (1993a) and results of short-term uplift capacities of piles were presented (Biggar and Sego 1993b). Aldaeef and Rayhani (2022) studied the axial short-term pull-out capacity and creep behavior of helical piles in frozen ice-rich silt in the field.

Because of the high cost of conducting field tests and the challenges of controlling soil parameters, such as temperature, laboratory tests of model piles are also adopted. For example, Biggar and Sego (1993c) examined the effects of soil salinity, shaft surface, and backfill modification on the axial performance of model piles. Tang et al. (2021) measured the frost heave and thaw settlement of frozen soils around concrete piles in the lab. Tang et al. (2019) investigated the short-term behavior of model reinforced-concrete piles subjected to degradation of warming permafrost, where quick axial compression tests were conducted in the cold room to primarily characterize the capacity of model piles in frozen soils with varying active layer thicknesses and temperature distributions. A primary objective of these field and laboratory studies was to determine the adfreeze strength (τ_{ad}) of piles under short-term axial loads. Adfreeze strength τ_{ad} is the shear strength between the pile shaft and the adjacent frozen soil at failure. The value of τ_{ad} generally increases with decreasing soil temperature and varies with type of shaft surface. The

[1] A version of this chapter has been accepted by the Canadian Geotechnical Journal

increased strength is attributed to the temperature's direct influence on the strength of intergranular ice and the reduced amount of unfrozen water within the colder soil.

Hivon and Sego (1993) reported saline frozen soils are widely distributed in the Canadian Arctic and salinity is shown to decrease the freezing point of pure water. Mechanical properties of saline frozen soil were comprehensively investigated in the laboratory (Nixon and Lem 1984, Hivon and Sego 1995). The short-term ultimate strength of soil was shown to decrease with an increase in salinity. Salinity accelerated the creep rate of frozen soil under constant load and reduced its shear strength owing to the greater unfrozen water content in the pores. When the soil temperature approaches the initial freezing point of pure water, the existence of ice crystals and unfrozen water within the pores of the soil can trigger a significant decrease of the short-term ultimate adfreeze strength and an increase of the pile’s long-term settlement rate (Biggar and Sego 1993c, Nixon 1988). Neukirchner and Nixon (1987) summarized the creep analysis for vertical and laterally loaded piles in saline and non-saline soils and presented the preliminary design charts for piles in saline permafrost.

The majority of the abovementioned literature on pile foundations was aimed at the performance of predrilled steel piles that were backfilled, which are the most common type used in the Canadian Arctic. Pipe piles with a prismatic shaft are placed in an oversized predrilled hole and then the annulus is backfilled with gravel or a cement-based slurry designed to cure (i.e. freeze-back) at cold temperatures (Biggar and Sego 1993a). However, this construction approach is labor-intensive and time-consuming. Since the construction season in the Canadian Arctic is short, typically from May to October, it is critical to shorten the duration of pile foundation construction. In addition, the failure surface of predrilled piles takes place along the cylindrical interface between the backfill and native permafrost, but the adfreeze bond at this interface may be low

(Biggar and Sego 1993c). Effects of climate change, which warms the permafrost and deepens the active layer, may require alternative pile types and installation methods.

The continuous-flight pile (also termed as screw micropiles in Guo and Deng 2018) has been recently introduced to the Canadian foundation construction industry. It consists of a steel tube with continuous spiral threads welded on the lower half of the pile shaft and a closed-end tapered pile tip, with a galvanized coating for corrosion resistance. The pile can be screwed into soils by applying torque and axial force on the pile head. Owing to the differences in pile installation method and soil-pile interface, continuous-flight piles possess many advantages over conventional smooth-shaft piles in unfrozen soils. The axial performance of continuous-flight piles in unfrozen soils was investigated by Guo and Deng (2018), Guo et al. (2019), and Khidri and Deng (2022). Installing a pile into frozen soils by torque is rare in the current practice of the Canadian Arctic. The continuous-flight pile may be a feasible foundation solution, because the torsion installation method will reduce the duration of foundation construction. The axial loads may be applied within hours rather than weeks. Moreover, warming permafrost owing to climate change might further ease the torsional installation. The engineering behavior of continuous-flight piles in frozen soils needs to be investigated since continuous-flight pile has not been tested in permafrost.

This study is aimed at understanding the side shear performance of continuous-flight pile segments embedded in a laboratory frozen soil under the short-term compressive loads. The results collected from short-term tests will then be used to obtain the axial loads for long-term creep tests. A primary objective of the present research is to examine the effects of soil temperature (T), gravimetric water content (w) and salinity (S) on the adfreeze strength τ_{ad} and the failure modes of the model piles. A series of axial load tests of pile segments with a shaft diameter of 89 mm and length of 300 mm were carried out under a constant displacement rate. The load versus displacement curves and axial force strain gauge (SG) readings along the pile length were measured to evaluate the load-transfer mechanism of the piles in frozen soils. Two failure modes were identified from the post-test visual inspection and data interpretation.

3.2 Laboratory Experimental Program

3.2.1 Test soil and piles

The continuous-flight piles studied in this research are intended to support the Arctic infrastructure. Hence, the laboratory testing selected silty sand, common for communities in the Mackenzie River delta area such as Tuktoyaktuk and Inuvik, NWT, Canada. The field investigation report (Thurber Consultants 1987) showed that the subsurface soils in these communities fell into the silty sand type and have a typical band of grain size distribution as shown in Figure 3.1. Hivon and Sego (1995), and Biggar and Sego (1993c) tested soils that had a similar grain size distribution. The present study adopted a mixture of silt and silica intended to be similar to the soil used by Hivon and Sego (1995).

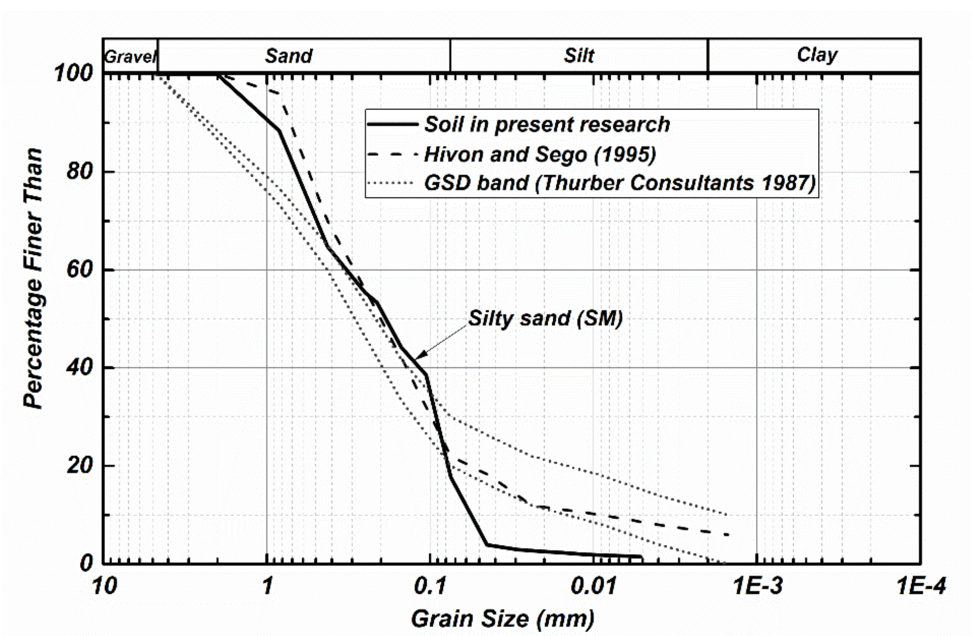

Figure 3.1 Grain size distribution (GSD) of test soil.

A full-size continuous-flight pile is shown in Figure 3.2a. In unfrozen soils, piles are installed by torquing the pile head and screwing the pile directly into the soil. The pile can vary in length and diameter to provide the desired performance. The original pile with a length of 1.5 m and a diameter of 89 mm was selected for the present research. The threads on the pile segments have a width (w_{th}) of 12 mm and a thickness of 2 mm. The spacing (S_{th}) between each thread is 50 ± 2 mm. The pile is made of structural steel with a Young's modulus of 210 GPa and a yield strength of 248 MPa (Guo and Deng 2018). The pile was cut into three segments to address the limitation of lab testing equipment (Figure 3.2b). A straight threaded and a straight smooth segment (Figure 3.2b) were used in this study to compare the axial performance of continuous-flight piles to the conventional piles.

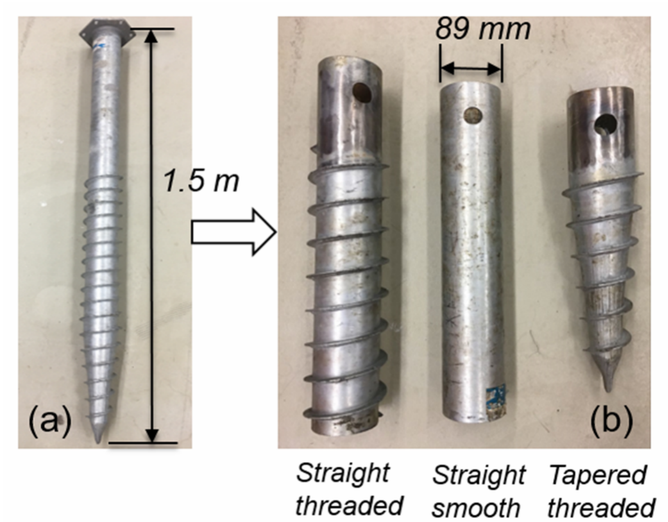

Figure 3.2 (a) A prototype screw pile; and (b) pile segments. Note: Results of cylindrical segments are presented herein.

3.2.2 Test Equipment Setup

This research characterized the axial behavior of continuous-flight piles subjected to rapid loading in frozen soils, using the facilities at the University of Alberta, Cold Regions Geotechnical Research Center. The model pile testing equipment was placed in the cold room capable of testing down to -40 °C. The testing system consists of test pile segments, test cell, temperature control system, servo-control hydraulic loading equipment, and data acquisition. The servo-control hydraulic loading equipment can provide constant loads or constant displacement rates via the load frame shown in Figure 3.3.

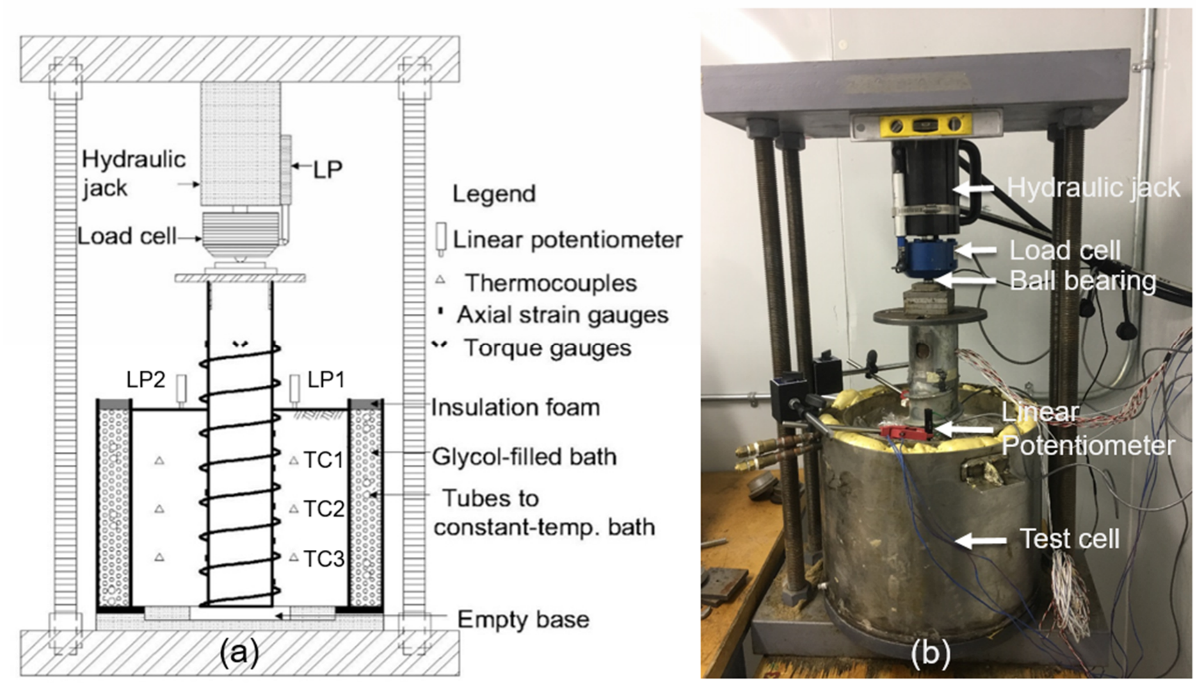

Figure 3.3 (a) Schematic of testing apparatus; and (b) testing apparatus that was placed inside a constant-temperature cold room during axial loading tests.

The frozen soil cell was composed of two concentric cells. The soil sample was placed in the inner cell and ethylene glycol was placed in the outer cell. To maintain the soil mass at a constant temperature, ethylene glycol from a constant temperature bath was circulated through copper coils located in the outer cell. At the bottom of the test cell, an aluminum base plate was inserted during the consolidation stage. During load testing, a PVC base plate with a center hole replaced the aluminum base plate. The hole in the base plate was slightly larger than the pile diameter to eliminate end bearing. A hydraulic jack was connected to the servo-control system providing a constant hydraulic oil pressure. A ball bearing was placed between the load cell and pile cap to eliminate loading eccentricity and application of a bending moment to the pile top.

3.2.3 Instrumentation

Strain gauges (SG) were installed to measure internal strains; thus, the load transfer mechanism and installation torque could be examined. Eight SGs were mounted and uniformly distributed along the pile shaft surface at different depths (Figure 3.3a). At each SG location, one axial and one hoop SGs were attached to the surface and connected to the data acquisition system to form a half Wheatstone bridge circuit. To measure the torque during pile installation, four torsional SGs were installed on the shaft near the pile head, forming a full Wheatstone bridge that compensates for the ambient temperature changes and eliminates the error due to other load types (such as axial loading during the installation stage). Three layers of protective coatings, including epoxy, modeling clay, and aluminum foil tape, were applied to prevent the SGs and wires from being damaged. The SG installation technique in the present study was shown to be effective at protecting the gauges and measuring the desired quantities. A majority of the SGs survived the installation and loading stages. SGs were calibrated against axial load or torque before the beginning of every test.

Six thermocouples (TC1 to TC6) were embedded in the soil at different depths and radial distances from the pile shaft to measure the soil temperature distribution during the entire test progress (Figure 3.3a). The top-layer thermocouples were embedded 7.5 cm below the ground surface, the mid-layer thermocouples were in the middle of the soil and bottom-layer thermocouples were 7.5 cm above the bottom of the test cell. A Linear Potentiometer (LP) was attached to the hydraulic cylinder to measure the axil pile displacements. To understand the effect of pile settlement on the adjacent soil, the ground surface settlements near the pile shaft were recorded using LP1 and LP2 (Figure 3.3b). A load cell was connected to the hydraulic jack to measure pile head load. The thermocouples, load cell and LPs were calibrated before use and the error of temperature was less than 0.2 °C.

3.2.4 Model Construction and Test Procedure

Dry soil was placed in a soil mixer with the appropriate amount of distilled water and NaCl as required. Mixed soil was placed in buckets with lids and stored in a moisture control room until ready for use. A PVC cylinder was left in the middle of the soil cell, and the moist soil of the same weight was placed in four layers loosely and homogenously. After each layer of soil placement, two thermocouples were placed into the soil at designated radial distances from the center of the cell. The test cell filled with soil was left in the temperature control room with an ambient room temperature of 2 °C for at least 24 h to allow for even distribution of moisture content and temperature inside the soil, self-weight consolidation and stabilization of the soil. Then a consolidation load plate was placed on top of the soil and a consolidation pressure was applied. The consolidation pressure of 80 kPa was used to simulate the consolidated soil buried in a depth of around 4 m. Consolidation pressure and settlement were recorded until 95% consolidation was achieved.

It can be concluded from the time history of applied normal stress and vertical strain that the consolidation was finished within 1 h for the soil with an initial gravimetric water content (w_0) of 20% while it took 60 h for the sample with a w_0 of 35% to complete the 95% consolidation. It was shown that the water content remained the same for the soil sample with w_0 of 20% after consolidation, whereas the water content decreased from 35% to approximately 26% for the soil sample with w_0 of 35%. Table 1 summarizes the w_0 of the mixed soil before consolidation preparation, the range and average w after consolidation preparation, and the bulk density measured from the excavated frozen soil samples at the end of load tests. The results showed that the densities at different locations were consistent. The bulk densities ranged from 1.47 to 1.64 g/cm^3, changing with the initial water content (Table 1).

Table 3.1 Test matrix

Test ID	**Pile shaft feature**	**Load type**	**Salinity S (ppt)**	**Initial water content w_0 (%)**	**Average and range of water content w (%)**	**Average unfrozen water content w_u (%)**	**Average bulk density (g/cm^3)**	**Average soil temperature T (°C)**
SCD1	Straight smooth (S)	Constant displ. rate (CD)	0	20	**20.2**	11.5	N/A	-0.7
SCD2			0	20	**19.9**	7.3		-4.5
SCD3			10	20	**20.0**	N/A		-0.8
SCD4			10	20	**19.7**	N/A		-4.6
TCD1	Straight threaded (T)		0	35	**25.5** (20.6-27.5)	10.5	1.47	-1.0
TCD2			0	20	**20.2** (18.5-24.1)	20.2	1.57	0
TCD3			0	35	**26.9** (25.2-29.1)	7.3	N/A	-4.5
TCD4			0	20	**19.5** (16.9-22.2)	7.2	1.57	-4.8
TCD5			10	35	**22.1** (20.1-27.6)	N/A	1.63	-1.6
TCD6			10	20	**19.8** (18.8-21.0)		1.64	-0.8
TCD7			10	35	**24.5** (21.3-31.9)		1.63	-4.3
TCD8			10	20	**20.1** (18.1-23.2)		N/A	-4.9

A pilot hole was constructed in the soil. The diameter of the pilot hole depends on the lab (or field) installation equipment and pile shaft size. Several pilot hole diameters were attempted in the present study, and a diameter of 80 mm was selected because this size enabled the smooth installation with existing torque equipment in the lab. Other pilot hole sizes may also be adopted in the laboratory or field, however, the effects of pilot hole size on the installation torque were not investigated in this study. To prepare the pilot hole, a PVC cylinder was left in the middle of the soil cell during the soil preparation and consolidation process; this cylinder was removed before the test pile segment was torqued into the pilot hole. The PVC cylinder had an outer diameter of 80 mm, to simulate a pilot hole that is slightly smaller than the diameter of a smooth pile shaft of 89 mm. In this case, a downsized ratio (pilot hole diameter/pile shaft diameter) of 0.9 was obtained. The torque value may change with the pilot hole size, soil temperature, or boundary condition, but this was not examined in the present work.

Ethylene glycol was circulated through the outer cell until the thermocouples indicated that the soil had reached the desired test temperature for installation. The installation method is different from the method for conventional piles (Nixon 1988; Biggar and Sego 1993a and 1993c). In order to keep the consistent construction method, the smooth segment was also screwed into the same size pilot hole by applying torque and compressive force on the pile head. Since backfilling and freeze-back are unnecessary, screw piles may be immediately loaded upon the completion of their installation. In the present study, the pile was loaded once the desired test temperature (T) of soil was reached, which usually took less than 24 h. Upon completion of axial loading tests, the frozen soil and model pile were excavated with care, physical properties (such as water content and bulk density) of soil were measured, and the pile failure modes were observed and photographed.

3.2.5 Test matrix

The constant displacement rate test is a typical method for determining the short-term shear resistance (τ_{ad}) of piles in frozen soils. 12 constant displacement rate tests were conducted in the present research (Table 1). The constant displacement rate was 2.2 mm/h, which was within the range adopted in the literature; for example, 0.5 mm/h was used in Biggar and Sego (1993c), 1.2 0.03 to 6 mm/h in Parameswaran (1978) and 1.8 to 18.3 mm/h in Ladanyi and Guichaoua (1985).

It is generally accepted that a higher rate increases the resistance of piles in frozen soils (Heydinger 1987).

As shown in Table 1, w of 20% and 25% and T of -1 °C and -5 °C were selected to cover the range of conditions encountered in Arctic communities. The value of w was 15% for ice-poor sandy silt and 35% for ice-rich silt in Inuvik, and the ground temperature below 5 m depth was from -0.3 to -4.1 °C (EBA 2004). Another reason for choosing a warm temperature of -1 °C was that research on the performance of piles in warm permafrost available in the literature is insufficient. The porewater salinity (S) is defined as:

$$S \text{ (in ppt)} = m_{\text{salt}} / m_{\text{water}} \tag{3-1}$$

where m_{salt} (in g) is the mass of salt ions and m_{water} (in kg) is the mass of porewater in the frozen soil. The salinity of 10 ppt of sodium chloride was selected in the present study. The porewater S was reported (EBA 2004; Hivon and Sego 1993) to vary from 5 to 11 ppt within a permafrost depth of 10 m in Inuvik, NWT, Canada.

3.3 Results

3.3.1 Soil Temperature Distribution

Figure 3.4a shows that the average soil temperature in tests TCD4 and TCD6 remained stable during the loading and consolidation period with a fluctuation of less than 1 ºC, which indicated the constant temperature bath worked effectively during the test. The average temperature was calculated from all thermocouples embedded in each soil sample. Figure 3.4b shows an example of soil temperature at different locations within the frozen soil. The temperature fluctuation of the three layers was less than 0.5 ºC during the loading period and a consistent and homogeneous temperature profile in the soil was maintained.

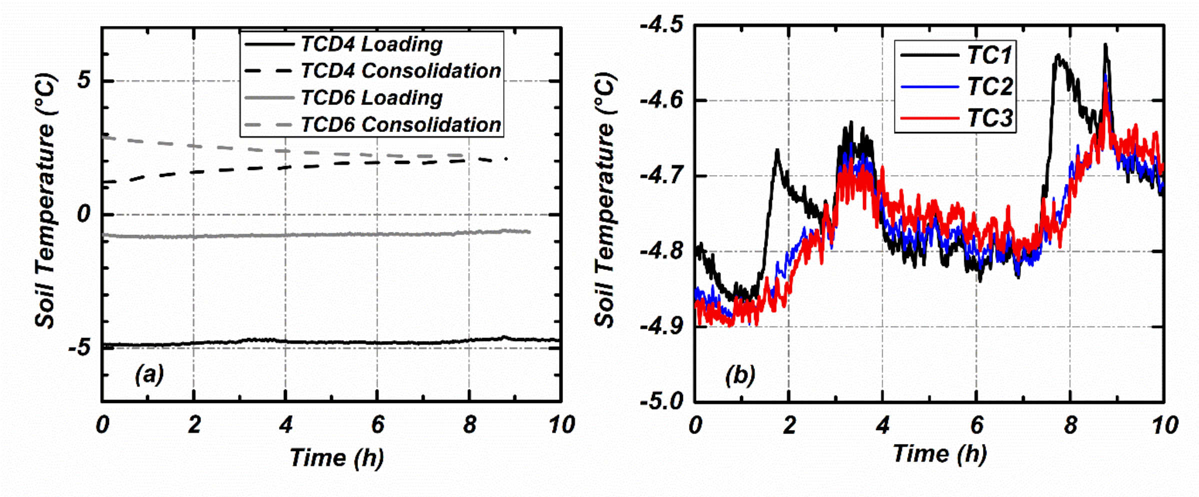

Figure 3.4 Example soil temperature readings: (a) Time histories of average soil temperature during consolidation and axial loading phases (TCD4 and TCD6); and (b) soil temperature in different layers during axial loading (TCD4).

3.3.2 Installation Torque

The installation torque of piles in unfrozen soils in the field is an important indicator of the potential axial performance of a screw pile. Empirical torque versus capacity correlation can be used for the pile design in unfrozen soils (Guo and Deng 2018). Figure 3.5 shows the relationship between the installation torque and penetration depth in test TCD6. It is observed that the installation torque increased with an increasing penetration depth of the pile segment. Torque refusal, due to the limitation of the electric torque driver in the laboratory, was observed at -1 ºC in non-saline soil and -2 ºC in 10 ppt soil. The soil between the threads was squeezed and damaged when refusal was observed. Also, the installation torque increased significantly with decreasing temperature and salinity. This can be attributed to the increased soil shear strength due to the increasing volume of ice crystals in the pores of frozen soil, when the temperature and salinity of soil decreased. The installation torque is also presumably dependent on the downsized ratio (pilot hole diameter/pile shaft diameter), but this was not studied in this research. The torque required to install a full-scale pile in the field may be approximately proportional to pile length if the boundary effects of the chamber are neglected.

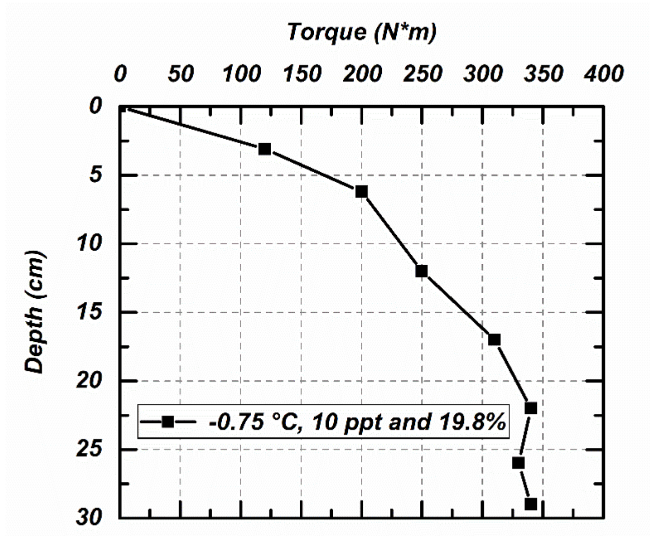

Figure 3.5 Example plot of installation torque vs. penetration depth (TCD6: -0.75 °C of *T*, 10 ppt of *S*, and 19.8% of *w*).

3.3.3 Ground Surface Settlement During Loading

To measure the ground surface settlement during the loading process, two LPs were placed at radial distances of 1.5 cm (LP1) and 2.5 cm (LP2) away from the pile shaft wall. Figure 3.6 compares typical ground surface settlements with pile head settlements. It can be seen that the ultimate ground surface settlement for a threaded segment (TCD3) in cold frozen soil (approximately at -5 ºC) ranged from 1 to 2.7 mm, which was 5% to 13.5% of the pile head settlement (=20 mm). The settlement for a smooth segment (SCD2) was 0.6 mm, which was only 3% of pile head settlement. This implies a limited soil settlement adjacent to the pile shaft when the pile was axially compressed at a constant displacement rate. The shear failure zone of the threaded segment (TCD3) was greater than that of the smooth segment (SCD2), when comparing the free-field soil settlement.

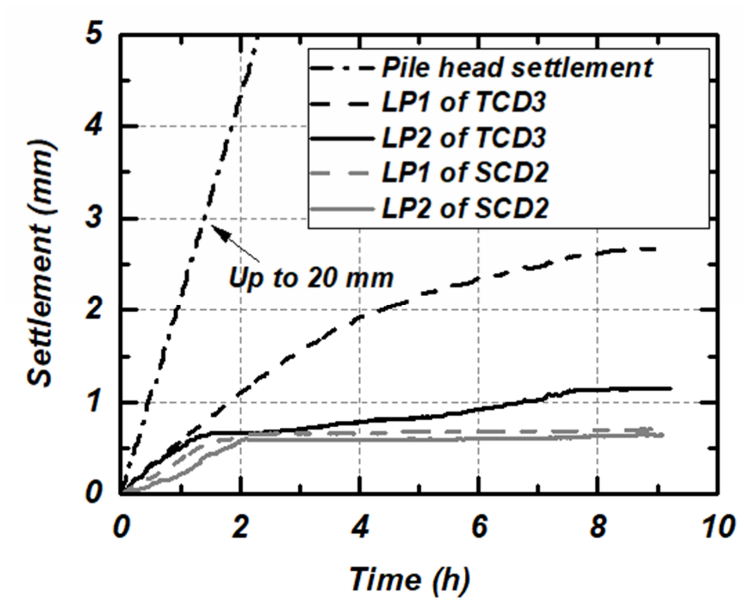

Figure 3.6 Example of ground settlement near the pile shaft and pile head settlement.

3.3.4 Axial Load vs. Displacement Behavior

The axial load vs. pile head displacement curves for all tests are summarized in Figure 3.7. Figures 3.7a and 3.7b show that threaded pile resistance increased significantly from 2.7 kN (TCD2) to 40 kN (TCD4) when the average *T* decreased from -1 ºC to -5 ºC. This can be attributed to the temperature's direct influence on the strength of intergranular ice and the reduced amount of unfrozen water within the colder soil. In general, a decrease in *T* increases the strength of frozen soil, but at the same time results in a more brittle behavior (Andersland and Ladanyi 2004), which is manifested by the post-peak softening (SCD2 in Figure 3.7a).

Figure 3.7a compares the behavior of threaded and smooth pile segments at -5 ºC. The limit capacities of threaded pile segments were 3 to 4 times of the smooth pile segments, because of the contribution of outward threads and the shearing of the frozen soil compared to the interfacial shearing along the smooth pile. Salinity also has a significant effect on the pile capacity at -5 ºC. Non-saline soil (TCD4 and SCD2) carried more load than the soil with *S* of 10 ppt (TCD8 and SCD4) because *S* decreased the strength and thus the capacity. This observation agreed with the conclusion that the adfreeze bond between piles and frozen soil is substantially reduced in the presence of saline pore fluid (Andersland and Ladanyi 2004). The reduction in strength was attributed to the formation of a liquid film at the ice and steel interface thereby reducing the effective contact area (Biggar and Sego 1993c).

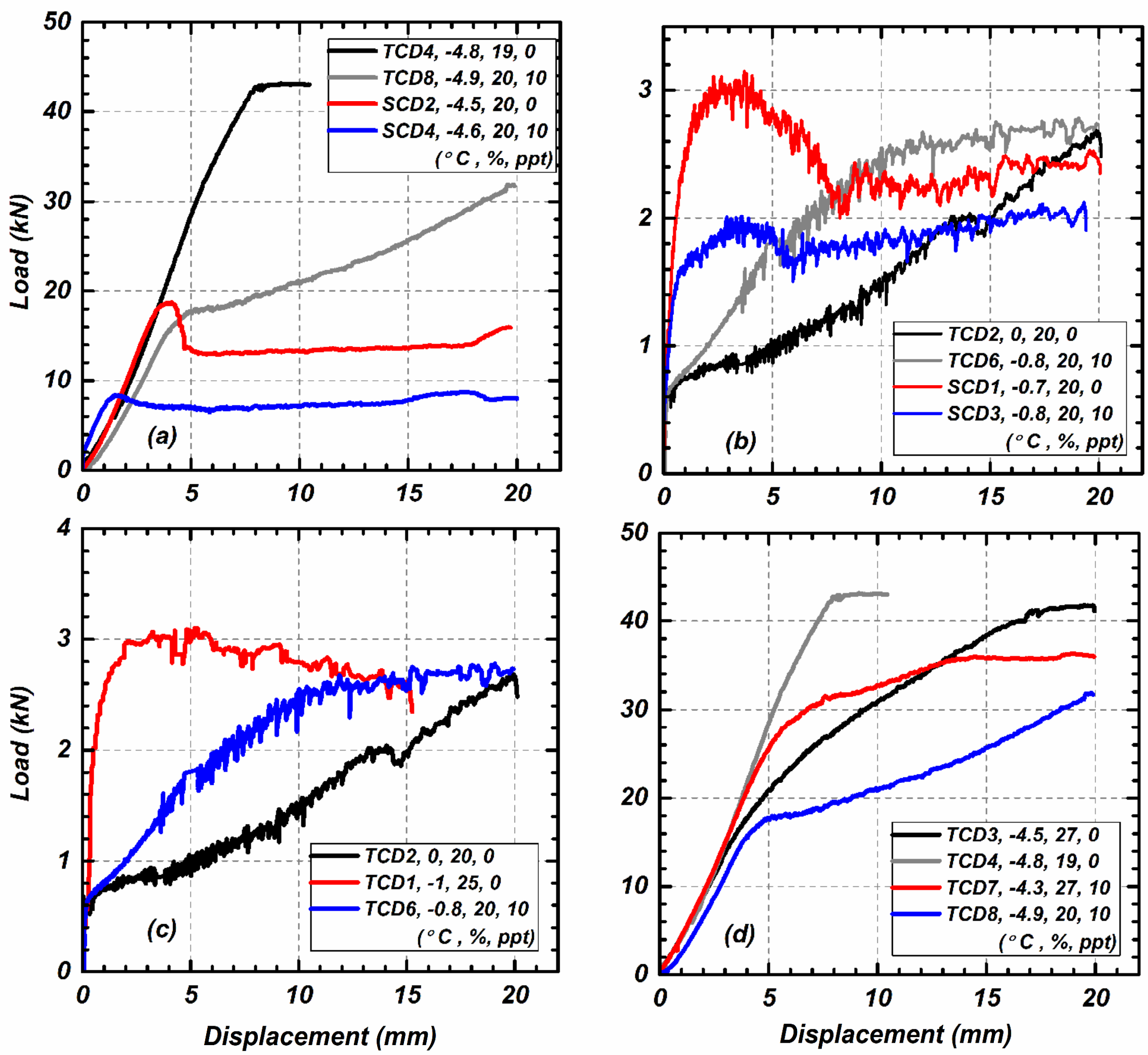

Figure 3.7 Axial load vs. displacement curves: (a) piles in soils with different salinity at approximately -5 °C; (b) piles in soils with different salinity at approximately -1 °C; (c) threaded piles in soils with different water contents and salinity at approximately -1 °C; (d) threaded piles in soils with different water content and salinity at approximately -5 °C.

Figure 3.7b shows the effects of pile type and soil salinity on the axial performances of the pile at a soil temperature of -1 ºC. The axial load versus displacement behavior of threaded segment in saline soils (TCD6) was not significantly different from that in non-saline soils (TCD2, Figure 3.7b). The performance of the smooth segment was affected by S at T of -5 ºC but there was no significant difference between saline and non-saline soil at approximately -1 ºC, as shown in the curves of SCD1 and SCD3 in Figure 3.7b. Furthermore, the ultimate capacity differences among threaded and smooth segments at -1 ºC (TCD2, TCD6, SCD1) were not significant.

Figures 3.7c and 3.7d show the impact of S and w on the performance of screw piles. Piles in soils with different w experienced different patterns of post-peak load vs. displacement behavior. However, ultimate resistances were not affected by w. It can be concluded the pile capacity decreased with increasing S for all of the threaded piles in cold frozen soil (-5 ºC). The presence of salt ion in frozen soil triggers a higher volume of unfrozen water and a lower amout of ice crystals compared to non-saline soil at the temperature of -5 ºC, thus, reducing the soil strength.

Azmatch et al. (2011) evaluated the gravimetric unfrozen water content (w_u) of Devon silt. The unfrozen water content curve indicates that w_u drops significantly from 25% to 9.5% when the temperature decreases from 0 ºC to -1 ºC within the temperature range of the frozen-fringe. The change in w_u is small (10.5% to 7.1%) from -1 ºC to -5 ºC. Then w_u remains almost constant at 6.5% when the temperature is below -7 ºC. Tice et al. (1976) suggested the following equation:

$$w_u = \alpha(\theta / \theta_0)^{\beta} \tag{3-2}$$

where θ is the negative temperature in ºC, θ_0 is a reference temperature taken as -1 ºC, and α and β are empirical parameters. According to the values α (= 10.5) and β (= -0.244) of Devon silt suggested by Azmatch et al. (2011), w_u of non-saline frozen soils in the present study are summarized in Table 1. The values of w_u ranged from 11.5% to 7.2% when the temperature decreases from -0.7 ºC to -4.8 ºC, except for sample TCD2 with a temperature of 0 ºC. In other words, the frozen water/ice lens changed by 4.2% when the temperature decreased by 4 ºC. The values of w_u of saline soil samples are unavailable herein because of a lack of predictive model.

3.3.5 Failure Mode Observation

Soil and piles were carefully excavated after each loading test so that the failure modes of the continuous-flight pile segments within the frozen soil could be assessed. Two major failure patterns were observed, photographed, and inferred from the measured data.

For piles in warm frozen soil approximately at T of -1ºC, soils around the threaded pile segment failed approximately in a cylinder shear mode (CSM, Figure 3.8a). The soil adjacent to the edge of the thread was sheared and a global failure occurred as shown in Figures 3.8b and 3.8c. In this failure mode, the soil's unit-area resistance is represented by the internal shear strength τ_u (in a unit of kPa) along the global failure surface, and the unit plate bearing resistance q_b (kPa) of the soil can be neglected (Figure 3.8a). The CSM is similar to conventional pile failure that takes place along the interface between the backfill and the native frozen soil, which is illustrated in Figure 3.9 (Biggar and Sego 1993c).

For piles in soil at T of approximately -5ºC, Figure 3.10 shows a schematic of individual bearing mode (IBM) of each pile thread and the soil rather than at the soil-shaft shear surface. The soil resistance can be represented by q_b of the threads and τ_{ad} between the soil and shaft, as shown in Figure 3.10a. A slipping wedge was observed below the threads (Figure 3.10b and 3.10c). The IBM may be attributed to a strong soil-pile bond at the cold temperature.

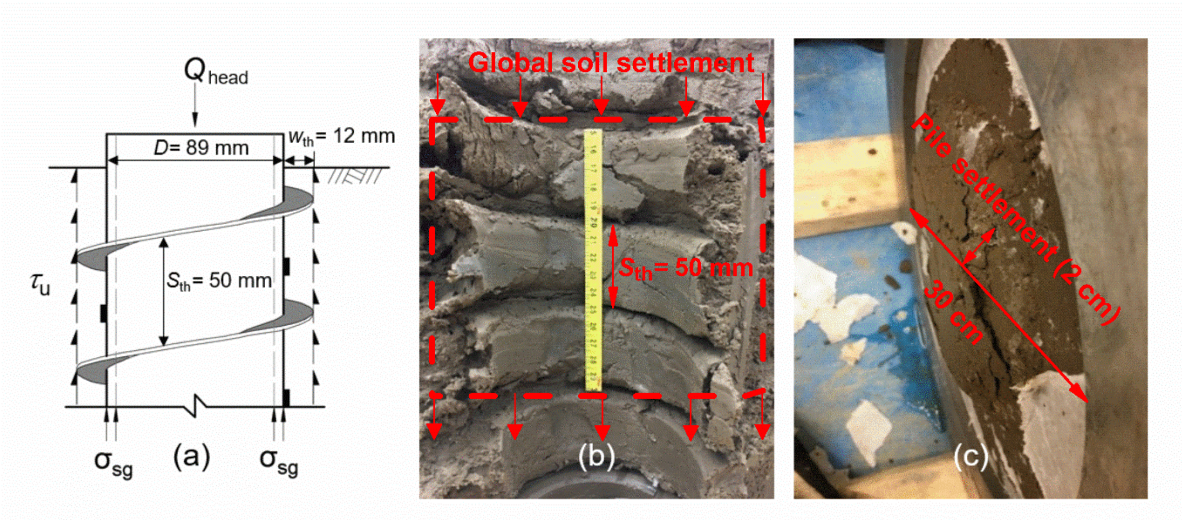

Figure 3.8 (a) Schematic of cylindrical shear mode of piles in warm frozen soil at approximately -1 °C; and (b) observed global failure; and (c) soil movement at the pile tip (TCD1).

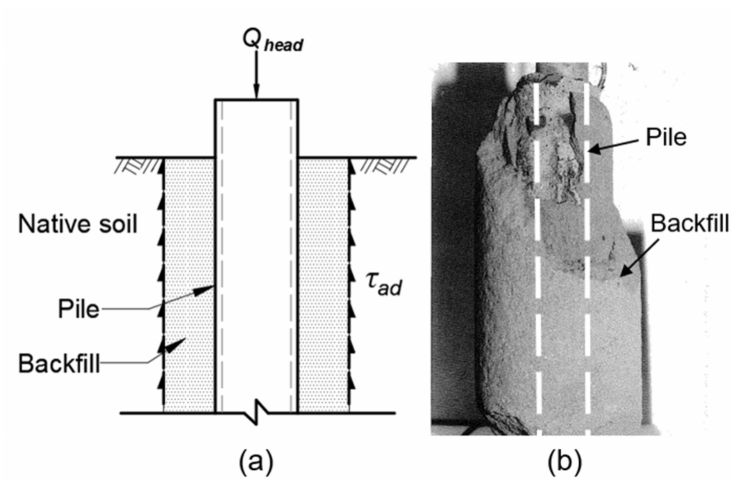

Figure 3.9 (a) Soil-pile failure pattern of conventional piles with backfill; and (b) conventional pile failure (adapted from Biggar and Sego 1993c, drawings are not to scale).

3.3.6 Axial Load Distribution and Adfreeze Strength – Smooth Pile Segment

For smooth pile segments instrumented with SGs, the internal shaft load Q at a SG location is calculated from Equation 3-3:

$$Q = \sigma_{sg} A = E\varepsilon_{sg} A \tag{3-3}$$

where σ_{sg} is the internal normal stress of the pile shaft, A is the cross-sectional area of the pile, E is Young's modulus of the pile shaft material, and ε_{sg} is the internal normal strain within the pile shaft measured using the SG. The average τ_{ad} between two SGs is estimated as:

$$\tau_{ad} = \frac{Q_i - Q_j}{\pi D L_{ij}} \tag{3-4}$$

where Q_i is the internal load at the limit state at i, D is the smooth shaft diameter and L_{ij} is the length of the shaft segment between i and j. In the present research, τ_{ad} was estimated at the pile's limit state corresponding to the peak from the load vs. displacement curves (Figure 3.7).

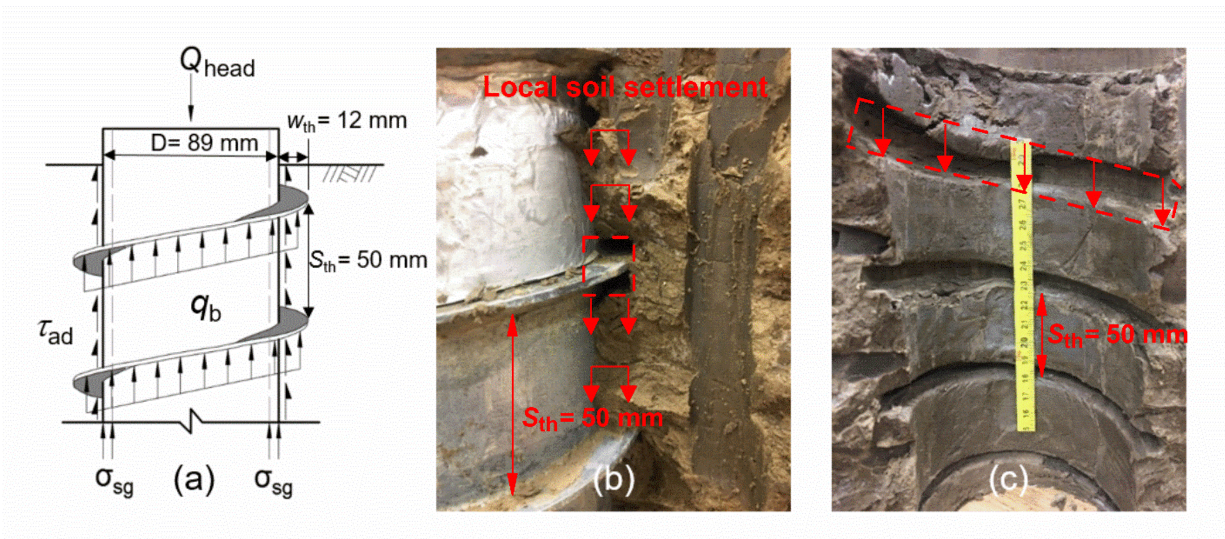

Figure 3.10 (a) Schematic of individual bearing mode for piles in cold permafrost at approximately -5 °C; and (b) observed slipping wedge; and (c) observed local failure (TCD7).

Figure 3.11a shows the load distributions measured from the load cell and SGs in warm frozen soil (approximately at -1 ºC). Figure 3.11b shows the average τ_{ad} obtained from the load cell and τ_{ad} between SGs. The average τ_{ad} was 38.2 kPa in this non-saline frozen soil, while τ_{ad} from SG readings varied along the depth, but in general showed a reasonable consistency. The average τ_{ad} was 27.9 kPa when the salinity was increased to 10 ppt. Salinity did not show a significant effect on the magnitude of τ_{ad} in the warm frozen soil; this phenomenon matched the observation from Figure 3.7b that the effect of salinity on the pile capacity in warm frozen soil was not significant.

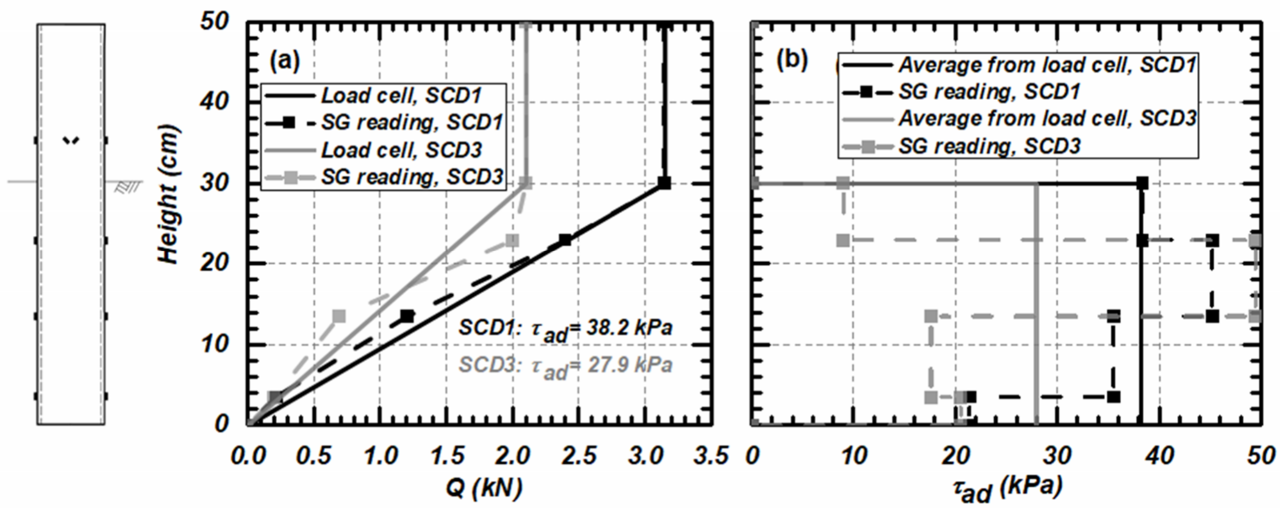

Figure 3.11 (a) Axial load distribution of SCD1 (-0.7 °C, 20.2% and 0 ppt) and SCD3 (-0.8 °C, 20% and 10 ppt); and (b) adfreeze strength distribution of SCD1 and SCD3. The "Average from load cell" is the averaged τ_{ad} estimated from the load cell readings and "SG reading" is obtained from strain gauge readings.

The average τ_{ad} increased from 38.2 kPa (SCD1) to 240 kPa (SCD2) in non-saline soil and from 27.9 kPa (SCD3) to 113 kPa (SCD4) in 10 ppt soil, when the average temperature decreased from -1 ºC to -5 ºC (Figure 3.12). In addition, τ_{ad} decreased with increasing salinity, as observed in test SCD2 to SCD4. It is also noted that the internal load measured from SGs had an acceptable consistency with the measured load from the load cell.

Values of τ_{ad} for straight pipe piles with backfill reported in literature are summarized in Table 3.2. The value of τ_{ad} of the smooth segment in non-saline cold frozen soil from the present research was 240 kPa comparable to the Johnston's (1981) 275 kPa, Biggar and Sego's (1993c) 220-390 kPa of untreated steel piles, and Tang et al.'s (2019) 154-347 kPa.

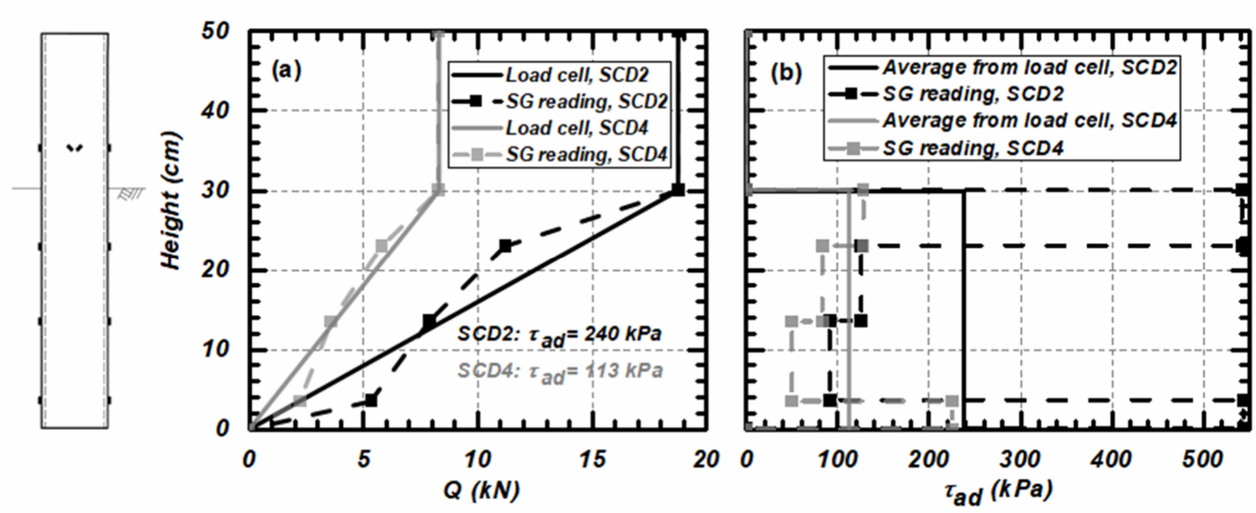

Figure 3.12 (a) Axial load distribution of SCD2 (-4.5 °C, 19.9 %, 0 ppt) and SCD4 (-4.6 °C, 19.7%, 10 ppt; and (b) adfreeze strength distribution of SCD2 and SCD4.

Table 3.2 Adfreeze bond strength τ_{ad} from selected literature

Reference	**Pile type**	**Backfill material and *w***	***T* (°C)**	***S* (ppt)**	**τ_{ad} (kPa)**
Johnston (1981)	Steel	Ice-rich clays or silts	-5	0	275
Linnel and Lobacz (1980)	Steel	Sand	-4	0	390
Tsytovich (1975)	Steel	Sand (18%)	-5	0	398
Weaver and Morgenstern (1981)	N/A	Sand	-5	0	294
Biggar and Sego (1993c)	Untreated steel	Sand (18%)	-5	0	220–390
	Sandblasted steel		-5	0	760–1100
	Sandblasted steel		-10	0	1240–1380
Tang et al. (2019)	Concrete	Silt (30%)	-1.1 – -2.35	0	564–962
		Clay (10%)	-1.2 – -2.29	0	154–347

3.3.7 Load Transfer of Continuous-Flight Piles in Warm Frozen Soil

In the warm frozen soil, the limit load transferred to the threaded segment under the CSM hypothesis, Q_{head}, was estimated using Equation 3-5:

$$Q_{head} = \tau_u \pi (D + 2w_{th}) L \tag{3-5}$$

where τ_{u} is the average shear strength of frozen soil and w_{th} is the thread width (Figure 3.8). The term $\pi(D+2w_{\mathrm{th}})L$ is essentially the presumed shear failure area between the soil and "enlarged" pile shaft associated with failure at the outside of the threads.

Figure 3.13a shows the load distribution of TCD1 measured from the load cell and internal load from SG readings; Figure 3.13b shows the average τ_{u} estimated from the load cell and SG readings. The value of average τ_{u} from load cell was 30.5 kPa for TCD1, while τ_{u} estimated from SGs varied from 28 to 37.5 kPa. Figure 3.14a shows the load distribution for TCD2. The value of average τ_{u} was estimated 32.4 kPa using Equation 4. In Figure 3.14b, τ_{u} of TCD2 and τ_{ad} of SCD1 in similar soil conditions were compared. It is noted that the shear strength at the failure surface decreased from 38.2 kPa (SCD1) to 32.4 kPa (TCD2) when the average T increased from -1 to 0 ºC.

The load distribution and shear strength of test TCD6 are shown in Figure 3.15. The value of τ_{u} was 31 kPa for TCD6, which is 11% greater than τ_{ad} of 27.9 kPa of test SCD3. The threads not only expanded the failure surface outward from the pile surface but also increased the unit area shear strength, because the failure surface occurred internally within the soil when threads were present. For conventional piles with backfill, the ratio of $\tau_{\mathrm{ad}}/\tau_{\mathrm{u}}$ is selected from the type and the roughness of the pile surface. Weaver and Morgenstern (1981) suggested a coefficient of 0.6 for steel piles and 1.0 for corrugated steel pipe piles with backfill. In the present study, the ratio of $\tau_{\mathrm{ad}}/\tau_{\mathrm{u}}$ was 0.9 in the 10 ppt soil with T of approximately -1 ºC.

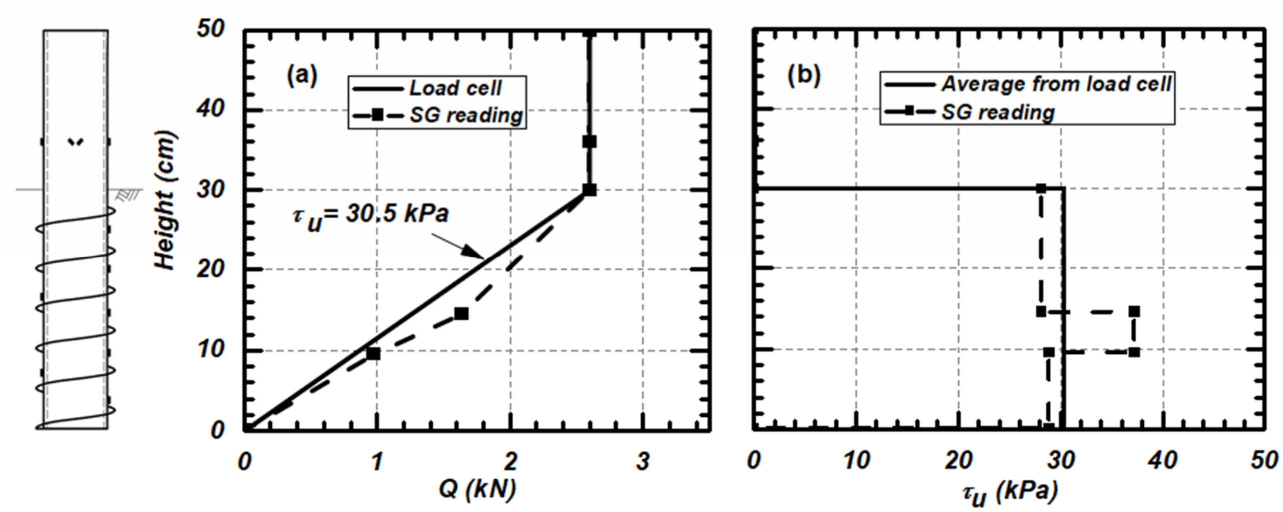

Figure 3.13 (a) Axial load distribution of TCD1(-1 °C, 25.5% and 0 ppt); and (b) strength distribution of TCD1. The “Average from load cell” is the estimated average τ_u from the load cell readings using Equation 5 and “SG reading” is measured from strain gauge readings.

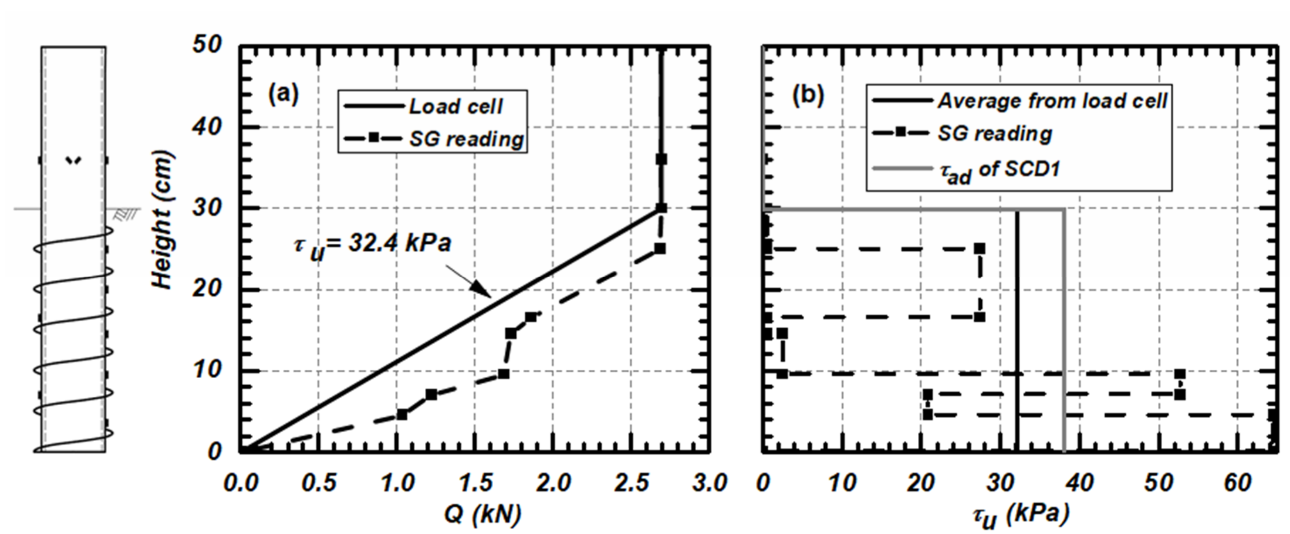

Figure 3.14 (a) Axial load distribution of TCD2 (0 °C, 20.2% and 0 ppt); and (b) strength distribution of TCD2.

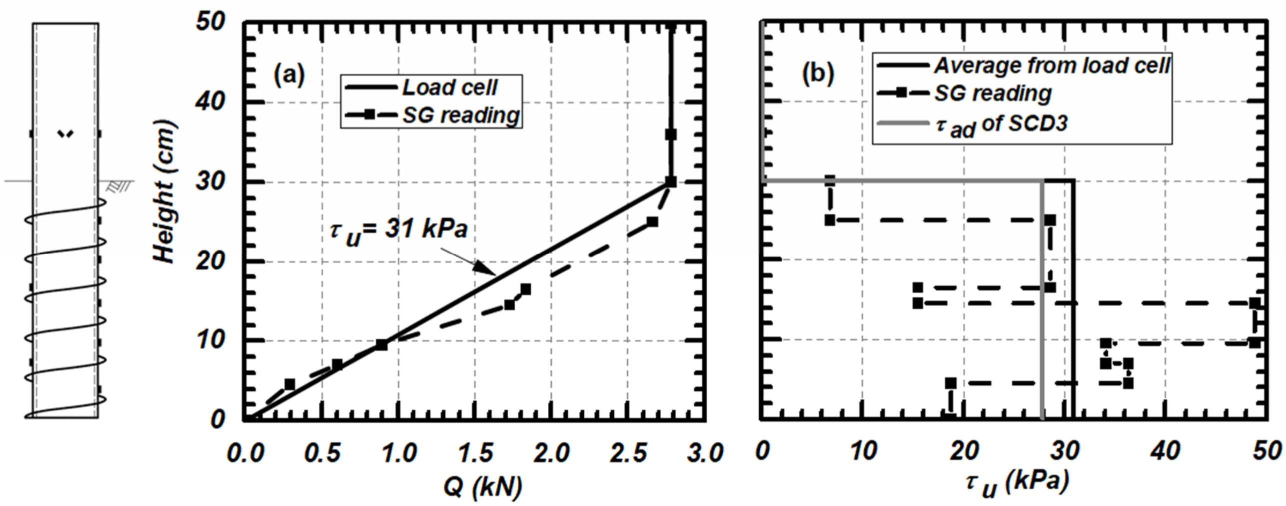

Figure 3.15 (a) Axial load distribution of TCD6 (-0.8 °C, 19.8% and 10 ppt); and (b) strength distribution of TCD6.

Hivon and Sego (1995) measured the strength τ_u of frozen soils with various w, T, and S from the unconfined compression tests. The values of τ_u of soils that are similar to the present soils are adopted to verify the measured strength in the present study. Table 3.3 summarizes the strength and τ_{ad}/τ_u ratios. It can be observed that τ_{ad}/τ_u in the present research ranged from 0.72 to 0.9, which are comparable to values suggested in Weaver and Morgenstern (1982). In addition, as shown in Figures 3.13 to 3.15, values of τ_u among TCD1 (30.5 kPa), TCD2 (32.4 kPa) and TCD6 (31 kPa) were not significantly different, which shows that the effect of w and T were not significant for piles in the warm frozen soil. This phenomenon agrees with the results from the load vs. displacement curves in Figure 3.7c.

In conclusion, continuous-flight piles in warm frozen soil failed under the CSM as suggested in Figure 8a. The effect of w and S on the value of τ_u in the warm frozen soil can be neglected. The ratios of τ_{ad}/τ_u in the present study were within the range suggested in the literature. The presence of threads pushed the shear failure outward to the edge of the threads where the soil shear strength was mobilized along the failure surface, and therefore enhancing the pile capacity.

Table 3.3 Summary of shear strength and end bearing resistance

<table>
<tr><th>Test ID</th><th>Average τ_u (kPa)</th><th>Average τ_{ad} (kPa)</th><th>Average q_b (kPa)</th><th>τ_u (kPa) [1]</th><th>τ_{ad}/τ_u</th><th>q_b/τ_u</th></tr>
<tr><td>SCD1</td><td rowspan="4">N/A</td><td>38.2 (Measured)</td><td rowspan="4">N/A</td><td colspan="3">N/A</td></tr>
<tr><td>SCD2</td><td>240 (Measured)</td><td>333</td><td>0.72</td><td>N/A</td></tr>
<tr><td>SCD3</td><td>27.9 (Measured)</td><td colspan="3">N/A</td></tr>
<tr><td>SCD4</td><td>113 (Measured)</td><td>151</td><td>0.75</td><td>N/A</td></tr>
<tr><td>TCD1</td><td>30.5</td><td colspan="5" rowspan="2">N/A</td></tr>
<tr><td>TCD2</td><td>32.4</td></tr>
<tr><td>TCD3</td><td rowspan="2">N/A</td><td>240 (From SCD2)</td><td>1420</td><td>333</td><td>0.72</td><td>4.26</td></tr>
<tr><td>TCD4</td><td>240 (From SCD2)</td><td>1410</td><td>333</td><td>0.72</td><td>4.23</td></tr>
<tr><td>TCD5</td><td colspan="6">N/A</td></tr>
<tr><td>TCD6</td><td>31</td><td>27.9 (From SCD3)</td><td colspan="2">N/A</td><td>0.9</td><td>N/A</td></tr>
<tr><td>TCD7</td><td rowspan="2">N/A</td><td>113 (From SCD4)</td><td>1610</td><td>151</td><td>0.75</td><td>9.66</td></tr>
<tr><td>TCD8</td><td>113 (From SCD4)</td><td>1370</td><td>151</td><td>0.75</td><td>8.22</td></tr>
</table>

Note: 1. Obtained from unconfined compression tests of similar frozen soils in Hivon and Sego (1995).

3.3.8 Load Transfer of Continuous-Flight Piles in Cold Frozen Soil

For the IBM shown in Figure 3.10a, the limit load Q_{head} transferred to the threaded segment was estimated as:

$$Q_{head} = \tau_{ad}\pi DL + q_b w_{th} L_{th} \tag{3-6}$$

where L_{th} is the length of helical threads that was embedded in the soil. In the following calculations, τ_{ad} of the screw pile was assumed the same as the measured values of τ_{ad} of the smooth pile in the same soil conditions. Thus, the average q_b for pile segment can be estimated as:

$$q_b = \frac{Q_{head} - \tau_{ad}\pi DL}{w_{th} L_{th}} \tag{3-7}$$

Figure 3.16a shows the load distribution measured from the load cell and SG readings for test TCD4 in cold frozen soil. Figure 3.16b shows the average q_b estimated from the load cell and SG readings. An average τ_{ad} of 240 kPa, obtained from the results of SCD2, was adopted when performing the q_b estimation. The average value of q_b was 1.41 MPa, whereas q_b estimated by SG readings ranged from 600 kPa to 1.9 MPa. The values of average q_b from the load cell were adopted in the present study for the convenience of comparison.

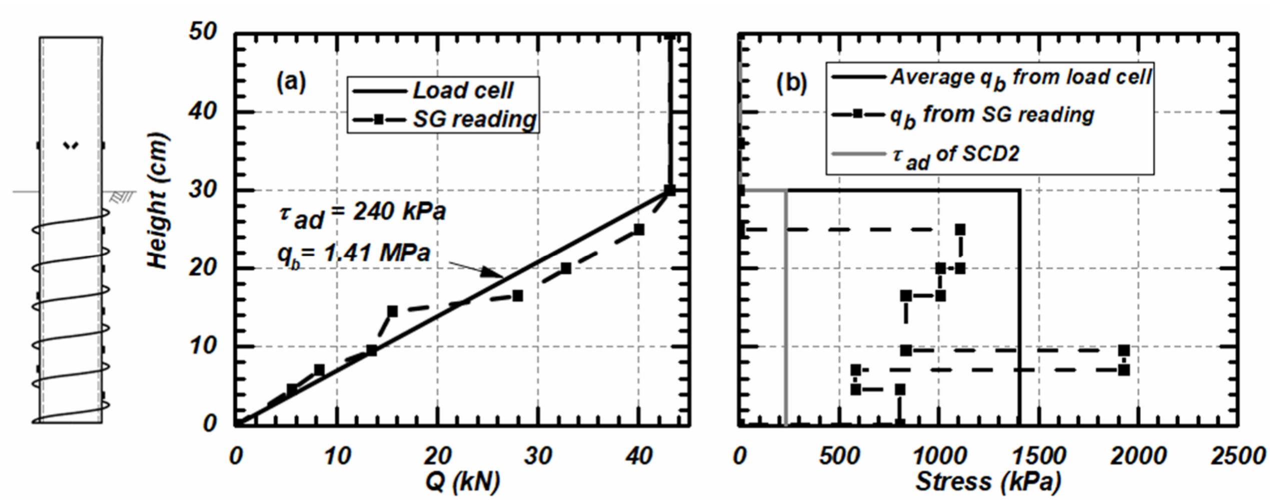

Figure 3.16 (a) Axial load distribution of TCD4 (-4.8 °C, 19.5% and 0 ppt); and (b) strength distribution of TCD4. The "Average q_b from load cell" is the average q_b estimated from the load cell reading and τ_{ad} was assumed equal to τ_{ad} of SCD2.

Figure 3.17a shows the load and strength distribution of TCD8. It appears that the load distribution from the load cell agrees well with the internal load distribution calculated from the SGs. In Figure 3.17b, an average τ_{ad} was assumed to be 113 kPa (SCD4) and q_b was estimated to be 1.37 MPa; q_b estimated from SGs ranged from 550 kPa to 2 MPa. Test results of TCD3 and TCD7 were processed in the same way as the data from Figures 3.16 to 3.17 were interpreted; the patterns of TCD3 and TCD7 were also deemed similar to Figures 3.16 to 3.17. The ratio of q_b / τ_u can be viewed as N_c, which is the bearing capacity factor in the frozen soil. Ladanyi (1975) proposed a simple mathematical model for determining the bearing capacity of strip footings in frozen soils and suggested values of N_c ranging from 4 to 16. Table 3 summarizes values of q_b and q_b / τ_u of all relevant tests in the present research. The estimated values of q_b for all tests ranged from 1.37 to 1.61 MPa were not significantly different, which shows that the effects of w and S on the unit plate bearing capacity of piles in the cold frozen soil could be negligible. The ratios of q_b / τ_u in the present study ranged from 4.2 to 9.7, which are comparable to values from Ladanyi (1975).

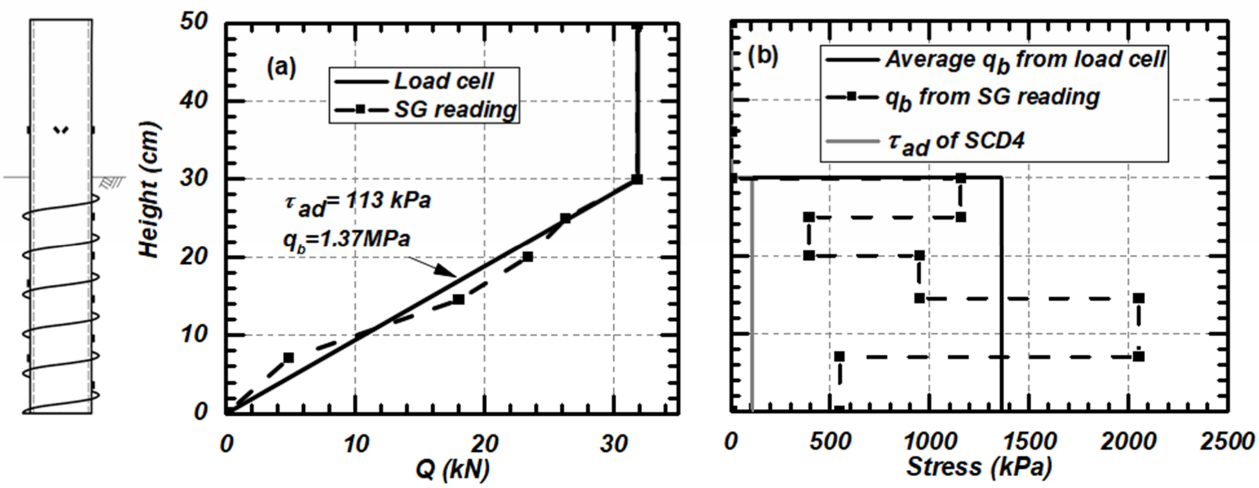

Figure 3.17 (a) Axial load distribution of TCD8 (-4.9 °C, 20.1% and 10 ppt); and (b) strength distribution of TCD8. Value of τ_{ad} was assumed equal to τ_{ad} of SCD4.

In conclusion, continuous-flight piles in cold frozen soil failed under the IBM. The effect of w and S on the value of q_b in the cold frozen soil is negligible. Because the plate bearing resistance is mobilized during loading, the IBM suggests a potential advantage of continuous-flight piles over conventional smooth piles.

3.4. Conclusions and Limitations

Twelve axial load tests of continuous-flight and smooth piles were conducted in the present study. The following conclusions can be drawn:

1. The continuous-flight pile can be installed in an undersized pilot hole in frozen soil using the laboratory equipment which can provide a maximum torque of 3.6 kN·m. Installation met refusal at a minimum temperature of -1.88 ºC in 10 ppt soil because the equipment

was unable to produce higher torque. The required installation torque increased with the penetration depth of the pile segment. The installation torque increased significantly with decreasing frozen soil temperature and salinity.

2. The continuous-flight pile carried more load than the smooth pile in the cold frozen soil. The ultimate pile capacity increased significantly when T decreased from -1 ºC to -5 ºC. The pile capacity increased with decreasing S in cold frozen soils (-5 ºC); the effect of S on the pile capacity in warm frozen soils (-1 ºC) could be neglected. The effect of w on the pile capacity was not significant at -5 ºC.
3. Cylindrical shearing mode (CSM) and individual bearing mode (IBM) were observed for continuous-flight piles in warm and cold frozen soils, respectively.
4. For pile failure in the warm frozen soil, the presence of threads pushed the shear failure outward to the edge of the threads, mobilizing the shear strength of the frozen soil, and therefore enhanced the pile capacity. The effect of w and S on the value of τ_u along this failure surface in the warm frozen soil can be neglected. The ratios of τ_{ad} / τ_u ranged from 0.72 to 0.9 in the present study, which are comparable to values suggested in the literature.
5. For pile failure in the cold frozen soil, the estimated values of q_b ranged from 1.37 to 1.61 MPa and the ratios of q_b / τ_u ranged from 4.2 to 9.7. The influences of w and S on the unit plate bearing resistance of piles in the cold frozen soil were not evident.

Continuous-flight piles may provide a viable solution for pile foundations in the Canadian Arctic; however, limitations of the present study should be noted. First, only one undersized pilot hole size was tested. If another hole size is used, the required installation torque would change. Second, the pile segment was installed in the frozen with a minimum temperature of -2 °C, owing to the limitation of the lab installation technique. Lastly, the long-term creep settlement rate of continuous-flight piles needs to be evaluated.

4 Long-Term Axial Performance of Continuous-Flight Pile in Frozen Soil[2]

4.1 Introduction

Research on pile foundations in permafrost is critically important to maintaining infrastructure in Arctic communities. The design of the piles is governed by the time-dependent creep settlement and the adfreeze strength between the pile shaft and frozen backfill (Weaver and Morgenstern 1981, Heydinger 1987, Ladanyi et al. 1995). Weaver and Morgenstern (1981) reviewed the principles for designing piles in permafrost and proposed procedures for predicting the settlement of piles in ice-rich and ice-poor soils based on the creep model of Morgenstern et al. (1980).

There are three types of creep behavior when frozen soil is subjected to a constant load (Figure 4.1a). For the ice-poor (typically <35% ice content by weight) soil under low stress, the soil experiences a small instantaneous deformation (i.e. elastic strain) at the outset and deforms at a rate that gradually decreased with time; the strain reaches a plateau after a certain time. This is defined as the primary creep stage. For ice-rich soils under moderate stress, the deformation tends to increase linearly with elapsed time, therefore steady-state or secondary creep dominants. The primary stage can often be neglected when the secondary creep is dominant (Hult 1966; Ladanyi 1972). For high-stress level, the creep rate of frozen soil may accelerate (termed the tertiary creep) until failure occurs. Figure 4.1b shows a typical time history of creep when the soil is under medium to high-stress levels. A comprehensive creep curve may include three stages, where the creep rate decreases (I), remains constant (II), and increases (III). From the time history of the pile displacement or creep curve, the pile settlement rate curve can be determined (Figure 4.1c). The three periods I to III correspond to the primary, secondary and tertiary creep respectively. The

[2] A version of this chapter has been accepted by the Canadian Geotechnical Journal

creep settlement of piles in frozen soils is a function of the time, rate of loading, pile type, soil type, and temperature (Parameswaran 1986).

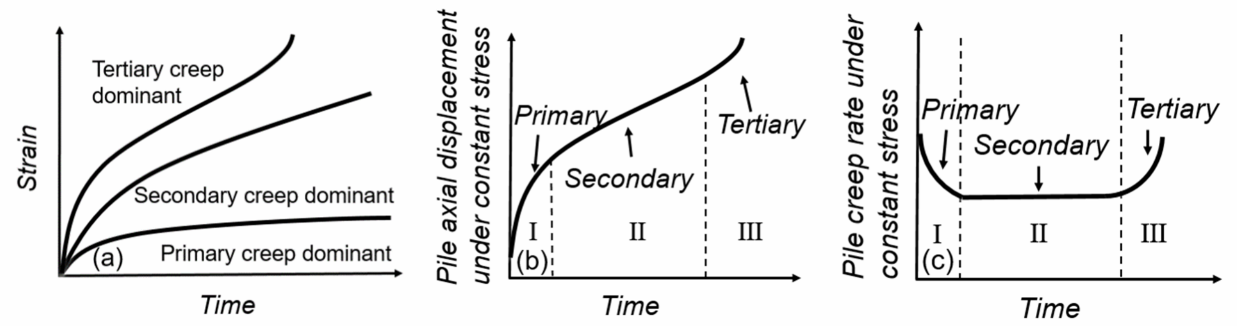

Figure 4.1 (a) Creep modes of frozen soil; and (b) potential pile axial displacement under constant stress; and (c) potential pile creep rate under constant stress (adapted from Andersland and Ladanyi 2004).

Straight-shaft smooth pipe piles are a conventional foundation in the Canadian Arctic. The conventional pile is usually placed in a pre-drilled borehole and backfilled with gravel, grout or slurries freeze (i.e. freezeback). Figure 4.2a shows a photo and schematic of a conventional straight pipe pile in Inuvik, NWT. Recently, helix thermopile (Figure 4.2b) has been introduced to the Canadian Arctic (Zhang and Hoeve 2015). Helix thermopile combines the function of thermosyphon and adfreeze pile that has continuous thin-bladed helixes on the pile surface to enhance the pile capacity. Despite the common use, conventional foundation types may possess several disadvantages. The pile is expensive and labor-intense; it takes time to freeze backfill before fully mobilize the pile capacity. The pile may be compromised because the capacity relies on the adfreeze strength along the pile shaft surface that is usually smaller than the strength of adjacent frozen soil (Biggar and Sego 1993c). Many buildings in the Canadian Arctic have demonstrated signs of failure due to excessive settlement or deterioration of the pile shaft (Liu et al. 2022).

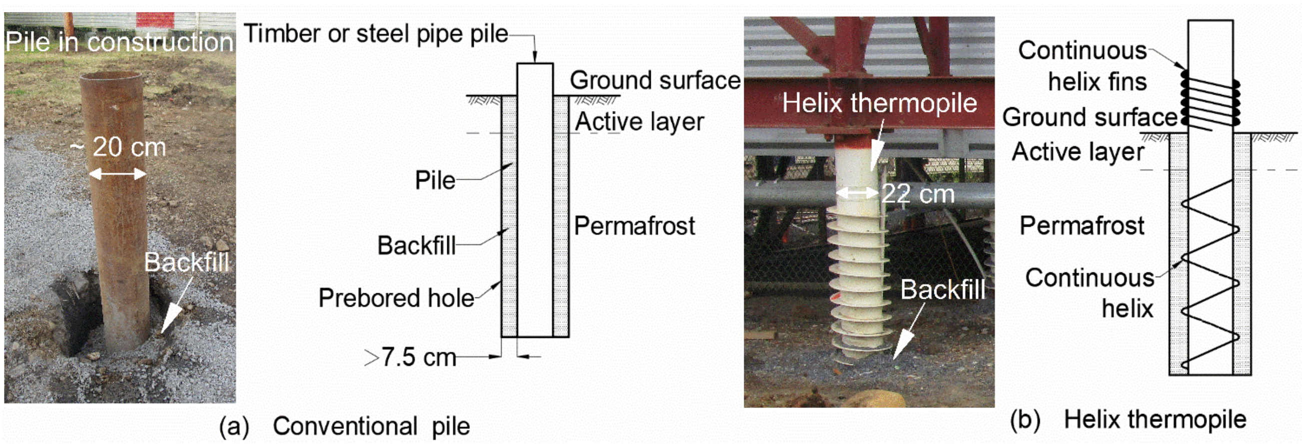

Figure 4.2 (a) Photo and schematic of a conventional smooth straight-shaft pile in Inuvik, NWT; and (b) photo and schematic of a helix thermopile supporting a commercial building in Inuvik, NWT.

Research on the performance of conventional piles was typically carried out in the lab or the field. Studies on the steel-pipe pile including both field testing (Johnston and Ladanyi 1974, Nixon 1988, Biggar and Sego 1993a, b, Biggar et al. 1996, Biggar and Kong 2001) and laboratory model-pile tests (Parameswaran 1978 and 1979, Sego and Smith 1989, Biggar and Sego 1993c) are available in the published literature. In these studies, short-term constant-displacement-rate and long-term constant applied load are the typical loading methods to obtain the adfreeze strength and creep settlement of piles respectively. Notably, there was a scarcity of research on the axial load distribution during constant load testing. Loading tests of model piles in frozen sand show that smooth straight-shaft piles fail in a brittle manner and have relatively low axial capacities because the shear failure is mobilized at the pile-backfill interface compared to failure of the surrounding soil (Ladanyi and Guichaoua 1985).

The present research evaluates an alternative foundation type that may be suitable for use in permafrost regions. The continuous-flight pile, also known as a ground screw or screw micropile (Guo and Deng 2018, Guo et al. 2019, Khidri and Deng 2022), has been adopted in southern Canada. Unlike conventional piles, this pile is screwed into the ground via torque. Compared to conventional piles of similar sizes, continuous-flight piles may have several advantages: low cost, reusability, larger capacities, faster installation, and immediate loading. Past studies of smooth and protruded (e.g., ribbed or helical) piles in permafrost imply that continuous-flight piles, as a result of the shaft screws and tapered shape, may provide larger capacities and smaller creep displacement than conventional pile foundations in permafrost (Holubec 1990; Johnston and Ladanyi 1972 and 1974; Liu et al. 1999 and 2007). It is anticipated that this pile type can be screwed into an undersized pilot hole of warm frozen soils induced by climate change. The installation process may further increase the confining stress on adjacent soils and therefore increase the pile capacities. Since freeze-back is unnecessary, this pile will reduce construction time and significantly reduce costs. These attributes of continuous-flight piles are expected to offer significant benefits to the Canadian Arctic communities.

The creep behavior of continuous-flight piles in permafrost is yet to be studied, although the adfreeze strength and axial failure mechanism of this pile type subjected to short-term loads have been reported in Gao et al. (2023a). The present study is focused on the axial creep behavior of continuous-flight piles in frozen soils under long-term constant applied loads. A primary objective is to examine the effects of soil temperature (T), water content (w), and soil salinity (S) on the stress, pile displacement rate, and failure mode of continuous-flight piles in frozen soils. A series of axial load tests of model continuous-flight piles with a shaft diameter of 89 mm and a length of 300 mm were carried out. The load cell (LC), Linear Potentiometers (LP), thermocouples

(TC), and strain gauges (SG) were used to evaluate the load-transfer mechanism and soil temperature profile.

4.2 Laboratory Experimental Program

4.2.1 Test Soil and Piles

The test soil was a mixture of Devon Silt and Silica sand. The selected silty sand was similar to the soil observed in Canadian Arctic communities near the Mackenzie River delta. The grain size distribution of the test soil was described by Gao et al. (2023a) and frozen soil properties were investigated by Hivon and Sego (1995).

Continuous-flight piles can have various lengths and diameters. Owing to the limitation of lab testing equipment, a straight threaded pile segment with a diameter (D) of 89 mm and a length (L) of 300 mm was tested in this research (Figure 4.3a). The threads on the pile segments have a width (w_{th}) of 12 mm and a thickness of 2 mm. The spacing between each thread (S_{th}) is 50 mm.

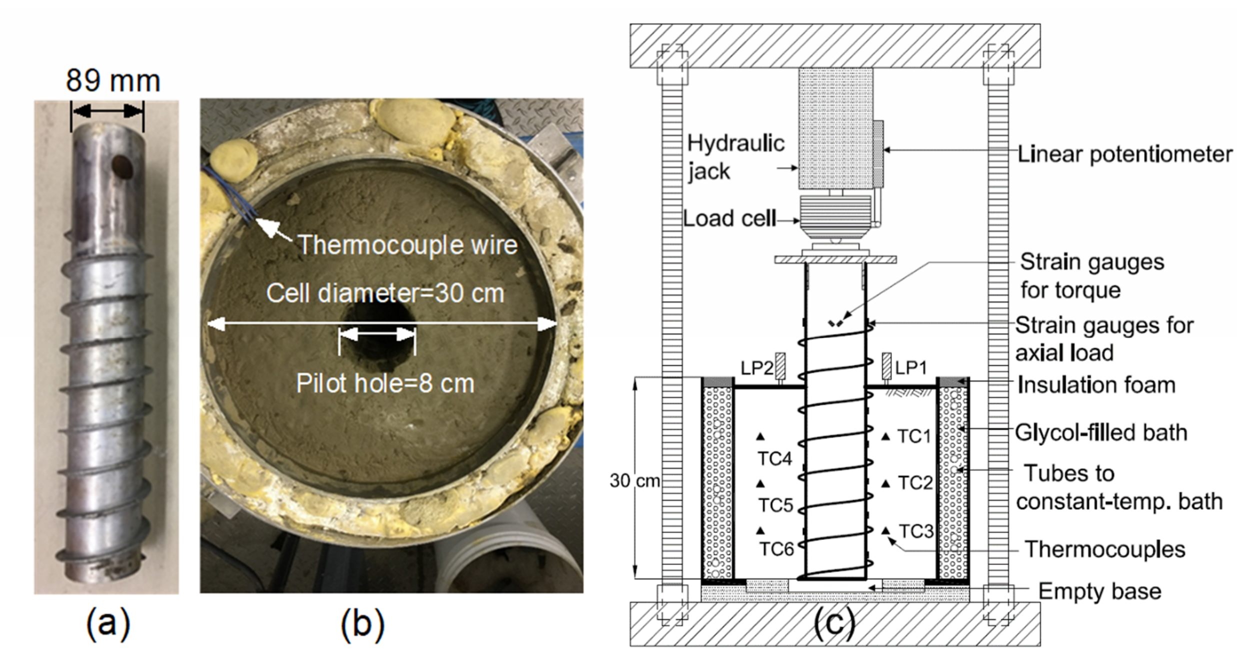

Figure 4.3 (a) Test pile segment; and (b) soil cell after consolidation or compaction; and (c) schematic of testing apparatus that was placed in a temperature control room.

4.2.2 Test Setup

The model pile tests were carried out in the Cold Regions Geotechnical Research Center at the University of Alberta. A series of short-term constant-displacement-rate axial load tests of continuous-flight piles were described by Gao et al. (2023a) to examine the adfreeze strength and pile failure modes. In the present research, the test setup (Figure 4.3c) identical to that in Gao et al. (2023a) was used for the constant load tests. The laboratory equipment consisted of a soil-pile test chamber, a servo-control hydraulic loading system, a temperature control bath, and a data logger. The soil was placed in the inner chamber and consolidated (or compressed) by applying 80 kPa of overburden pressure on the consolidation loading cap before use (Figure 4.3b). The outer chamber was filled with ethylene glycol for temperature control. To freeze the soil, ethylene glycol from a constant temperature bath was circulated through copper coils located in the fluid-filled outer chamber. The pile segment was twisted into a pilot hole in frozen soil using an electric driver by applying torque and compressive force on the pile head (Figure 4.4). The pile was then loaded under a series of constant applied loads. Details of model construction and test procedures are presented in Gao et al. (2023a).

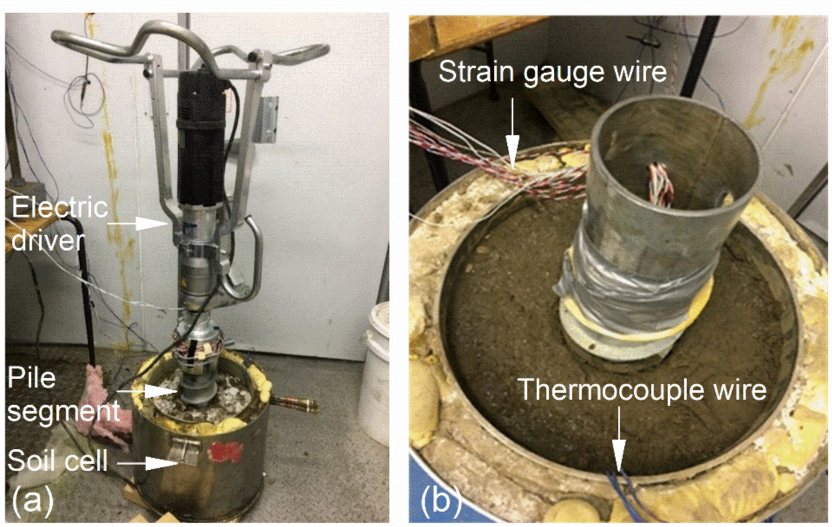

Figure 4.4 (a) Pile installation; and (b) test pile and cell after installation.

4.2.3 Instrumentation

During the testing, pile head loads Q_{head} were recorded using a load cell. Pile head displacement and ground surface settlement were recorded from the corresponding Linear Potentiometers (i.e., LP1 and LP2 in Figure 4.3c). A series of thermocouples (i.e., TC1-6 in Figure 4.3c) were embedded in the soil chamber at various depths and radial distances to record soil temperature during the entire test progress.

Research that addresses the internal load distribution of piles in permafrost is rare. Resistance strain gauges (SGs) were selected to measure installation torque and internal axial loads. Four torsional SGs were mounted on the same elevation near the pile head to form a full-Wheatstone bridge circuit that can compensate for the ambient temperature variation and eliminate the effects of axial loading (Figure 4.3c). For axial SGs, eight locations were selected along the pile shaft from the pile head to the tip. At each location, two SGs were mounted to the pile shaft surface and connected to a data acquisition system to form a half-Wheatstone bridge circuit. SGs were tested for survival and calibrated against axial load and torque before use.

4.2.4 Test Matrix

As shown in Table 4.1, four constant tests TCL1 to TCL4, which had various water content, freezing soil temperature and soil salinity, were conducted. A water content of 16 to 25%, a temperature of -0.6 to -4.8 ºC, and a salinity of 0 and 10 ppt were selected to cover the range of conditions encountered in coastal Arctic communities. Salinity *S* ppt (parts per thousand), is defined as the ratio of the mass of salt ions to the mass of porewater. The water content was reported as 15% for ice-poor soil and 35% for ice-rich soil in Inuvik, NWT (EBA 2004). Meanwhile, the soil temperature ranged from -0.3 to -4.1 ºC below 5 m depth and the salinity ranged from 5 to 11 ppt within a permafrost depth of 10 m in Inuvik, NWT (EBA 2004; Hivon and Sego 1993).

Table 4.1 Constant load test matrix

Test ID	Pile axial capacity (kN) [1]	Load increment, Q_{head} (kN)	Salinity, S (ppt)	Average and range of soil temperature, T (°C)	Average and range of water content, w (%) [2]	Degree of Saturation (%) [2]	Estimated unfrozen water content, w_u (%)	w_u (%) of Hivon and Sego (1995)
TCL1	2.8	0.3	0	**-0.9** (-0.6– -1)	**24.1** (23.5–25)	**66.9** (65.9–68.4)	**1.62** (1.5–2.14)	2.8
TCL2	Not measured	1, 4, 6, 9	0	**-2.2** (-1.1– -2.9)	**18.4** (17.1–20.4)	**56.3** (53.6–60.3)	**0.86** (0.71–1.4)	1.68
TCL3	43.2	15, 20, 30, 35, 40	0	**-4.7** (-3.5– -4.8)	**18** (17–18.6)	**56.6** (53.8–56.8)	**0.51** (0.5–0.62)	1.4
TCL4	31.9	10, 20	10	**-3.9** (-3.7– -4.2)	**16.9** (16.1–17.8)	**53.2** (51.4–55.1)	**2.51** (2.24–2.78)	3.63

Note: 1. The pile axial capacity was obtained from the short-term axial loading test of the continuous-flight pile in frozen soil (Gao et al. 2023a); 2. soil properties before freezing.

The constant load test is a common method to study the settlement rate and creep behavior of piles in frozen soil, since pile foundations are subjected to constant load rather than constant-displacement-rate during the service life. Johnston and Ladanyi (1974) conducted field constant load tests of screw anchors (i.e. helical piles) in permafrost, where the loads were applied in increments of 8.9 kN to a maximum of 22.2 kN and each load was maintained until a constant rate of strain was obtained. The duration of each load increment ranged from 1 to 18 h. Biggar (1991) examined the laboratory time-dependent behavior of model piles in saline frozen soils, for which a load increment of 5 kN was selected and the loading duration for each constant load ranged from 1 h to 83 days. In these constant load tests, the load increment was usually taken as a fraction of the pile axial capacities. For example, Fish (1982) adopted a load increment equal to 10-20% of the estimated pile capacity, and each load was held until the settlement rate is less than 0.2 mm/day. Heydinger (1987) suggested a criteria to stop the load in the constant load tests when the settlement rate is less than 0.5 mm/day.

The pile resistances at the ultimate limit states obtained from short-term constant-displacement-rate tests (Gao et al. 2023a) were referenced when determining the load increment in the present research. The initial constant loads were started from 10-35% of the limit pile resistance, which was the maximum load from the short-term load vs. displacement curves. If a minimum of 0.001 mm/h of displacement rate (i.e. primary creep) or a constant displacement rate (i.e. secondary creep) was obtained, the axial load would then be increased by 10-30% of the limit pile resistance. Load increments were continued until the failure was indicated by the acceleration of the pile displacement rate (tertiary creep), however, no tertiary creep was observed in the present study. The load was increased to the limit pile resistance or until the cumulative pile displacement reached a maximum of 20 mm the limit of the space available at the base of the pile (see Figure 4.3c).

4.3 Results

4.3.1 Installation Torque

The installation torque is one of the primary parameters in the evaluation of axial capacities for continuous-flight piles. Empirical or theoretical torque-capacity correlation can be applied to the pile design in unfrozen soils. Guo and Deng (2018) proposed a theoretical torque model to estimate the torsional resistance of continuous-flight piles installed in cohesive soils. However, there is no research on the torque-capacity relationship for continuous-flight piles in frozen ground. It is noticed in the present laboratory installation that the torque increased with the penetration depth and the maximum torque was observed at the last rotation during installation. Table 4.2 summarizes the maximum installation torque of the tests TCL1-4. The TCL1 with a temperature of -1.5 ºC experienced a maximum installation torque of 560 N·m and TCL3 with a temperature of 3 ºC reached a torque of 110 N·m. The installation torque decreased with warmer temperatures.

This can be attributed to the decreased soil shear strength due to the increasing volume of unfrozen water content in the pores of frozen soil when the temperature of soil increases. The test TCL4 with a salinity of 10 ppt and a temperature of 1.1 ºC experienced an installation torque of 165 N·m. The installation torque could be dependent on the soil temperature, salinity, and downsized ratio (pilot hole diameter/pile shaft diameter). The required installation torque in the field for full-scale continuous-flight pile is presumably proportional to the pile length.

Table 4.2 Soil temperature and maximum torque during installation

Test ID	**Soil temperature, *T* (ºC)**	**Maximum torque (N·m)**
TCL1	**1.3** (3 to 0)	57.0
TCL2	**-0.02** (0.38 to -0.39)	500
TCL3	**3.36** (3.88 to 2.6)	228
TCL4	**1.19** (2.1 to 1.05)	251

4.3.2 Soil Temperature Distribution

Figure 4.5a shows the time history of the average soil temperature of samples TCL1 and TCL3. The average soil temperature remained constant during the consolidation and loading phase, which indicated an effective temperature control system during the test. The average temperature was calculated from all six thermocouples (TC1-6 in Figure 4.3c) embedded at different depths and radial distances to the pile shaft. Figure 4.5b shows an example of the soil temperature (TCL3) at three different depths within the frozen soil. It is seen that the temperature differences among TC1-3 were negligible and a homogeneous temperature profile was obtained. In addition, the temperature fluctuation was less than 0.5 ºC during the loading period. Table 4.1 summarizes the average, maximum, and minimum soil temperature of tests TCL1-4.

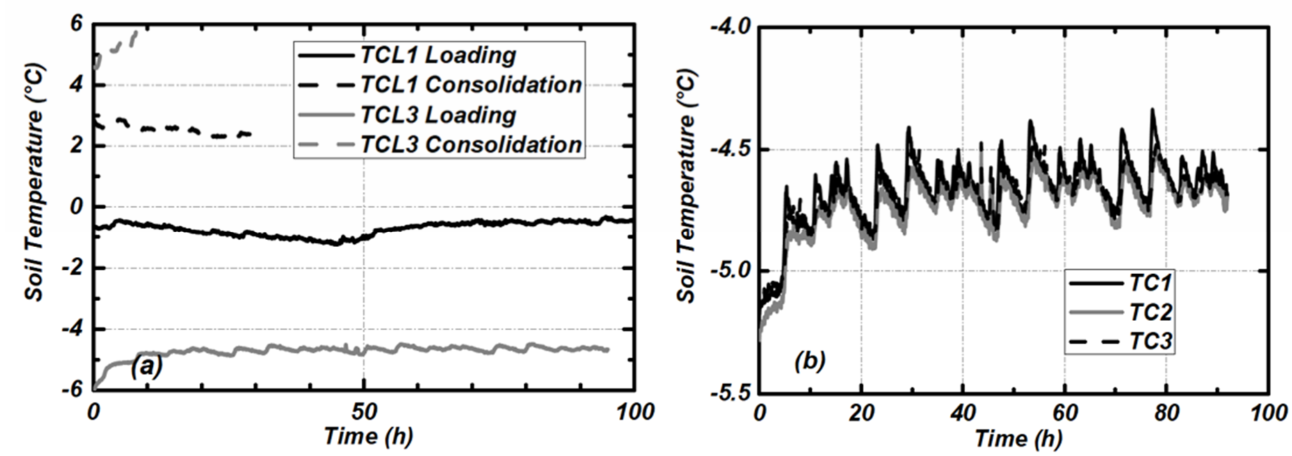

Figure 4.5 Example soil temperature readings: (a) Time histories of average soil temperature during consolidation and axial loading phases (TCL1 and TCL3); and (b) soil temperature in different layers during axial loading (TCL3).

4.3.3 Ground Surface Settlement During Loading

The ground surface settlement near the pile shaft was used to compare the pile displacement, therefore the soil-pile interaction can be inferred. Two Linear Potentiometers LP1 and LP2 were placed 1.5 cm and 2.5 cm away from the pile shaft wall to record the ground surface settlement during the loading of the test (Figure 4.3c). Figure 4.6a shows the comparison between pile head settlement and ground settlement in test TCL1 at the constant load Q_{head} of 300 N, where Q_{head} denotes the load applied to the pile head and recorded by the load cell. It is observed from Figure 4.6a that the pile settlement reached 16.3 mm within 5 h of loading, while limited ground settlements were observed (LP1=0.49 mm and LP2=0.13 mm). Figure 4.7a compares the ground surface settlements with pile head settlements when the value of Q_{head} was 9 kN in TCL2. It can be observed that the ultimate ground surface settlements ranged from 0.07 to 0.28 mm, which was 3.5-14% of the pile head settlement (=2 mm). When the soil temperature decreased from -2.2 ºC to -4.7 ºC, the comparison between ground surface settlement and pile head settlement in TCL3 is shown in Figure 4.8a. The ground settlements for LP1 and LP2 at Q_{head} of 40 kN were 0.45 mm and 0.34 mm respectively, which was 9-12% of pile head settlement (=3.7 mm). For the colder frozen soil (-3.9 ºC) with a salinity of 10 ppt, the ground settlements of TCL4 at Q_{head} of 10 kN were 3.4 mm and 2 mm (Figure 4.9a), which were 18% and 31% of pile head settlement (=11 mm). It implies limited soil settlement adjacent to the pile shaft when axially compressed under a constant load. The shear failure zone of the test TCL4 was greater than that of the TCL3 when the soil salinity decreased from 10 ppt to non-saline soil. It is also noted from Figures 4.7a and 4.9a that the ground settlement of LP1 was significantly larger than the value of LP2, which indicated a curve-shaped soil settlement zone near the pile shaft for each constant load test.

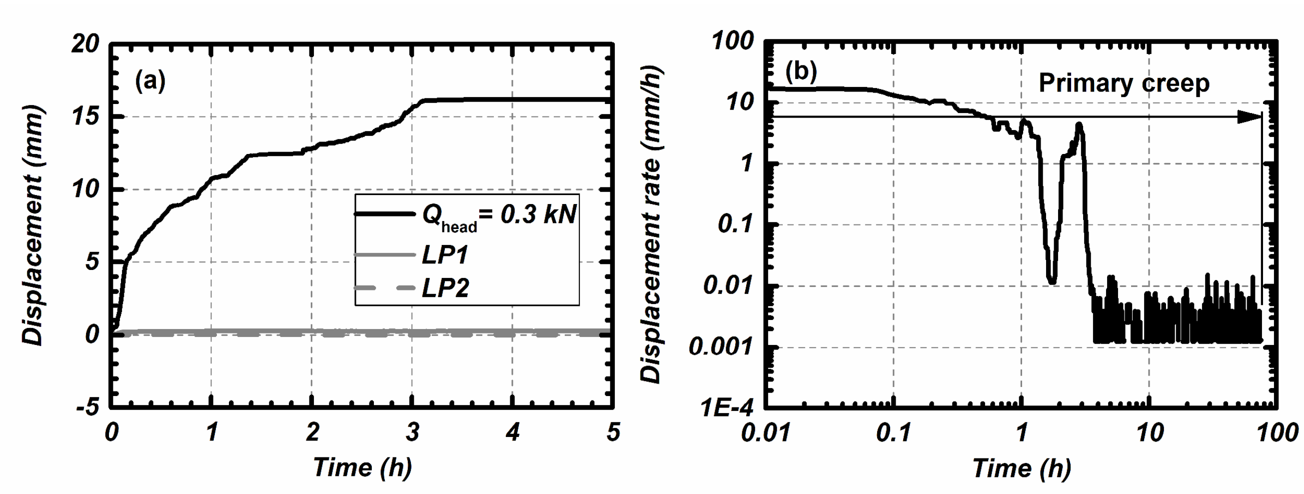

Figure 4.6 (a) Time history of pile displacement of TCL1; and (b) time history of pile displacement rate of TCL1. Note: LP1 and LP2 are the ground surface settlements at Qhead of 0.3 kN.

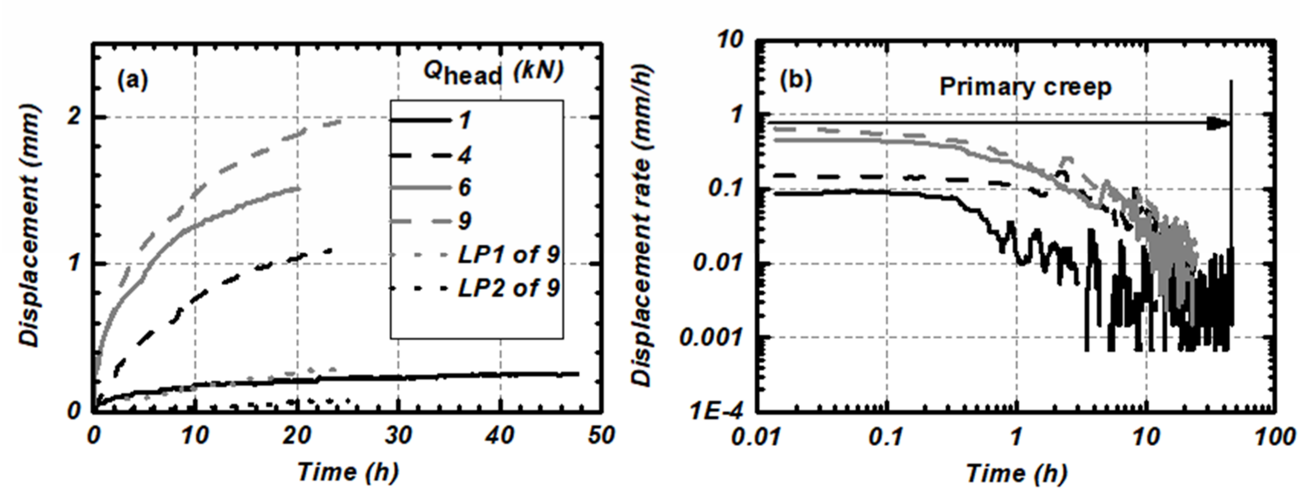

Figure 4.7 (a) Time history of pile displacement of TCL2; and (b) time history of pile displacement rate of TCL2. Note: LP1 and LP2 are the ground surface settlements at Q_{head} of 9 kN.

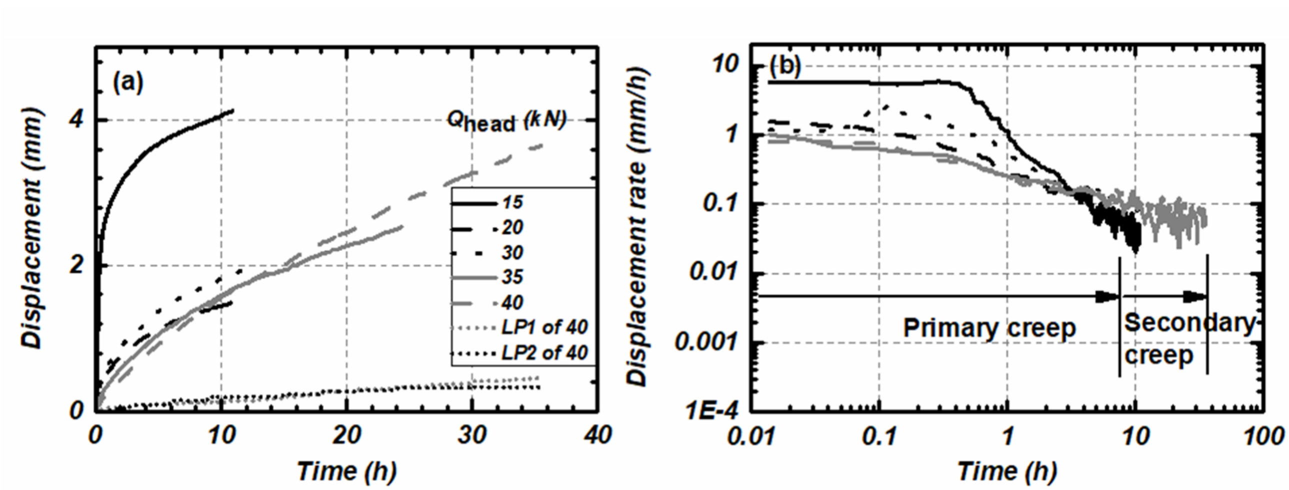

Figure 4.8 (a) Time history of pile displacement of TCL3; and (b) time history of pile displacement rate of TCL3. Note: LP1 and LP2 are the ground surface settlements at Q_{head} of 40 kN.

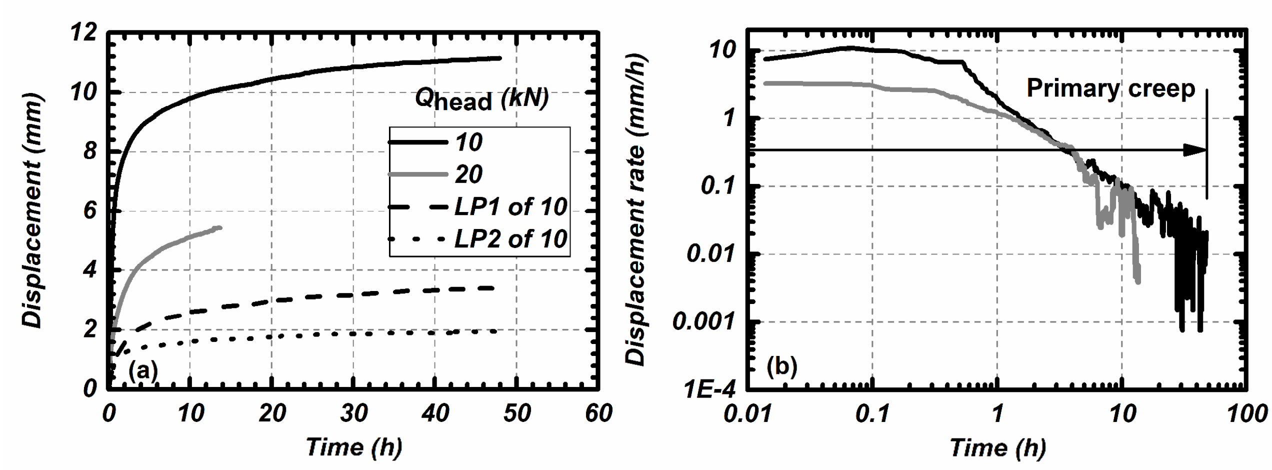

Figure 4.9 (a) Time history of pile displacement of TCL4; and (b) time history of pile displacement rate of TCL4. Note: LP1 and LP2 are the ground surface settlements at Q_{head} of 10 kN.

4.3.4 Estimated Unfrozen Water Content in Frozen Soil

The relationship between gravimetric unfrozen water content (w_u) and soil temperature (T), defined as the soil freezing characteristic curve, is essential in predicting the mechanical behavior of frozen soil. Tice et al. (1976) suggested the following equation to estimate w_u upon T:

$$w_u = \alpha |T|^{\beta} \tag{4-1}$$

where T is the soil temperature in ºC, and α and β are empirical parameters. Smoltczyk (2002) suggested the values α (= 1.5) and β (= -0.699) for silty sand; according to these parameters, the calculated w_u in the present study decreased from 1.62% to 0.51% when the temperature decreased from -0.9 ºC to -4.7 ºC, which indicates the ice lens changed by 1.1% when the temperature decrease by 3.8 ºC. The values of estimated w_u and initial saturation of each soil sample are listed in Table 4.1.

When the salt ions are present in the frozen soil, Andersland and Ladanyi (2004) proposed the following equation to determine w_u:

$$w_u = \frac{wS}{1000}\left(1 - \frac{54.11}{T}\right) \tag{4-2}$$

where S is the salinity in ppt. Therefore, the value w_u of TCL4 with 10 ppt of salinity is estimated to be 2.51% when the soil temperature is -3.9 ºC (Table 4.1). The presence of salt ions in the saline frozen soil enhances w_u compared to non-saline soil at the same T. Hivon and Sego (1995) measured the unfrozen water content of similar silty sand using the time-domain reflectometry (TDR) method. Table 4.1 shows the estimated w_u are comparable with the results from Hivon and Sego (1995), an increase in T and S causes an increase in w_u.

4.3.5 Pile Displacement Rate

The time history of pile head displacement and pile head displacement rate curves for tests TCL1-4 are summarized in Figures 4.6-4.9. A load of 300 N was initialized in test TCL1 (Figure 4.6a) and the corresponding pile head displacement increased to a steady value of 16.3 mm in 3 h. The pile displacement rate reached zero after 3 h of loading (Figure 4.6b), so the primary creep was observed. Four constant load tests, where the applied axial load Q_{head} equals 1, 4, 6, and 9 kN, were conducted in TCL2 and the loading durations of each load increment ranged from 20 to 48 h (Figure 4.7a). The load was paused and increased to the next high-level loads when the pile displacement rate was lower than 0.001 mm/h. It can be seen from Figure 4.7b that the pile displacement rates dropped to practically zero for all four loads. Hence it is reasonable to argue that the primary creep is dominant for TCL2. In addition, the pile at a maximum Q_{head} of 9 kN experienced a maximum displacement of 2 mm. However, Q_{head} did not show a significant influence on the pile displacement rates in test TCL2.

Loading steps in TCL3 ranged from 15 to 40 kN (Figure 4.8a). The time histories of displacement rates show that all creep rates reached constant values from 0.02 to 0.1 mm/h and steady creeps (secondary creep) were obtained (Figure 4.8b). In this case, the secondary creep was dominant and the primary creep could be negligible. Figure 4.9 shows the time history of the pile displacement rate of TCL4 with a salinity of 10 ppt. Only primary creep was observed during the two constant loading periods when Q_{head} equals 10 and 20 kN.

In a summary, secondary creep only was observed in test TCL3 with a temperature of -4.7 ºC and a salinity of 0 ppt. When the pore fluid became saline or the temperatures were relatively warm (-0.9 and -2.2 ºC), primary pile creep behavior was dominant.

4.3.6 Failure Mode Observation

Gao et al. (2023a) suggested two failure modes for continuous-flight piles under short-term axial loading. For piles in warm permafrost (at -1 ºC), soils around the pile segment failed as a cylinder shear mode (CSM, i.e global failure). The failure surface took place along the outer edge of the continuous threads. In this failure mode, the strength developed from the plate bearing is negligible and the shear resistance of the surrounding soil dominates. For piles in cold permafrost (at -5 ºC), an individual bearing mode (IBM) was observed by Gao et al. (2023a).

To assess the failure mode of piles under constant loads, the soil-pile model was excavated and examined after each loading test. Two failure modes were observed and inferred from the measured data (e.g. ground surface settlement). The CSM was observed in tests TCL1 and TCL2, then the load transfer mechanism from Gao et al. (2023a) was adapted for the shear stress calculation. For piles in the colder permafrost (TCL3 and TCL4), Figure 4.10a shows that the failure occurs locally in the soil beneath the pile threads rather not at the soil-shaft shear surface. The soil capped between threads was pushed down by the axial force (Figures 4.10b and 4.10c). In this IBM, the plate bearing stress and the shear stress are dominant.

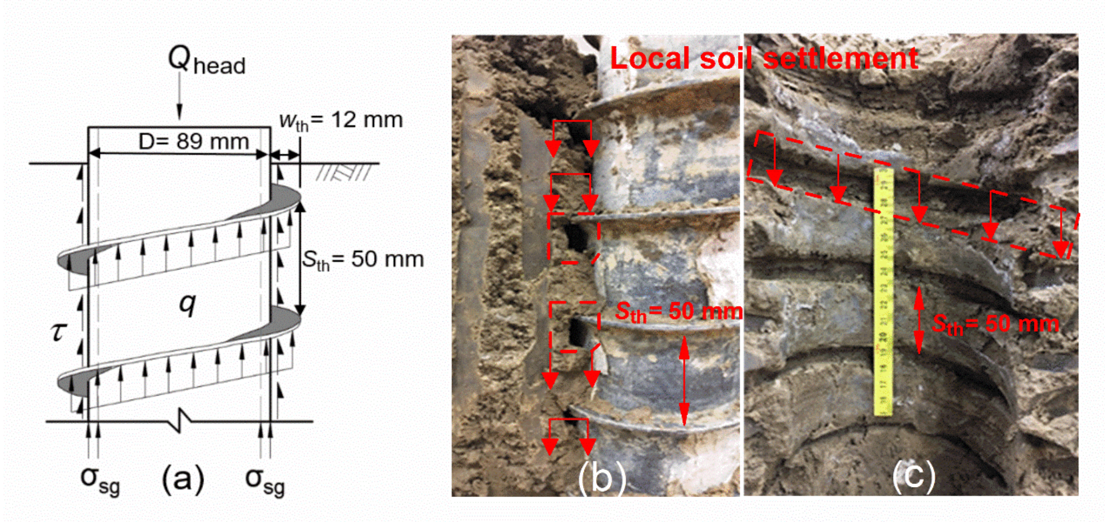

Figure 4.10 (a) Schematic of individual bearing mode for piles in cold permafrost at approximately -5 °C; and (b) observed slipping wedge; and (c) observed local failure (TCL3).

4.3.7 Load Transfer to Continuous-Flight Piles in Warm Frozen Soil

The axial load transferred to the continuous-flight pile segment under the CSM hypothesis, Q_{head}, was estimated using Equation 4-3 (Gao et al. 2023a):

$$Q_{head} = \tau\pi(D + 2w_{th})L \qquad (4\text{-}3)$$

where τ is the average shear stress of frozen soil; D is the pile diameter; w_{th} is the thread width; L is the pile segment length embedded in the soil.

Figure 4.11a shows the internal load distribution of TCL2 at Q_{head} of 4 and 5 kN; the values of Q_{head} were measured from LC and the internal loads Q were calculated from SG readings. It can be seen that the load distribution estimated from LC was consistence with the values of SGs. Figure 4.11b shows the values τ estimated from LC and SGs using Equation 4-3. The value of τ from LC was 49 kPa at Q_{head} of 4 kN, while τ estimated from SGs varied from 6 to 72 kPa. The value of τ from LC was 61 kPa at Q_{head} of 5 kN, while τ estimated from SGs ranged from 7 to 84 kPa. Figure 4.12a shows the internal load distribution of TCL2 at Q_{head} of 6 and 9 kN. The value of the average

τ was estimated at 73 kPa of 6 kN and 111 kPa of 9 kN. In Figure 4.12b, τ calculated from LC and SGs were compared. It is seen that τ at the failure surface was from 10 to 155 kPa. The values of τ from SGs were comparable to the values of τ estimated from LC.

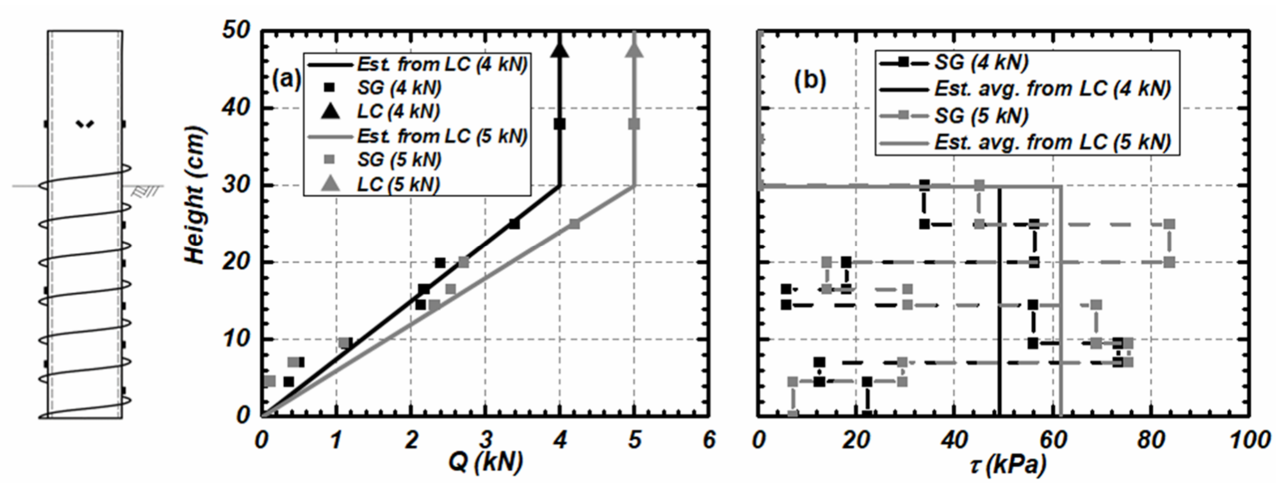

Figure 4.11 (a) Axial load distribution at Q_{head} of 4 and 5 kN of TCL2 (-2.2 °C, 18.4% and 0 ppt); and (b) shear stress distribution of TCL2. The "Est. avg. from LC" is average τ estimated from the load cell readings and "SG" is obtained from the strain gauge readings.

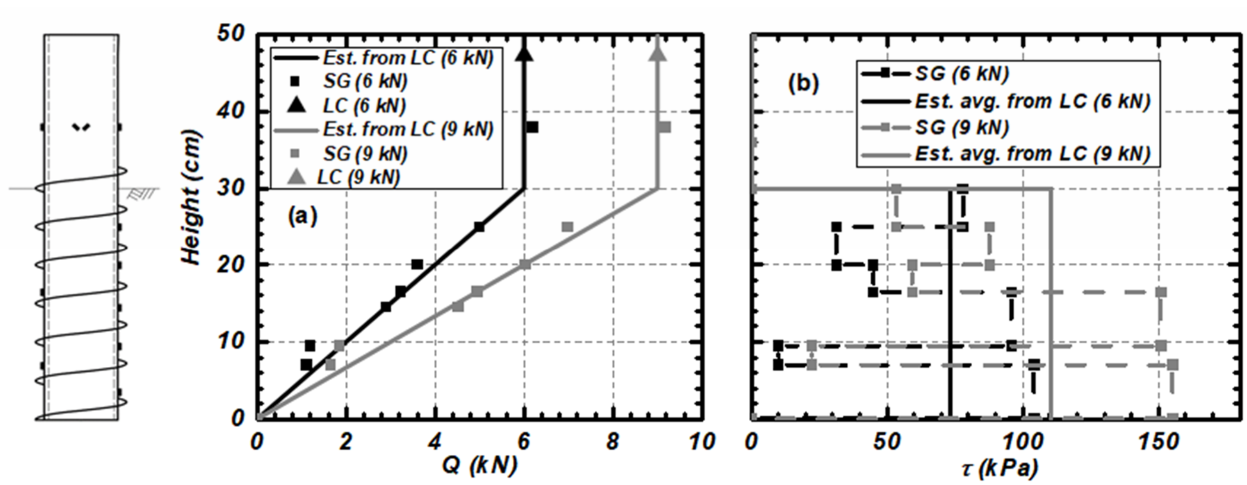

Figure 4.12 (a) Axial load distribution at Q_{head} of 6 and 9 kN of TCL2; and (b) shear stress distribution of TCL2.

In conclusion, the load distribution of test TCL2 calculated from the proposed load transfer mechanism was validated. Internal load distribution estimated from LC and SGs showed a favourable comparison using Equation 4-3. The estimated average shear stress τ increased with the increasing constant load.

4.3.8 Load Transfer to Continuous-Flight Piles in Cold Frozen Soil

The point resistance of a pile in frozen soil or ice tends to become proportional to the penetration rate after a mobilization period (Ladanyi and Paquin 1978; Sego 1980). Nixon (1978) applied a theory of creep settlement of strip footings in frozen soils (Ladanyi and Johnston 1974) to determine the dependence of the pile point resistance q (kPa) on the settlement rate $\dot{s} = ds/dt$ (mm/h), where s denotes the pile settlement (Figure 4.13a). This relationship is expressed as:

$$\dot{s} = I \cdot a \cdot B \cdot q^n \tag{4-4}$$

where I denote an influencing factor, which depends only on n; a is the pile toe radius or half-width of a strip footing; B (kPa^{-n}·h^{-1}) and n are the experimental creep parameters.

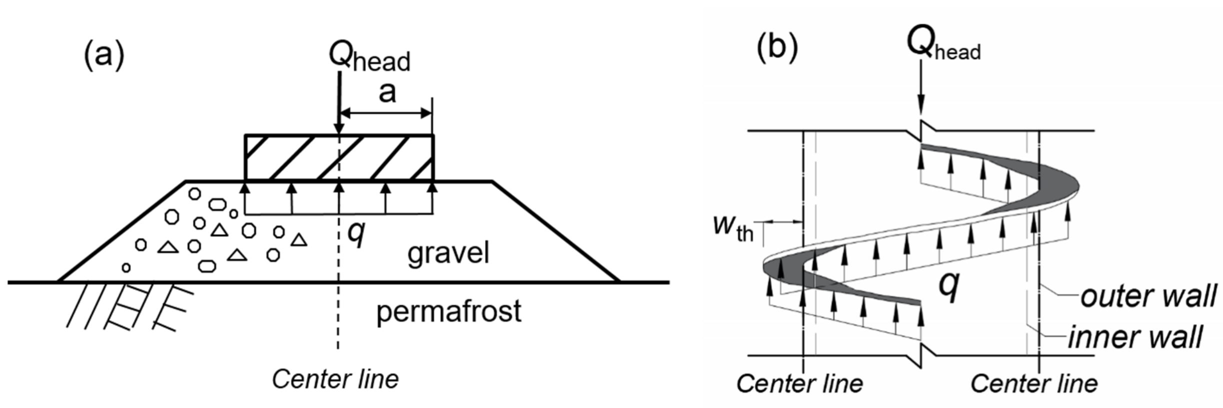

Figure 4.13 (a) Creep settlement of strip footings in frozen soil (adapted from Nixon 1988); and (b) schematic load transfer mechanism for continuous-flight piles in cold frozen soil.

The continuous thread embedded in the frozen soil is similar to the strip footing in the permafrost. A schematic load transfer mechanism for continuous-flight piles is drawn in Figure 4.13b based on the observation above. Because it is difficult to measure q directly although the pile had been instrumented, Equation 4-4 could be used for determining the relationship between the pile settlement rate $\dot{s}$ and the plate bearing stress q on the continuous threads. Following Equation 4-4, the average q provided by the continuous threads was estimated from the creep rate:

$$q = \left(\frac{\dot{s}}{I \cdot w_{th} \cdot B} \right)^{\frac{1}{n}} \tag{4-5}$$

where $\dot{s}$ is obtained from the present creep test results in Figure 4.8b. In the calculation, the width of threads w_{th} is taken as the same as the half-width a of a strip footing.

For the IBM shown in Figure 4.10a, the axial load Q_{head} transferred to the threaded segment is estimated as:

$$Q_{head} = \tau \pi DL + q w_{th} L_{th} \tag{4-6}$$

where L is the length of the pile segment and L_{th} is the length of the continuous helical threads that are embedded in the soil. Once q has been estimated, the average adfreeze shear stress τ along the pile shaft can be estimated as:

$$\tau = \frac{Q_{head} - q w_{th} L_{th}}{\pi DL} \tag{4-7}$$

It should be noted that the secondary creep only existed in test TCL3 with a stable minimum displacement rate $\dot{s}$ while the values of $\dot{s}$ for TCL1, 2, and 4 were practically zero, therefore the results of TCL3 are discussed herein.

Table 4.3 summarizes the values of $\dot{s}$, I, B, and n in Equation 4-5 for the estimation of q in TCL3. It is noted that q increased with the increasing $\dot{s}$. Figure 4.14a shows the load distribution at Q_{head} of 15 and 20 kN in test TCL3. Both curves show a linear load distribution between the loads estimated from LC and SGs. Figure 4.14b shows the values of q calculated from Equation 4-5 and the average τ calculated from Equation 4-7. The value of q was 680.4 kPa and τ was 13.4 kPa at Q_{head} of 15 kN. The values of q and τ were 745.4 and 49.5 kPa respectively when the load was increased to 20 kN. Meanwhile, the values of q calculated from the SG readings at Q_{head} of 15 and 20 kN ranged from 108 kPa to 2.5 MPa which were comparable with values from the calculations.

Table 4.3 Parameters used to estimate q in test TCL3

Q_{head} (kN)	Minimum pile displacement rate $\dot{s}$ (mm/h)	Width of threads w_{th} (mm)	Influence factor I [1]	B (kPa^{-n}·h^{-1}) [2]	n [3]	q (kPa)
15	0.02					680.4
20	0.024					745.4
30	0.05	12	0.4	$9 \cdot 10^{-9}$	2	1076
35	0.024					745.4
40	0.028					805.1

Note: 1. I was obtained from Nixon (1988); 2. B was obtained from unconfined compression tests of similar frozen soils in Hivon (1991); 3. n was obtained from Andersland and Ladanyi (2004).

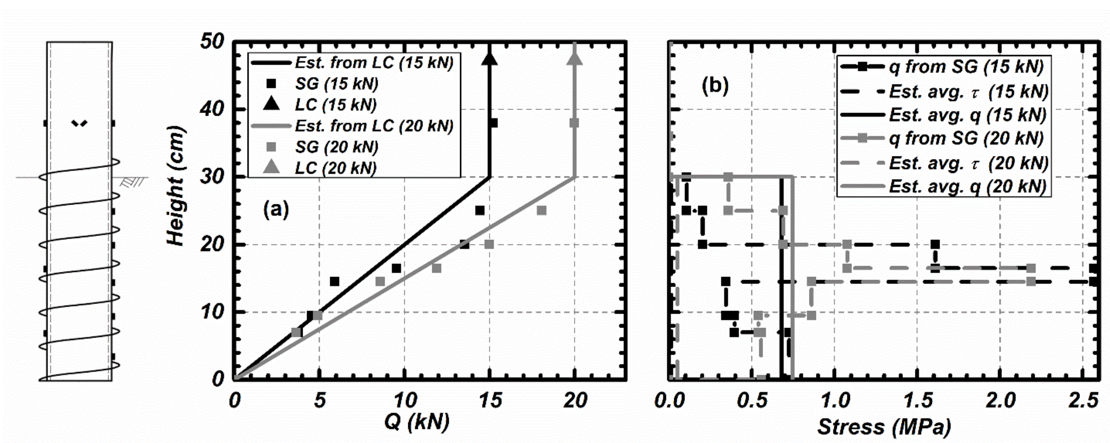

Figure 4.14 (a) Axial load distribution at Q_{head} of 15 and 20 kN in TCL3 (-4.7 °C, 18% and 0 ppt); and (b) stress distribution of TCL3. The "Est. avg. q and τ" is estimated from Equations 4-5 and 4-7, and "q from SG" is obtained from strain gauge readings.

The load and stress distribution at Q_{head} of 30, 35, and 40 kN in test TCL3 are shown in Figures 4.15-4.16. The linear load distribution and comparable stress distribution were also observed.

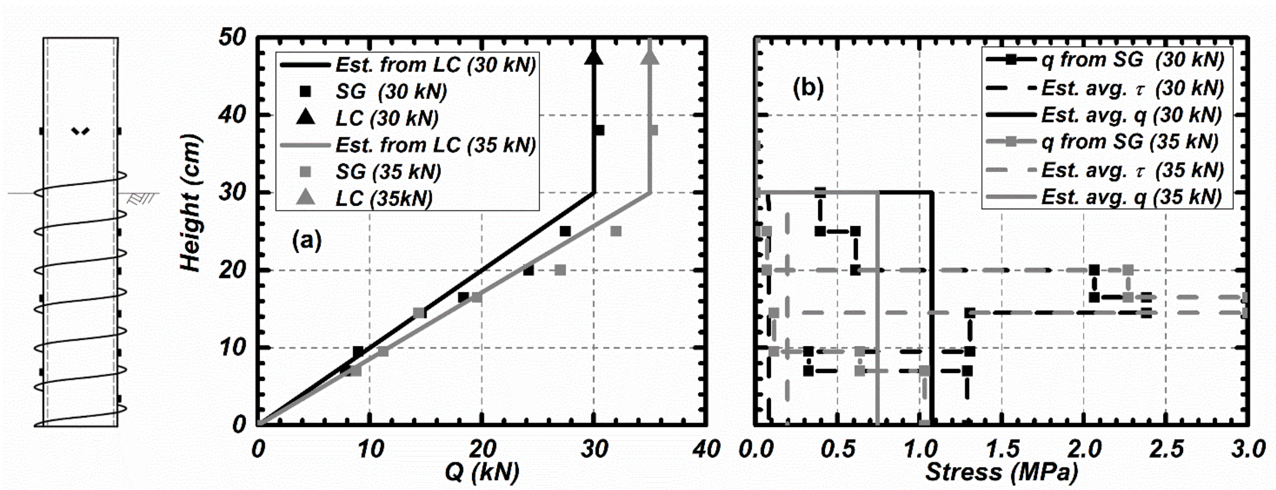

Figure 4.15 (a) Axial load distribution at Q_{head} of 30 and 35 kN of TCL3; and (b) stress distribution of TCL3.

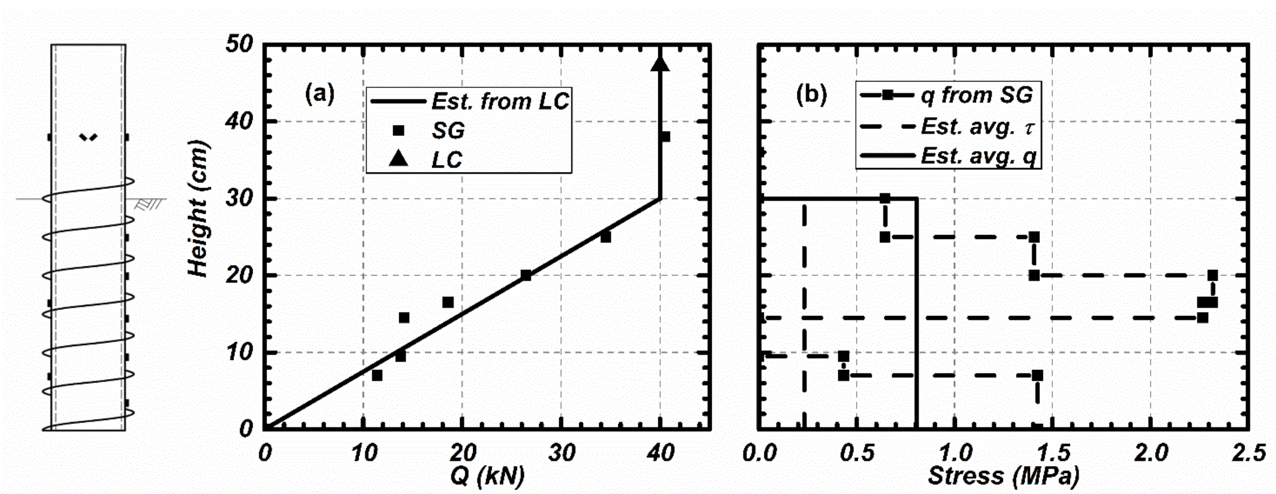

Figure 4.16 (a) Axial load distribution at Q_{head} of 40 kN of TCL3; and (b) stress distribution of TCL3.

Table 4.4 summarizes the values of τ and the corresponding adfreeze resistance ($Q_{shaft}=\tau \cdot \pi \cdot D \cdot L$), and q and the corresponding plate bearing resistance ($Q_{plate}=q_{th} \cdot w_{th} \cdot L_{th}$) at Q_{head} of 15-40 kN in test TCL3. The values of τ increased from 13.4 to 232.1 kPa when Q_{head} was increased from 15 to 40 kN. The shaft resistances Q_{shaft} were re-distributed as the Q_{head} increased. The value of the q was from 680.4 to 1076 kPa when $\dot{s}$ was increased. The adfreeze strength (τ_{ad}=240 kPa) and plate bearing strength (q_b=1410 kPa) from the short-term axial loading test (Gao et al. 2023a) with the same soil parameters were used to verify the estimated stress in the present study. It shows τ/τ_{ad} ranged from 0.06 to 0.97 when Q_{head} was increased from 10 to 40 kN. The value of τ shows a favourable agreement with τ_{ad} (τ/τ_{ad} =0.97) when Q_{head} reached the limit pile capacity (40 kN) of the short-term constant-displacement-rate test. The ratios of q/q_b ranged from 0.48 to 0.76, which indicates the plate bearing stresses calculated from the constant load tests were smaller than the strengths in the constant-displacement-rate tests in the same soil conditions. q/q_b ratios are reasonable because it is accepted that q increased with $\dot{s}$, and $\dot{s}$ in short-term loading (2.2 mm/h) is dramatically greater than $\dot{s}$ in the long-term constant load tests (0.02-0.05 mm/h).

Table 4.4 Summary of shear and plate bearing stress of TCL3

Q_{head} (kN)	Min. normalized pile displacement rate $\dot{s}/w_{th}$ (day^{-1})	Average τ (kPa)	Adfreeze shear Q_{shaft} (kN)	Average q (kPa)	Plate bearing Q_{plate} (kN)	τ/τ_{ad}[1]	q/q_b[1]
15	0.04	13.4	1.4	680.4	13.6	0.06	0.48
20	0.048	49.5	5.1	745.4	14.9	0.21	0.53
30	0.1	82.6	8.5	1076	21.5	0.34	0.76
35	0.048	195.2	20.1	745.4	14.9	0.81	0.53
40	0.056	232.1	23.9	805.1	16.1	0.97	0.57

Note: 1. τ_{ad}=240 kPa and q_b =1410 kPa, were obtained from the short-term axial loading test of the continuous-flight pile in frozen soil (Gao et al. 2023a).

Ladanyi and Johnston (1974) predicted and measured the values of q and $\dot{s}/b$ of screw anchors installed in permafrost, where b is the diameter of the screw anchor. In the present study q vs. $\dot{s}/w_{th}$ was used to compare the results from Ladanyi and Johnston (Figure 4.17). It can be seen that the estimated q from the present study was consistent with the values calculated from the creep date in Ladanyi and Johnston (1974).

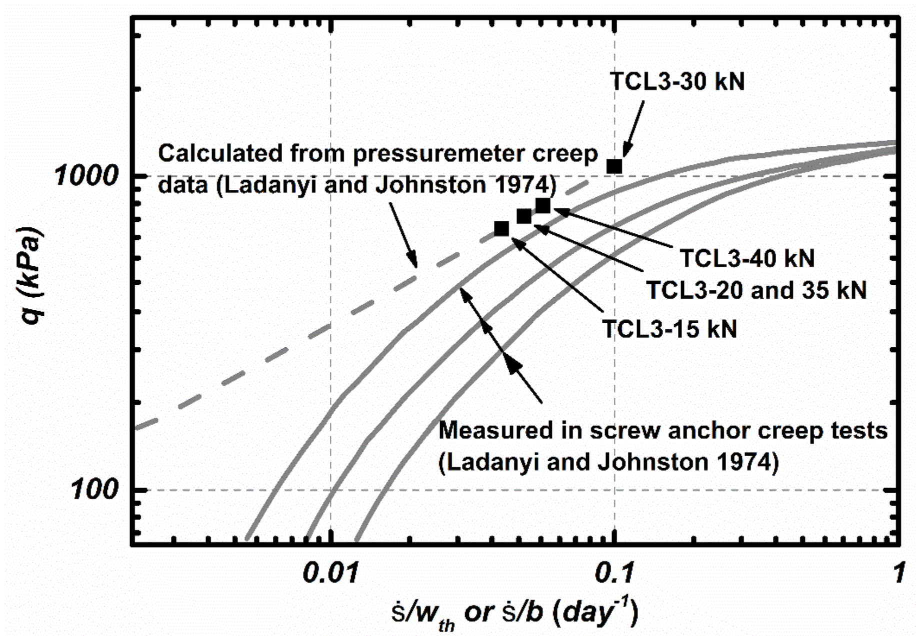

Figure 4.17 Plate bearing stress vs. minimum normalized pile displacement rate $\dot{s}/w_{th}$ ($\dot{s}/b$ in Ladanyi and Johnston, 1974).

In conclusion, the values of q and τ of piles under constant loads were estimated and verified from the literature. The values of q increased with the increasing $\dot{s}$ and mobilized when the constant load was increased. The shaft resistances were re-distributed as Q_{head} increased.

4.4 Conclusions and Limitations

In the present research, four continuous-flight piles were loaded under a series of constant load increments. The following conclusions can be drawn:

1. The continuous-flight pile can be screwed into an undersized hole in frozen soil by applying compressive load and torque. The required maximum installation torque increased with increasing penetration depth and decreasing temperature.

2. Limited soil settlement adjacent to the pile shaft was observed when the pile was axially compressed under a constant load. CSM and IBM were observed and inferred from the measured data. The two failure modes suggest beneficial larger capacity and smaller creep displacement compared to conventional smooth piles.
3. Primary and secondary dominant creeps were observed from the constant load tests. The estimated τ in CSM increased with the increasing constant load. The values of q in IBM increased with the increasing $\dot{s}$ and mobilized when the constant load was increasing. Pile shaft loads were re-distributed as the Q_{head} increased. The mobilized q suggests a potential increasing capacity of the continuous-flight pile over conventional smooth piles.

Limitations of the present research may be noted. First, the required installation torque would change if a different pilot hole size and temperature are selected. The effects of pilot hole size, soil temperature, and salinity on the pile installation performance are not discussed herein; second, due to the lack of load increments and duration criteria in the constant load tests, the results in the present research might be different if the load increments and load duration changes; lastly, the values of q and τ are estimated from the equation rather than measurement.

5 Laboratory Investigation of Torsional Installation Method for Continuous-Flight Pile in Frozen Soil[3]

5.1 Introduction

Pile foundations are widely used in the Canadian Arctic. Timber piles were used in the 1950s for residential homes and above-ground infrastructure; in the past decades, commercial structures are commonly supported by steel pipe piles or recent thermopiles. Guo and Deng (2018) introduced screw micropiles, also termed continuous-flight piles by Gao et al. (2023a), into the foundation industry of southern Canada. This pile type, unlike aforementioned piles, is directly screwed into unfrozen ground by torque. Gao et al. (2023a) investigated the short-term axial behavior of continuous-flight piles in different frozen soil conditions. Gao et al. (2023b) studied the load transfer mechanism and failure modes associated with the shaft resistance of the continuous-flight piles; in the study, they evaluated the effects of soil temperature, water content, and soil salinity on the long-term creep rate of piles. These studies verified that continuous-flight pile is a viable foundation solution in permafrost of the Canadian Arctic.

Traditional steel piles are placed in an oversized predrilled hole and then the annulus is backfilled with gravel or cement-based slurry intended to freezeback at cold temperatures (Biggar and Sego 1993). The duration of the freezeback waiting period required to fully mobilize the pile capacity may vary from several days to months (Shang et al. 2018), depending on the air temperature at the site. Moreover, the freezeback and pile construction process may disturb the thermal regime of the surrounding permafrost. Specifically, during the cement hydration process, heat is released as a result of the exothermic reaction between cement and water (Hou et al. 2022). This can cause the temperature of the surrounding permafrost to increase, which in turn affects the

[3] A version of this chapter will be submitted to a peer-reviewed journal

mechanical properties of the soil and reduce the pile capacity at the early stage (Shang et al. 2018). Since climate change warms permafrost and thickens the active layer, alternative installation technology, such as torsional or driving methods, may be feasible for piles in permafrost. Gao et al. (2023a, 2023b) installed continuous-flight piles by torque into undersized pilot holes of warm frozen soils. To extend the technology to field application, it is meaningful to investigate the torque required to install the continuous-flight pile into warm frozen soils that are widespread in the Canadian Arctic due to climate change. This torsional installation method may promise a fast construction process, reduced noise and vibration, and a cost-effective solution compared to conventional methods. The absence of backfilling and freezeback may minimize thermal disturbance to the ground and allow the pile to be immediately loadable. The torsional method also aims to improve the vertical alignment of the pile, minimize the ground heave and fully displace the soil to maximize the lateral earth pressure on the pile shaft, ultimately increasing the pile capacities.

Current guidance on screw piles in unfrozen soils recommends pitch-matched installation method to minimize soil disturbance and maintain post-installation pile capacity (Perko 2009). Understanding installation torque or torsional resistance is crucial for helical piles and continuous-flight piles. The required installation torque and pile capacity can be estimated upon the soil shearing resistance developed along the embedded area of the pile, including the shaft and helical plates (Harnish and El Naggar 2017). While there are several studies on the installation torque of screw piles in unfrozen soil (Ghaly and Hanna 1991; Sakr 2013; Guo and Deng 2018; Cerfontaine et al. 2021; Sharif et al. 2021a and 2021b), there is no published research on the torque of continuous-flight piles required to install the pile in frozen soils.

The present study is aimed at understanding the performance of continuous-flight pile during the installation stage in laboratory-frozen soils, in order to guide the field application of this pile type in permafrost of Canada. A primary objective of the present research is to examine the effects of soil temperature (t_{soil}), gravimetric water content (w), and salinity (S) on the installation torque (T) of pile segments. A series of installation tests of pile segments with a shaft diameter of 88.9 mm and a length of 300 mm at various frozen soil parameters were carried out in the laboratory. A simple analytical model for torque based on sleeve resistance was developed. The study also examined the thermal stability of frozen soil when piles were installed.

5.2 Laboratory Experimental Program

5.2.1 Test Soil and Piles

Silty sand is commonly distributed in the Mackenzie River delta area in Northwest Territories, Canada. The present study uses a mixture of silt and silica similar to the soil examined by Hivon and Sego (1995). Biggar and Sego (1993) and Hivon and Sego (1993 and 1995) thoroughly tested the properties of these frozen soils.

Continuous-flight piles can have different lengths and diameters to meet specific performance requirements in the field. In this study, a straight threaded segment (Figure 5.1a) and a straight smooth segment with a diameter of 88.9 mm and a length of 300 mm were utilized. Further description of the pile type and their engineering behavior in unfrozen soils can be found in Guo and Deng (2018).

5.2.2 Test Equipment setup

This research characterized the torque of continuous-flight piles and soil temperature subjected to the torsional installation method, using the facilities of the Cold Regions Geotechnical Research Center at the University of Alberta. The applied axial compressive load on a pile head when a pile is screwed into the soil is termed crowd load (N). The installation tests were performed in a temperature-controlled cold room that was equipped to maintain temperatures as low as -40 °C.

The laboratory system consists of test pile segments, an electric rotary motor with a reaction bar (Figure 5.1a), a soil cell (Figure 5.2a), a temperature control system, and a data logger.

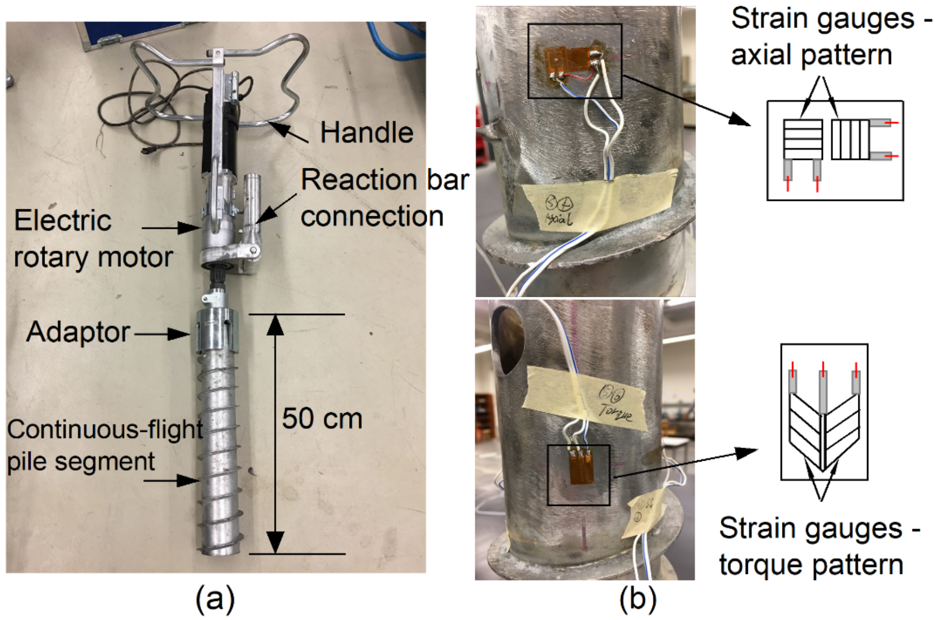

Figure 5.1 (a) photo of continuous-flight pile segment and electric rotary motor; (b) photo and schematic strain gauges pattern.

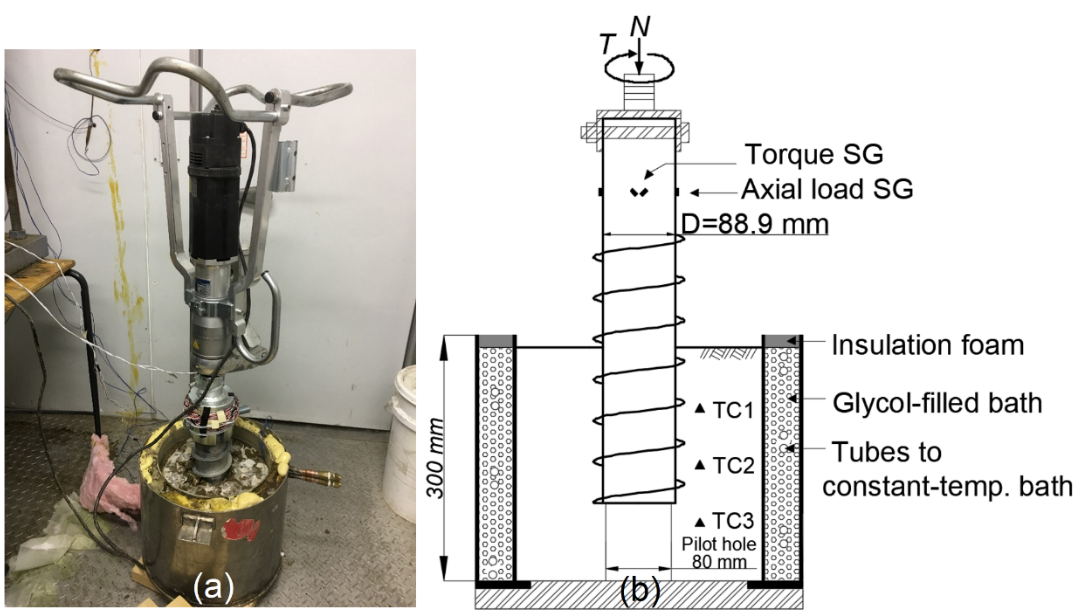

Figure 5.2 (a) photo of pile installation; and (b) schematic of soil cell and pile segment.

As shown in Figure 5.2b, the soil sample was housed within an inner cell that was surrounded by an outer cell filled with ethylene glycol. The outer cell was utilized to maintain a constant temperature for the soil mass. The temperature was regulated by circulating ethylene glycol (a refrigerant) from a constant temperature bath through copper coils in the outer cell. The electric rotary motor can maintain proper pile alignment and position. The reaction bar on the side of the rotary motor prevents the rotation of the motor head.

5.2.3 Instrumentation

Resistance strain gauges (SG) are electrical resistors that measure strain, according to the principle that a change in specimen length results in a change in SG diameter and resistance. In this study, strain gauges were glued on the pile shaft's outer surface to measure internal strains, and thus the installation torque and axial crowd load could be examined. At the pile head, four strain gauges were mounted at 45° and 135° relative to the pile's axial direction and at the same elevation (Figure 1b), forming a full-Wheatstone bridge circuit that can compensate for ambient temperature changes and cancel the errors from the axial loading. Once the shear strain ($\gamma = 2\varepsilon$, where ε is the normal strain along the strain gauge's direction, according to the strain transformation principle) is obtained, the installation torque is calculated by:

$$T = \frac{\tau J}{R} = \frac{\gamma G J}{R} = \frac{\gamma G}{R}\frac{\pi}{2}(R^4 - r^4) \tag{5-1}$$

where τ is the shear stress, G is the shear modulus of pile material (steel), R (= 44.45 mm) is the outer radius of the pile shaft, J is the polar moment of inertia of the tubular cross-section, and r (= 40.85 mm) is the inner radius of the pile shaft. The yield shear strength (τ_y) of steel when subjected to simple shear could be estimated to be $1/\sqrt{3}$ times its tensile yield strength (σ_y) based on the Von Mises criteria or $0.5\sigma_y$ based on the Tresca criteria. The pile shaft and threads in this research are made from structural steel, which has a Young's modulus of 210 GPa and σ_y of 248 MPa. Thus, the estimated τ_y ranges from 124 to 143 MPa. The first yield torque T_y ranges from 5.1 kN·m to 5.9 kN·m using Equation 5-1.

To measure the axial load during the stages of installation or axial loading, two pairs of axial and hoop strain gauges (Figure 5.1b) were mounted on the pile shaft outer surface at the same elevation to form a full-Wheatstone bridge circuit. The axial crowd load (*N*) has a crucial importance in selecting appropriate equipment or inferring in-situ soil strength. The crowed load is calculated by:

$$N = \sigma A = \varepsilon E A \tag{5-2}$$

where *E* is the Young's modulus of the pile shaft material (steel), ε is the axial strain, and *A* is the cross-sectional area of the pile shaft. Given σ_y of 248 MPa, the yield crowd force (N_y) is 239 kN using Equation 5-2. The maximum allowable crowd force shall be significantly lower than N_y as the pile shaft may buckle. Strain gauges were calibrated against torque and crowd load before each test.

Thermocouples (TC) were placed at the top, middle, and bottom layers (TC1, TC2, and TC3 in Figure 5.2b) to monitor the soil temperature distribution during the entire test progress. The thermocouples were calibrated before each test.

5.2.4 Test Matrix

To investigate the performance of continuous-flight piles at the stage of torsional installation in frozen soils, twenty-three pile segments were installed in the soil with temperatures ranging from 3.43 to -1.88 °C. As shown in the test matrix (Table 5-1), the water contents of 16.9% to 26.9% were selected. The porewater salinity (*S*, in ppt) of frozen soil is defined as:

$$S = \frac{m_{salt}}{m_{water}} \tag{5-3}$$

where m_{salt} (in g) is the mass of salt ions and m_{water} (in kg) is the mass of porewater in the frozen soil. The salinity of 10 ppt of sodium chloride was selected to mimic the soil conditions in the coastal Canadian Arctic communities (see detail in Gao et al. 2023a). In addition to the tests SCD1 to SCD4 (Table 1), which utilized a straight smooth pile segment, the remaining installation tests employed a straight threaded pile segment (Figure 5.1a).

Table 5.1 Test matrix

Test ID [1]	**Pile type**	**Salinity, S (ppt)**	**Average water content, w (%)**	**Average and range of soil temperature, t_{soil} (°C)**	**Max torque, T (N·m)**	**Average sleeve resistance, f_s (kPa), and pile depth at max torque (cm)**
IN1	Threaded	0	20.0	**-0.25** (0.19– -0.72)	535	108@25.5
IN2		0	20.0	**-0.8** (-0.49– -1.0)	211	86.8@12.5
IN3		10	20.0	**0.14** (0.34– 0.01)	110	21.8@25.0
IN4		10	20.0	**-1.38** (-0.85– -2.12)	317	81.6@20.0
IN5		10	20.0	**-1.25** (-1.12– -1.44)	772	153@26.0
IN6		10	20.0	**-1.88** (-1.67– -1.93)	Refused	NA
IN7		0	20.0	**-1.0**	Refused	NA
TCD1		0	25.5	TC Malfunction	21.0	4.08@23.0
TCD2		0	20.2	**-0.07** (-0.03– -0.13)	340	76.1@23.0
TCD3		0	26.9	**-0.54** (0– -1.37)	195	41.1@24.5
TCD4		0	19.5	**0.67** (0.86– 0.49)	137	25.9@27.3
TCD5		10	22.1	**-0.44** (-0.23– -0.77)	263	63.6@21.3
TCD6		10	19.8	**-0.76** (-0.63– -0.92)	326	66.3@25.3
TCD7		10	24.5	**-0.09** (0.82– -0.43)	149	30.7@25.0
TCD8		10	20.1	**-0.63** (-0.53– -0.76)	141	25.9@28.0
TCL1		0	24.1	**1.30** (3.87– 0.90)	57.0	11.5@25.5
TCL2		0	18.4	**-0.02** (0.38– -0.39)	500	92.1@28.0
TCL3		0	18.0	**3.36** (3.88– 2.60)	228	40.5@29.0
TCL4		10	16.9	**1.19** (2.10– 1.05)	251	51.6@25.0
SCD1	Smooth	0	20.2	**-0.08** (0.29– -0.29)	9.12	2.82@26.0
SCD2		0	19.9	**0.08** (0.41– -0.11)	5.07	1.46@28.0
SCD3		10	20.0	**0.08** (0.34– -0.26)	10.7	3.26@26.4
SCD4		10	19.7	**-0.18** (0.13– -0.40)	6.76	2.09@26.0

Note: 1. IN = Piles installed without subsequent axial loading tests; TCD and SCD = Piles installed with subsequent short-term axial loading tests; TCL = Piles installed with subsequent long-term axial loading tests.

5.2.5 Model Construction and Test Procedure

Before installing a pile, the soil sample with the desired water content and salinity was prepared and consolidated in the inner test cell. A pilot hole was constructed while the soil was compacted and consolidated. The diameter of the pilot hole depends on the laboratory or field installation equipment and pile shaft size. In the present study, a diameter of 80 mm was selected after trying several pilot hole diameters, simulating a pilot hole slightly smaller than the diameter of a pile shaft (D = 88.9 mm). This resulted in a downsized ratio of 0.9 (pilot hole diameter/pile shaft diameter). Other pilot hole sizes may also be adopted in the laboratory or field, however, the effects of pilot hole size on the installation torque were not investigated in this study. To create the pilot hole, a PVC cylinder was left in the center of the soil cell during the preparation and consolidation process. The PVC cylinder was removed before installing the test pile segment. Ethylene glycol was circulated through the outer cell until the desired test temperature was reached, as indicated by the thermocouples. To maintain consistency in the construction method, the smooth segment was also screwed into the same size pilot hole by applying torque and crowd force on the pile head.

The installation procedure involves several steps to ensure a successful and accurate measurement. Firstly, the test cell was fixed on the ground and the center pile segment was positioned over the pilot hole. Then, the continuous-flight pile head was attached to the torque adaptor using a screw pin. The pile segment was pushed downwards until the bottom flight contacts the ground surface, and the alignment of the rotary motor was checked using a level gauge and stabilized with a reaction bar. The installation process begins with the rotation of the pile while applying a crowd force, and depth was recorded at select intervals. Upon completion, the final depth, torque, and temperature were recorded.

5.3 Results

5.3.1 Soil Temperature During Installation

Figures 5.3a to 5.5a illustrate the measured soil temperatures in tests SCD1, TCD6, and TCD7 during the installation period. The average temperature was determined by averaging the readings from all thermocouples placed in the soil sample. TC1 thermocouples were situated 7.5 cm below ground surface, TC2 thermocouples were located at the center of the soil, and the TC3 thermocouples were 7.5 cm above the bottom of the test cell (Figure 5.2b). The soil cell has a total depth of 30 cm. It is observed that all soil temperatures in different layers remained stable with a variation of less than 0.1 ºC and the temperature fluctuation of the three layers remained under 0.9 ºC during the installation period. A consistent and uniform temperature profile throughout the soil was observed. The results indicate a negligible thermal disturbance of the soil during the torsional installation.

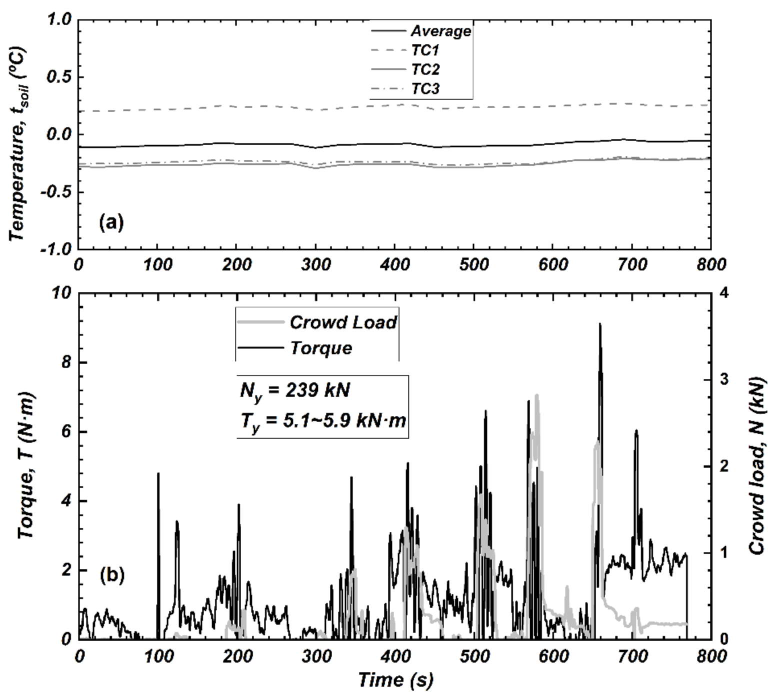

Figure 5.3 (a) Time history of soil temperature during installation; and (b) time history of installation torque and crowd load (SCD1).

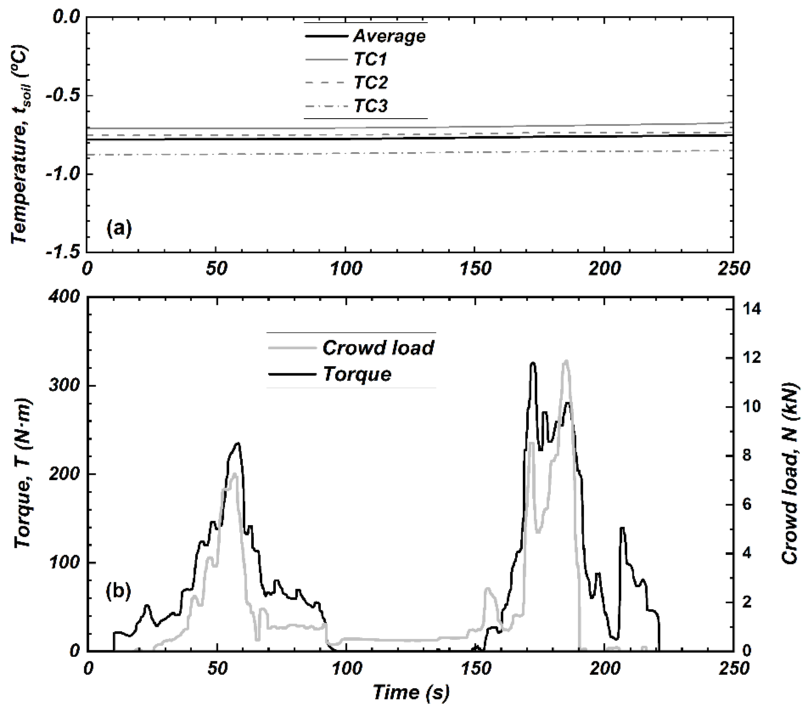

Figure 5.4 (a) Time history of soil temperature during installation; and (b) time history of installation torque and crowd load (TCD6).

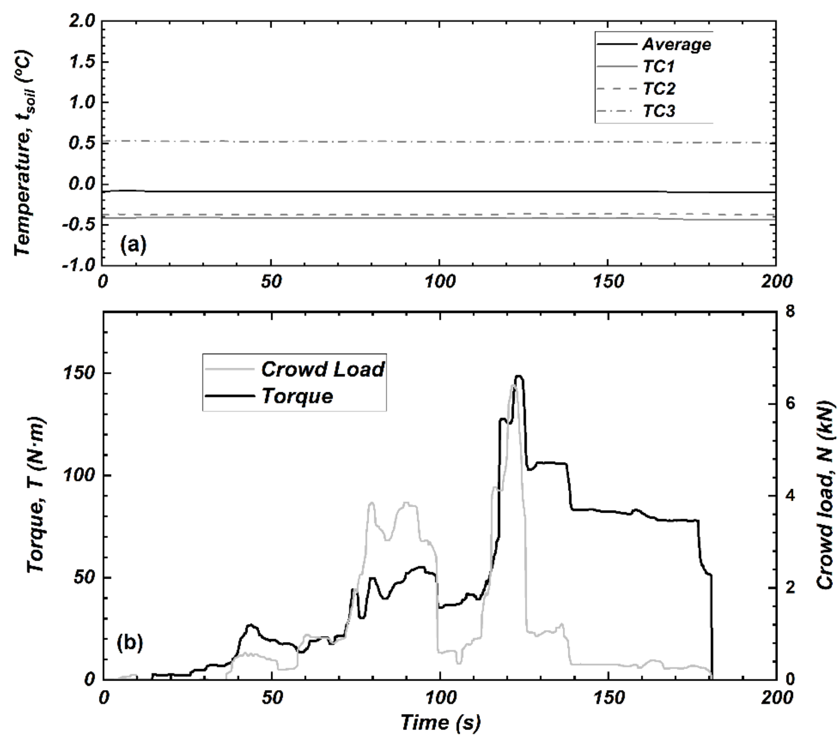

Figure 5.5 (a) Time history of soil temperature during installation; and (b) time history of installation torque and crowd load (TCD7).

5.3.2 Installation Torque

The torque required for installing piles in the soil is crucial in determining the potential axial capacity of continuous-flight piles and selecting field equipment. Table 1 summarizes the required maximum torques of all piles installed in the present study. It is observed that the smooth pile exhibited the lowest torque from 5.07 to 10.7 N·m at average soil temperatures from 0.08 to -0.18 ºC. Due to the lack of threads on smooth piles and the use of a rotary motor for installation, the smooth piles were primarily pushed in under the influence of crowd force instead of torque.

The required maximum torque for continuous-flight piles ranged from 21.0 to 772 N·m with different soil conditions. These torque values are significantly lower than the yield torque T_y (5.1 to 5.9 kN·m). This is important for ensuring the integrity of the pile shaft, because excessive torque can lead to permanent twisting failure of the pile shaft. The range of torque values highlights the importance of considering specific soil conditions when designing and installing continuous-flight piles into the permafrost. Test IN5 with an average temperature of -1.25 ºC, a water content of 20%, and a salinity of 10 ppt exhibited a maximum installation torque of 772 N·m. It is generally recognized that the required torque increases with decreasing temperature. However, salinity and water content do not show a significant impact on the required installation torque within the temperature from 3.43 ºC to -1.88 ºC.

Torque refusal, caused by the limited capacity of the electric rotary motor in the laboratory, was observed at -1.0 ºC in 0 ppt soil (IN6) and -1.88 ºC in 10 ppt soil (IN7). When torque refusal was reached, the pile stopped advancing downward and instead rotated in place. The soil between the threads was compressed and shredded as shown in Figure 5.6.

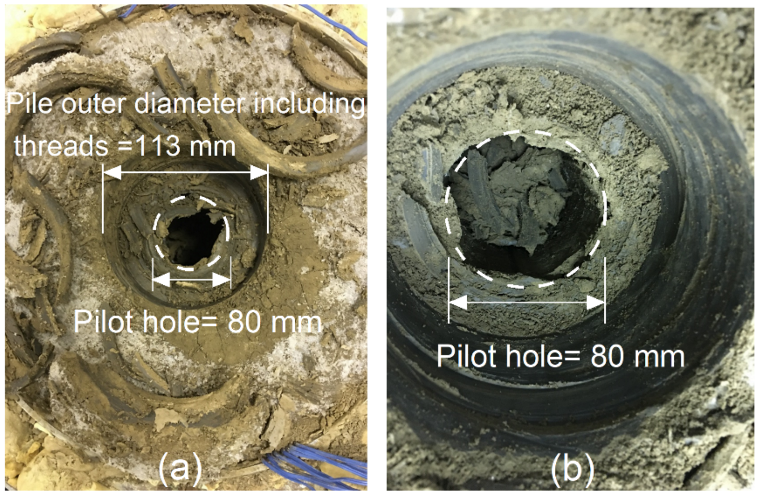

Figure 5.6 Photos showing the refusal: (a) IN7: -1 °C, 20% and 0 ppt; and (b) IN6: -1.88 °C, 20% and 10 ppt.

Figures 5.3b to 5.5b show the time history of installation torque and the corresponding crowd load in selected tests SCD1, TCD6, and TCD7. The torque and crowd load were manually imposed onto the pile head using the electric rotary motor. Each spike value in the time histories corresponds to a revolution when the pile was rotated and advanced downward, and the history valley usually suggested a manual break in advancing. It is observed from Figures 5.3b to 5.5b that the peak values of torque and crowd load almost occurred simultaneously. The values of crowd load measured in these tests ranged from 2.82 to 11.9 kN, which are significantly lower than the yield crowd force (N_y) of 239 kN. This indicates that piles were able to withstand the crowd loads applied during the installation process without undergoing permanent deformation or failure.

5.3.3 Relationship between Installation Torque and Penetration Depth

Because axial advancing displacement of piles was not measured, time histories of torque were used to infer the penetration depth. The torques were manually selected from the peak value of each revolution, and axial penetration depths were calculated from the final depth and the total revolution number. Following this estimative methods, Figure 5.7b illustrates the selected peak torques of each revolution in TCD4 and Figure 5.8b depicts the selected peak torque in IN3. Figures 5.7c and 5.8c show the relationship between the measured installation torque and the penetration depth. It is seen from Figures 7c and 8c that the measured installation torque mainly increased with the increasing embedment of the pile segment.

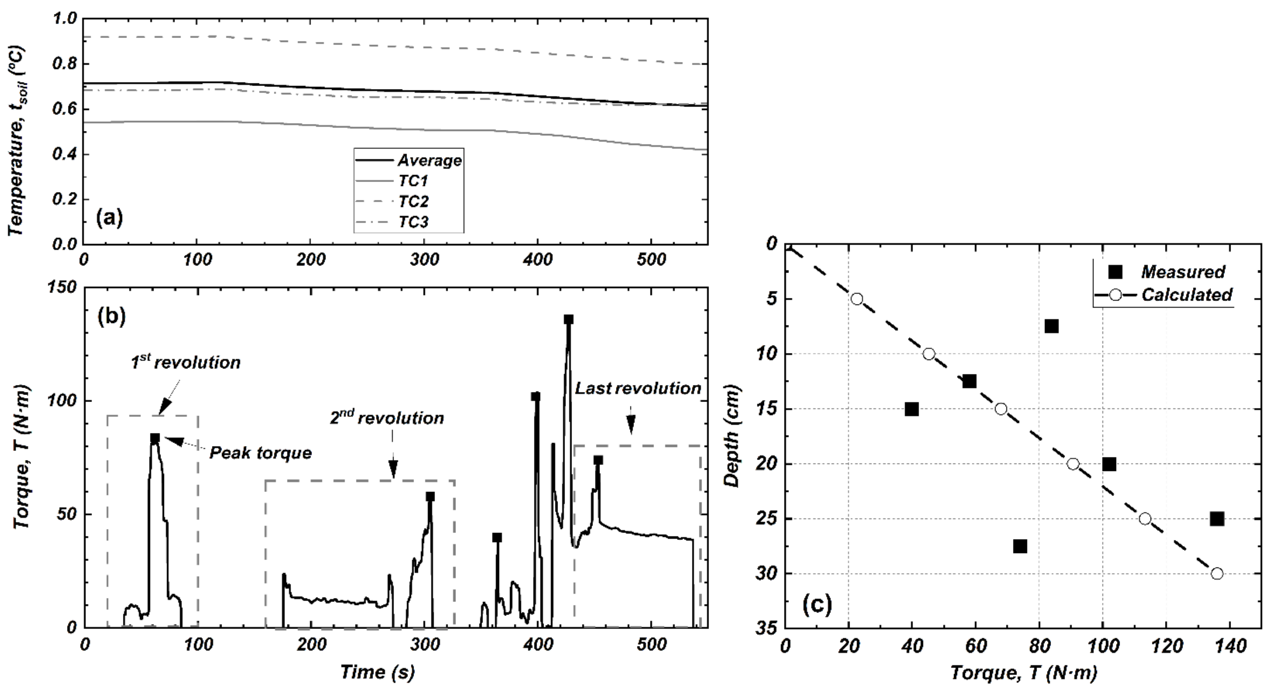

Figure 5.7 (a) Time histories of soil temperature during installation; (b) manually selected peak torque at each torsional revolution; and (c) correlation between peak installation torque and penetration depth (TCD4).

Guo and Deng (2018) assumed that the installation torque is counterbalanced by the torque produced by unit-area resistance (for both shaft and threads) acting on the pile shaft and the threads. The model was adopted in the present study to infer the unit-area resistance f_s of frozen soils (Figure 5.9). The installation torque (T) is estimated by:

$$T = f_s A_{shaft} R + f_s A_{threads} \left(R + \frac{w_{th}}{2}\right) \tag{5-4}$$

where A_{shaft} is the contacting area of the pile shaft, $A_{threads}$ is the area of two-sided threads contacting soil, and w_{th} is the thread width (= 12 mm). Once the maximum installation torque at the final depth is determined from the torque history, one can back-calculate the average f_s using Equation 5-4. Assuming the average sleeve f_s calculated from maximum torque is constant throughout the soil, torque versus pile embedded depth could be estimated. Figures 5.7c and 5.8c show the relationship between calculated torque and embedded depth. The calculated torques agreed reasonably with the measured torques at various depths.

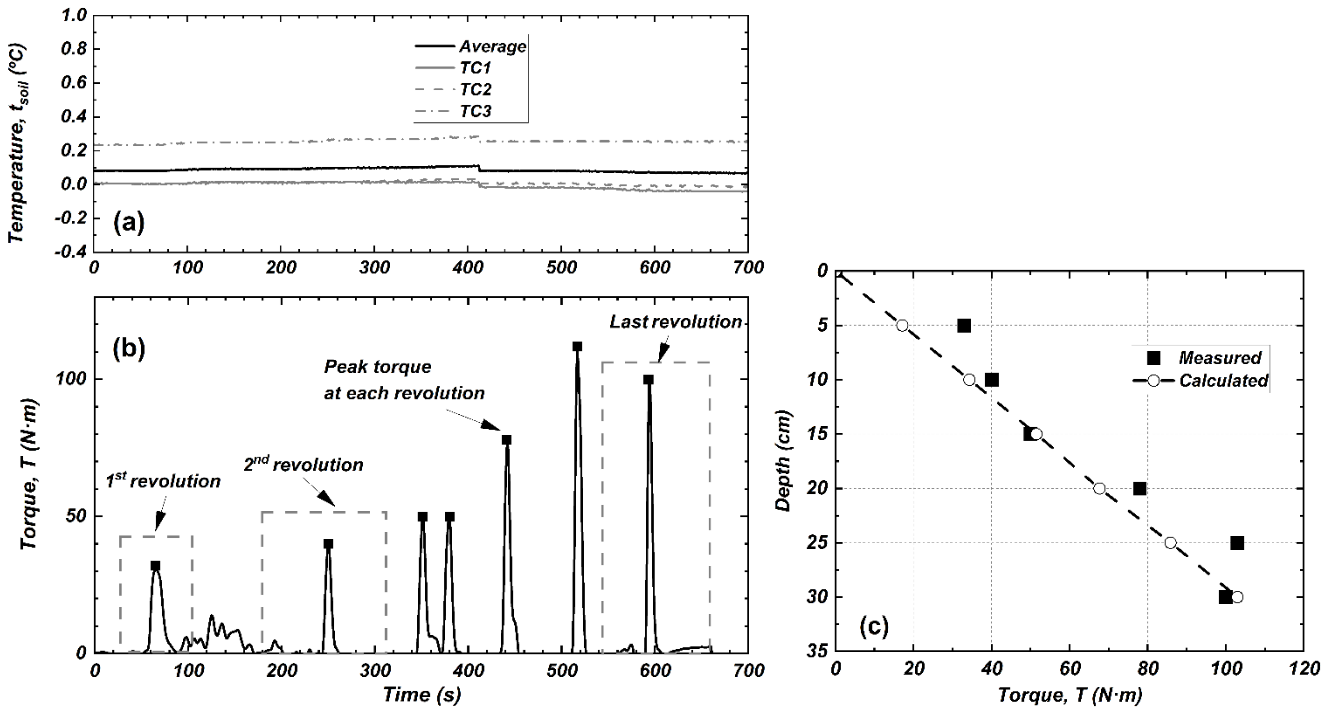

Figure 5.8 (a) Time histories of soil temperature during installation; (b) manually selected peak torque at each revolution; and (c) correlation between installation torque and penetration depth (IN3).

Figure 5.10a summarizes the maximum torques of threaded pile segments in different soil conditions. Polynomial fitting curves of the scattered data point were drawn to show the trend. It is shown from the fitting curves that the maximum torque increases with decreasing soil temperature. This phenomenon can be attributed to the rise in soil shear strength due to an increase in ice crystal volume within the soil pores as the temperature of the soil decreased. The required maximum torques in the temperature from 3.43 ºC to -1.88 ºC were not significantly influenced by changes in water content and salinity. The torque is also likely to depend on the pilot hole diameter, but this was not explored in the research. If chamber boundary effects are disregarded, the torque needed for installing full-scale piles in the field will be possibly proportional to pile length.

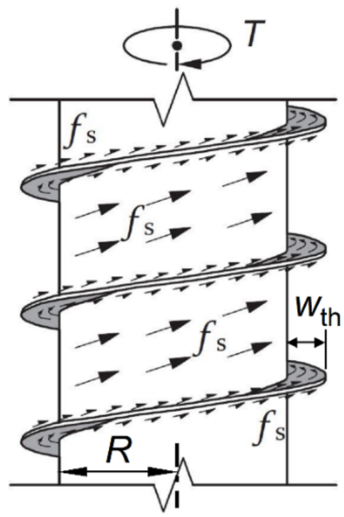

Figure 5.9 Proposed model relationship between applied torque and sleeve resistance (adapted from Guo and Deng 2018).

Figure 5.10b summarizes the back-calculated average f_s according to the maximum torque values. It is seen from Figure 10b fitting curves that the sleeve resistance increased significantly with the decreasing soil temperature. When comparing sleeve resistances at the same soil temperature, it is generally recognized that the average f_s in 0 ppt soil was slightly higher than the average f_s in 10 ppt soil. This observation suggests that the average f_s decreases slightly with increasing salinity.

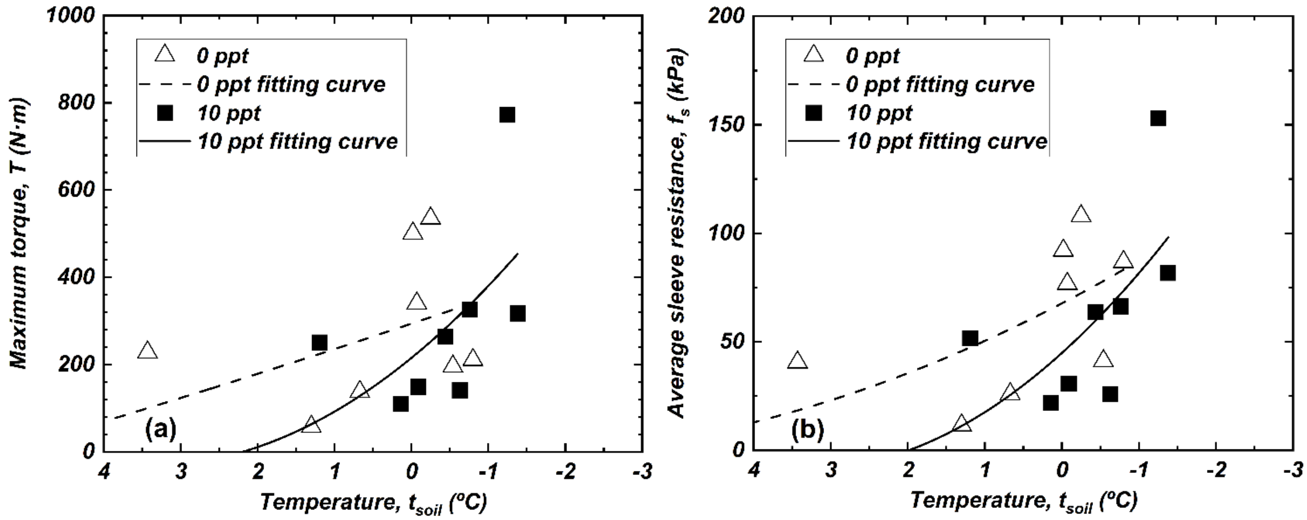

Figure 5.10 (a) summarized the required maximum torque versus installation temperature; and (b) summarized the calculated average sleeve resistance versus installation temperature

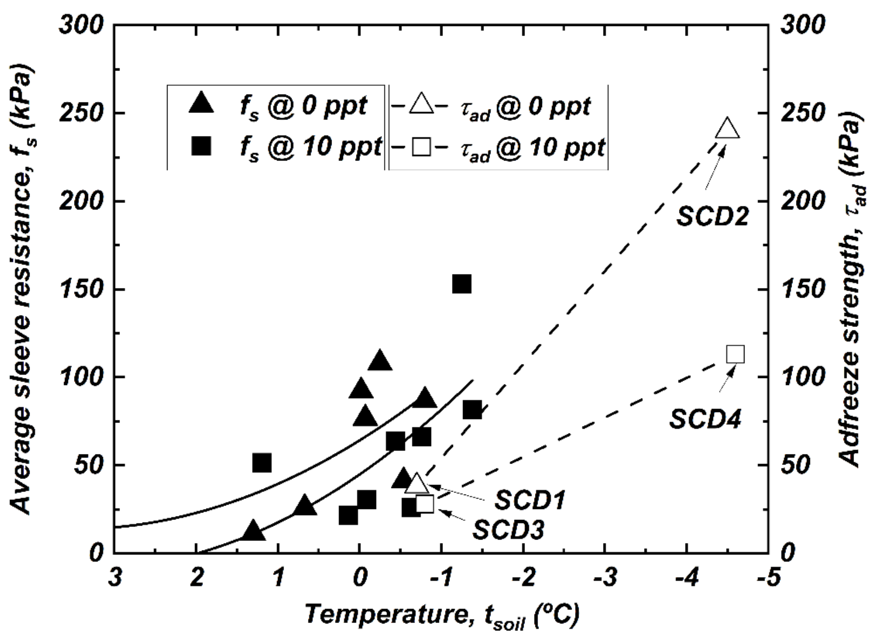

Figure 5.11 Comparison of average sleeve resistance (f_s) and adfreeze strength (τ_{ad}) at different temperatures and salinities. Note: τ_{ad} was obtained from short-term axial loading tests of smooth pile from Gao et al. (2023a).

The values of average f_s, ranging from 21.8 kPa to 153 kPa, are comparable to the adfreeze strength (τ_{ad}) measured by Gao et al. (2023a) who investigated the average τ_{ad} of continuous-flight and smooth piles in short-term axial loading tests. As shown in Figure 5.11, the measured τ_{ad} of smooth pile segments ranged from 38.2 kPa (SCD3) to 240 kPa (SCD2) with the temperature from -0.7 to -4.5 ºC in a 0 ppt frozen soil with a water content of 20%. In 10 ppt frozen soil with a water content of 20%, the measured τ_{ad} of smooth pile segments ranged from 27.9 kPa (SCD3) to 240 kPa (SCD4) with the temperature from -0.8 to -4.6 ºC. The measured τ_{ad} increased dramatically with the decreasing temperature and salinity.

5.4 Conclusions

Continuous-flight piles may provide a viable solution for pile foundations in the Canadian Arctic, and they could be installed into warm permafrost using a rotary motor. Twenty-three installation tests of continuous-flight and smooth pile segments were reported in the present study. The following conclusions can be drawn:

1. Continuous-flight pile segments were installed in an undersized pilot hole (0.9 times shaft diameter) in warm frozen soils using the electric rotary motor. The required maximum torque for continuous-flight piles segment ranged from 21 to 772 N·m depending on frozen soil conditions. The smooth pile segment experienced a required torque from 5.07 to 10.7 N·m.
2. Installation was halted at a minimum temperature of -1.88 ºC in 10 ppt soil and -1.0 ºC in 0 ppt soil because the equipment was unable to produce higher torque.
3. The soil temperature remained stable with a variation of less than 0.1 ºC on average during the installation. Negligible thermal disturbance of the soil was observed during the installation.
4. The installation torque increased with the penetration depth of the pile segment. The required maximum installation torque increased significantly with decreasing soil

temperature. The water content and the salinity did not show a significant impact on the required maximum torque in the temperature from 3.43 ºC to -1.88 ºC.

5. An analytical model was proposed, and the estimated average sleeve resistances for the contimuous-flight pile segment ranged from 21.8 to 153 kPa. These values were observed to be comparable to the adfreeze strengths of smooth pile in frozen soils with similar water content and salinity.

Limitations of the present study should be noted. First, only one undersized pilot hole size was tested. If another hole size is used, the required installation torque would change. Second, the pile segment was installed in the frozen soil with a minimum temperature of -1.88 °C, owing to the limitation of the lab installation technique.

6 Conclusions, Limitations, and Recommendations

Continuous-flight piles may provide a viable solution for pile foundations in the Canadian Arctic, and they could be installed into warm permafrost using a rotary motor. This research characterizes conclusions of the short-term and long-term axial, and installation performance of continuous-flight pile in frozen soils based on laboratory tests. Also, limitations of the present study and recommendations for design of continuous-flight pile in warm permafrost is illustrated herein.

6.1 Short-term Axial Performance of Continuous-flight Piles in Frozen Soil

Twelve axial load tests of continuous-flight and smooth piles were conducted in the present study. The following conclusions can be drawn:

1. The continuous-flight pile can be installed in an undersized pilot hole in frozen soil using the laboratory equipment which can provide a maximum torque of 3.6 kN·m. Installation met refusal at a minimum temperature of -1.88 ºC in 10 ppt soil because the equipment was unable to produce higher torque. The required installation torque increased with the penetration depth of the pile segment. The installation torque increased significantly with decreasing frozen soil temperature and salinity.
2. The continuous-flight pile carried more load than the smooth pile in the cold frozen soil. The ultimate pile capacity increased significantly when soil temperature decreased from -1 ºC to -5 ºC. The pile capacity increased with decreasing S in cold frozen soils (-5 ºC); the effect of salinity on the pile capacity in warm frozen soils (-1 ºC) could be neglected. The effect of water content on the pile capacity was not significant at -5 ºC.
3. Cylindrical shearing mode (CSM) and individual bearing mode (IBM) were observed for continuous-flight piles in warm and cold frozen soils, respectively.

4. For pile failure in the warm frozen soil, the presence of threads pushed the shear failure outward to the edge of the threads, mobilizing the shear strength of the frozen soil, and therefore enhanced the pile capacity. The effect of water content and salinity on the value of τ_u along this failure surface in the warm frozen soil can be neglected. The ratios of τ_{ad} / τ_u ranged from 0.72 to 0.9 in the present study, which are comparable to values suggested in the literature.
5. For pile failure in the cold frozen soil, the estimated values of unit plate bearing resistance q_b ranged from 1.37 to 1.61 MPa and the ratios of q_b / τ_u ranged from 4.2 to 9.7. The influences of water content and salinity on the unit plate bearing resistance of piles in the cold frozen soil were not evident.

6.2 Long-Term Axial Performance of Continuous-Flight Pile in Frozen Soil

In this chapter, four continuous-flight piles were loaded under a series of constant load increments. The following conclusions can be drawn:

1. The continuous-flight pile can be screwed into an undersized hole in frozen soil by applying compressive load and torque. The required maximum installation torque increased with increasing penetration depth and decreasing temperature.
2. Limited soil settlement adjacent to the pile shaft was observed when the pile was axially compressed under a constant load. CSM and IBM were observed and inferred from the measured data. The two failure modes suggest beneficial larger capacity and smaller creep displacement compared to conventional smooth piles.
3. Primary and secondary dominant creeps were observed from the constant load tests. The estimated adfreeze strength τ in CSM increased with the increasing constant load. The values of unit plate bearing resistance q in IBM increased with the increasing $\dot{s}$ and

mobilized when the constant load was increasing. Pile shaft loads were re-distributed as the pile head load Q_{head} increased. The mobilized q suggests a potential increasing capacity of the continuous-flight pile over conventional smooth piles.

6.3 Torque Correlation

Twenty-three installation tests of continuous-flight and smooth pile segments were reported in the present study. The following conclusions can be drawn:

1. Continuous-flight pile segments were installed in an undersized pilot hole (0.9 times shaft diameter) in warm frozen soils using the electric rotary motor. The required maximum torque for continuous-flight piles segment ranged from 21 to 772 N·m depending on frozen soil conditions. The smooth pile segment experienced a required torque from 5.07 to 10.7 N·m.
2. Installation was halted at a minimum temperature of -1.88 ºC in 10 ppt soil and -1.0 ºC in 0 ppt soil because the equipment was unable to produce higher torque.
3. The soil temperature remained stable with a variation of less than 0.1 ºC on average during the installation. Negligible thermal disturbance of the soil was observed during the installation.
4. The installation torque increased with the penetration depth of the pile segment. The required maximum installation torque increased significantly with decreasing soil temperature. The water content and the salinity did not show a significant impact on the required maximum torque in the temperature from 3.43 ºC to -1.88 ºC.
5. An analytical model was proposed, and the estimated average sleeve resistances for the contimuous-flight pile segment ranged from 21.8 to 153 kPa. These values were observed

to be comparable to the adfreeze strengths of smooth pile in frozen soils with similar water content and salinity.

6.4 Limitations and Recommendations for Further Research

It is convinced that continuous-flight piles could provide a better solution for pile foundations in the Canadian Arctic upon the findings from this research; however, limitations of the present study should be noted. First, only one undersized pilot hole size was tested. If another hole size and installation temperature are used, the required installation torque would change. Second, the pile segment was installed in the frozen soil with a minimum temperature of -1.88 °C, owing to the limitation of the laboratory installation technique. Third, due to the lack of load increments and duration criteria in the constant load tests, the results in the present research might be different if the load increments and load duration changes. Lastly, the values of adfreeze strength τ and unit plate resistance q are estimated from the proposed analytical equation rather than measurement.

Compared to conventional steel pipe piles, continuous-flight piles provide a variety of pile shaft feature (e.g., threaded or tapered at desired location) and dimension, which results in a cost-effective deep foundation solution. To further guide the application of continuous-light pile in the permafrost of Canada, full-scale short-term and long-term pile loading tests in the field is highly recommended in future research. Although the required installation torque measured in the laboratory tests could be referenced to guide the field application of continuous-flight piles, it is still suggested that installation tests of the continuous-flight piles in warm or cold permafrost with a varietry of pilot hole dimensions need to be investigated. Also, the impact of cold frozen soil temperature down to -10 °C on the installation performance is recommended to study by using improved installation technique. Small temperature interval from -1 °C to -3 °C near the pure water freezing point is also recommended in the future study.

6.5 Recommendations for Design of Continuous-Flight Pile in Warm Permafrost

Due to the effect of climate change in the next decades, the permafrost is getting warm and the active layer is deepened. Also, it is more conservative to design pile in warm temperature rather than in cold permafrost. Based on the literature review in Chapter 2 and findings from the present work in Chapter 3 to 5, the design of continuous-flight pile should consider three criteria: 1) long-term load capacity; 2) potential of frost heave and frost jacking; and 3) long-term settlement rate.

For the design criteria against pile capacity in warm permafrost approximate at -1 °C, it is recommended that the long term adfreeze strength should follow Weave and Morgenstern's (1981) method in equation:

$$\tau_{lt} = m \cdot c_{lt} \tag{6-1}$$

The selection of an appropriate shear strength or cohesion c_{lt} of a specific type of soil is critical in the pile design. A roughness coefficient m of 1.0 is an appropriate value in theory because of the failure mode in warm permafrost. For design purpose, m of 0.6 may also be selected to be conservative for continuous-flight pile. To determine the pile capacity, the cylindrical shear mode is suggested based on the findings from the present laboratory model pile tests:

$$Q = \tau_{lt}\pi(D + 2w_{th})L \tag{6-2}$$

The projected contacting area should be "enlarged" to the outer edge of the threads.

In addition to compressive load capacity, design of continuous-flight pile should consider the detrimental seasonal frost effects associated with heave and jacking. The stress caused by frost heave may be assumed to be 150 kPa (Hoeve and Trimble 2018), which is a conservative value. The sum of the structure's load and the load allowed by adfreeze bond capacity must be greater than the resulting force from frost heave. Accurate prediction of the active layer depth and providing a sufficient embedded length are critical factors in ensuring the correct pile design when consider frost heave and jacking. The active layer thickness depends on many factors; because of climate change, the thickness may be as deep as 3 m in the next few decades. It is not uncommon that the design pile length may be governed by the criteria of frost heave stress.

The design of continuous-flight pile foundations in frozen soils is mainly based on limiting long-term creep settlements. Creep settlements are a function of the pile-soil adfreeze stress and temperature. It has been established that the long-term settlement for a common building should be designed for 50 mm over a period of 50 years, equivalent to an annual settlement of 1.0 mm/year (Hoeve and Trimble 2018). It is recommended that the steady-state creep settlement calculation should follow the equation proposed by Nixon and McRoberts (1976):

$$\frac{\dot{u}}{\mathrm{a}} = \frac{3^{(\mathrm{n}+1)/2}\,\mathrm{B}\tau^{\mathrm{n}}a}{\mathrm{n}-1} \tag{6-3}$$

where $\dot{u}$ is steady pile displacement rate, a is pile radius a, τ_{a} is applied shear stress, and the constant B and n determined from uniaxial creep data for the frozen soil. The cylindrical shear mode is also assumed herein.

References

Aldaeef, A.A. and Rayhani, M.T. 2019. Load transfer of pile foundations in frozen and unfrozen soft clay. International Journal of Geotechnical Engineering, 14(6): 653-664.

Aldaeef, A.A. and Rayhani, M.T. 2021a. A quick approach for estimating load transfer of conventional and helical piles in ice-rich frozen soils. Geotechnical and Geological Engineering, 39: 2927-2944.

Aldaeef, A.A. and Rayhani, M.T. 2021b. Pile-soil interface characteristics in ice-poor frozen ground under varying exposure temperature. Cold Regions Science and Technology, 191: 103377.

Aldaeef, A.A. and Rayhani, M.T. 2022. Pull-out capacity and creep behavior of helical piles in frozen ground. ASCE Journal of Geotechnical and Geoenvironmental Engineering, 146(12): 04020140.

Andersland, O.B. and Al-Nouri, I. 1970. Time dependent strength behavior of frozen soils. Journal of the Soil Mechanics and Foundations Division, ASCE96 (SM4): 1249-1265.

Andersland, O.B. and Ladanyi, B. 2004. Frozen Ground Engineering, 2nd ed., John Wiley & Sons, Inc., Hoboken, New Jersey, USA.

Andersland, O.B., and Alwahhab, M.R.M. 1983. Lug behavior for model steel piles in frozen sand. Proceedings of 4th International Conference on Permafrost, National Academy of Sciences, National Research Council, Washington, DC, PP. 16-21.

Andersland, O.B., and Anderson, O.B. 1978. Geotechnical Engineering for Cold Regions, McGraw-Hill Inc., New York.

Anderson, D. M., and Tice, A.R. 1972. Predicting unfrozen water contents in frozen soils from surface area measurements. In Frost Action in Soils. Washington, D.C.: National Academy of Sciences, pp. 12-18 (Highway Resc. Rec. 393).

Azmatch, T.F., and Sego, D.C., Arenson, L.U., and Biggar, K.W. 2011. Tensile strength and stress-strain behavior of Devon silt under frozen fringe conditions, Cold Regions Science and Technology, 68: 85-90.

Biggar, K. W. 1991. Adfreeze and grouted piles in saline permafrost. Ph.D. dissertation, University of Alberta, Edmonton, Canada.

Biggar, K. W., and Kong, V. 2001. An analysis of long-term pile load tests in permafrost from the Short Range Radar site foundations. Canadian Geotechnical Journal, 38(3): 441–460.

Biggar, K.W., and Sego, D.C. 1989. Field load testing of various pile configurations in saline permafrost and seasonally frozen rock. Proceedings of 42nd Canadian Geotechnical Conference, Winnipeg, Manitoba, Canada, pp. 304-312.

Biggar, K.W., and Sego, D.C. 1993a. Field pile load tests in saline permafrost. I. Test procedures and results, Canadian Geotechnical Journal, 30(1): 34-45.

Biggar, K.W., and Sego, D.C. 1993b. Field pile load tests in saline permafrost. II. Analysis of results, Canadian Geotechnical Journal, 30(1): 46-59.

Biggar, K.W., and Sego, D.C. 1993c. The strength and deformation behaviour of model adfreeze and grouted piles in saline frozen soils, Canadian Geotechnical Journal, 30(2): 319-337.

Biggar, K.W., Sego, D.C., and Stahl, R. P. 1996. Long-term pile load testing system performance in saline and ice-rich permafrost, Journal of Cold Regions Engineering, ASCE, 10(3): 149-162.

Cerfontaine, B., Knappett, J., Brown, M.J., Davidson, C., Al-Baghdadi, T., Sharif, Y.U., Brennan, A., Augarde, C., Coombs, W.M., Wang, L., Blake, A., Richards, D., Ball, J. 2021. A Finite Element approach for determining the full load-displacement relationship of axially loaded shallow screw anchors, incorporating installation effects, Canadian Geotechnical Journal, 58(4): 565-582.

Chen, S., and Lin, B. 2019. Contrast test on uniaxial compression of undisturbed and remolded frozen clay. Safety in Coal Mines, 50(06): 62-66.

Crowther, G.S. 1990. Analysis of laterally loaded piles embedded in layered frozen soil, Journal of Geotechnical Engineering, 116(7): 1137-1152.

Crowther, G.S. 2013. Frozen soil strength criteria for lateral pile analysis, Journal of Cold Regions Engineering, ASCE, 27(3): 155-167.

Cuthbertson-Black, R. 2001. The interaction between a flighted steel pipe pile and frozen sand. MSc Thesis, Department of Civil and Geological Engineering, University of Manitoba, Winnipeg, MB.

Dillon, H.B., and Andersland, O.B. 1966. Predicting unfrozen water contents in frozen soils. Canadian Geotechnical Journal, 3(2): 53-60.

Dubois, D.P. 1994. Load transfer from thermopiles with and without continuous flighting. M.Eng. Report, Department of Civil and Geological Engineering, University of Manitoba, Winnipeg, MB.

EBA. 2004. Geotechnical Characterization for Inuvik, NT: Report submitted to Natural Resources Canada, Ottawa, Canada.

Ersoy, T., Torgrol, E. 1978. Temperature and strain rate effects on the strength of compacted frozen silty clay. Proceedings of 3rd International Conference on Permafrost, Edmonton, Alberta, vol. 1, pp. 642-647.

Fish, A.M. 1982. Comparative analysis of the USSR construction codes and the U.S. Army technical manual for design of foundations on permafrost, CRREL Report 82-14, U.S. Army Cold Regions Research and Engineering Laboratory.

Foriero, A., and Ladanyi, B. 1990. Finite element simulation of behavior of laterally loaded piles in permafrost. Journal of Geotechnical Engineering, ASCE, 116(2): 266-284.

Foriero, A., and Ladanyi, B. 1991a. Design of piles in permafrost under combined lateral and axial loads. Journal of Cold Regions Engineering, ASCE, 5(3): 89-105.

Foriero, A., and Ladanyi, B. 1991b. Generalized finite-element algorithm for laterally loaded piles in permafrost in comparison with measurements, Canadian Geotechnical Journal, 28(4): 523-541.

Foriero, A., and Ladanyi, B. 1995. FEM simulation of interface problem for laterally loaded piles in permafrost, Cold Regions Science and Technology, 23: 121-136.

Foriero, A., St-Laurent, N., and Ladanyi, B. 2005. Laterally loaded pile study in permafrost of Northern Quebec, Canada, Journal of Cold Regions Engineering, ASCE, 19(3): 61-84.

Frederking, R.M.W. 1979. Laboratory tests on downdrag loads developed by floating ice covers on vertical piles. Proceedings of 5th International Conference on Port and Ocean Engineering under Arctic Conditions, NGI, Trondheim, Norway, Vol. 2, pp. 1097-1110.

Gao, S., Bin, J., Sego, D., and Deng, L. 2020. Axial performance of screw micropiles subjected to quick loads in frozen soils. GeoVirtual 2020, the annual conference of Canadian Geotechnical Society, pp. 8.

Gao, S., Sego, D., and Deng, L. 2021. Pile foundations in permafrost, Canadian Geotechnique, 2 (4): 42-45.

Gao, S., Sego, D.C., and Deng, L. 2023a. Short-term axial loading of continuous-flight pile segment in frozen soil, Canadian Geotechnical Journal, 60(4): 541-554.

Gao, S., Sego, D.C., and Deng, L. 2023b. Long-term axial performance of continuous-flight pile in frozen soil, Canadian Geotechnical Journal, e-first article, doi: 10.1139/cgj-2022-0461.

Gardner, A.R., Jones, R.H., and Harris, J.S. 1984. A new creep equation for frozen soils and ice, Cold Regions Science and Technology, 9, 271-275.

Ghaly, A., and Hanna, A. 1991. Experimental and theoretical studies on installation torque of screw anchors, Canadian Geotechnical Journal, 28(3): 353-364.

Glen, J.W. 1955. The creep of polycrystalline ice, Proceedings, Royal Society of London, 228 A, 519-538.

Goughnour, R.R., and Andersland, O.B. 1968. Mechanical properties of a sand-ice system, Journal of the Soil Mechanics and Foundation Division, ASCE94 (SM4): 923-950.

Guo, Z., and Deng, L. 2018. Field behavior of screw micropiles subjected to axial loading in cohesive soils, Canadian Geotechnical Journal, 55(1): 34-44.

Guo, Z., Khidri, M., and Deng, L. 2019. Field loading tests of screw micropiles under axial cyclic and monotonic loads, Acta Geotechnica, 14: 1843-1856.

Hanna, A.J. 1989. Baffin region salinity, pile design basis and recent pile modifications, Saline Permafrost Workshop, Winnipeg, Manitoba.

Harnish, J., and El Naggar, M.H. 2017. Large-diameter helical pile capacity-torque correlations, Canadian Geotechnical Journal, 54(7): 968-986.

Heydinger, A. G. 1987. Piles in permafrost. Journal of Cold Regions Engineering, ASCE, 1(2): 59-75.

Hivon, E.G. 1991. Behaviour of saline frozen soils. Ph.D. dissertation, University of Alberta, Edmonton, Canada.

Hivon, E.G., and Sego, D.C. 1993. Distribution of saline permafrost in the Northwest Territories, Canada, Canadian Geotechnical Journal, 30(3): 506-514.

Hivon, E.G., and Sego, D.C. 1995. Strength of frozen saline soils, Canadian Geotechnical Journal, 32(2): 336-354.

Hivon, E.G., Sego, D.C. 1991. Distribution of saline permafrost in the Northwest Territories, Proceedings of 44th Canadian Geotechnical Conference, Calgary, Alberta, Vol. 1, Paper 38.

Hoeve, T.E., and Trimble, J.R. 2018. Rationalizing the design of adfreeze piles with limit states design, Proceedings of 71st Canadian Geotechnical Conference, Edmonton, Alberta, Paper 136.

Holubec, I. 1990. Thread bar pile for permafrost. Proceedings of 5th Canadian Permafrost Conference, University of Laval Collection Nordiana No. 54, pp. 341–348.

Holubec, I. 2008. Flat loop thermosyphon foundations in warm permafrost. Government of the Northwest Territories Asset Management Division of Public Works and Services and the Climate Change Vulnerability Assessment of the Canadian Council of Professional Engineers.

Holubec, I., and Brzezinski, L.S. 1989. Arctic grout pile, Proceedings of 8th International Conference on Offshore Mechanics and Polar Engineering, Hague, the Netherlands, ASME, PP. 731-737.

Hou, X., Chen, J., Yang, B., Wang, J., Dong, T., Rui, P. 2022. Monitoring and simulation of the thermal behavior of cast-in-place pile group foundations in permafrost regions, Cold Regions Science and Technology, 196: 103486.

Hoyt, R.M., and Clemence, S.P. 1989. Uplift capacity of helical anchors in soil. Proceedings of 12th International Conference on Soil Mechanics and Foundation Engineering, Rio de Janeiro, Brazil, 2: 1019-1022.

Hult, J. A. H. 1966. Creep in Engineering Structures, Waltham, Mass.: Blaisdell.

Johnston, G. H., and Ladanyi, B. 1972. Field tests of grouted rod anchors in permafrost. Canadian Geotechnical Journal, 9(2): 176–194.

Johnston, G. H., and Ladanyi, B. 1974. Field tests of deep power-installed screw anchors in permafrost, Canadian Geotechnical Journal, 11(3): 348–358.

Johnston, G.H. (Editor). 1981. Permafrost engineering design and construction, John Wiley & Sons, New York.

Kaplar, C.W. 1974. Freezing test for evaluating reactive frost susceptibility of various soils, U.S. Army CRREL, Technical Report NO. 250, Hanover, N.H.

Khidri, M., and Deng, L. 2022. Field axial loading tests of screw micropiles in sand, Canadian Geotechnical Journal, 59(3): 458-472.

Ladanyi, B. 1972. An engineering theory of creep of frozen soils. Canadian Geotechnical Journal, 9(1): 63–80.

Ladanyi, B. 1972b. In situ determination of undrained stress-strain behavior of sensitive clays with pressuremeter. Canadian Geotechnical Journal, 9(3): 313–319.

Ladanyi, B. 1975. Bearing capacity of strip footings in frozen soil, Canadian Geotechnical Journal, 12(3): 393-407.

Ladanyi, B., and Guichaoua, A. 1985. Bearing capacity and settlement of shaped piles in permafrost, Proceedings of 9th ICSMFE, San Francisco, pp. 1421-1427.

Ladanyi, B., and Johnston, G.H. 1974. Behavior of circular footings and plate anchors embedded in permafrost, Canadian Geotechnical Journal, 11(4): 531-553.

Ladanyi, B., and Morel, J.-F. 1990. Effect of internal confinement on compression strength of frozen sand, Canadian Geotechnical Journal, 27(1): 8-18.

Ladanyi, B., and Paquin, J. 1978. Creep behavior of frozen sand under a deep circular load. Proceedings of 3rd International Conference on Permafrost, Edmonton, Alberta, vol. 1, pp. 679-686.

Ladanyi, B., and Theriault, A. 1990. A study of some factors affecting the adfreeze bond of piles in permafrost. Proceedings of 5th Canadian Permafrost Conference. University of Laval Collection Nordiana No. 54, pp. 327-334.

Ladanyi, B., Lunne, T., Vergobbi, P., and Lhuillier, B. 1995. Predicting creep settlements of foundations in permafrost from the results of cone penetration tests. Canadian Geotechnical Journal, 32(5): 835–847.

Li, H., Zhu, Y., Zhang, J., and Lin, C. 2004. Effects of temperature, strain rate and dry density on compressive strength of saturated frozen clay. Cold Regions Science and Technology, 39(1): 39-45.

Linnel, K.A., and Lobacz, E.F. 1980. Design and construction of foundations in areas of seasonal frost and permafrost. United States Army Corps of Engineers, Cold Regions Research and Engineering Laboratory, Hanover, N.H., Special Report 80-34: 320.

Liu, C., Anderson, R., Gopie, N., and Deng, L. 2022. Field performance of wood blocking method for remediating a building in the Canadian Arctic. Journal of Civil Structural Health Monitoring,12: 875-889.

Liu, H., Zubeck, H. K., and Schubert, D.H. 2007. Finite-element analysis of helical piers in frozen ground. Journal of Cold Regions Engineering, ASCE, 21(3): 92–106.

Liu, H., Zubeck, H.K., and Baginski, S. 1999. Evaluation of helical piers for use in frozen ground. Proceedings of 10th International Conference on Cold Regions Engineering, ASCE, Reston, VA., pp.232–242.

Long, E.L. 1973. Designing friction piles for increased stability at lower installed cost in permafrost. Proceedings of 2nd International Conference on Permafrost, National Academy of Sciences, National Research Council, Washington, DC, pp. 693-699.

Miller, D.E., and Johnson, L.A. 1990. Pile settlement in saline permafrost - a case history, Proceeding 5th Canadian Permafrost Conference, Quebec City, Quebec, 371-378.

Morgenstern, N. R., Roggensack, W. D., and Weaver, J. S. 1980. The behavior of friction piles in ice and ice-rich soils. Canadian Geotechnical Journal, 17(3): 405–415.

Neresova, Z.A., and Tsytovich, V.A. 1963. Unfrozen water in frozen soils. Proceedings of Permafrost International Conference, NAS-NRC Publ., Vol. 1287, pp. 230-234.

Neukirchner, R.J., and Nixon, J.F. 1987. Behavior of laterally loaded pile in permafrost, ASCE Journal of the Geotechnical Engineering, 113(1): 1-14.

Nixon, J.F. 1978. Foundation design approaches in permafrost areas, Canadian Geotechnical Journal, 15(1): 96-112.

Nixon, J.F. 1988. Pile load tests in saline permafrost at Clyde River, Northwest Territories, Canadian Geotechnical Journal, 25(1): 24-32.

Nixon, J.F. and Lem, G. 1984. Creep and strength testing of frozen saline fine-grained soils. Canadian Geotechnical Journal, 21(4): 518-29.

Nixon, J.F. and McRoberts, E.C. 1976. A design approach for pile foundations in permafrost. Canadian Geotechnical Journal, 13(1): 40-57.

Nixon, J.F., Pharr, G.M. 1984. The effects of temperature, stress and salinity on the creep of frozen saline soil, Transactions of the ASME Journal of Energy Resources Technology, 106: 344-348.

Nottingham, D., and Christopherson, A.B. 1983. Driven piles in permafrost: state of the art, Proceedings of the 4th International Conference on Permafrost, Fairbanks, Alaska. Washington, D.C.: National Academy Press, pp. 928-933.

Odqvist, F.K.G. 1966. Mathematical theory of creep and creep rupture, Oxford Mathematical Monographs, Oxford: Clarendon Press.

Ogata, N., Yasuda, M., and Kataoka, T. 1983. Effects of salt concentration on strength and creep behaviour of artificially frozen soils. Cold Regions Science and Technology, 8, 139-153.

Oliphant, J.L., and Tice, A.R. 1982. Comparison of unfrozen water contents measured by DSC and NMR, Proceedings of the 3rd International Symposium on Ground Freezing, Hanover, New Hampshire, USA, 115-121.

Parameswaran, V.R. 1978. Adfreeze strength of frozen sand to model piles, Canadian Geotechnical Journal, 15(4): 494-500.

Parameswaran, V.R. 1979. Creep of model piles in frozen soil, Canadian Geotechnical Journal, 16(1): 69-77.

Parameswaran, V.R. 1980. Deformation behaviour and strength of frozen sand, Canadian Geotechnical Journal, 17(1): 74-88.

Parameswaran, V.R. 1986. Bearing capacity calculations for piles in permafrost, Proceedings of the 4th International Conference, Anchorage, Alaska, Cold Regions Engineering, pp. 751-759.

Perko, H.A. 2009. Helical piles: A practical guide to design and installation. 1st ed. John Wiley & Sons, Inc., Hoboken, New Jersey, USA.

Ren, Z., Liu, J., Jiang, H., and Wang, E. 2023. Experimental study and simulation for unfrozen water and compressive strength of frozen soil based on artificial freezing technology, Cold Regions Science and Technology, 205: 103711.

Rowley, R.K., Watson, G.H., and Ladanyi, B. 1973. Vertical and lateral pile load test in permafrost, North American Contribution, 2nd International Conference on Permafrost, Yakutsk, USSR. Washington, D.C.: National Academy of Sciences, pp. 712-721.

Rowley, R.K., Watson, G.H., and Ladanyi, B. 1975. Prediction of pile performance in permafrost under lateral load, Canadian Geotechnical Journal, 12(4): 510-523.

Saeki, H., Ono, T., Takeuchi, T., Kanie, S., and Nakazawa, N. 1986. Ice forces due to changes in water level and adfreeze bond strength between sea ice and various materials. Fifth Offshore Mechanics and Arctic Engineering Conference, Vol. 4, pp. 534-540.

Sakr, M. 2013. Relationship between installation torque and axial capacities of helical piles in cohesive soils, The Journal of the Deep Foundations Institute, 7(1): 44-58.

Sayles, F.H. 1968. Creep of frozen soils, U.S. Army CRREL Technical Report 190, pp.5.

Sayles, F.H., and Haines, D. 1974. Creep of frozen silt and clay, U.S. Army CRREL technical report 252.

Scher, R.L. 1996. Geotechnical considerations. In: Smith D.W., ed. Cold Regions Utilities Monograph, 3rd ed. New York, NY. American Society of Civil Engineers, 3.1-3.115.

Sego, D. C. 1980. Deformation of ice under low stress. Ph.D. dissertation, University of Alberta, Edmonton, Alberta, Canada.

Sego, D. C., and Smith, L. B. 1989. Effect of backfill properties and surface treatment on the capacity of adfreeze pipe piles. Canadian Geotechnical Journal, 26(4): 718–725.

Sego, D.C., Morgenstern, N.R. 1983. Deformation of ice under low stresses, Canadian Geotechnical Journal, 20(4), 587-602.

Shang, Y.H., Niu, F.J., Wu, X.Y., and Liu, M.H. 2018. A novel refrigerant system to reduce refreezing time of cast-in-place pile foundation in permafrost regions. Applied Thermal Engineering, 128: 1151-1158.

Sharif, Y.U., Brown, M.J., Cerfontaine, B., Davidson, C., Ciantia, M.O., Knappett, J.A., Ball, J.D., Brennan, A., Augarde, C., Coombs, W., Blake, A., Richards, D., White, D., Huisman, M., and Ottolini, M., 2021a. Effects of screw pile installation on installation requirements and in-service performance using the discrete element method, Canadian Geotechnical Journal, 58(9): 1334-1350.

Sharif, Y.U., Brown, M.J., Ciantia, M.O., Cerfontaine, B., Davidson, C., Knappett, J., Meijer, G.J., and Ball, J., 2021b. Using discrete element method (DEM) to create a cone penetration test

(CPT)-based method to estimate the installation requirements of rotary-installed piles in sand. Canadian Geotechnical Journal, 58(7): 919-935.

Sheng, D., Axelsson K., Knutsson, S. 1995. Frost heave due to ice lens formation in freezing soils: 1. Theory and verification. Nordic Hydrol, 26(2): 125-146.

Smoltczyk, U. (Editor). 2002. Geotechnical Engineering Handbook (Vol. 2 Procedures), John Wiley & Sons.

Tang, L., Wang, K., Deng, L., Yang, G., Chen, J., and Jin L. 2019. Axial loading behaviour of laboratory concrete piles subjected to permafrost degradation, Cold Regions Science and Technology, 166: 102820.

Tang, L., Wang, X., Jin, L., Deng, L., and Di, W. 2021. Frost heave and thawing settlement of frozen soils around concrete piles: a laboratory model test. ASTM Journal of Testing and Evaluation, 49(2): 949-966.

Thomas, H.P., and Luscher, U. 1980. Improvement of bearing capacity of pipe piles by corrugations, Building under Cold Climates and on Permafrost: Collection of Papers from a US-Soviet Joint Seminar, US Department of Housing and Urban Development, Washington, DC, pp. 229-234.

Thurber Consultants. 1987. North Warning System, Short Range Radar Sites - Zone 2, Pile Load Test Program, Model Pile Load Tests – Phase 1, Edmonton, Canada.

Tice, A.R., Anderson, D.M., and Banin, A. 1976. The prediction of unfrozen water content in frozen soils from liquid limit determinations. US Army Cold Regions Research. Engineering Laboratory. Rep. 76-8.

Tsytovich, N.A., and Sumgin, M.I. 1959. Principles of mechanics of frozen ground. U.S. Army Snow, Ice and Permafrost Research Establishment (Cold Regions Research and Engineering Laboratory, Hanover, NH), Translation 19. (288p).

Tsytovich, N.A. 1975. The Mechanics of Frozen Ground. McGraw Hill, New York.

Velli, Y.Y., Lenzniiep, Karpunina, A.A. 1973. Saline permafrost as bearing ground for construction. Proceedings of 2nd International Conference on Permafrost, USSR Contribution, Yakutsk, USSR, 545-550.

Vyalov, S.S., Maximyak, R.V., Razbegin, V.N., Slepak, M.E., and Chapayev, A.A. 1988. Stress-strain behavior of frozen soils. Proceedings of 5th International Conference on Permafrost, Trondheim, Norway, 1186-1191.

Wang, S., Qi, J., Yin, Z., Zhang, J., and Ma, W. 2004. A simple rheological element based creep model for frozen soils, Cold Regions Science and Technology, 106-107: 47-54.

Weaver, J.S., and Morgenstern, N.R. 1981. Pile design in permafrost, Canadian Geotechnical Journal, 18(3): 357-370.

Yang, Y., Lai, Y., Chang, X. 2010. Experimental and theoretical studies on the creep behavior of warm ice-rich frozen sand, Cold Regions Science and Technology, 63: 61-67.

Yao, X., Qi, J., Liu, M., and Yu, F. 2017. A frozen soil creep model with strength attenuation, Acta Geotechnica, 12: 1385-1393.

Zhang, G., and Hoeve, E. 2015. Geotechnical design of thermopile foundation for a building in Inuvik. Proceedings of 68th Canadian Geotechnical Conference, Quebec, Québec, September 20 to 23, 2015.

Zubeck, H.K., and Liu, H. 2003. Design of helical pier foundations in frozen ground. Proceedings of 8th International Conference on Permafrost, Philips, M., Springman, S., and Arenson, L. (eds.), Swets & Zeitlinger Publishers, Lisse, the Netherlands.

Appendix A: Additional Laboratory Test Photos and Drawings

This appendix illustrates additional laboratory photos and drawings including soil preparation, instrumentation, calibration, and pile loading test.

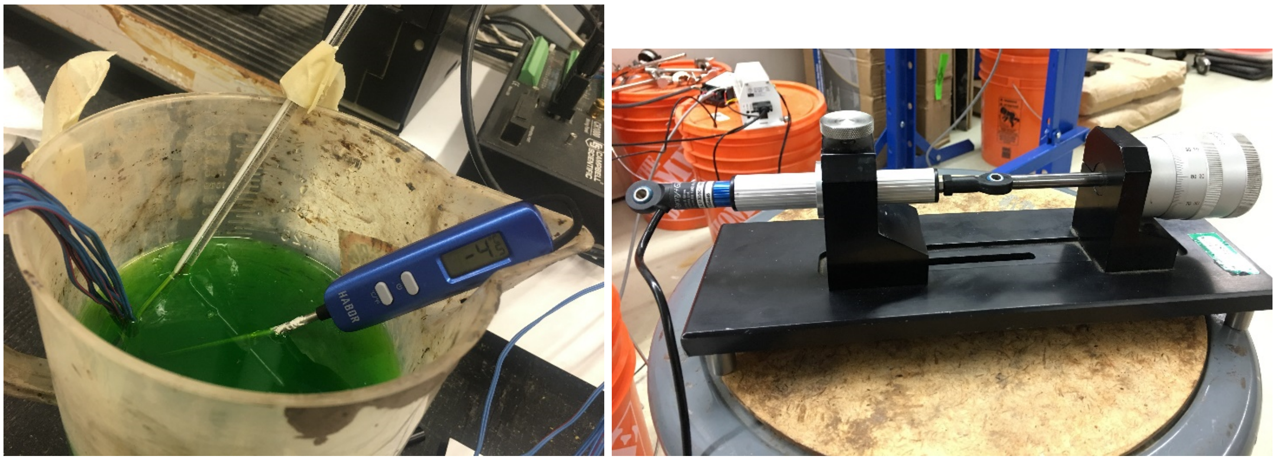

Figure A.1 Thermocouples and linear potentiometer calibration.

Figure A.2 Strain gauges installation and calibration.

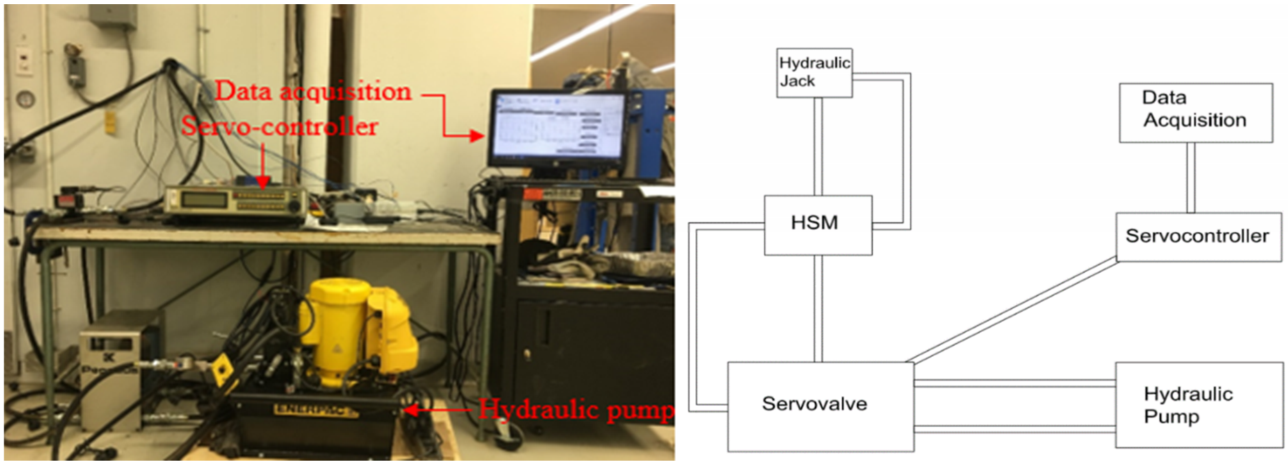

Figure A.3 Photo and schematic of loading equipments and data acquisition system.

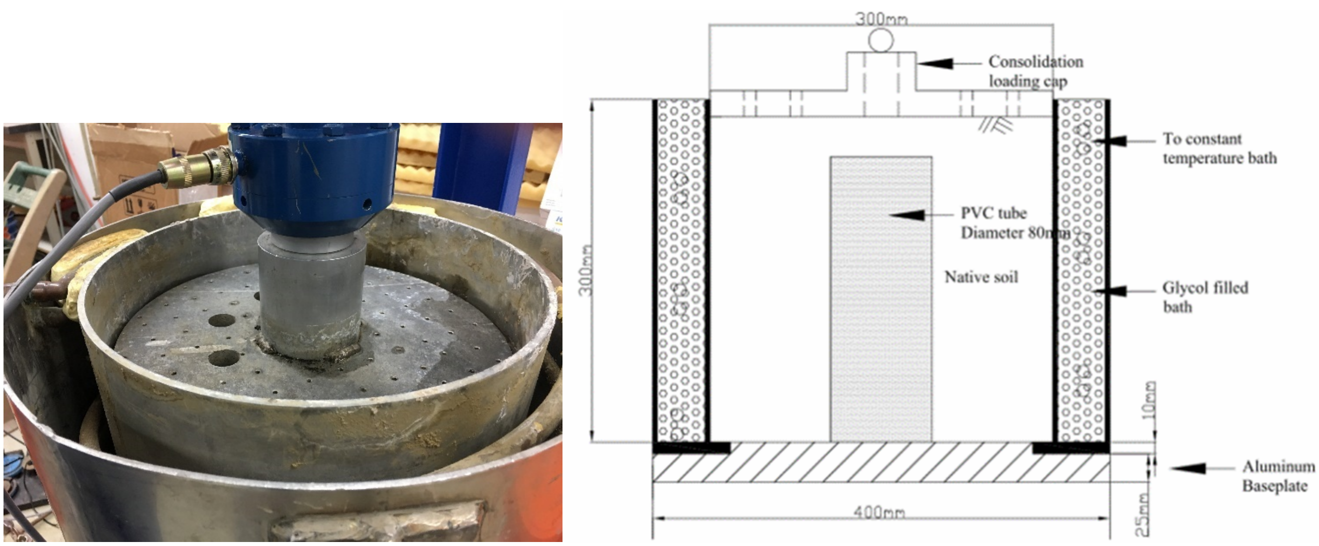

Figure A.4 Photo and schematic of soil consolidation in the test cell.

Figure A.5 Ice lenses in ice-rich soil sample after short-term axial loading (Test ID: TCD3).

Appendix B: Additional Laboratory Test Results

This appendix describes comprehensive test results in addition to short-term axial loading test results in Chapter 3, long-term axial loading test results in Chapter 4, and installation test results in Chapter 5. The results of consolidation, time history of soil temperature during the entire test progress, installation torque, calculated force from strain gauges, ground settlements are illustrated. Table B.1 summarizes the pile type, test type, soil salinity, soil water content, and soil temperature for all tests.

Table B.1 Test matrix

Test ID	Pile type	Test type	Salinity (ppt)	Average water content (%)	Average soil temperature (℃)
IN1	Straight threaded	Installation without loading	0	20.0	-0.3
IN2			0	20.0	-0.8
IN3			10	20.0	0.1
IN4			10	20.0	-1.4
IN5			10	20.0	-1.3
IN6			10	20.0	-1.9
IN7			0	20.0	-1.0
TCD1		Short-term axial loading	0	25.5	-1.0
TCD2			0	20.2	0
TCD3			0	26.9	-4.5
TCD4			0	19.5	-4.8
TCD5			10	22.1	-1.6
TCD6			10	19.8	-0.8
TCD7			10	24.5	-4.3
TCD8			10	20.1	-4.9
TCL1		Long-term axial loading	0	24.1	-0.9
TCL2			0	18.4	-2.2
TCL3			0	18.0	-4.7
TCL4			10	16.9	-3.9
SCD1	Smooth	Short-term axial loading	0	20.2	-0.7
SCD2			0	19.9	-4.5
SCD3			10	20.0	-0.8
SCD4			10	19.7	-4.6

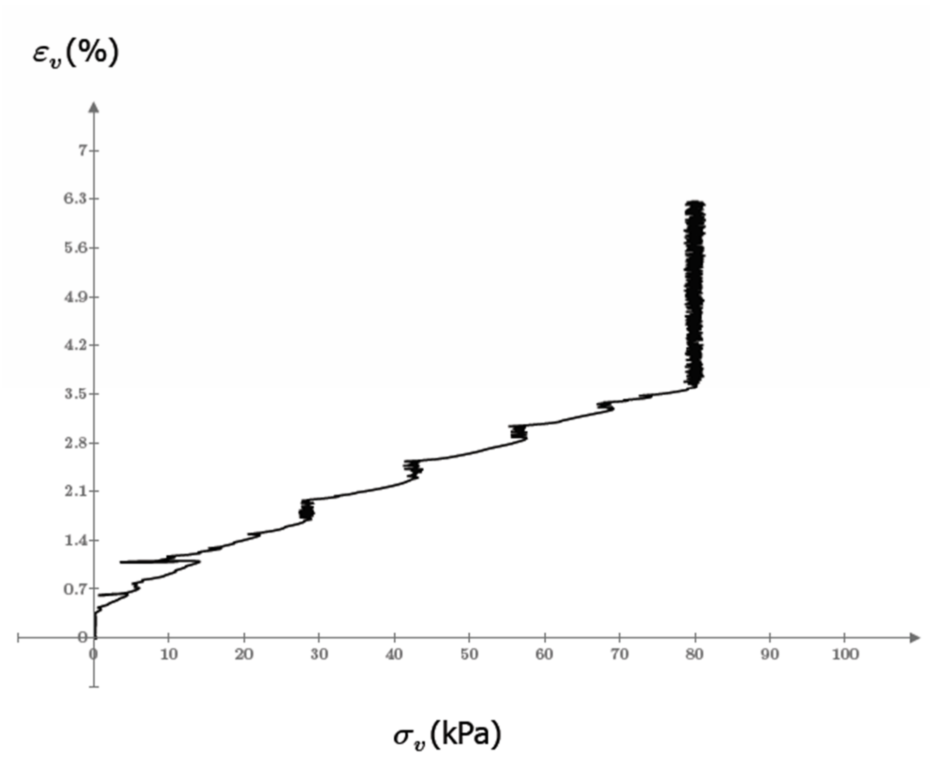

Figure B.1 Vertical strain (ε_v) versus stress (σ_v) during consolidation of TCD1.

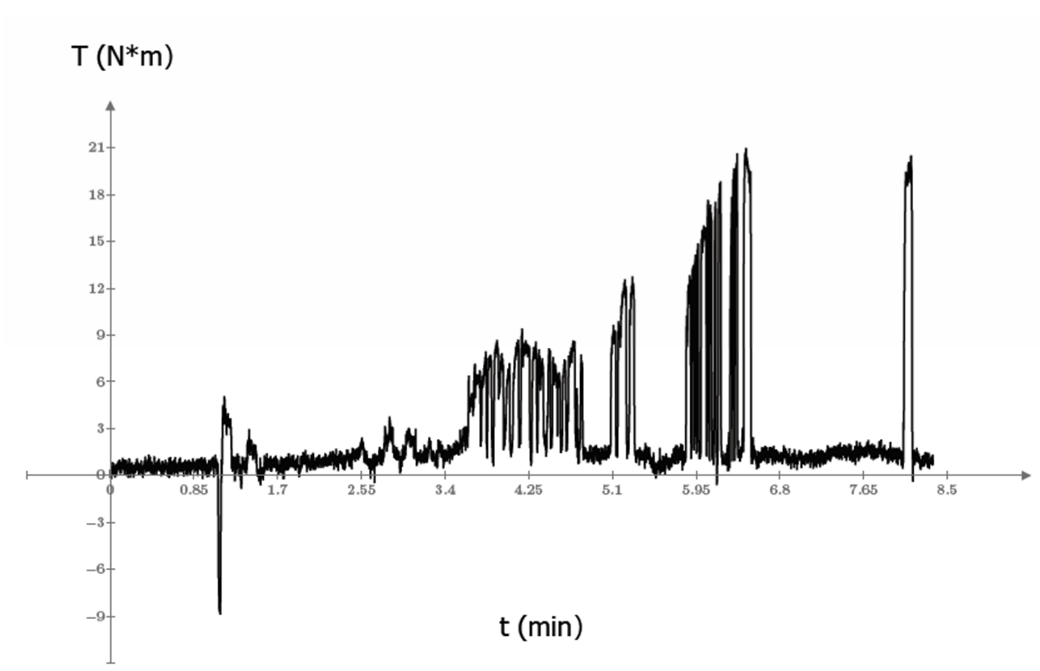

Figure B.2 Installation torque of TCD1.

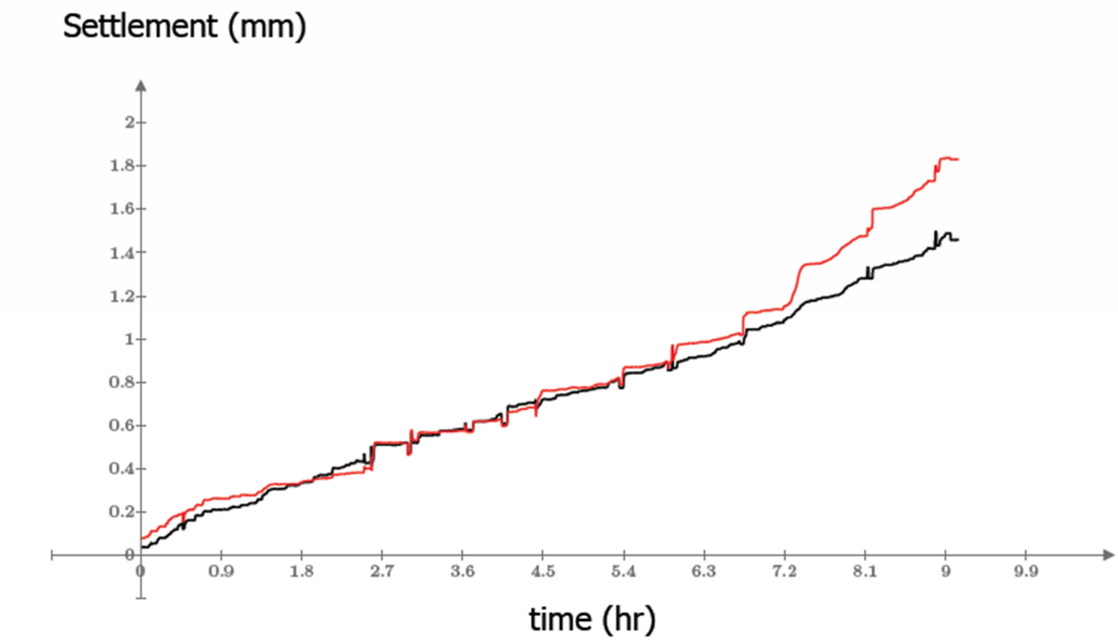

Figure B.3 Ground settlements during axial loading of TCD1.

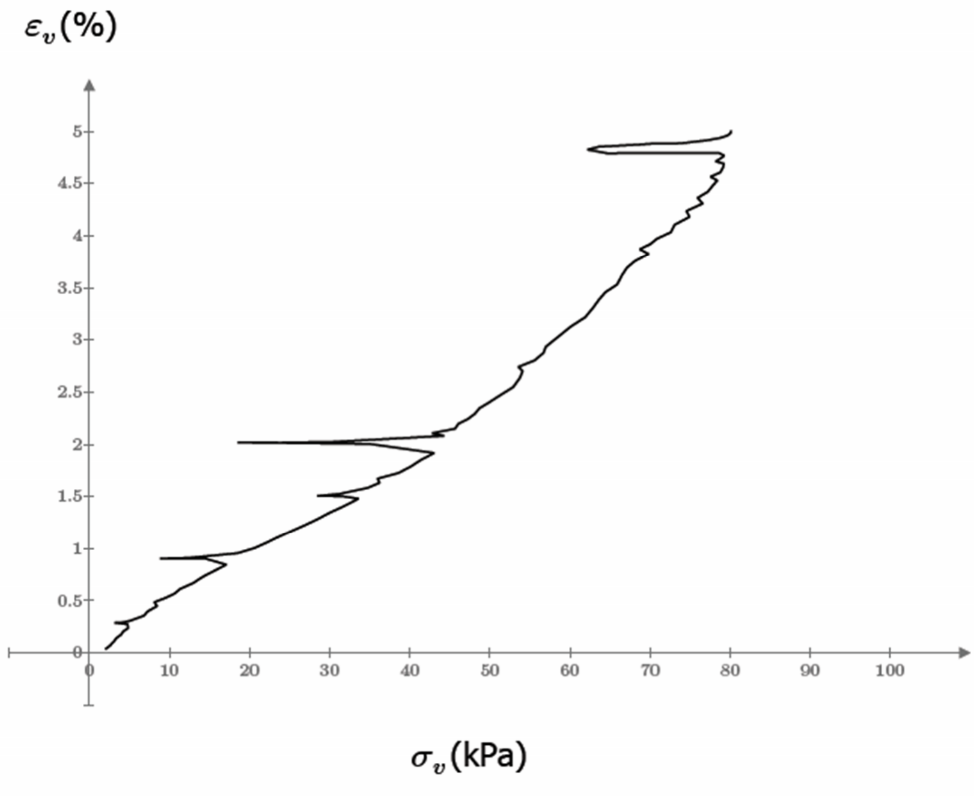

Figure B.4 Vertical strain (ε_v) vs. stress (σ_v) during consolidation of TCD2.

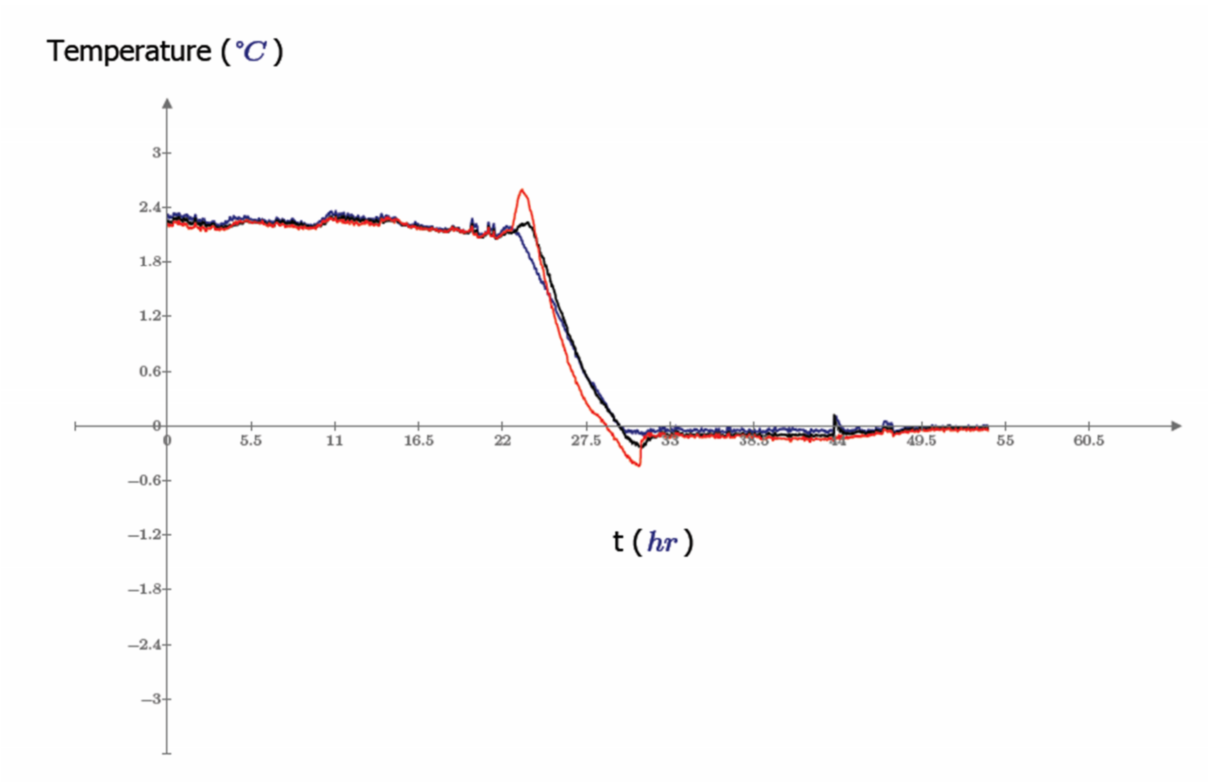

Figure B.5 Soil temperature during entire testing progress of TCD2.

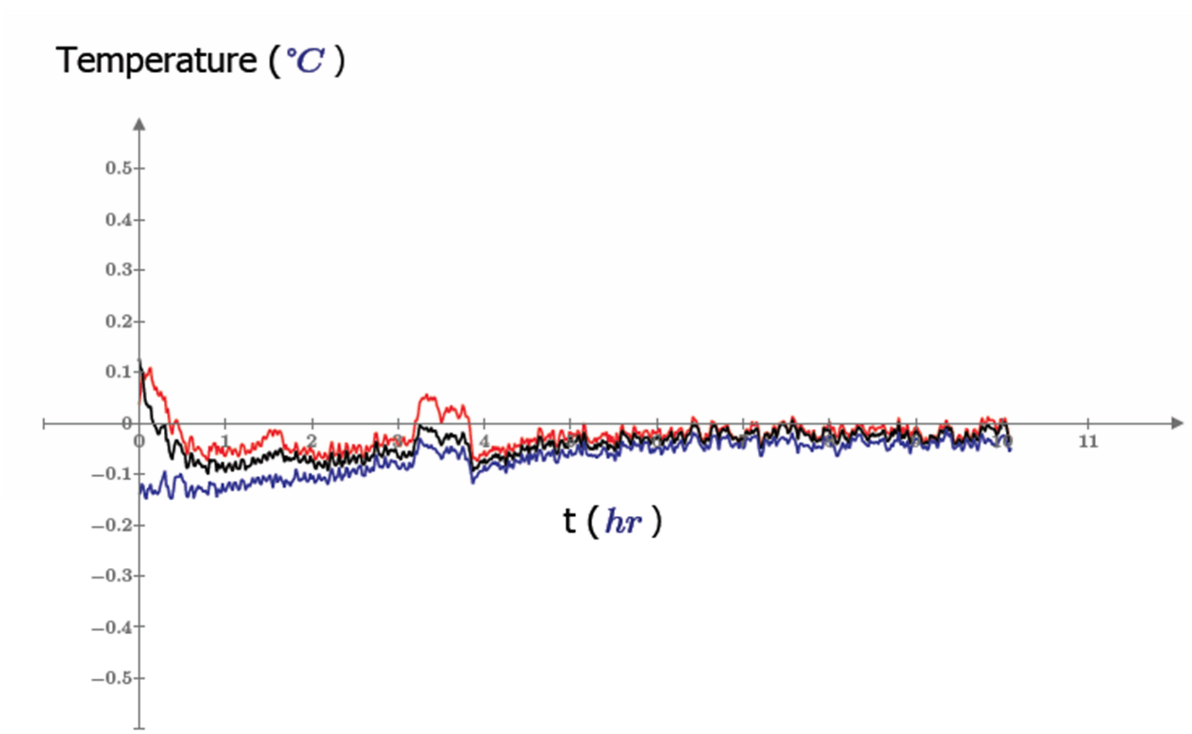

Figure B.6 Soil temperature during axial loading of TCD2.

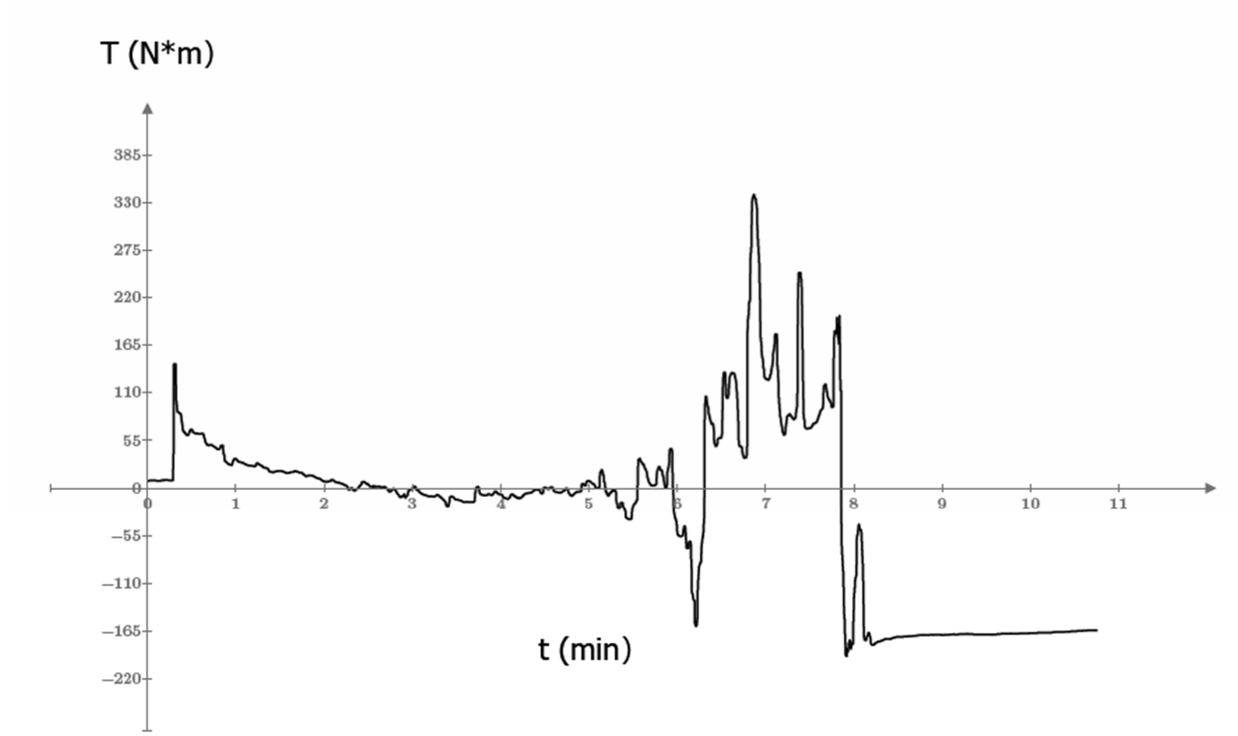

Figure B.7 Installation torque of TCD2.

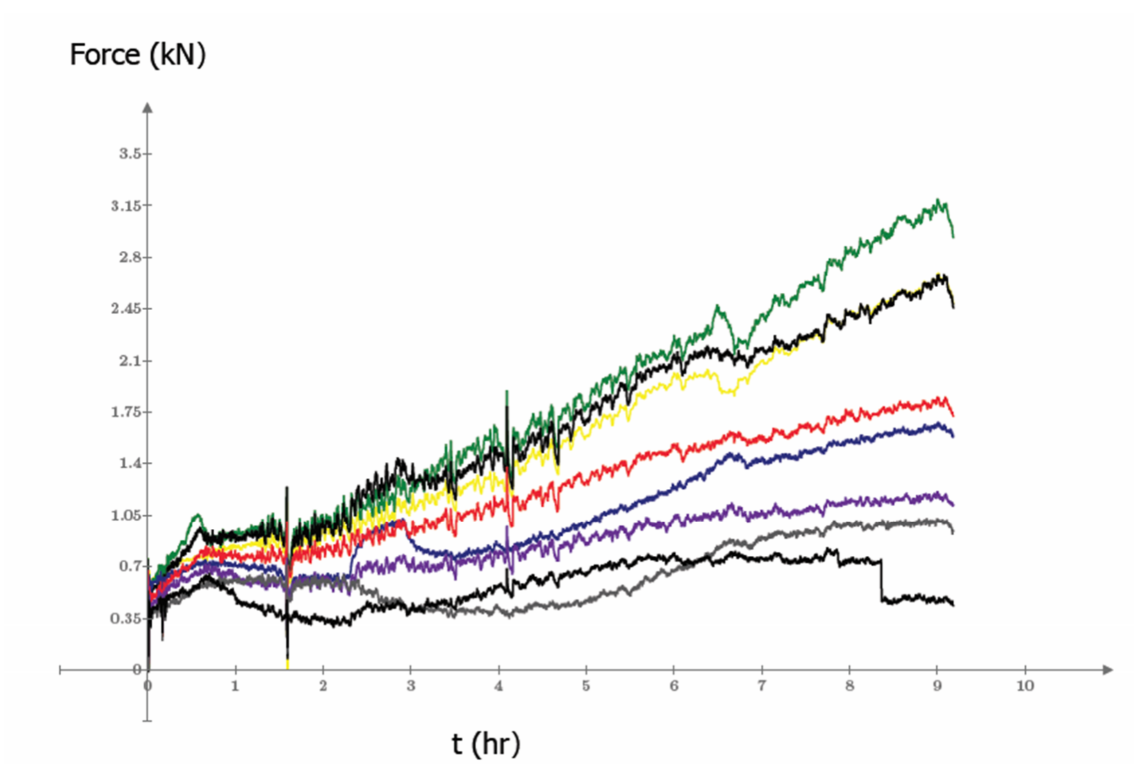

Figure B.8 Calculated axial force from strain gauges during pile loading of TCD2.

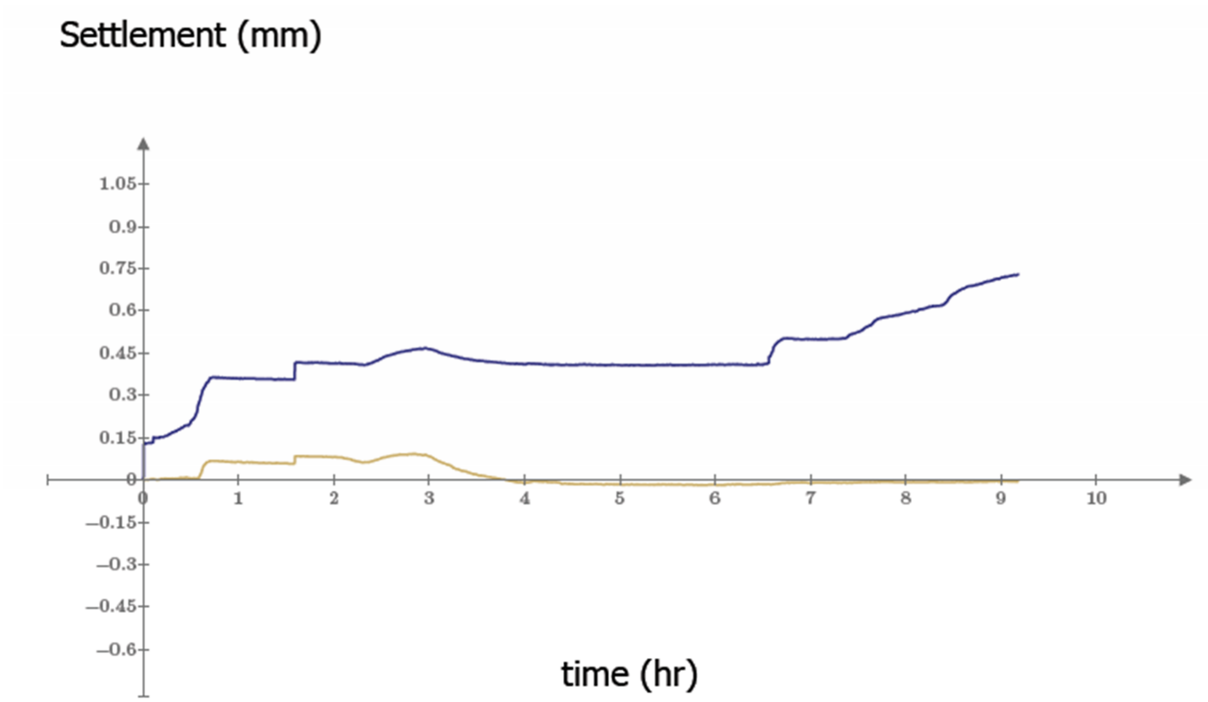

Figure B.9 Ground settlements during axial pile loading of TCD2.

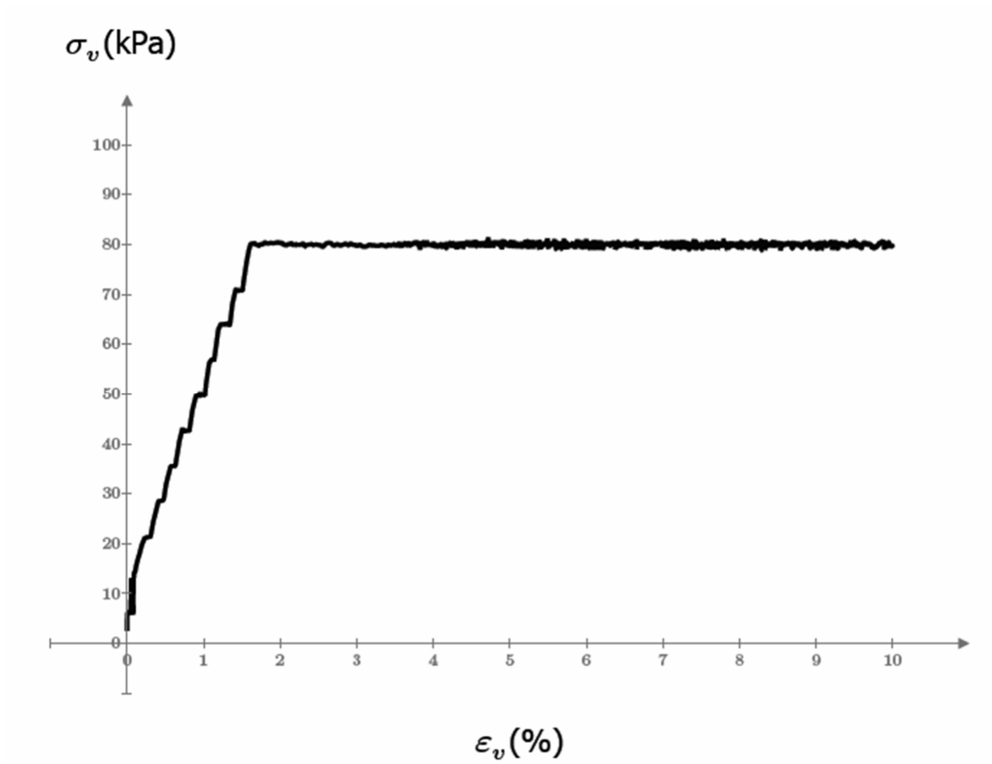

Figure B.10 Vertical strain (ε_v) vs. stress (σ_v) during consolidation of TCD3.

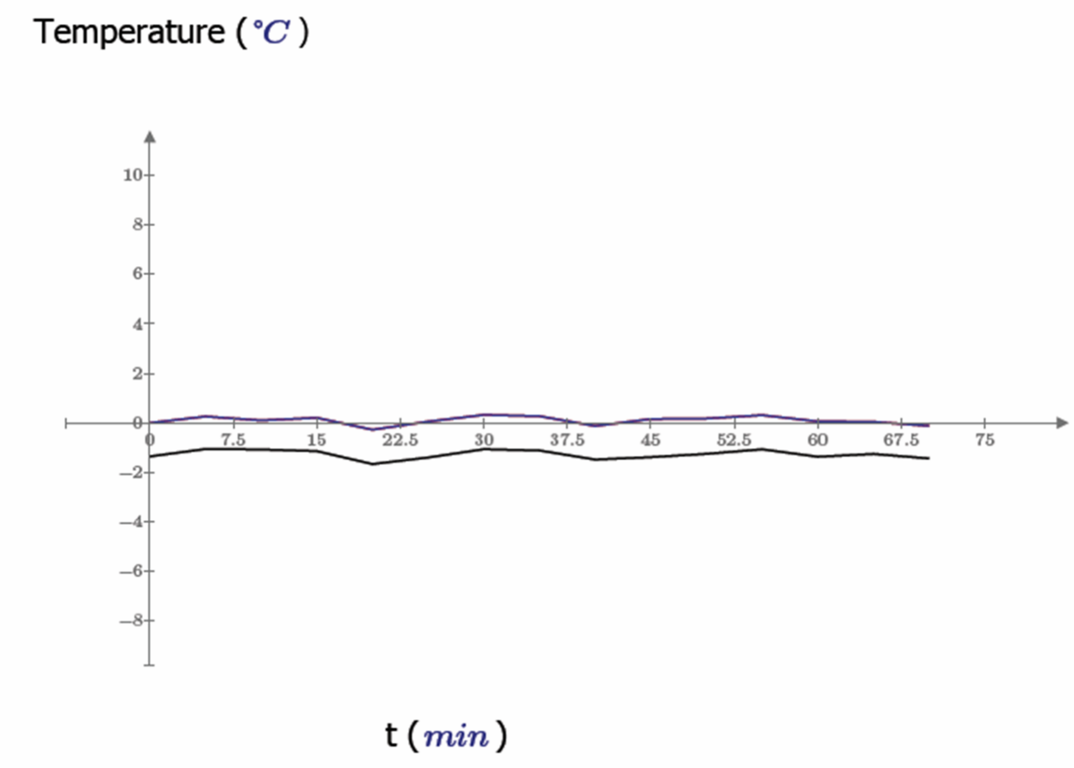

Figure B.11 Soil temperature during installation of TCD3.

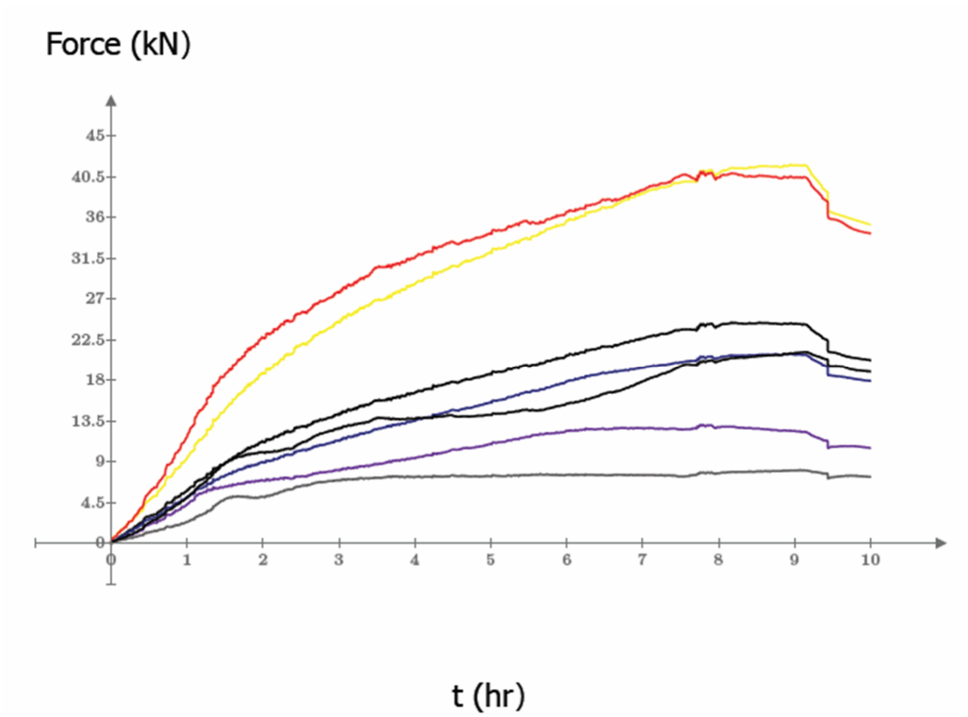

Figure B.12 Calculated axial force from strain gauges during pile loading of TCD3.

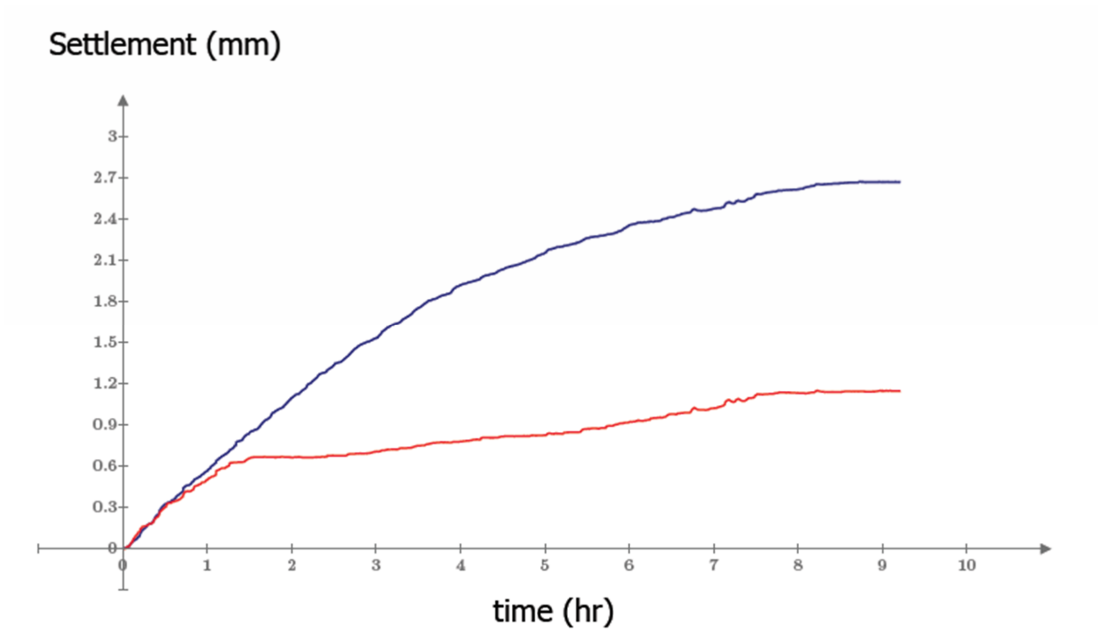

Figure B.13 Ground settlements during axial pile loading of TCD3.

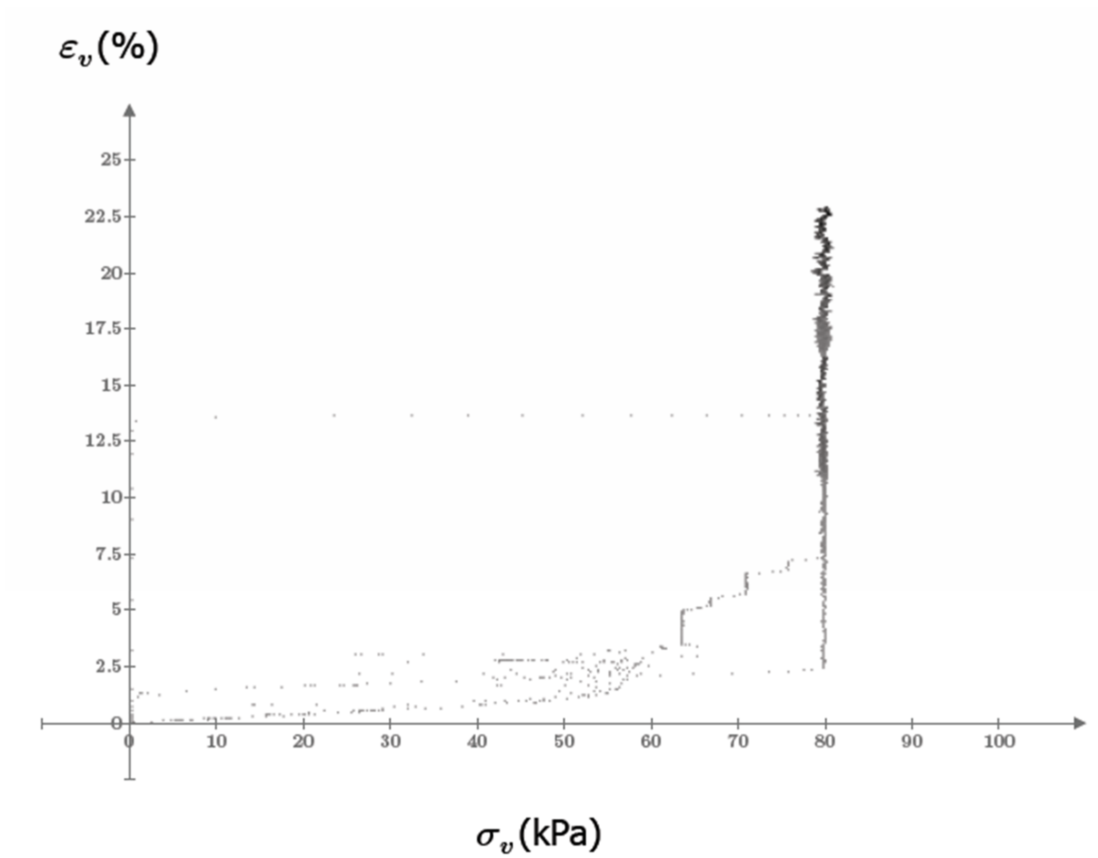

Figure B.14 Vertical strain (ε_v) vs. stress (σ_v) during consolidation of TCD5.

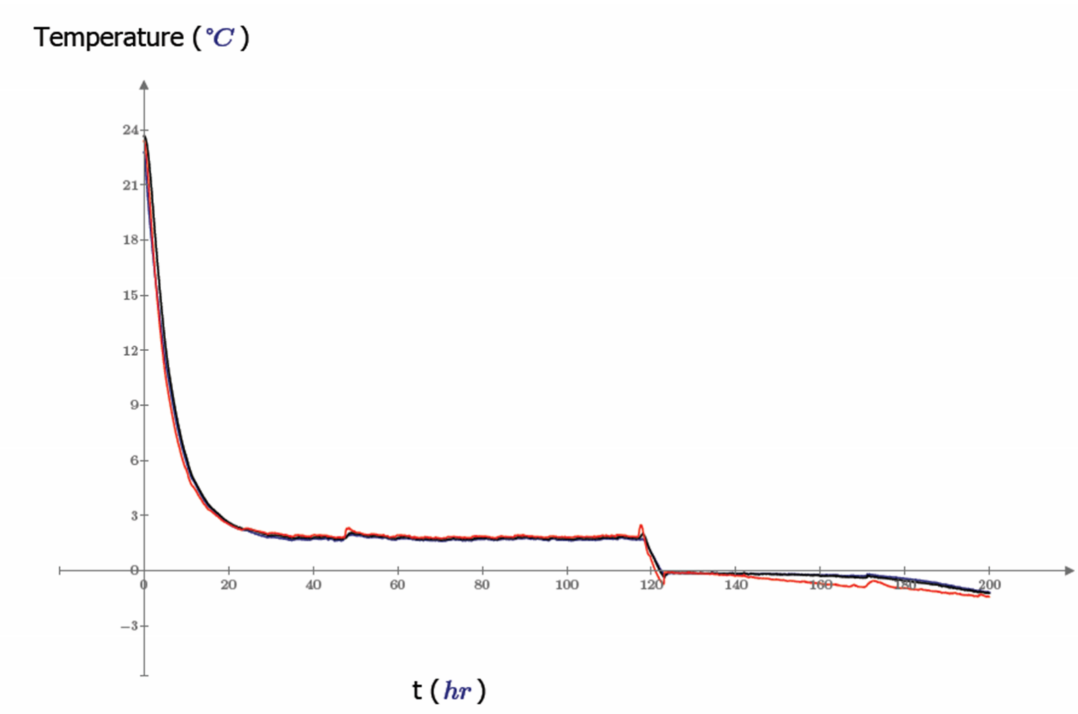

Figure B.15 Soil temperature during entire testing progress of TCD5.

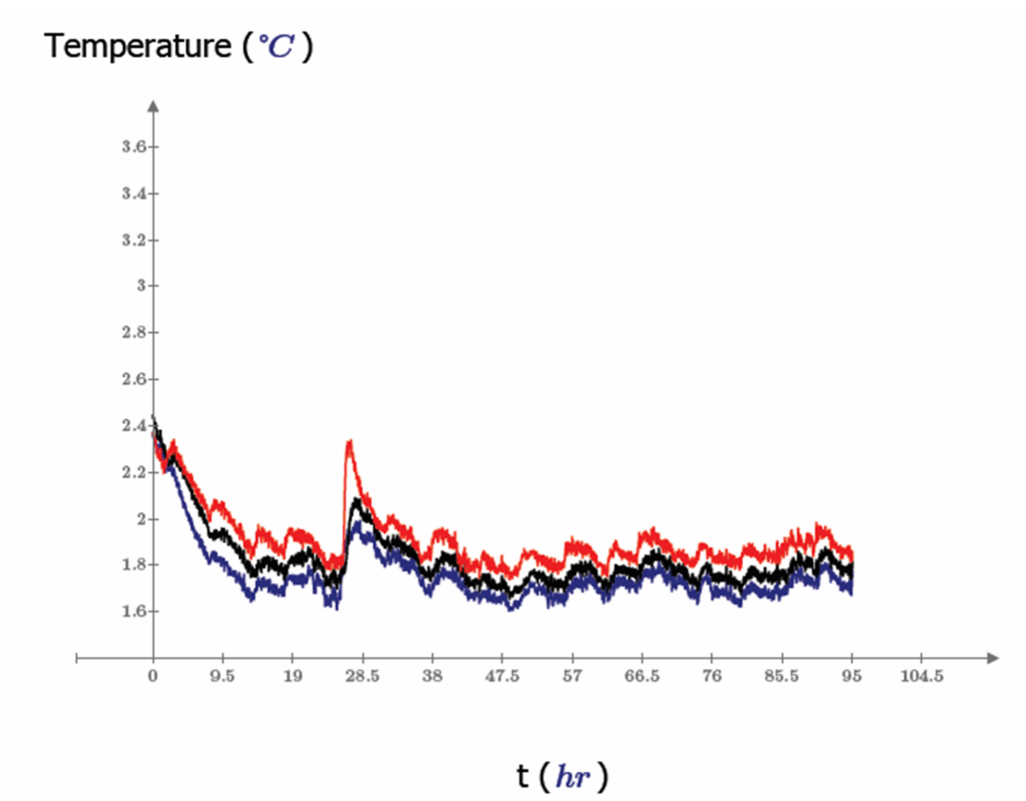

Figure B.16 Soil temperature during consolidation of TCD5.

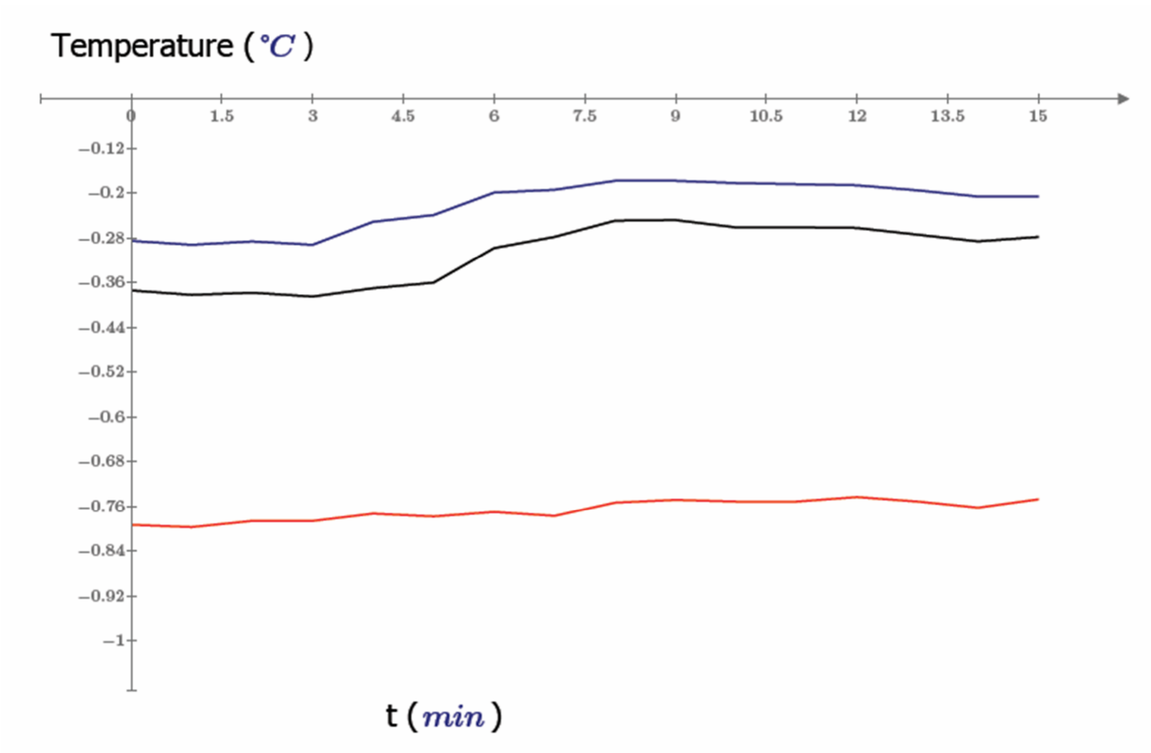

Figure B.17 Soil temperature during installation of TCD5.

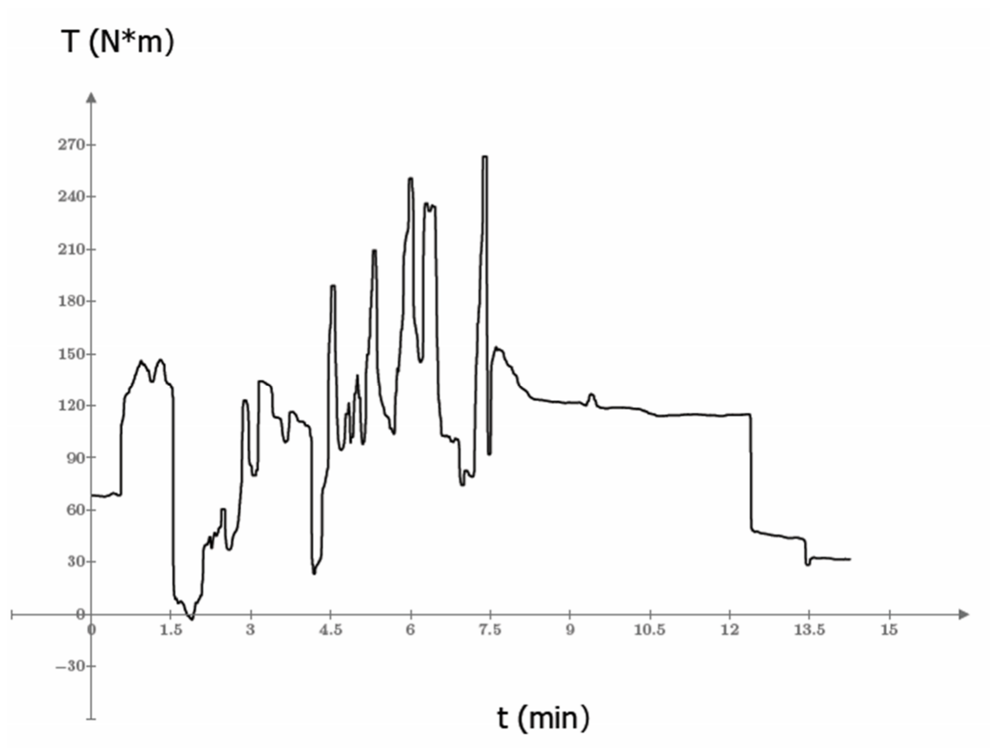

Figure B.18 Installation torque of TCD5.

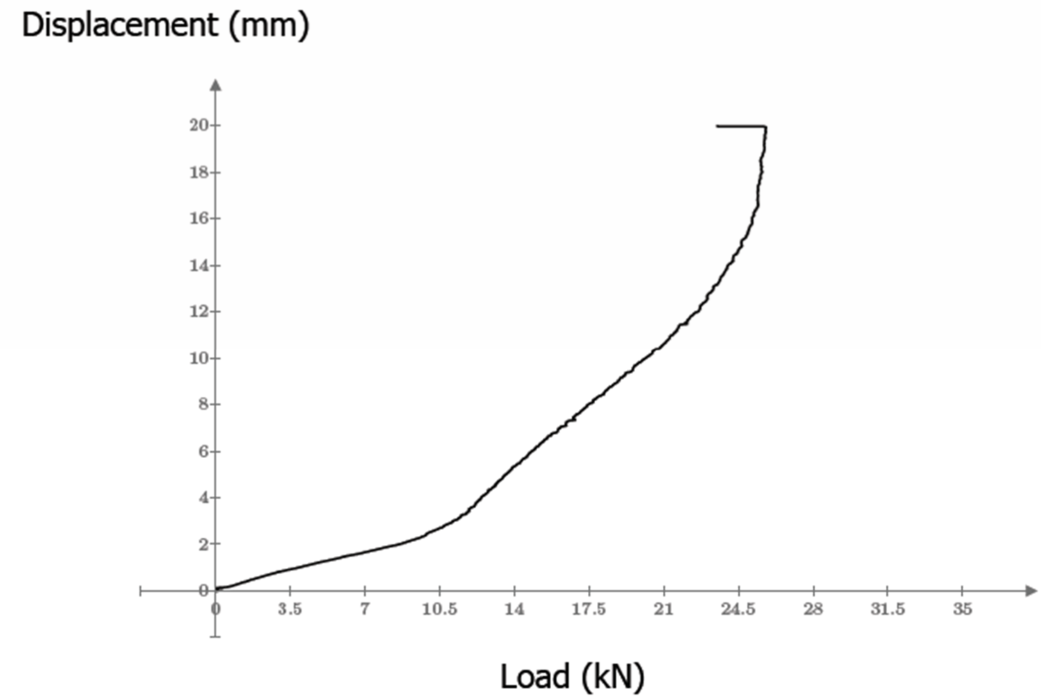

Figure B.19 Pile head load versus displacement during axial loading of TCD5.

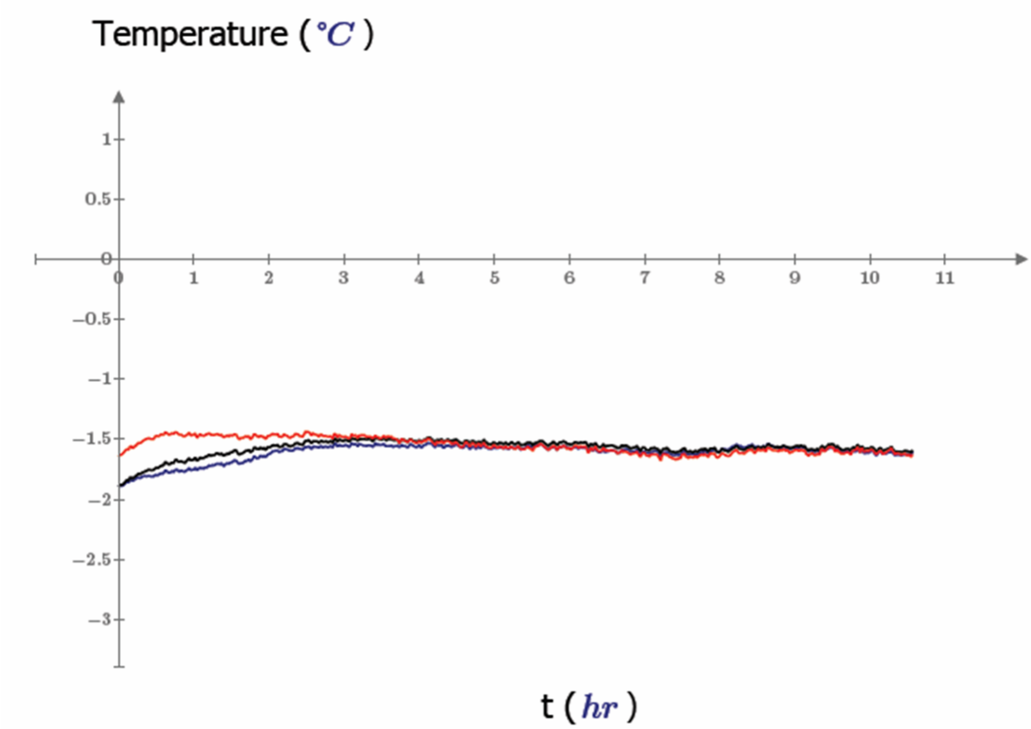

Figure B.20 Soil temperature during loading of TCD5.

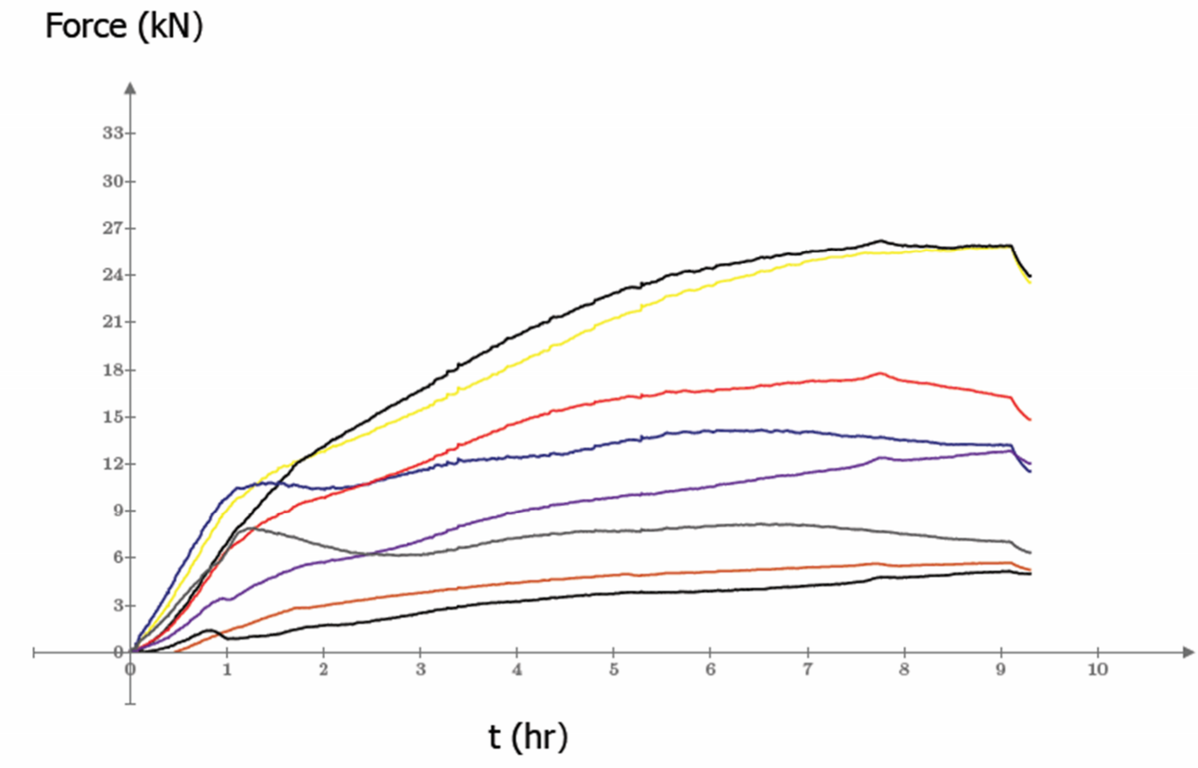

Figure B.21 Calculated axial force from strain gauges during axial pile loading of TCD5.

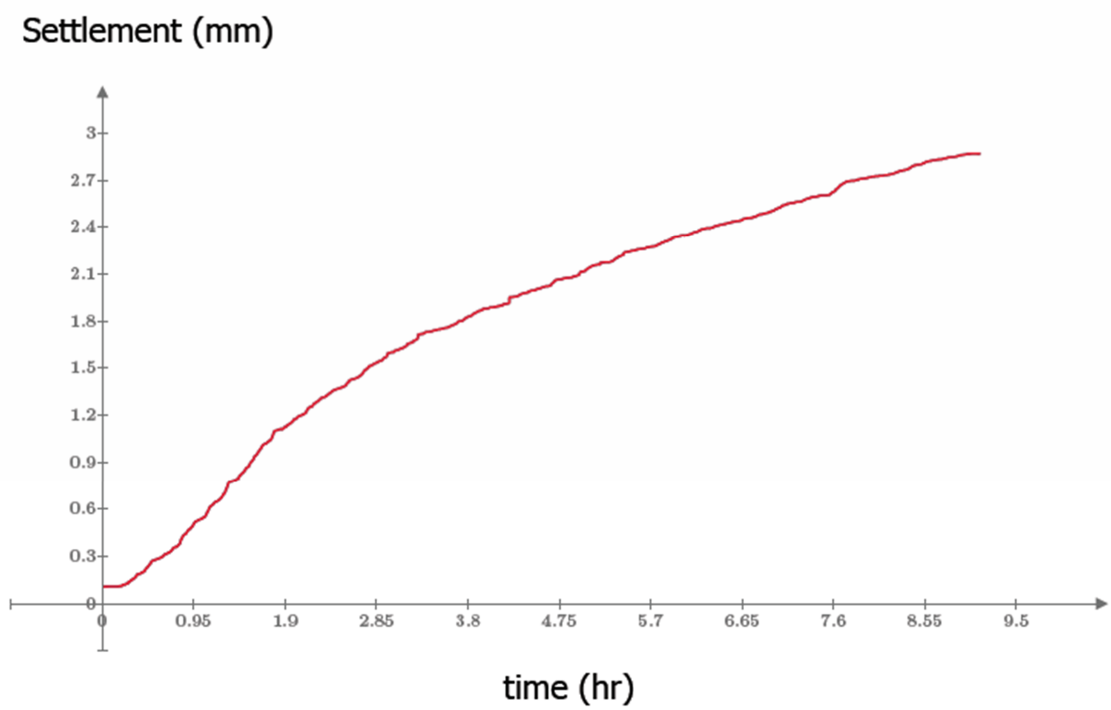

Figure B.22 Ground settlement during axial pile loading of TCD5.

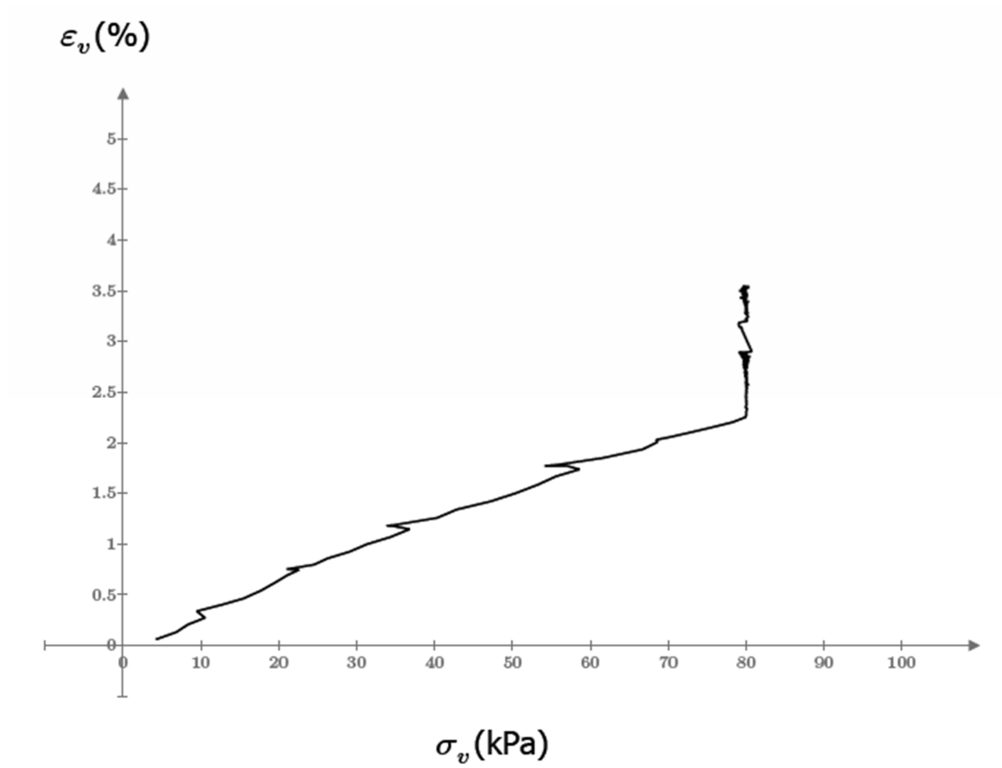

Figure B.23 Vertical strain (ε_v) vs. stress (σ_v) during consolidation of TCD6.

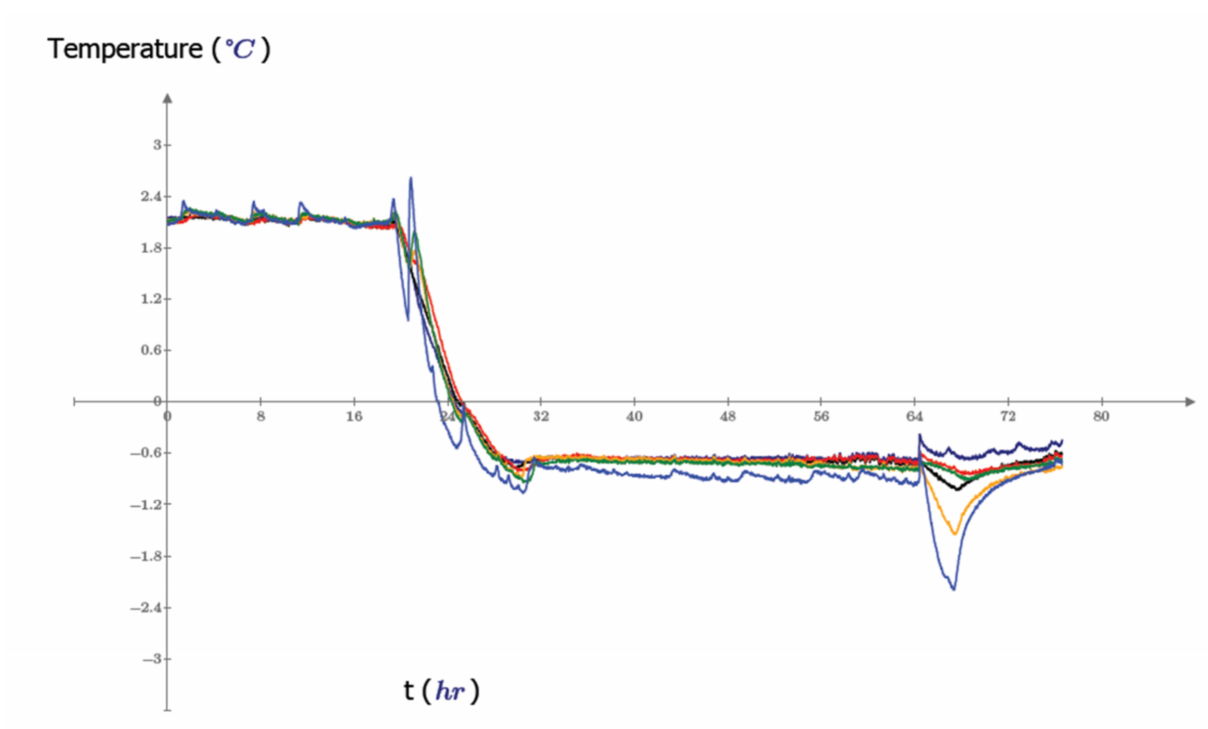

Figure B.24 Soil temperature during entire testing progress of TCD6.

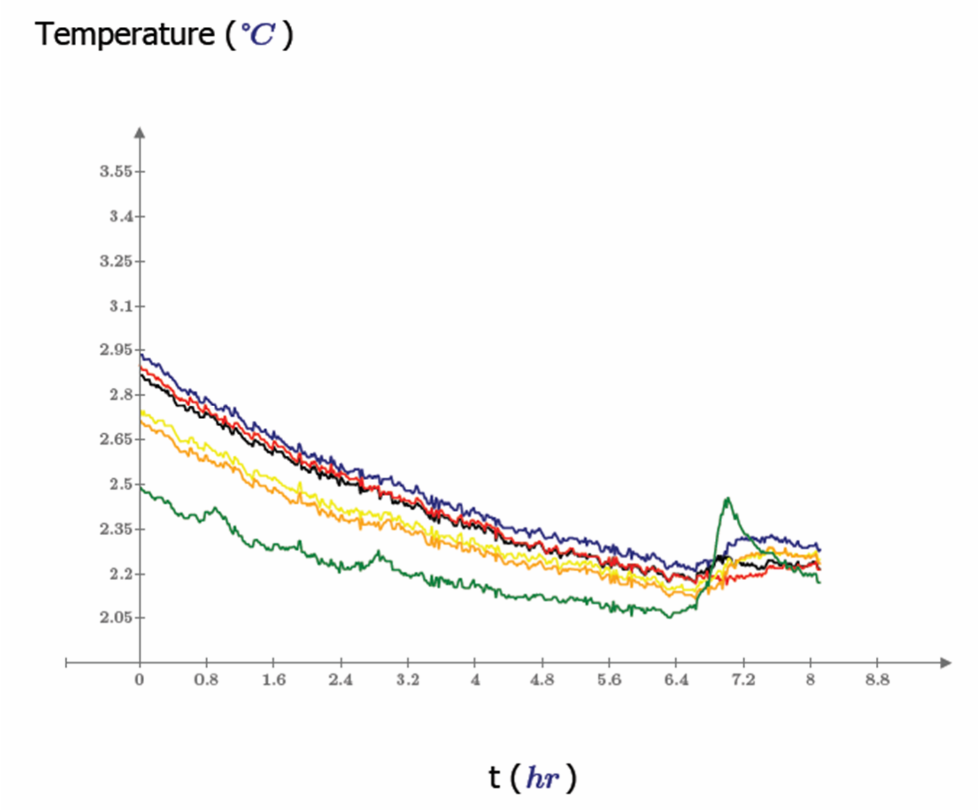

Figure B.25 Soil temperature during consolidation of TCD6.

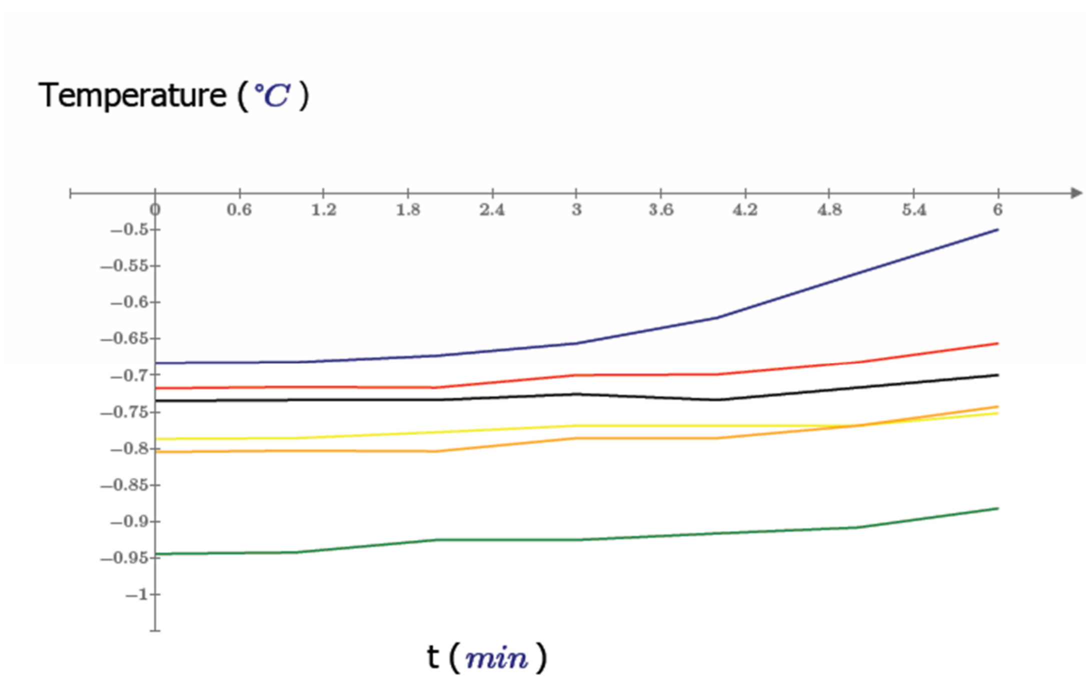

Figure B.26 Soil temperature during installation of TCD6.

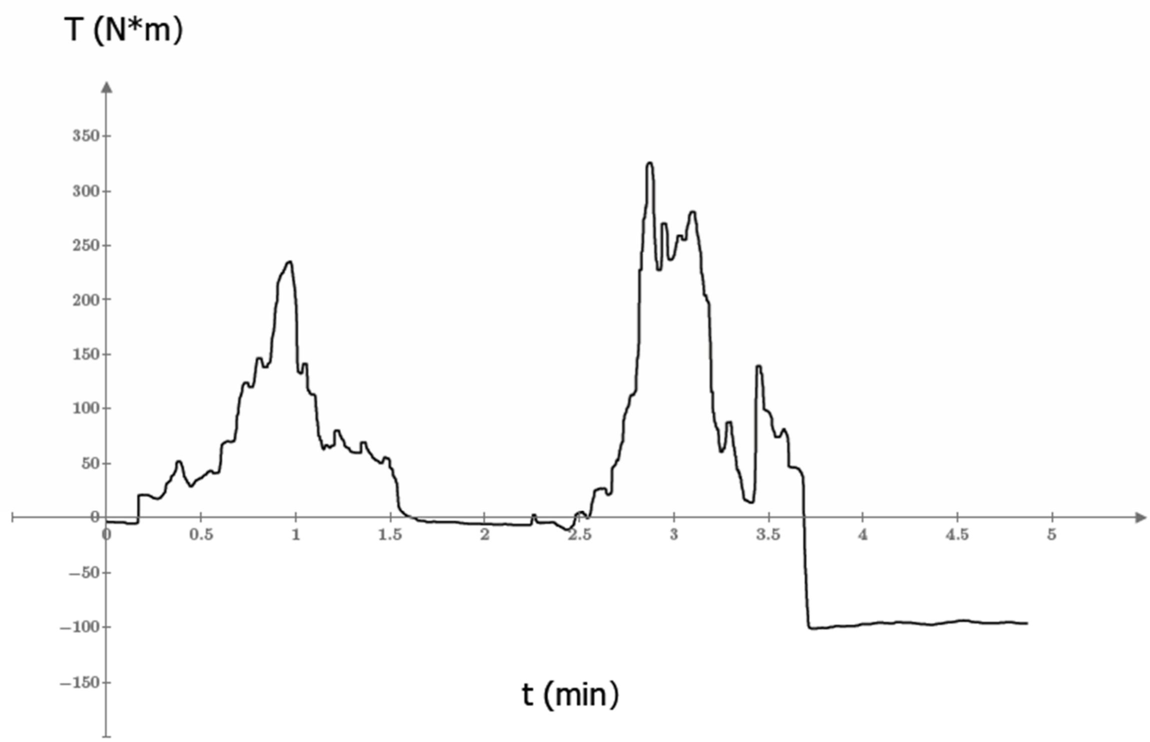

Figure B.27 Installation torque of TCD6.

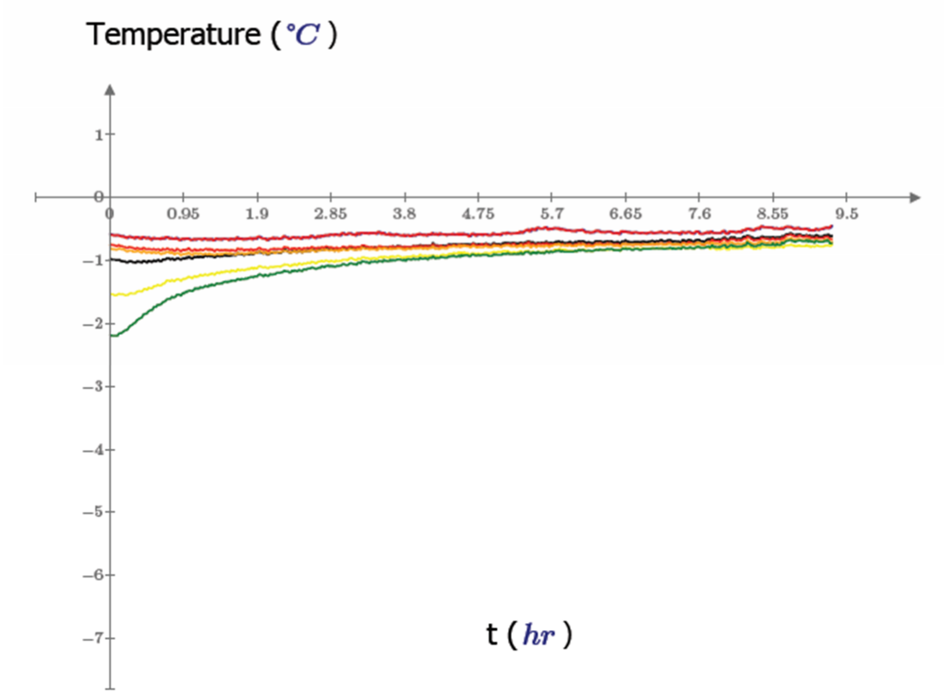

Figure B.28 Soil temperature during loading of TCD6.

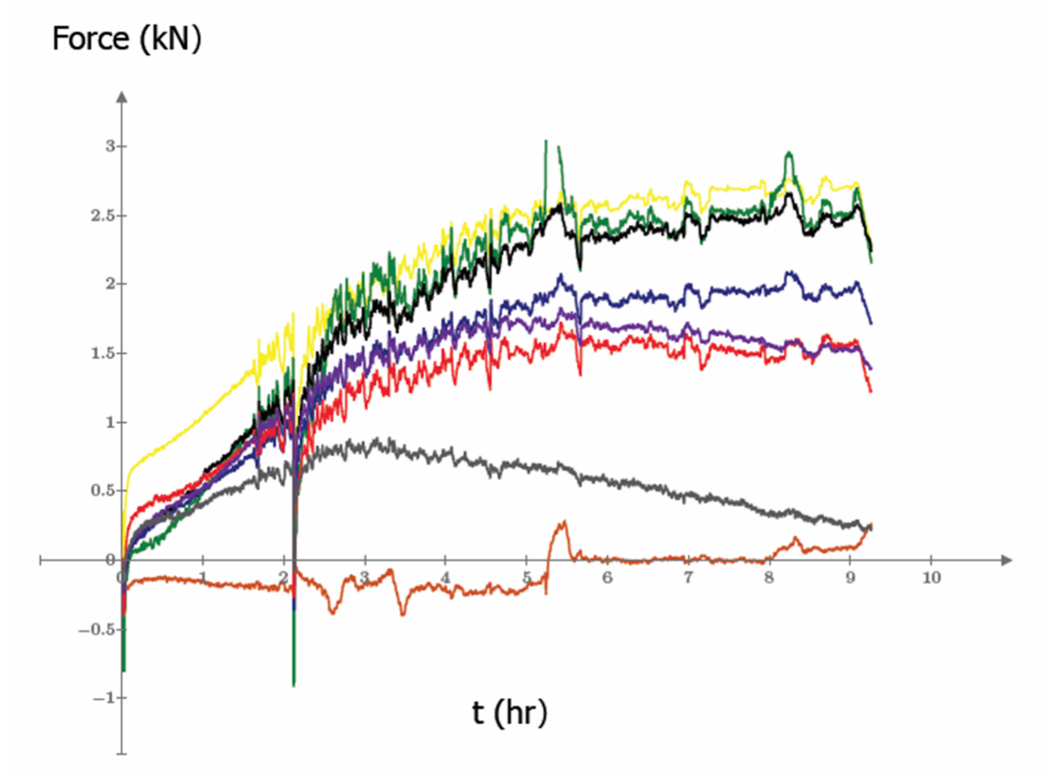

Figure B.29 Calculated axial force from strain gauges during axial pile loading of TCD6.

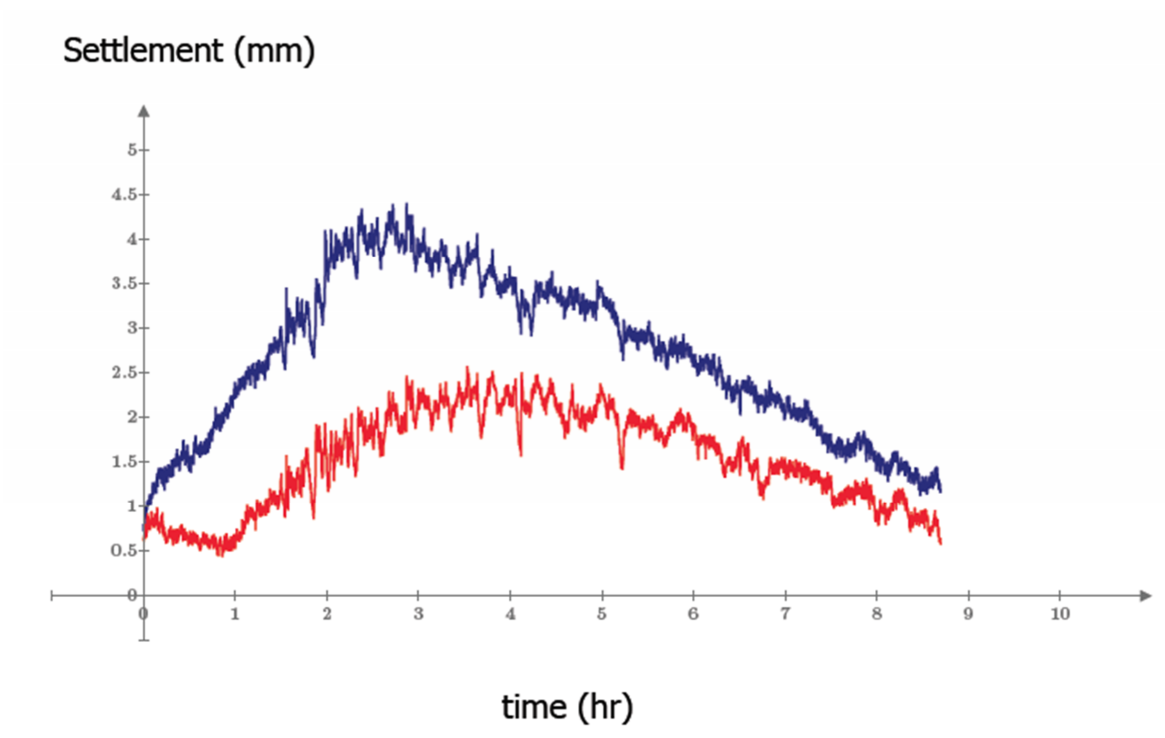

Figure B.30 Ground settlement during axial pile loading of TCD6.

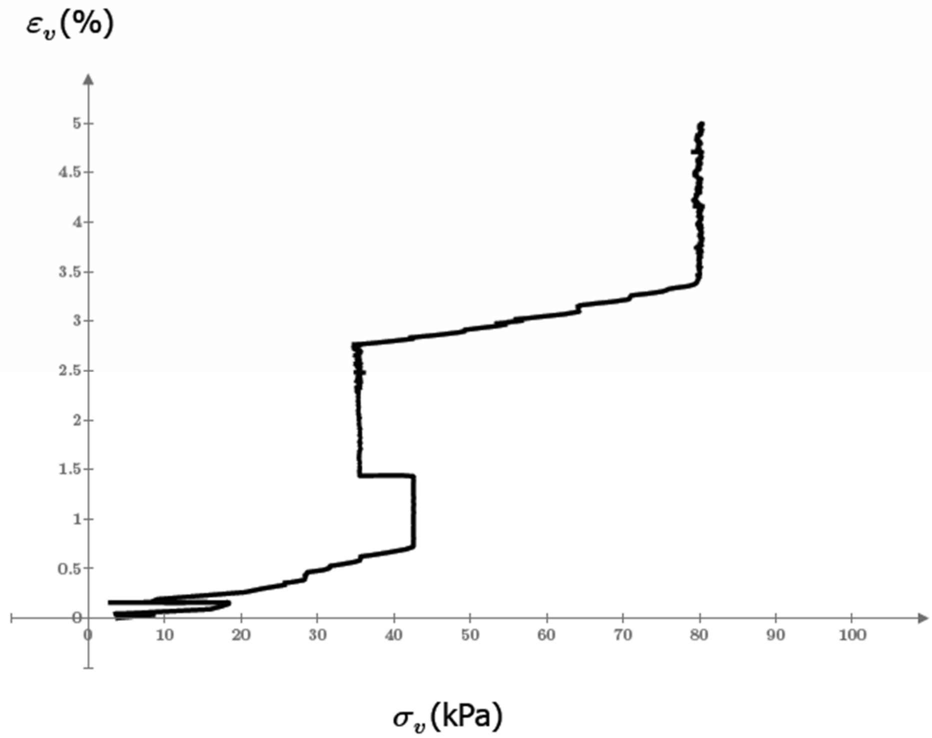

Figure B.31 Vertical strain (ε_v) vs. stress (σ_v) during consolidation of TCD7.

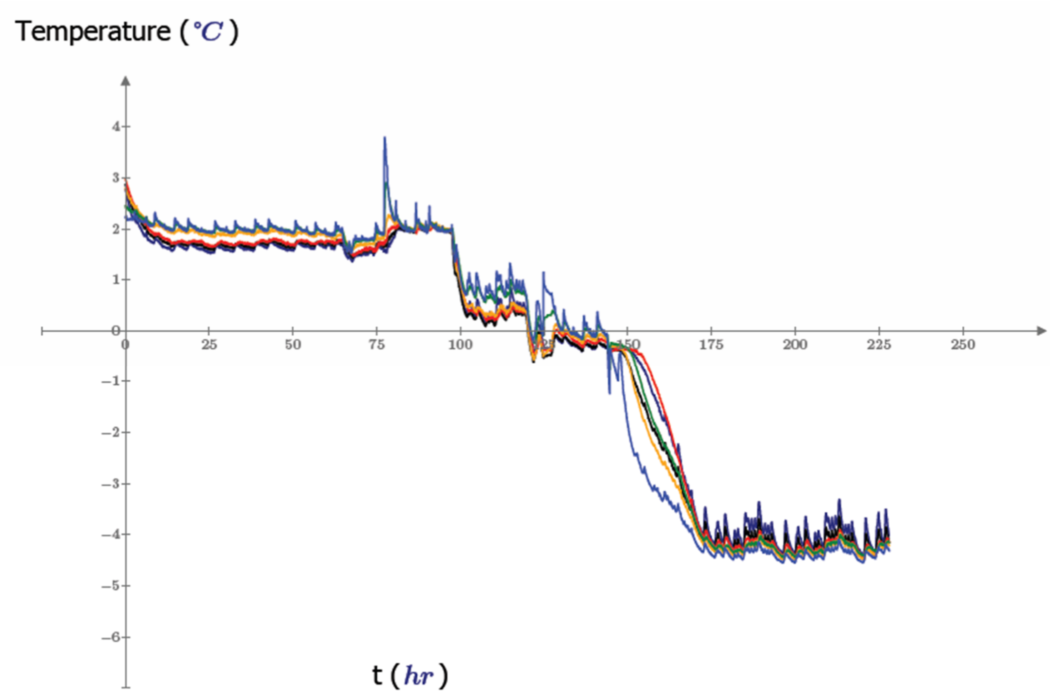

Figure B.32 Soil temperature during entire testing progress of TCD7.

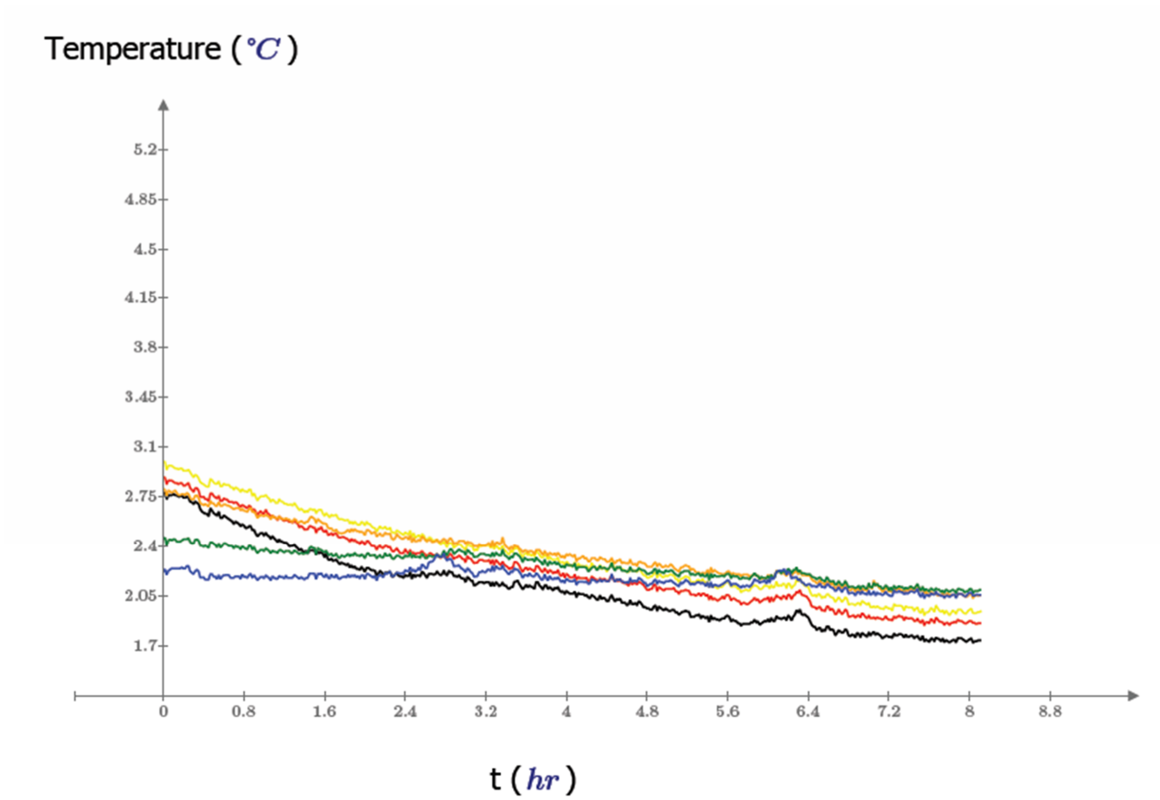

Figure B.33 Soil temperature during consolidation of TCD7.

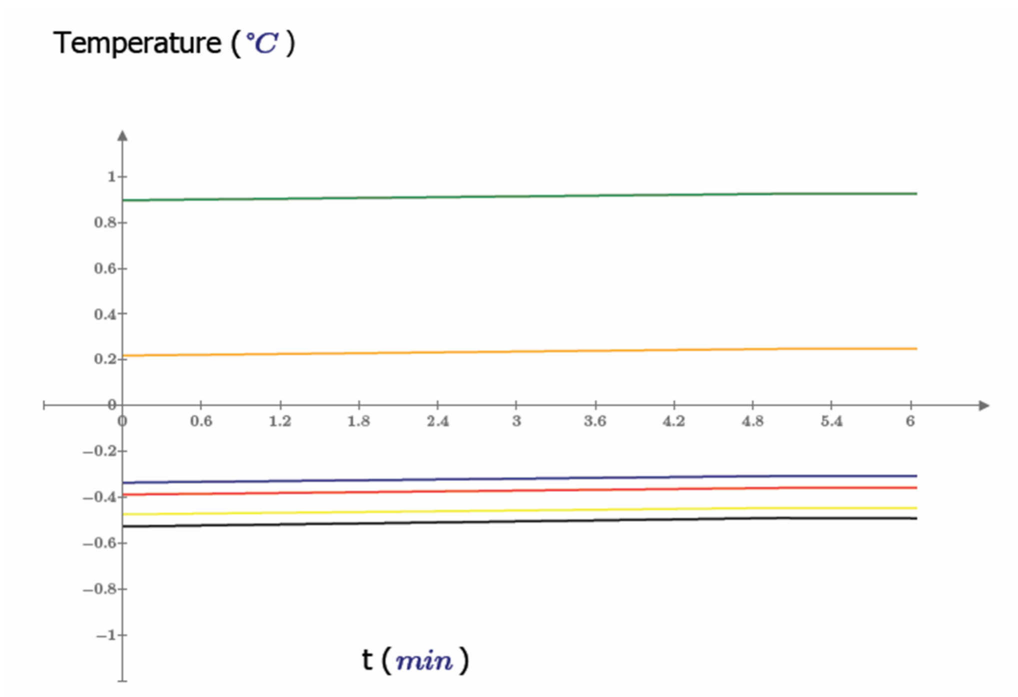

Figure B.34 Soil temperature during installation of TCD7.

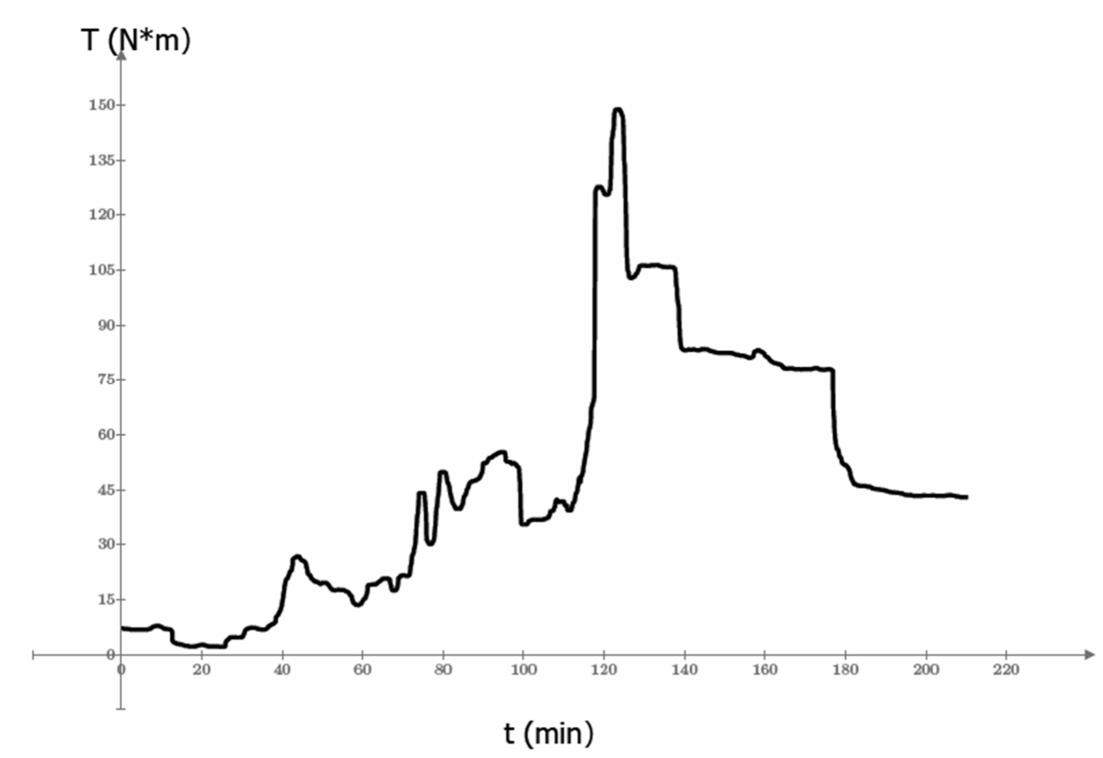

Figure B.35 Installation torque of TCD7.

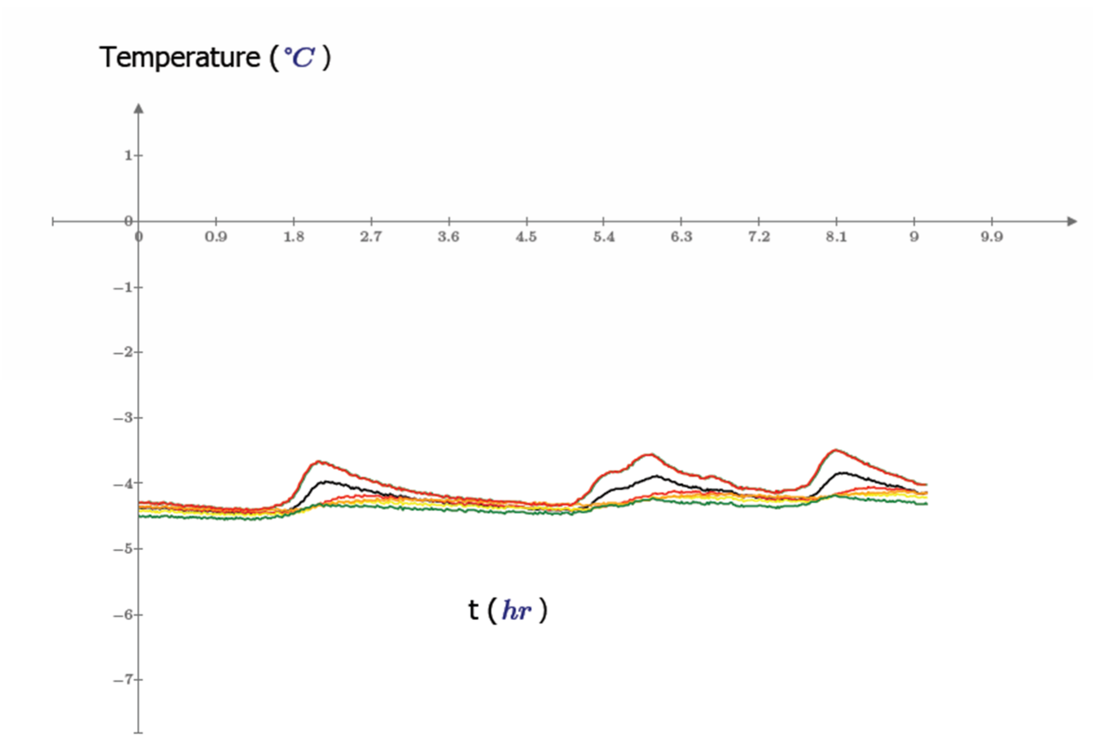

Figure B.36 Soil temperature during loading of TCD7.

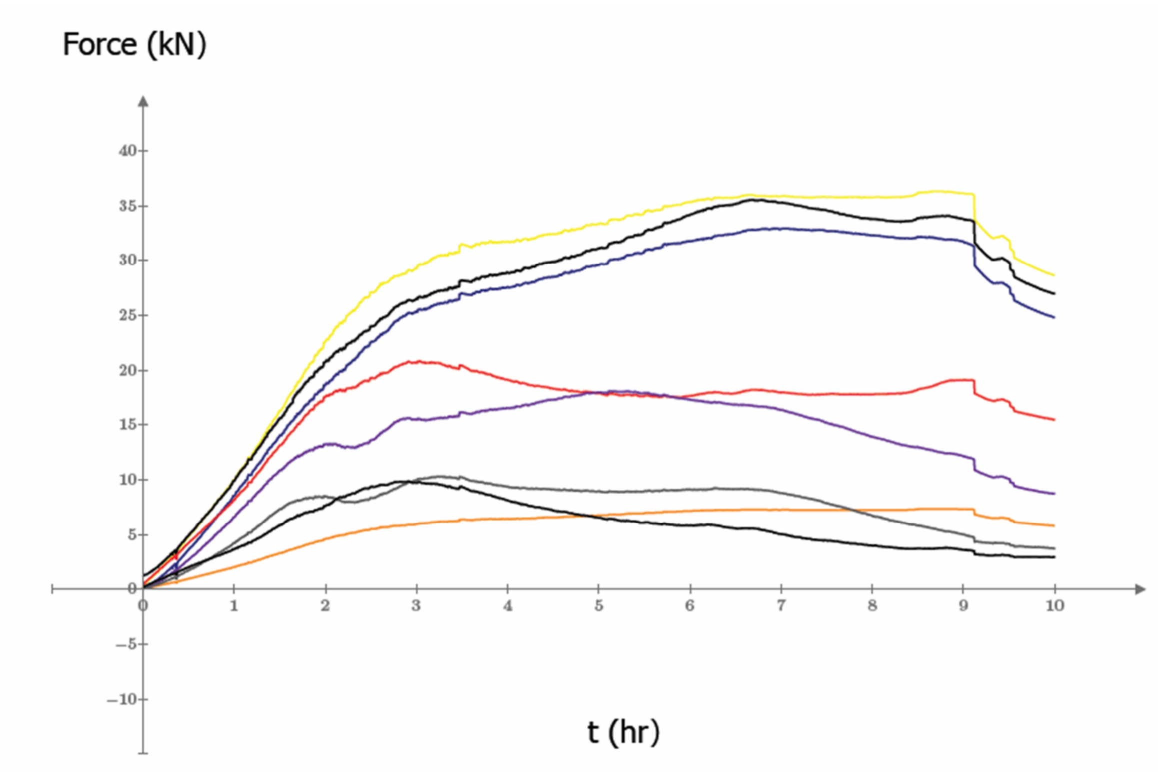

Figure B.37 Calculated axial force from strain gauges during axial pile loading of TCD7.

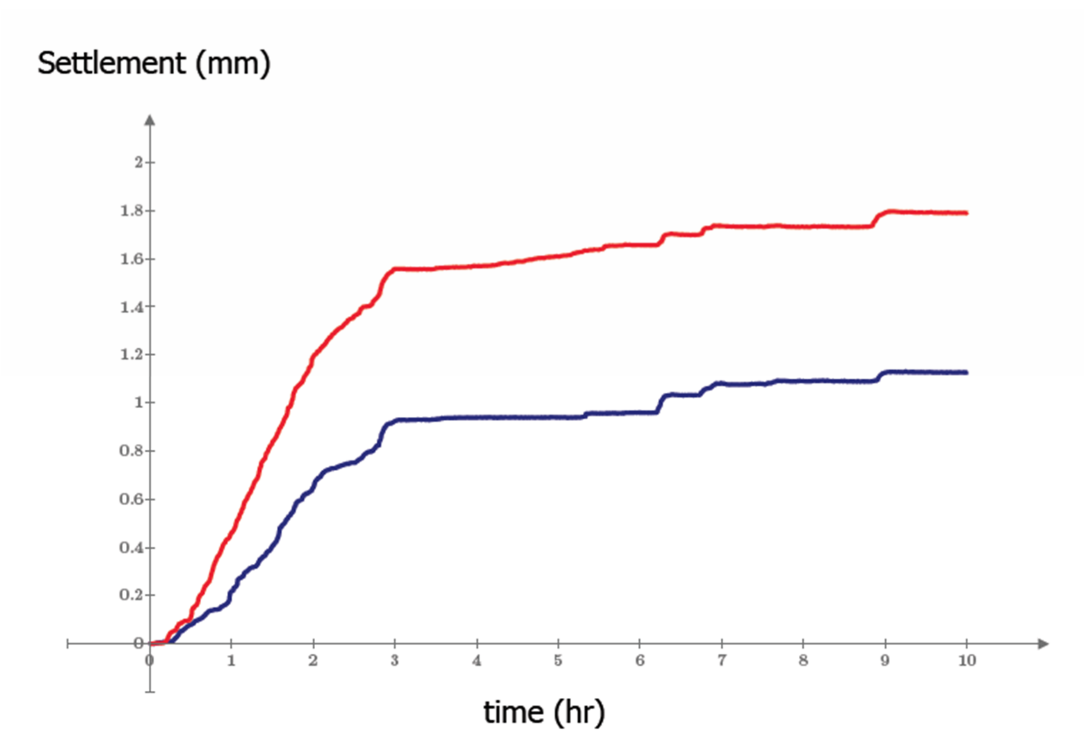

Figure B.38 Ground settlement during axial pile loading of TCD7.

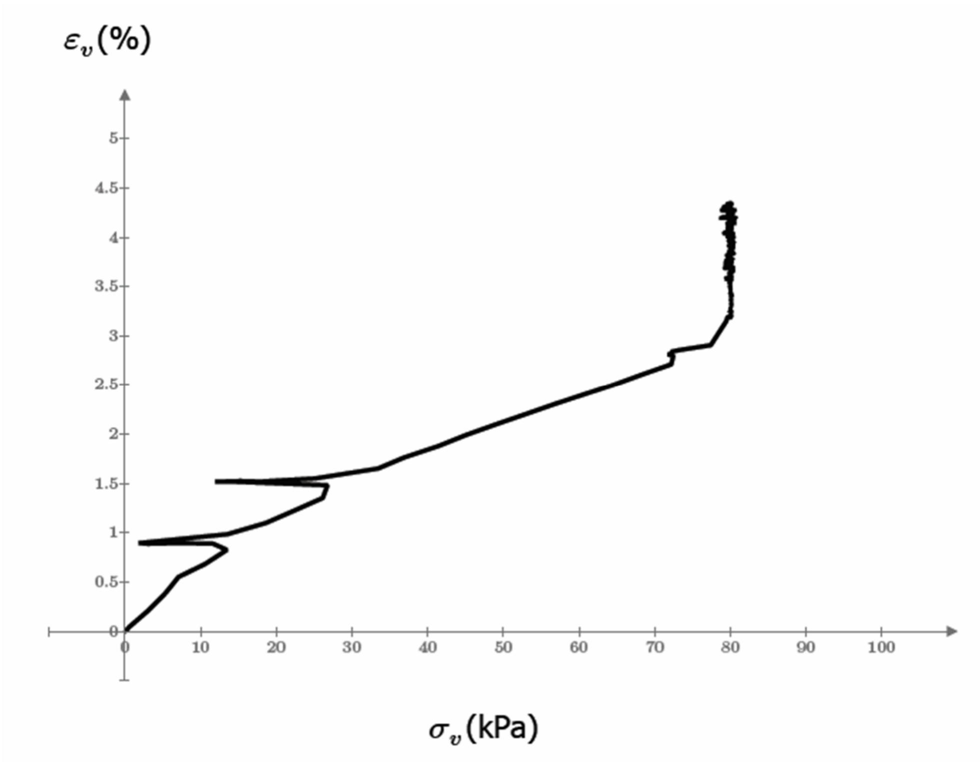

Figure B.39 Vertical strain (ε_v) vs. stress (σ_v) during consolidation of TCD8.

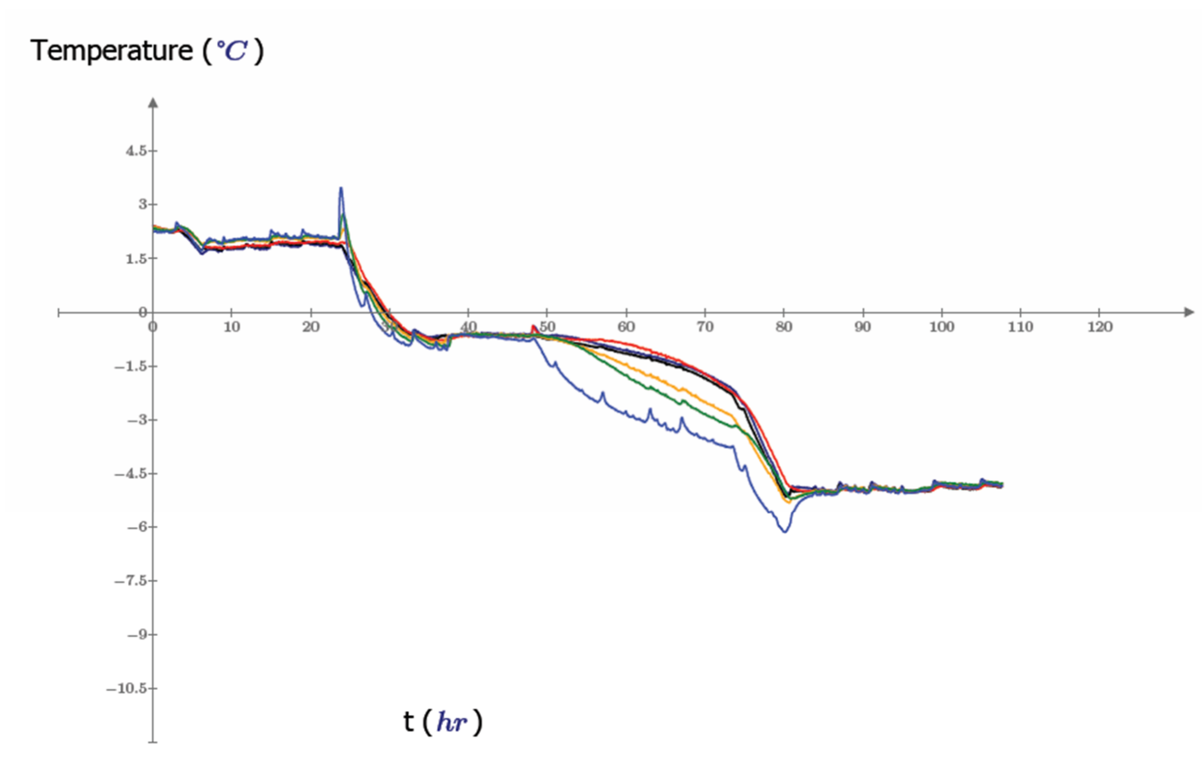

Figure B.40 Soil temperature during entire testing progress of TCD8.

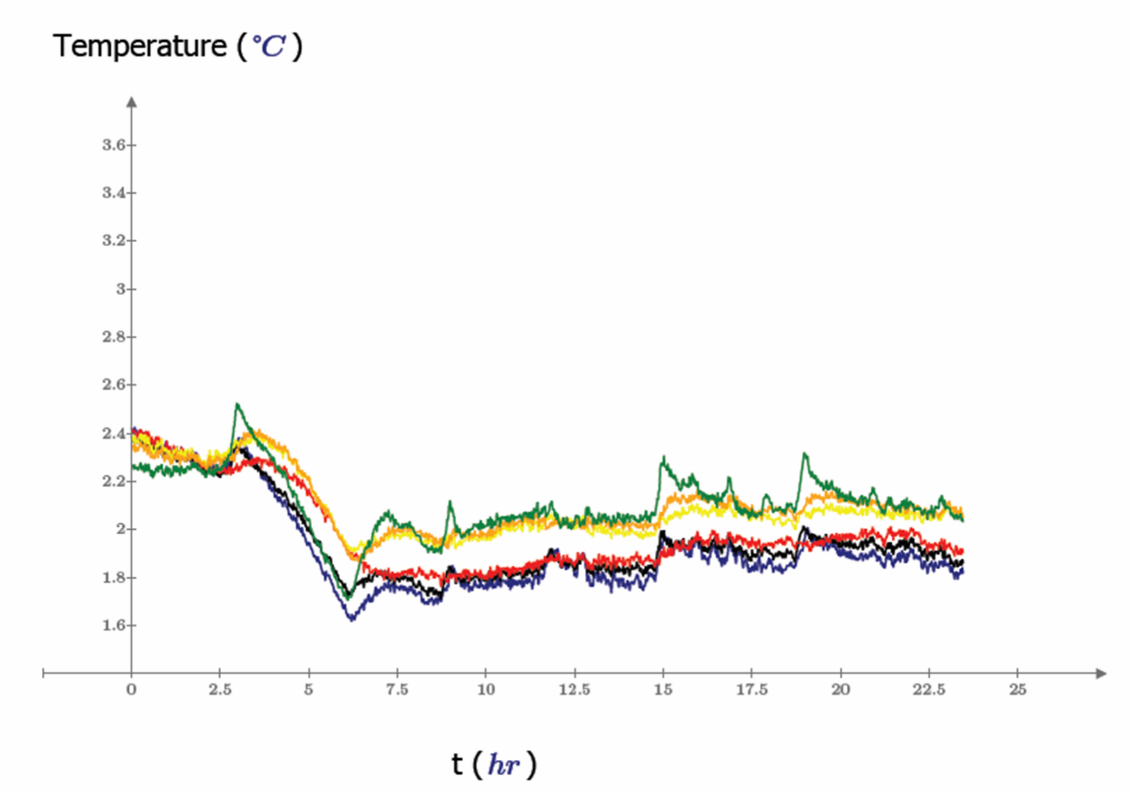

Figure B.41 Soil temperature during consolidation of TCD8.

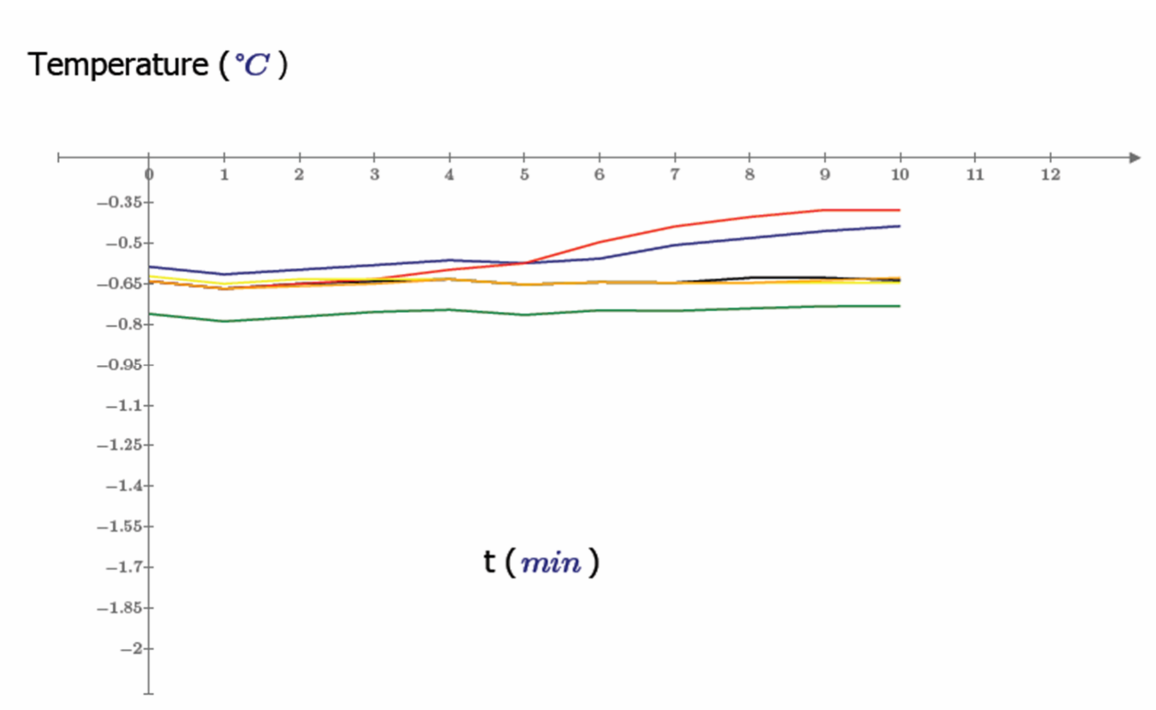

Figure B.42 Soil temperature during installation of TCD8.

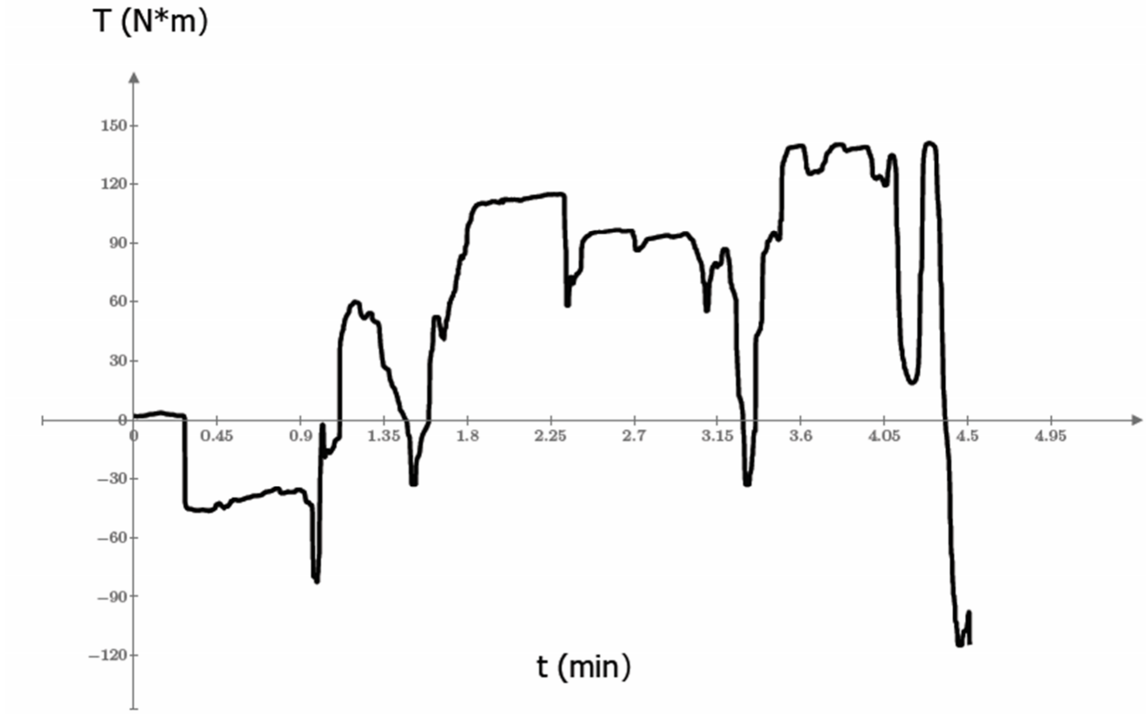

Figure B.43 Installation torque of TCD8.

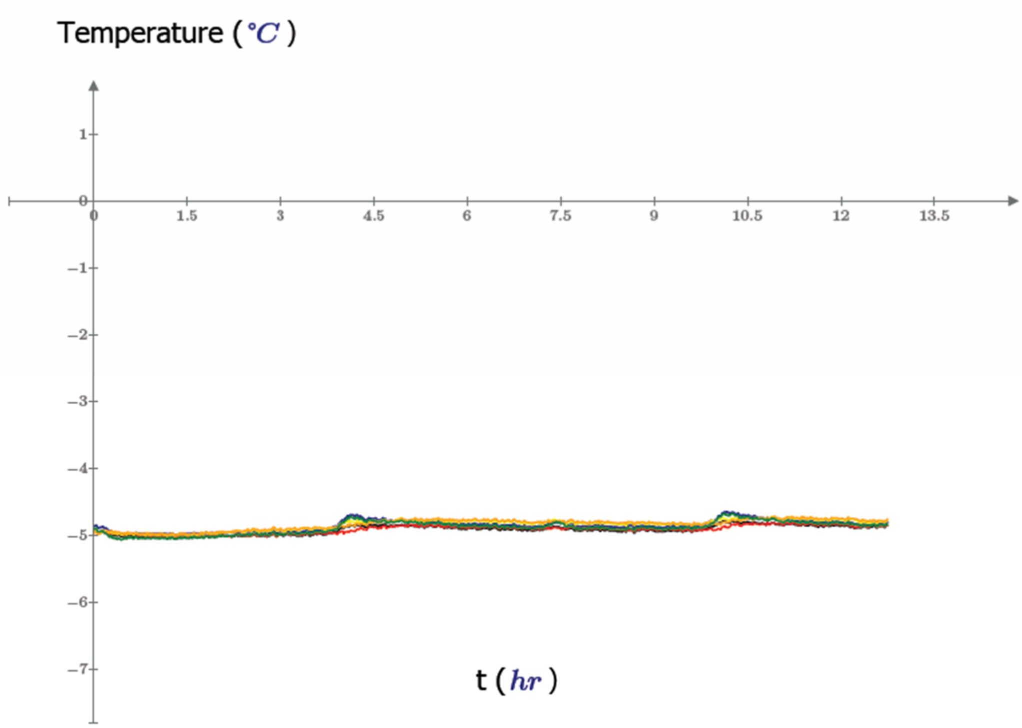

Figure B.44 Soil temperature during loading of TCD8.

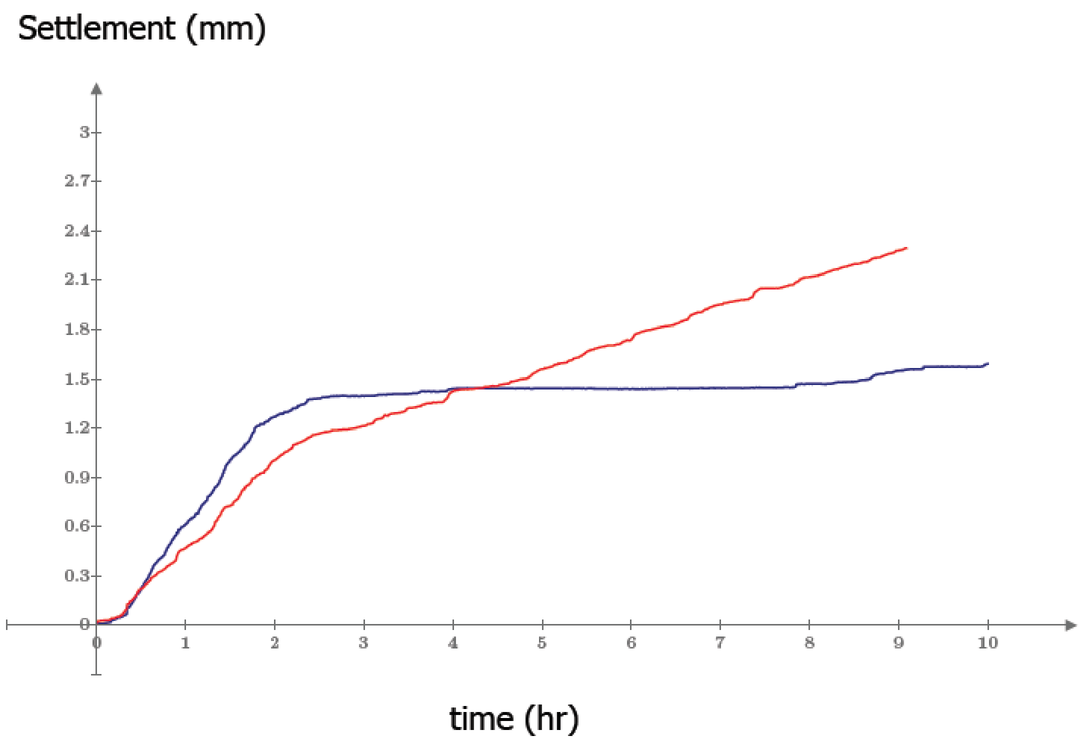

Figure B.45 Ground settlement during axial pile loading of TCD8.

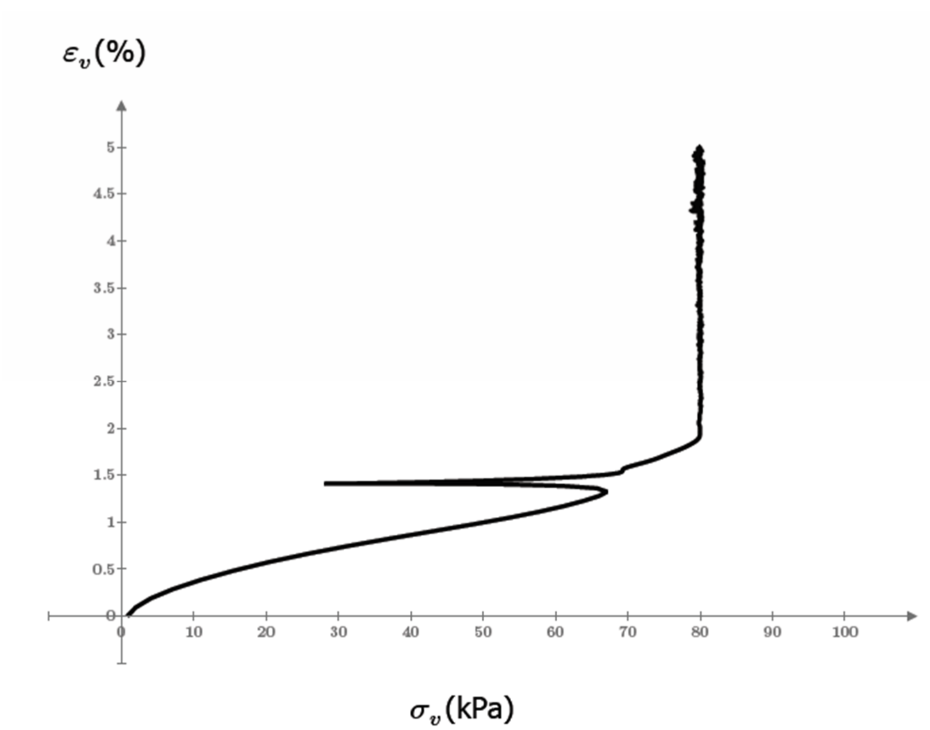

Figure B.46 Vertical strain (ε_v) vs. stress (σ_v) during consolidation of SCD1.

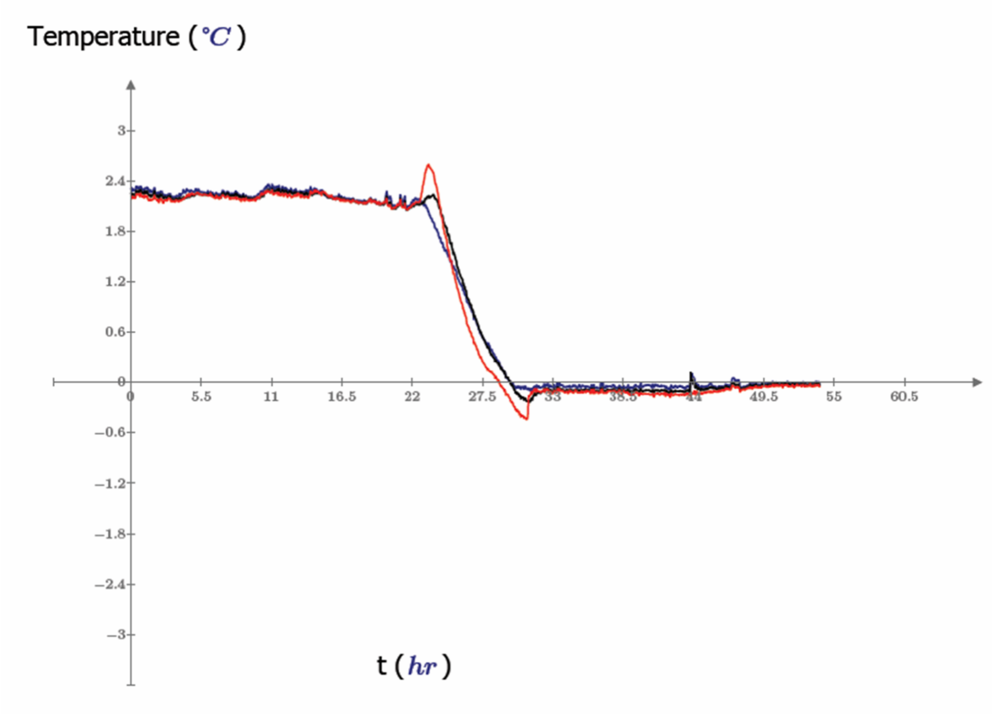

Figure B.47 Soil temperature during entire testing progress of SCD1.

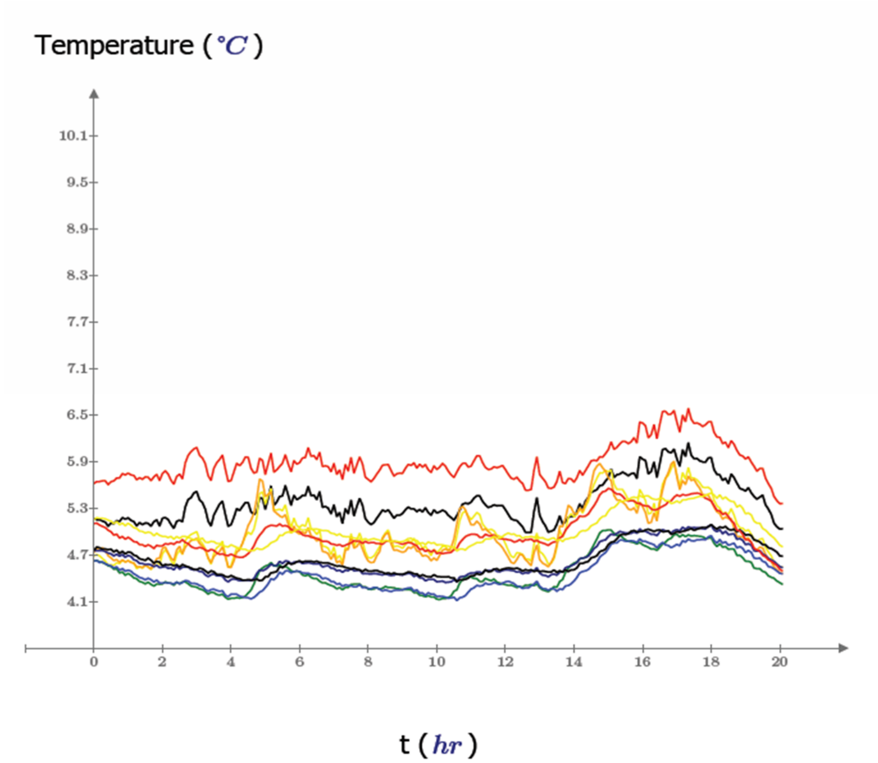

Figure B.48 Soil temperature during consolidation of SCD1.

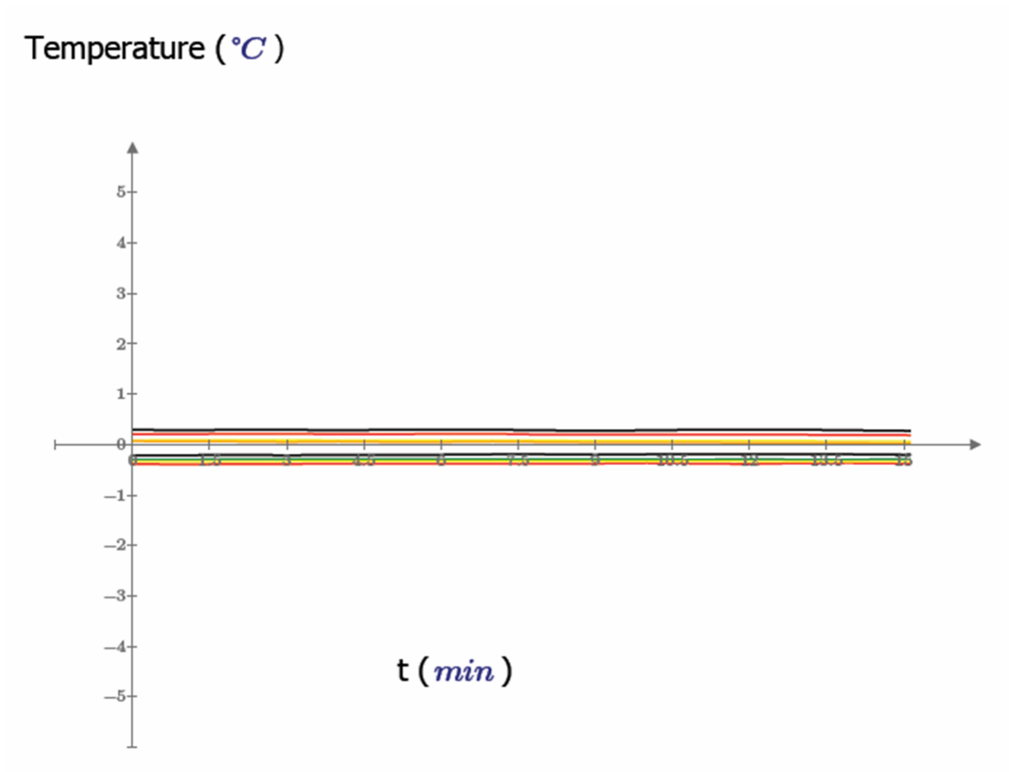

Figure B.49 Soil temperature during installation of SCD1.

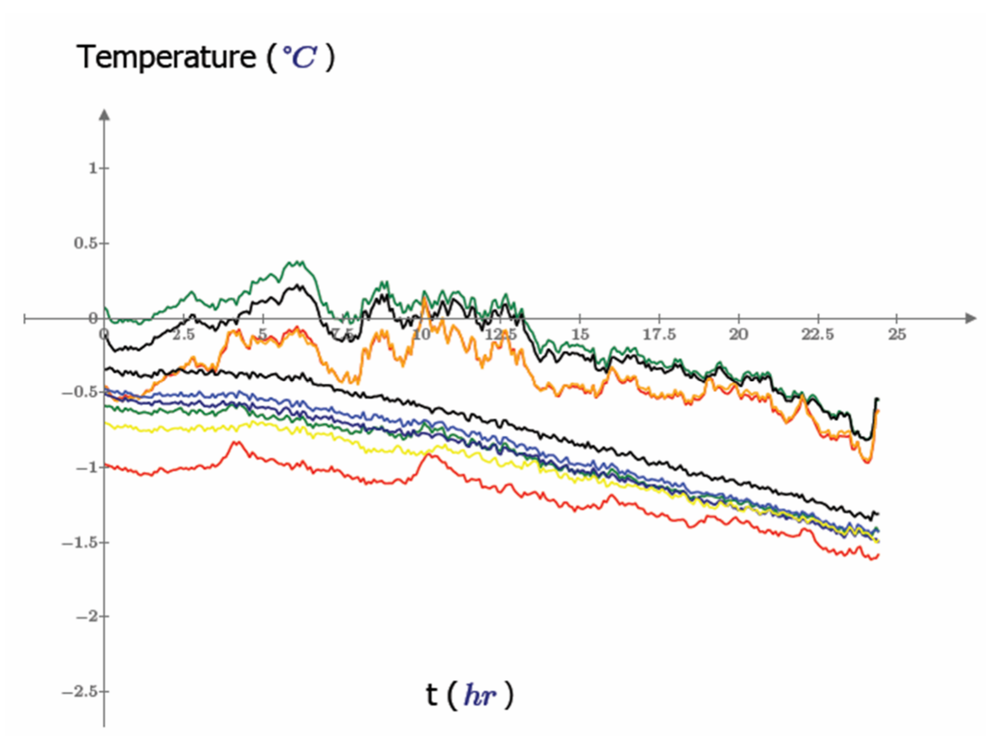

Figure B.50 Soil temperature during axial pile loading of SCD1.

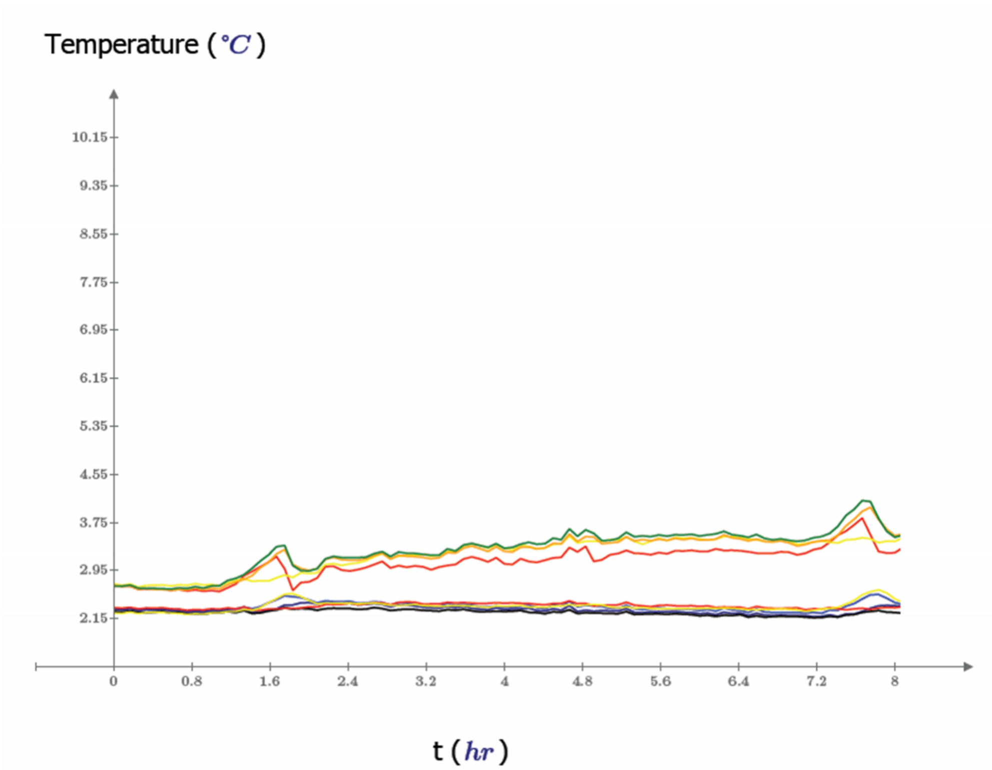

Figure B.51 Soil temperature during consolidation of SCD2.

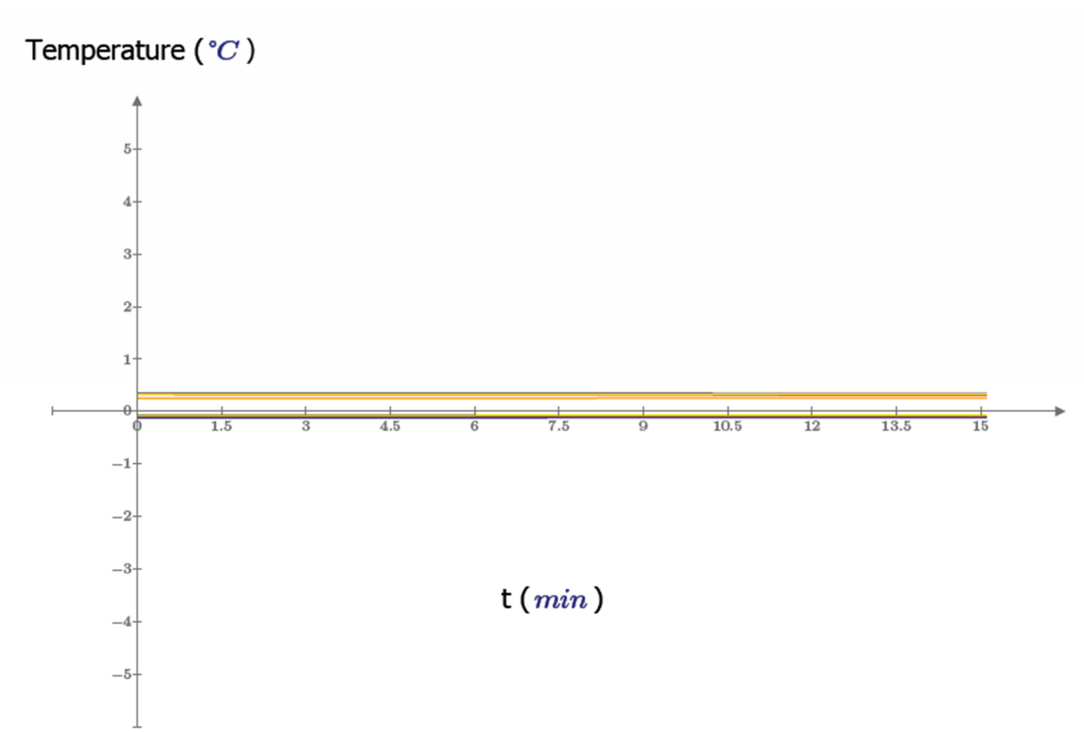

Figure B.52 Soil temperature during installation of SCD2.

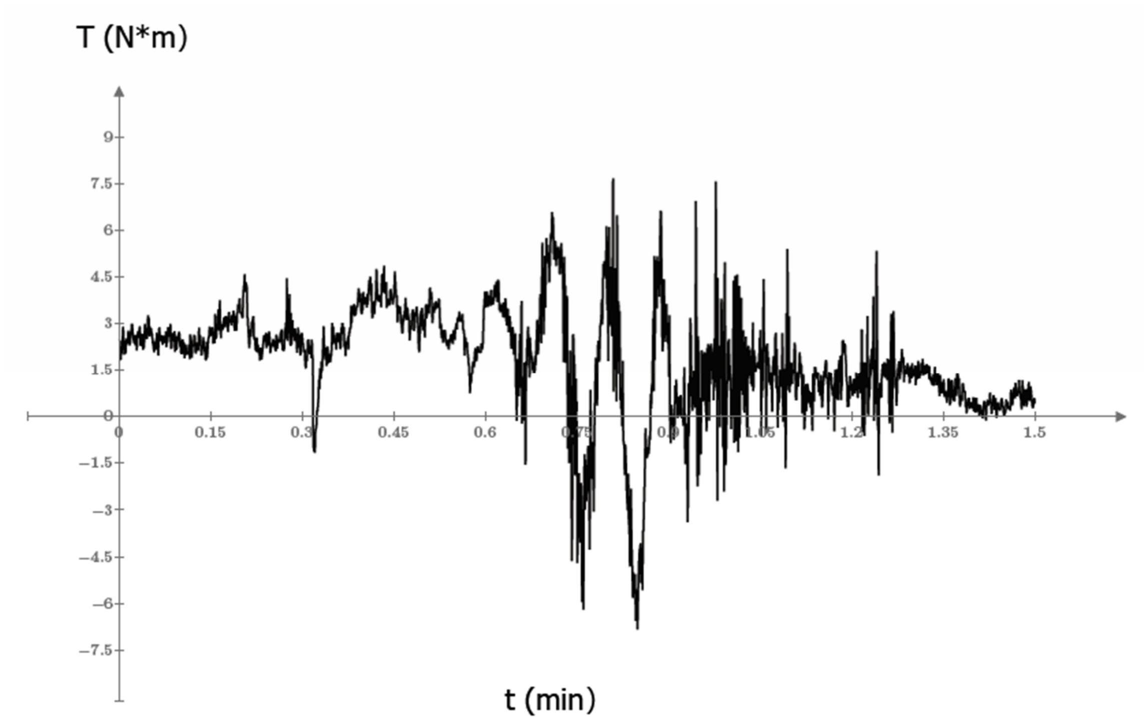

Figure B.53 Installation torque of SCD2.

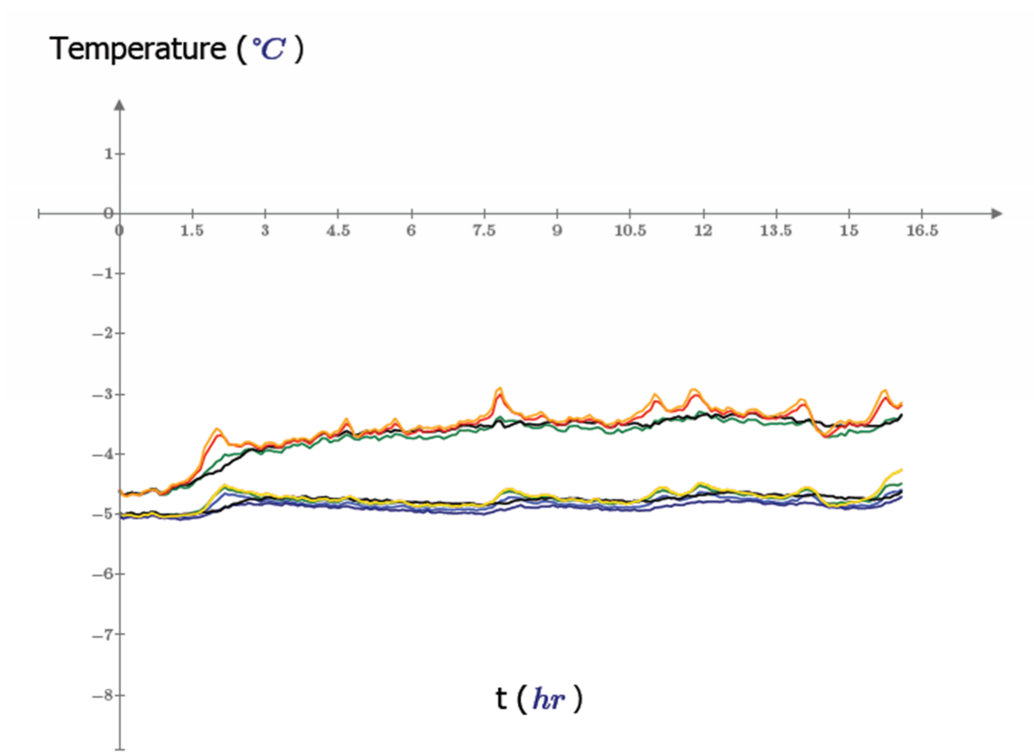

Figure B.54 Soil temperature during axial pile loading of SCD2.

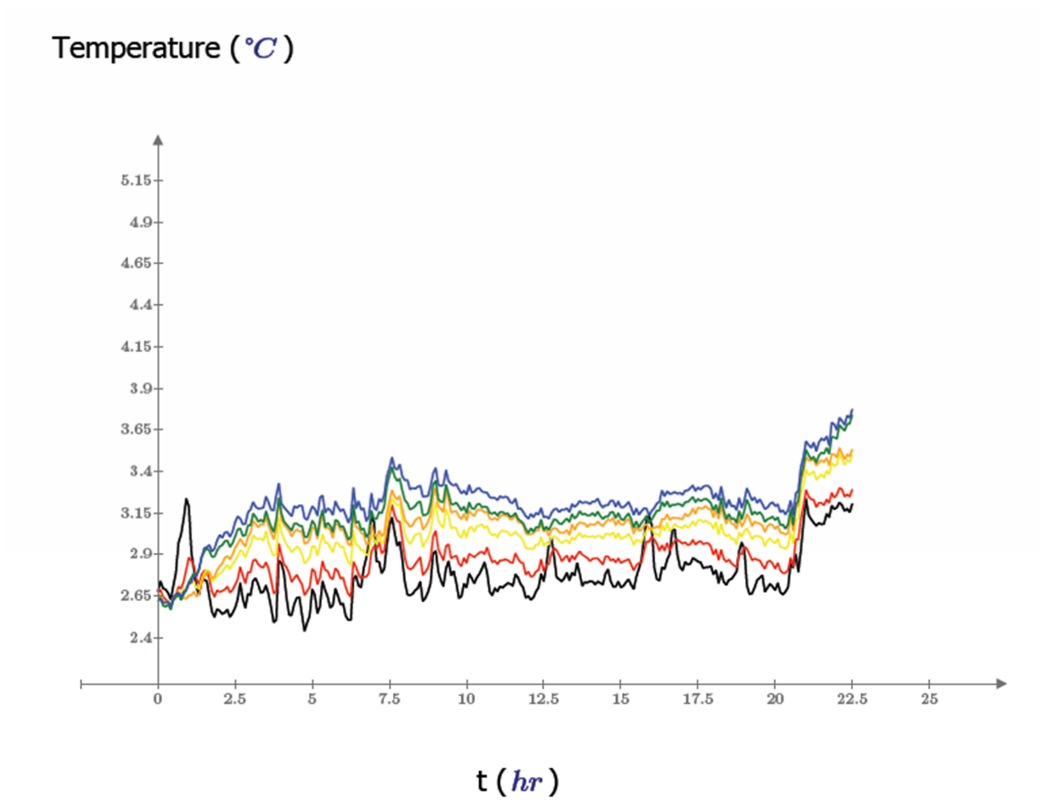

Figure B.55 Soil temperature during consolidation of SCD3.

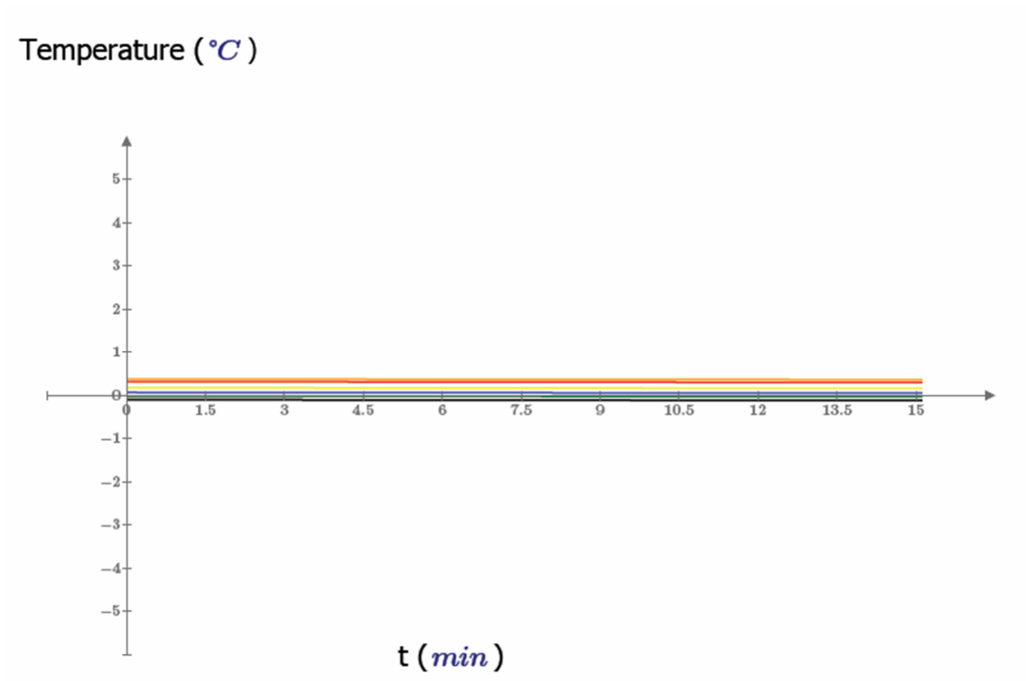

Figure B.56 Soil temperature during installation of SCD3.

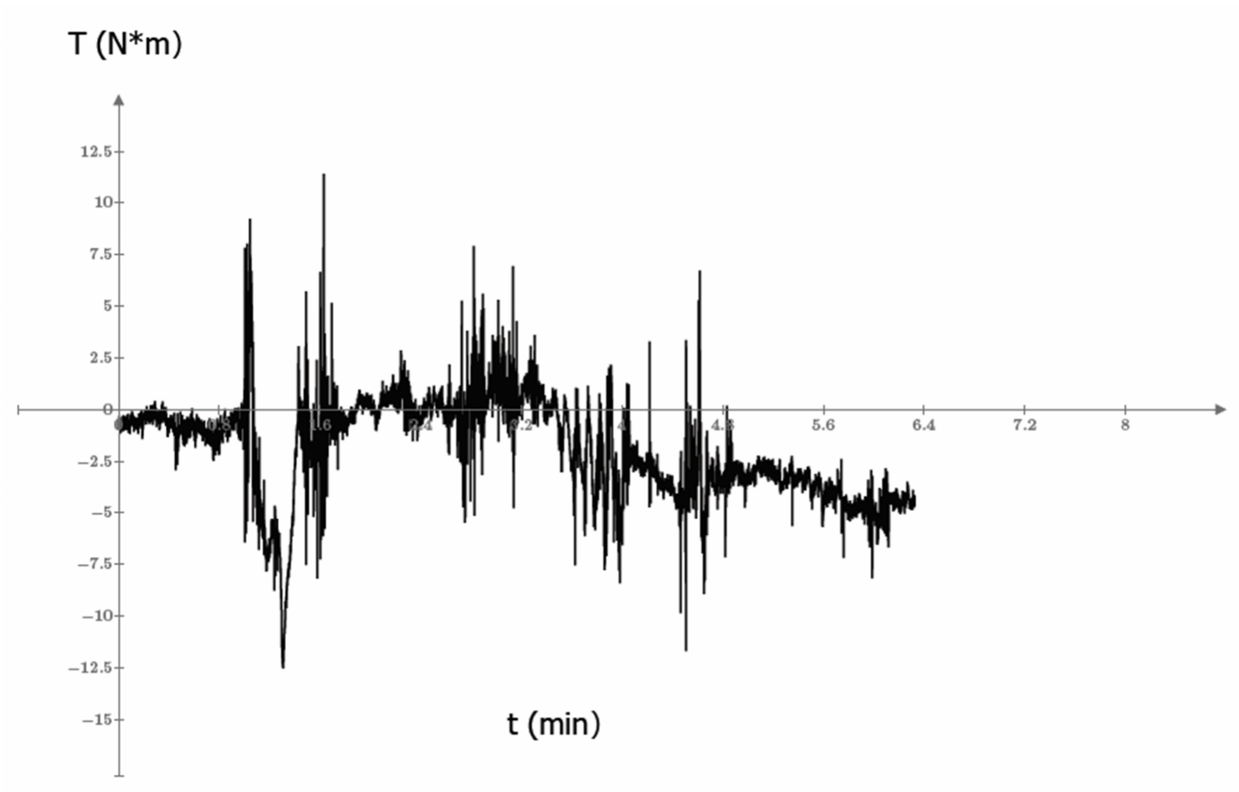

Figure B.57 Installation torque of SCD3.

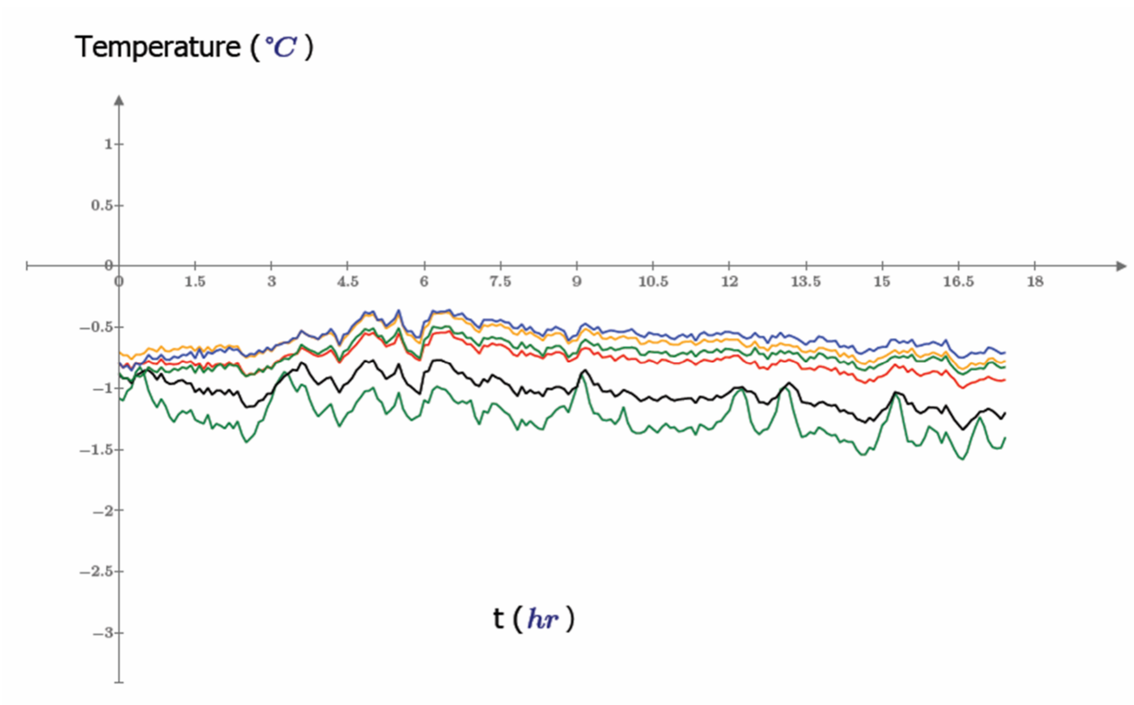

Figure B.58 Soil temperature during axial pile loading of SCD3.

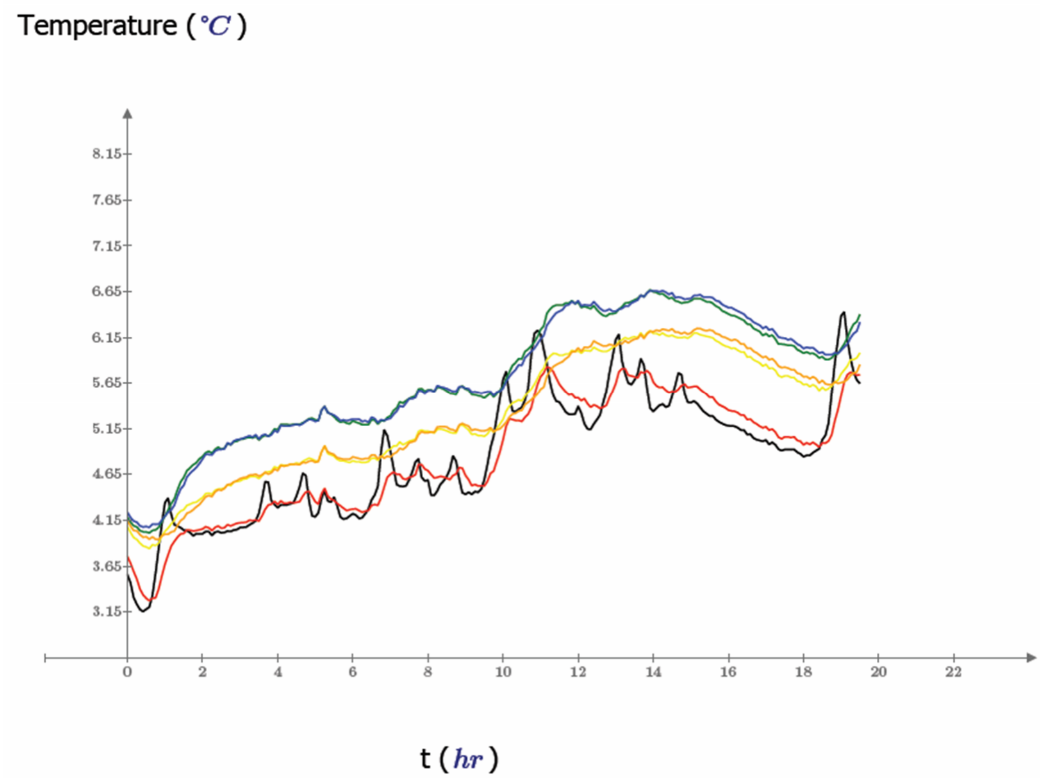

Figure B.59 Soil temperature during consolidation of SCD4.

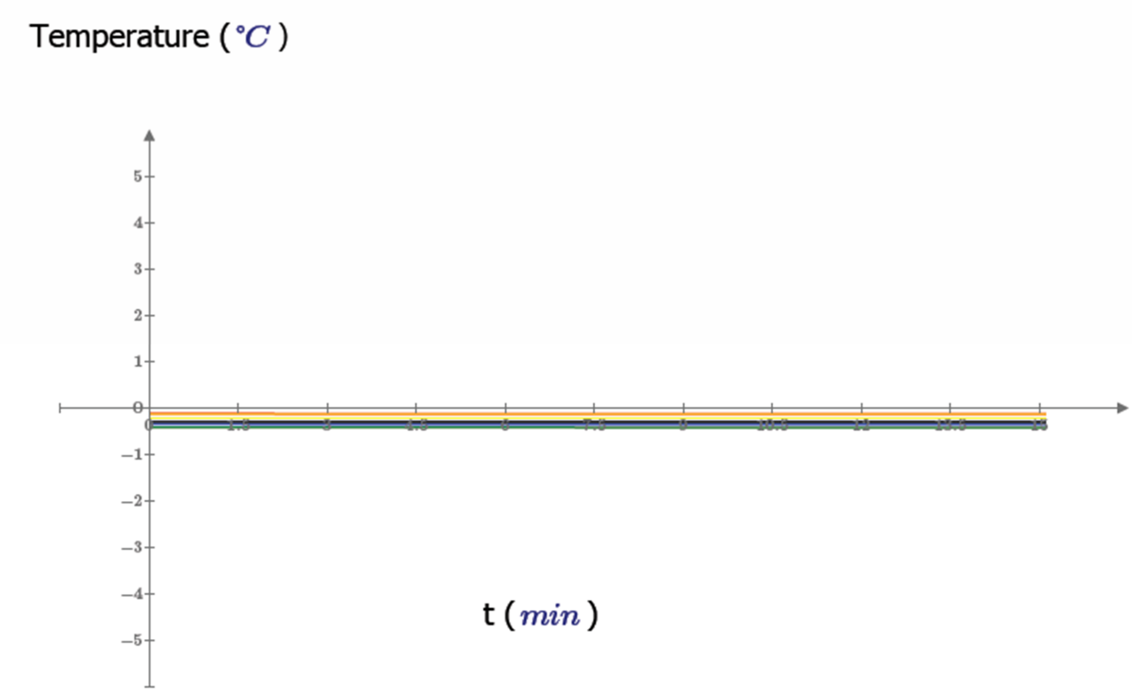

Figure B.60 Soil temperature during installation of SCD4.

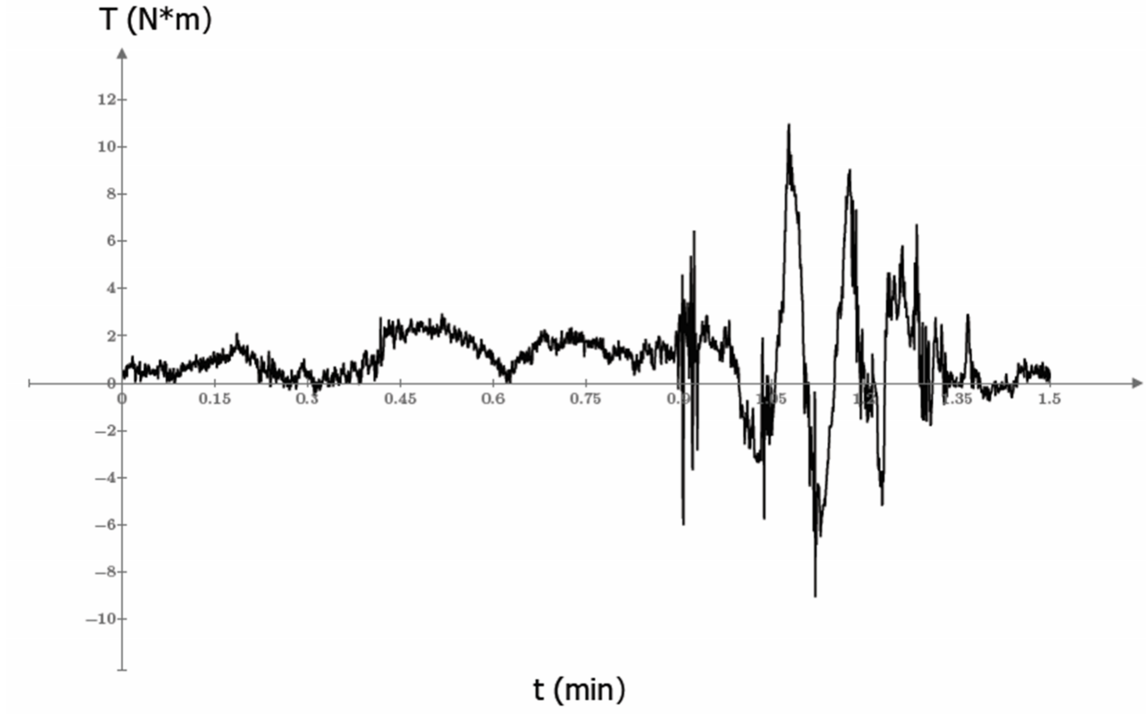

Figure B.61 Installation torque of SCD4.

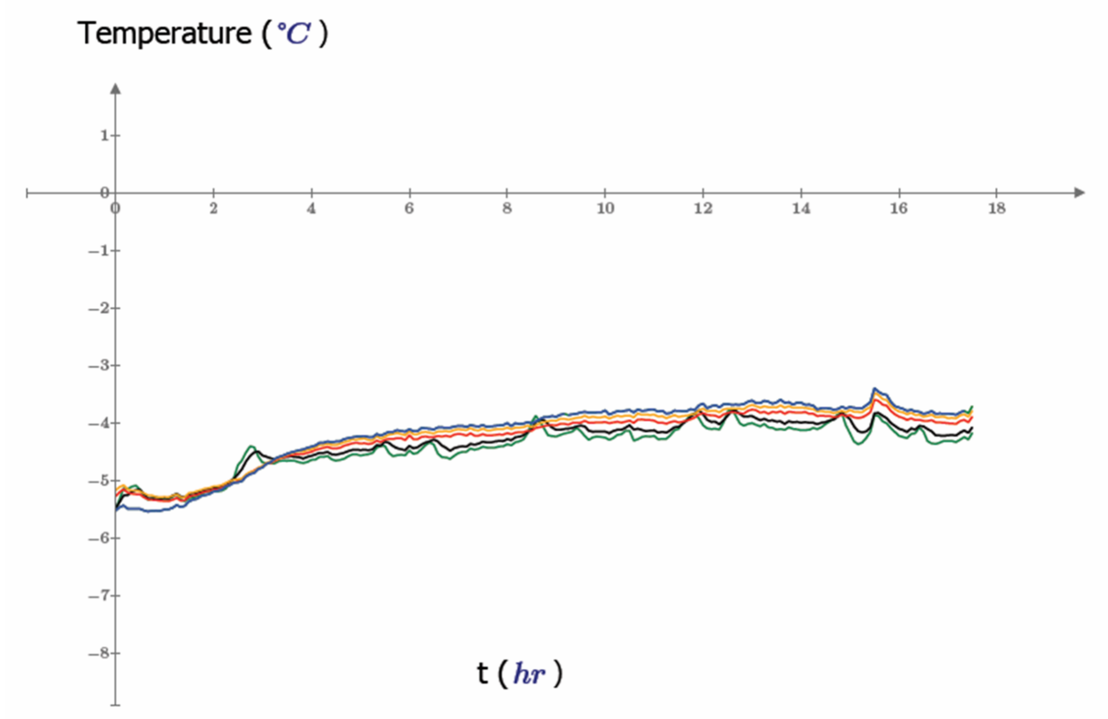

Figure B.62 Soil temperature during axial pile loading of SCD4.

$^{\circ}C$

mm

s

kN

cm

π cm

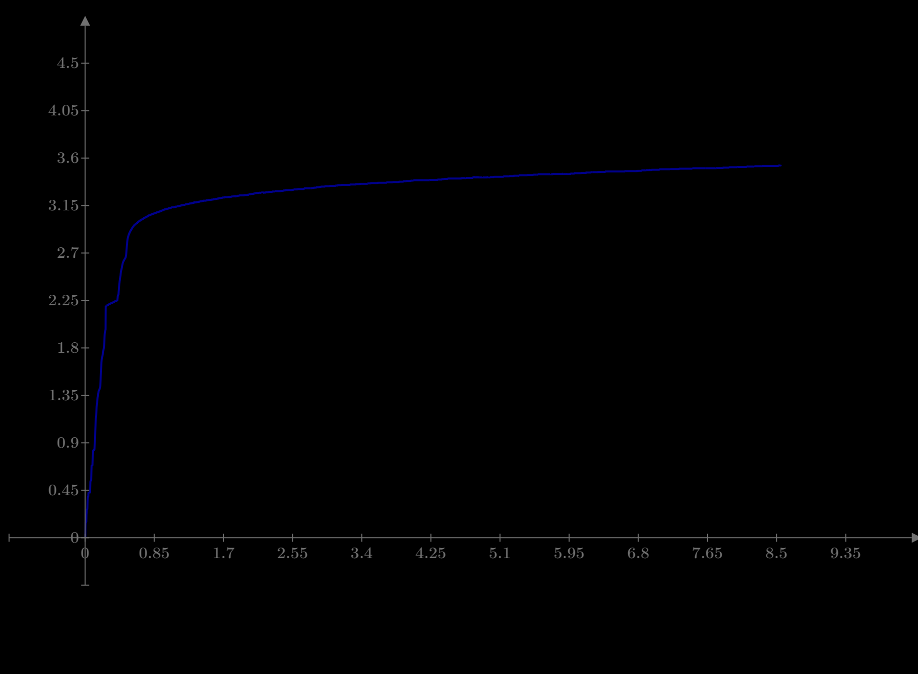

[redacted]

[redacted]

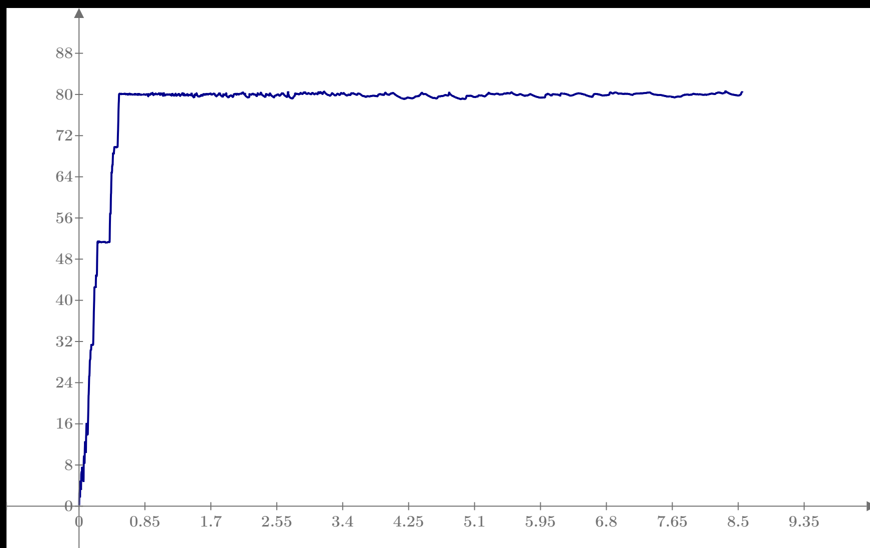

[redacted]

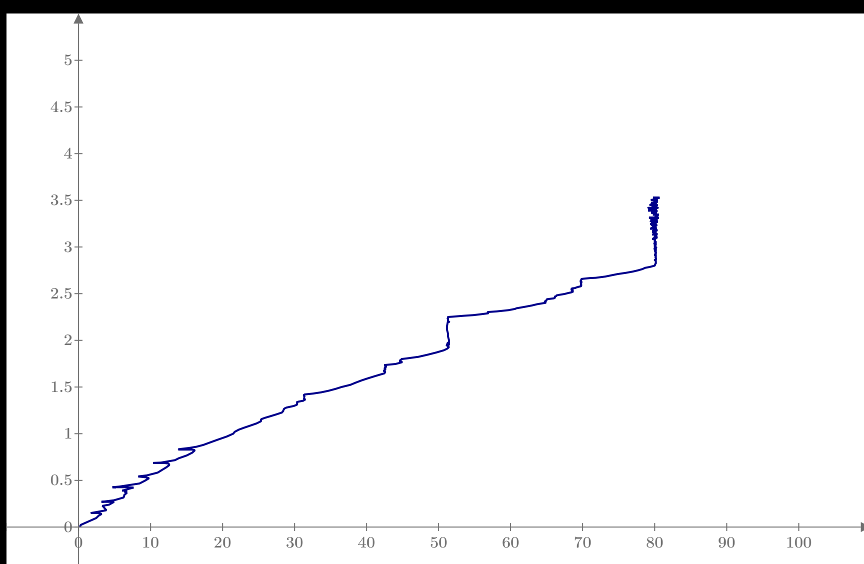

[redacted]

[redacted]

[redacted]

[redacted] min [redacted]

[redacted] $^\circ C$ [redacted]

[redacted] $^\circ C$ [redacted]

[redacted] $^\circ C$ [redacted]

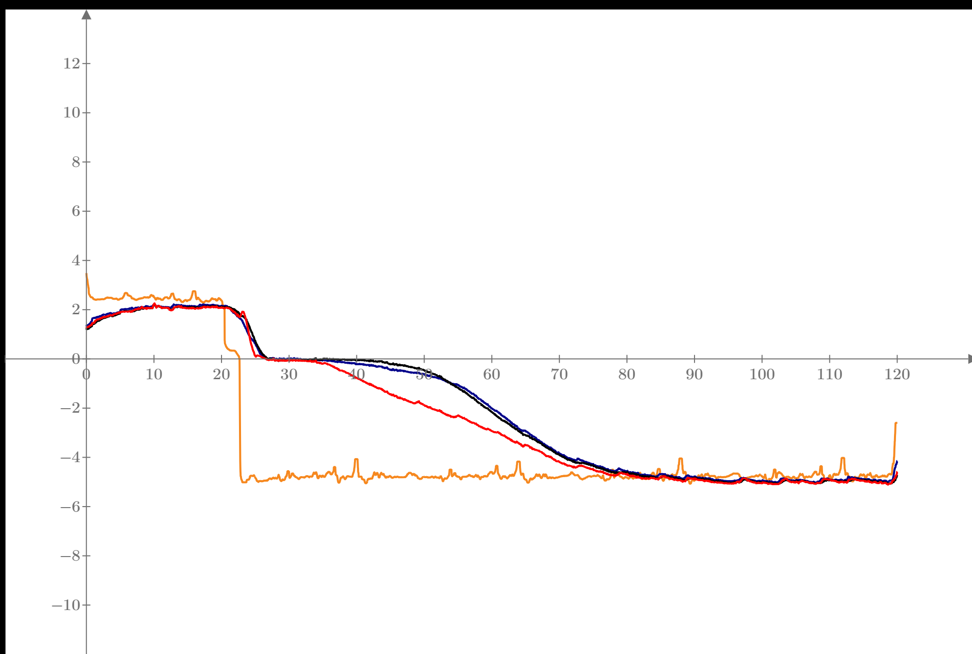

[redacted] hr [redacted]

[redacted] min [redacted]

[redacted] $^\circ C$ [redacted]

[redacted]

[redacted] $^{\circ}C$ [redacted]

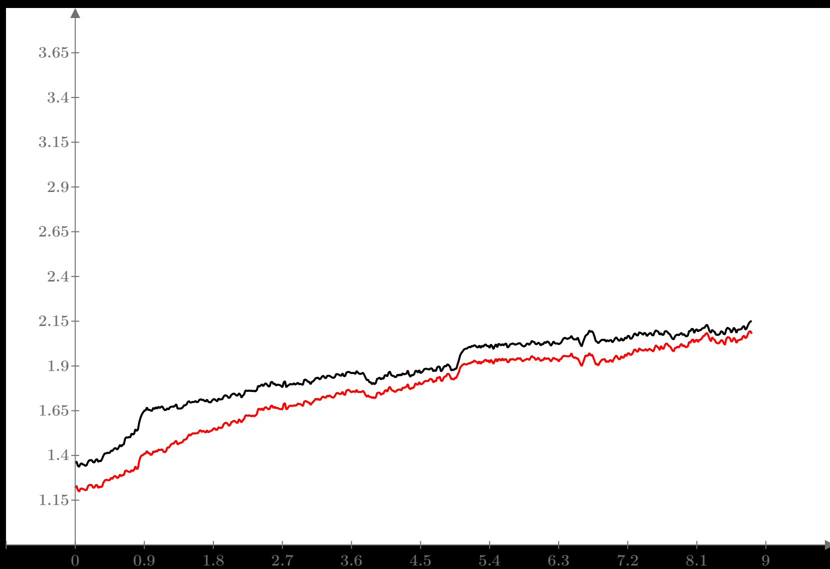

[redacted] hr [redacted]

[redacted] GPa [redacted] mm [redacted] m [redacted]

[redacted] π [redacted] mm [redacted] mm [redacted] m [redacted]

[redacted] s [redacted]

[redacted]

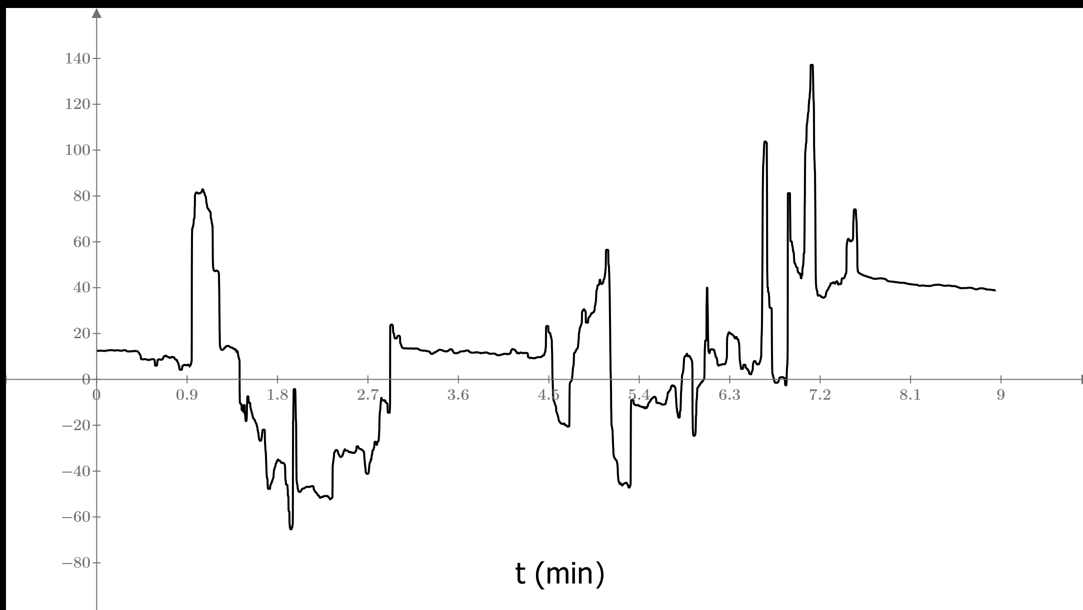

[redacted] $N\ m$ [redacted] $N{\cdot}m$ [redacted] $N{\cdot}m$ [redacted] $N\ m$ [redacted] cm [redacted]

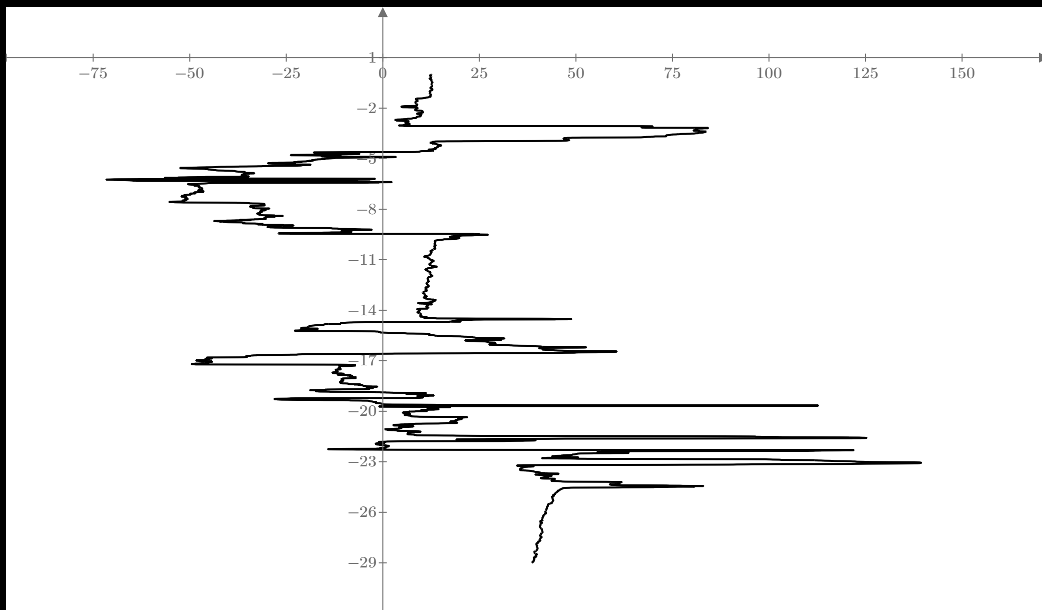

$N{*}m$

cm

s

$N \quad m$

kPa

$cm \quad mm \quad mm \quad \pi \quad mm \quad mm \quad cm$

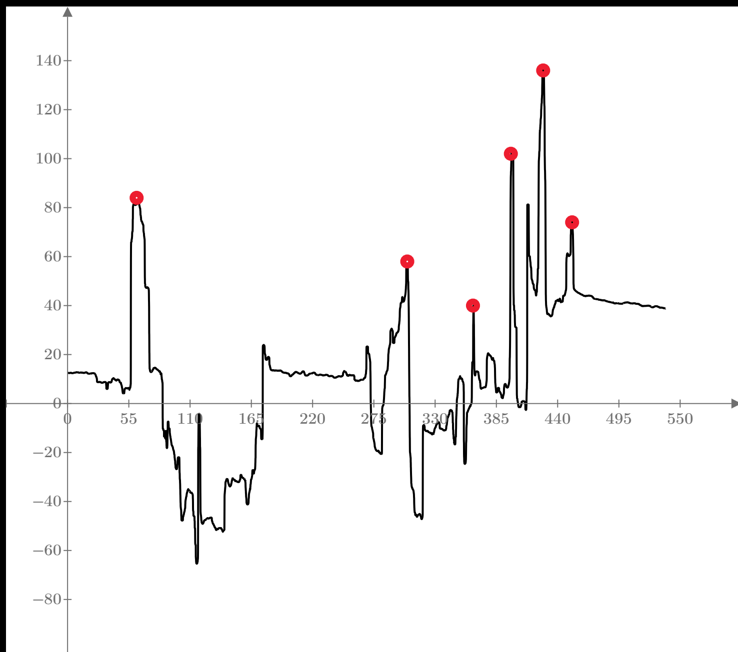

140
120
100
80
60
40
20
0
−20
−40
−60
−80
0
55
110
165
220
275
330
385
440
495
550

$N\ m$

$N\ m$

s

s

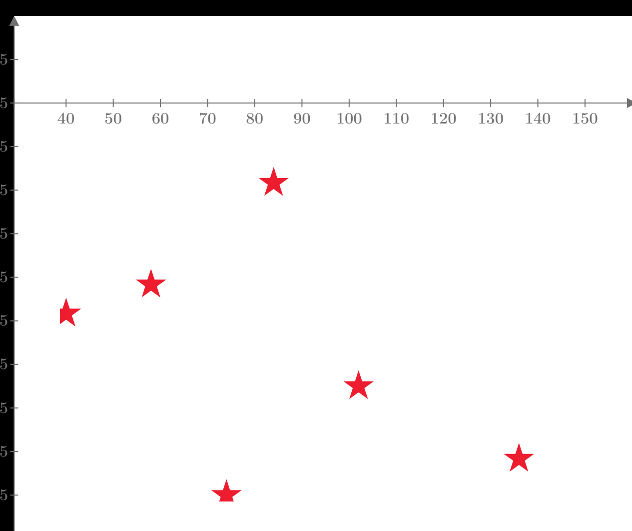

2.5
−0.5
−3.5
−6.5
−9.5
−12.5
−15.5
−18.5
−21.5
−24.5
−27.5
40
50
60
70
80
90
100
110
120
130
140
150

[redacted] $^{\circ}C$ [redacted] min [redacted] $^{\circ}C$ [redacted]

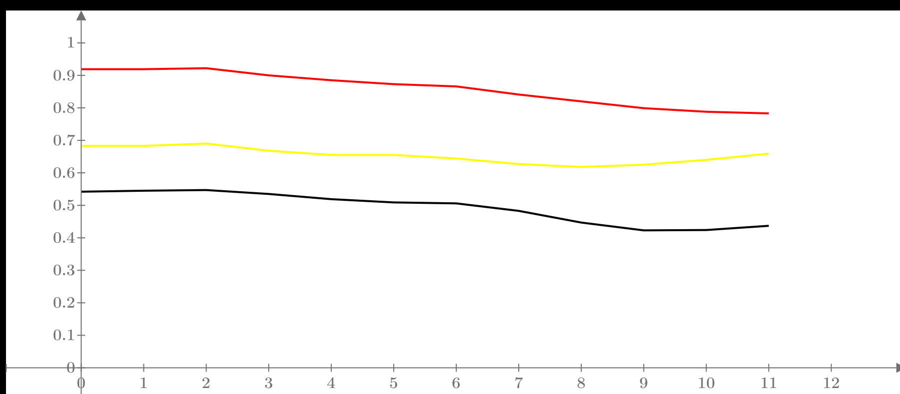

[redacted] min [redacted] s [redacted] kN [redacted]

[redacted]

[redacted] mm [redacted] kN [redacted]

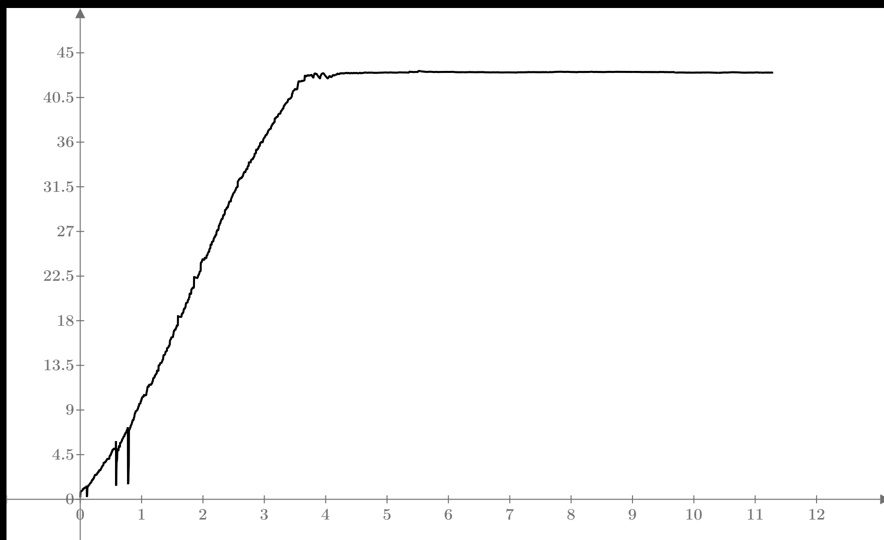

[redacted]

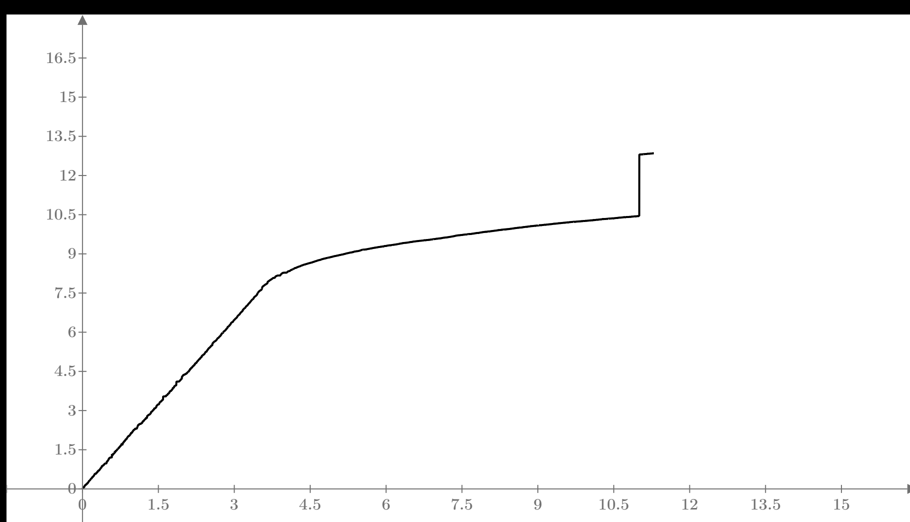

[redacted]

[redacted]

[redacted]

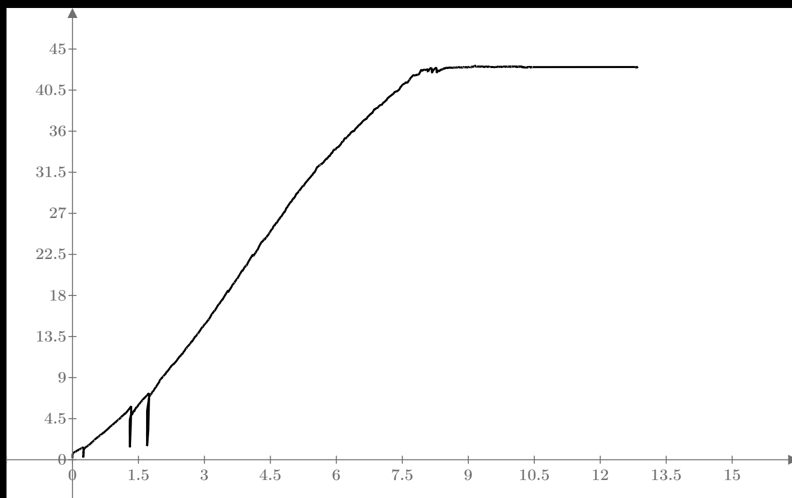

[redacted] hr [redacted] $°C$ [redacted] $°C$ [redacted]

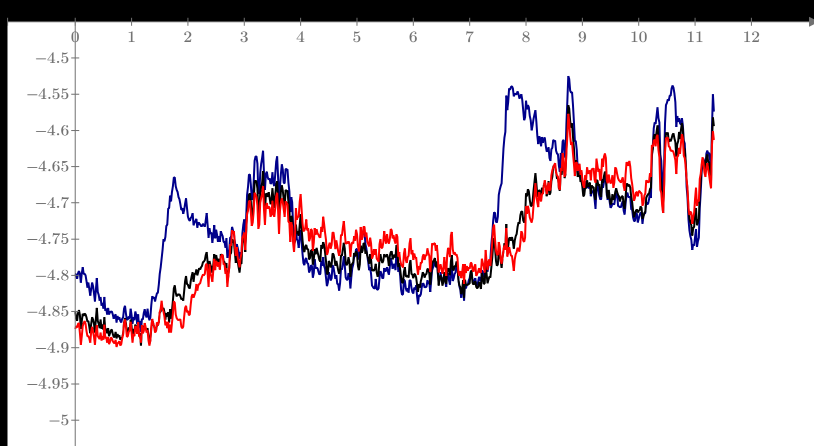

[redacted] hr [redacted]

[redacted] GPa [redacted]

[redacted] π [redacted] mm [redacted] mm [redacted] m [redacted]

[redacted] mm [redacted]

[redacted] mm [redacted] mm [redacted]

[redacted] cm [redacted]

[redacted] kPa [redacted]

[redacted] π [redacted] kN [redacted]

[redacted] kN [redacted]

[redacted] mm [redacted] cm [redacted] m [redacted]

[redacted] MPa [redacted]

[redacted]

[redacted]

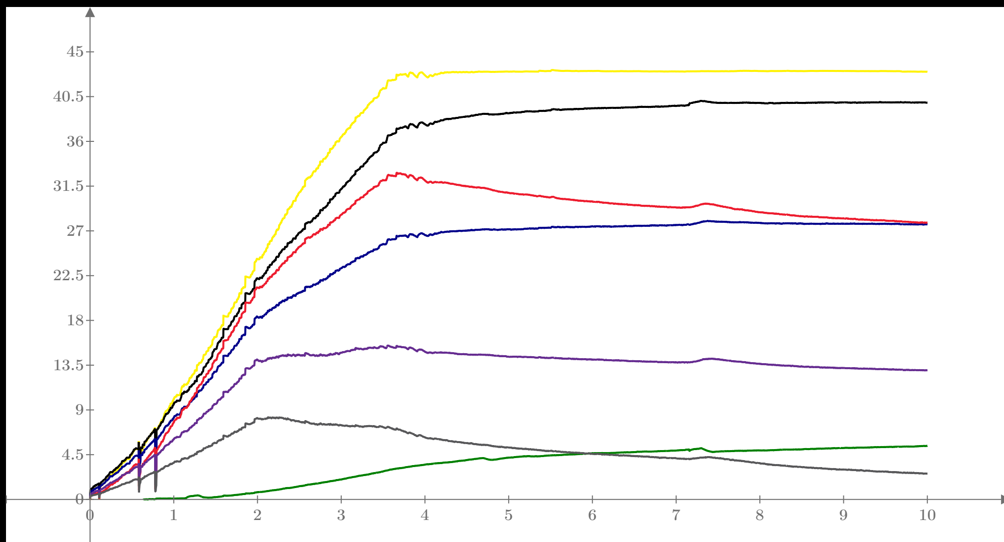

[redacted] mm [redacted] mm [redacted]

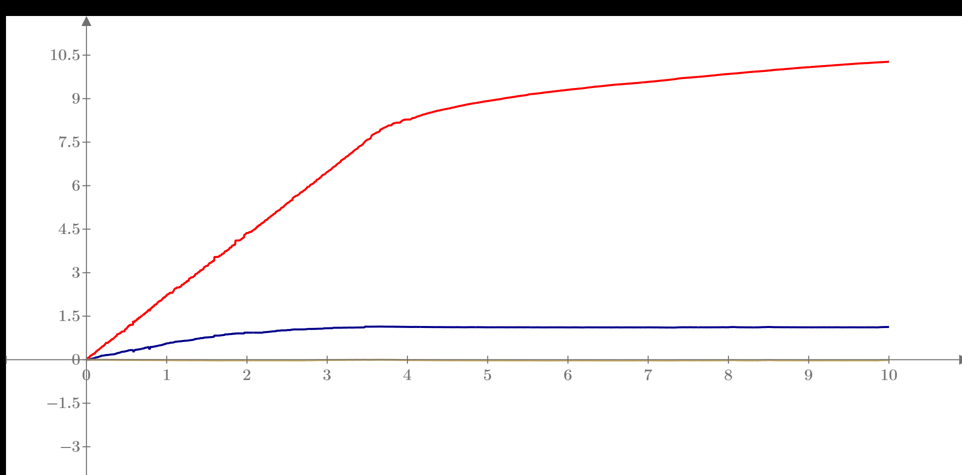

[redacted]

[redacted]